Constraints on the sources and impacts of volatile organic compounds (VOCs) over North America from tall tower measurements

A Dissertation
SUBMITTED TO THE FACULTY OF
UNIVERSITY OF MINNESOTA
BY

Lu Hu

IN PARTIAL FULFILLMENT OF THE REQUIREMENTS
FOR THE DEGREE OF
DOCTOR OF PHILOSOPHY

Dylan B. Millet, Advisor

June 2014

Acknowledgements

Special thanks to my wife Yurong Luan for her full, unconditional, and continued support. She has been my inspiration and motivation for continuing to move my career forward!

I also thank my wonderful advisor and mentor, Dylan Millet. Thank you so much for your inspiring discussions and ideas, and for believing in me. I really appreciate your guidance and mentoring over the years!

Thanks to Tim Griffis, Peter Snyder, and Matt Simcik for your ideas and inputs, and for serving in my thesis committee and reviewing this dissertation. I thank current and past members of the UMN Atmospheric Chemistry Group and the Biometeorology Group, who provided a very supportive environment to work and learn, and helped to make my life very enjoyable.

A huge thank you to Mike Mohr, Matt Erickson, Ming Chen, and Zewei Song for your generous help during the long-term field campaign. Without your help, the field work would be even more challenging. I thank The Current from Minnesota Public Radio (KCMP 89.3FM) for hosting this field campaign.

I would also like to thank many collaborators who have made significant contributions to this dissertation: Kelly Wells, Su Youn Kim, Munkhbayar Baasandorj, Detlev Helmig, Emily Fischer, Jacques Hueber, Abigale Curtis, Joost de Gouw, and Carsten Warneke.

Finally, I acknowledge the funding sources that made this work possible. Research was supported by the National Science Foundation (Grant #0937004), by the National Aeronautics and Space Administration (Grant #NNX10AG65G), by the Minnesota Supercomputing Institute, and by the University of Minnesota Doctoral Dissertation Fellowship.

Dedication

To my father,
a cancer survivor,
a brave fighter to a rare lung disease (pulmonary fibrosis),
who motivates and encourages me
to continually pursue research in atmospheric chemistry.

Abstract

This dissertation presents the first-ever in-situ tall tower measurements of volatile organic compound (VOC) concentrations. The data span August 2009 through July 2012, and provide new constraints on seasonal and long-term controls on VOC sources and their atmospheric effects. The 200 m sampling height provides a large-scale footprint, while the tall tower location, near the intersection of the main North American ecosystems and at times downwind of the Twin Cities, affords information on natural emissions from some of the most important US landscapes as well as on anthropogenic sources.

I interpret the dataset using an atmospheric chemical transport model (GEOS-Chem CTM), with a focus on several key atmospheric VOCs. This dissertation finds that current models underestimate methanol emission rates for younger versus older leaves. This biased seasonality means that the photochemical role for methanol early in the growing season is presently underestimated.

A Bayesian inverse analysis of the tall tower observations reveals that the prior estimate of North American anthropogenic acetone sources (based on the US EPA's NEI05 inventory) is accurate to within 20%. However, biogenic acetone emissions from broadleaf trees, shrubs, and herbaceous plants are presently underestimated (~37%), while emissions from needleleaf trees plus secondary production from biogenic precursors are overestimated by a similar amount (~40%).

Model-measurement comparisons imply that isoprene emissions in the immediate vicinity of the tall tower are accurately captured by the MEGANv2.1 biogenic inventory, but that larger-scale regional emissions are underestimated, reflecting the heterogeneous land cover in this transitional landscape. Isoprene emissions play a key role in seasonal shifts between VOC-limited chemistry in the spring and fall and NO_x-limited or transitional chemistry in the summer.

A Bayesian inverse analysis based on the tall tower measurements suggests that: *i*) the RETRO global emission inventory significantly overestimates (> two-fold) US C_6-C_8

aromatic emissions; *ii*) the US EPA's NEI08 inventory likewise overestimates the toluene flux by a factor of 3, partly reflecting a bias in the estimated non-road emissions; and *iii*) total annual emissions of benzene and C_8 aromatics in the EPA's NEI08 are accurate to within the analysis uncertainty, but with some seasonal biases for on-road emissions.

Table of Contents

List of Tables

List of Figures

1 Introduction

Volatile organic compounds (VOCs) play a key role in the atmosphere as precursors of ozone and secondary organic aerosol, both of which are known to have serious deleterious effects on human and ecosystem health, and to affect Earth's radiation balance and thus the climate system. Once in the atmosphere, photochemical reactions involving VOCs modulate the oxidizing capacity of the troposphere and thus affect the lifetime of methane (a greenhouse gas) and other air pollutants. Despite their importance for the atmosphere-climate system, understanding the sources and chemistry of atmospheric organic compounds remains one of the core challenges in the field of atmospheric chemistry.

VOCs are emitted from various anthropogenic sources, including solvent use, industrial processes such as oil refining and petrochemical manufacturing, as well as combustion and evaporation of fossil fuels (Parrish, 2006; Chapter 5). Other sources of atmospheric VOCs include biomass burning (Holzinger et al., 1999) and photochemical and biological processes in the ocean (Williams et al., 2004; Sjostedt et al., 2012). Globally, however, biogenic emissions from terrestrial plants make up the largest source of atmospheric VOCs; these emissions are currently thought to be several times larger than those from anthropogenic sources (Piccot et al., 1992; Guenther et al., 2012). Plants produce and emit a wide range of VOCs - including alkenes, terpenoid compounds such as isoprene and monoterpenes, alcohols, ketones, and aldehydes – through a variety of biochemical pathways (Fall, 2003; Monson et al., 2012).

Over the last two decades, atmospheric chemists have made great strides in building emission inventories to better describe the chemical composition of our atmosphere. However, large uncertainties remain for these so-called bottom-up inventories. For example, state-of-the-science biogenic VOC inventories such as MEGAN (Model of Emissions of Gases and Aerosols from Nature) are mainly based on extrapolation of very localized (leaf to canopy scale) measurements and are highly uncertain (Guenther et al., 1995; Chapter 2-4). Data are lacking for understanding how biogenic VOC emissions

depend on season and phenology (Chapter 2), and the photochemical role these species play during the spring and fall transitions (Jacob et al., 1995; Chapter 2 and 4). According to the most recent version of the MEGAN inventory (v2.1), the total magnitude of global biogenic VOC emissions is uncertain by at least a factor of two (Guenther et al., 2012). For a specific locations and times, this error can be substantially larger (Guenther et al., 2006; Warneke et al., 2010). Errors in our understanding of how emissions change with environmental conditions (e.g., light, temperature, etc.) can be particularly significant, mainly because there is a lack of sustained atmospheric measurements that can provide robust constraints (Lamb et al., 1987). Uncertainties in anthropogenic VOC emission inventories are commonly at least as large as those in biogenic VOC emission inventories (Warneke et al., 2007), with errors for individual compounds and specific source sectors often reaching several hundred percent (Chapter 5). These poorly constrained source terms limit our ability to model air pollution and climate, and to predict future atmospheric composition.

This dissertation aims to advance scientific understanding of the sources of several key atmospheric VOCs and their impacts on other air pollutants. I performed the first-ever long-term in-situ VOC concentration measurements from a tall tower (244 m above ground level), providing a high-resolution atmospheric dataset with a regional- to continental-scale footprint. The University of Minnesota tall tower Trace Gas Observatory (KCMP tall tower) is located near the confluence of the three great ecosystems of North America (western prairie, northern coniferous forests, and eastern deciduous forests). This region also contains the largest agricultural ecosystem in the United States. In addition, the tower is sometimes downwind of the Twin Cities, allowing us to investigate the nature and importance of urban as well as biogenic emission processes.

I used a high-sensitivity proton transfer reaction mass spectrometer (PTR-MS) to measure 13 different VOCs every ~3 minutes at the KCMP tall tower. I designed and built online sampling and automatic calibration systems, and deployed them with the PTR-MS to the tall tower from July 2009 to August 2012. This dataset thus provides rich

opportunities to examine atmospheric processes across multiple temporal scales, from minutes to years.

This dissertation interprets these VOC measurements using an atmospheric chemical transport model (GEOS-Chem CTM) in terms of the constraints they provide on the following guiding questions:

- What is the regional distribution of VOC emissions, and how do they vary seasonally and with environmental conditions?
- How accurate are current VOC emission inventories? Are there discrepancies between field measurements and model predications? If so, what do these discrepancies imply for our understanding of emission processes?
- How do VOCs affect the productions of other air pollutants such as CO and ozone, especially during the seasonal transitions from spring-to-summer and summer-to-fall?

I focus on the following key atmospheric VOCs: isoprene (C_5H_6), methanol (CH_3OH), acetone ($CH_3C(O)CH_3$), and C_6-C_8 aromatic compounds including benzene (C_6H_6), toluene (C_7H_8), and ethylbenzene + xylenes (C_8H_{10}). According to current estimates, the first three species account collectively for nearly 70% of biogenic VOC emissions and 60% of all VOC emissions globally, while C_6-C_8 aromatic compounds are air toxics that account for ~25% of global anthropogenic VOC emissions (Figure 1.1 and its cited references).

The following science chapters (2-5) are self-contained, each with an abstract, introduction, method description, result/discussion, and conclusion. Chapter 2 focuses on atmospheric methanol observations at the KCMP tall tower, Chapter 3 on acetone, Chapter 4 on isoprene, and Chapter 5 on C_6-C_8 aromatic compounds. Chapter 6 provides a summary of the research and recommendations for future study.

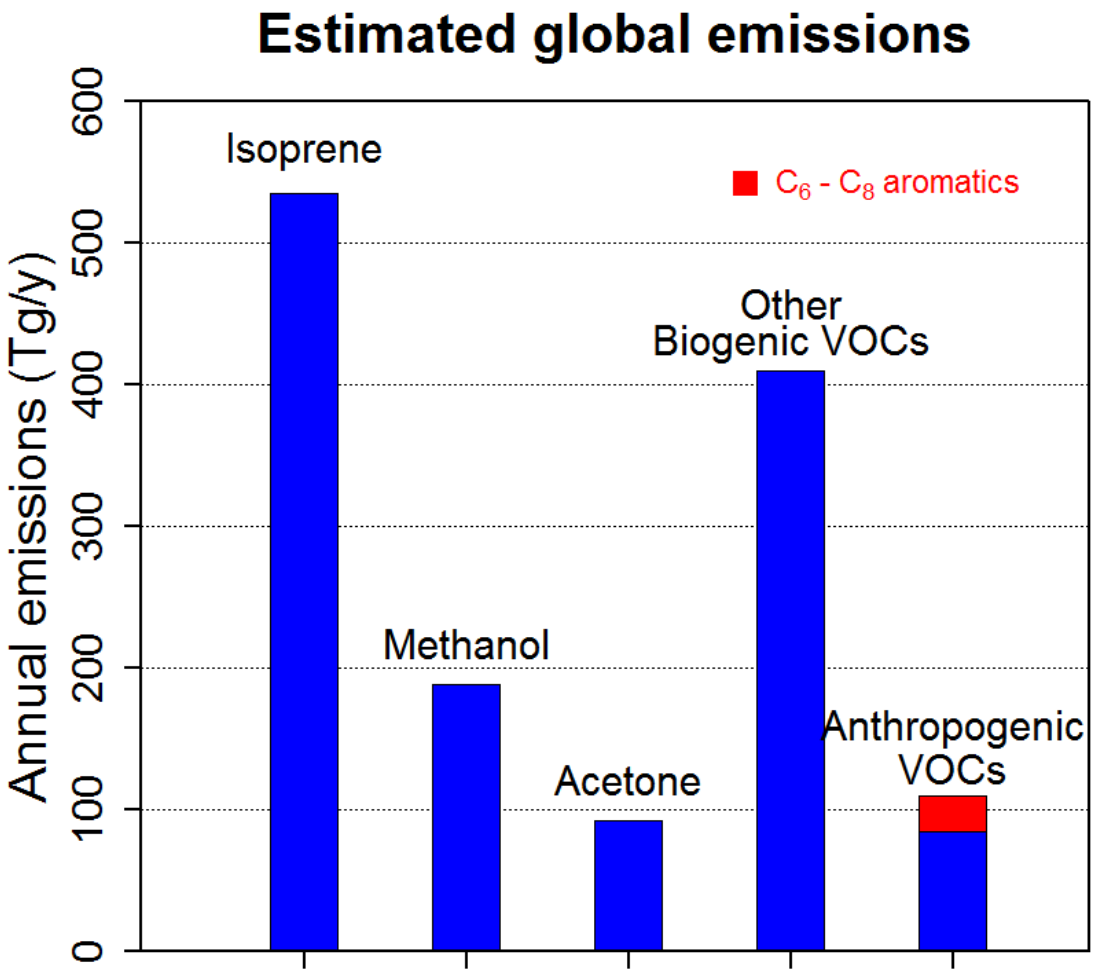

Figure 1.1. Estimated global emissions for several key atmospheric VOCs: isoprene; methanol, acetone, other biogenic VOCs, C_6-C_8 aromatics and other anthropogenic VOCs (Piccot et al., 1992; Millet et al., 2008; Fischer et al., 2012; Guenther et al., 2012; Wells et al., 2014; Chapter 5).

2 Sources and seasonality of atmospheric methanol based on tall tower measurements in the US Upper Midwest

Abstract

We present over one year (01/2010-02/2011) of continuous atmospheric methanol measurements from the University of Minnesota tall tower Trace Gas Observatory (KCMP tall tower; 244 m a.g.l.), and interpret the dataset in terms of constraints on regional methanol sources and seasonality. The seasonal cycle of methanol concentrations observed at the KCMP tall tower is generally similar to that simulated by a global 3-D chemical transport model (GEOS-Chem, driven with MEGANv2.0 biogenic emissions) except the seasonal peak occurs ~1 month earlier in the observations, apparently reflecting a model underestimate of emission rates for younger versus older leaves. Based on a source tracer approach, which we evaluate using GEOS-Chem and with multiple tracers, we estimate that anthropogenic emissions account for approximately 40% of ambient methanol abundance during winter and 10% during summer. During daytime in summer, methanol concentrations increase exponentially with temperature, reflecting the temperature sensitivity of the biogenic source, and the observed temperature dependence is statistically consistent with that in the model. Nevertheless, summertime concentrations are underestimated by on average 35% in the model for this region. The seasonal importance of methanol as a source of formaldehyde (HCHO) and carbon monoxide (CO) is highest in spring through early summer, when biogenic methanol emissions are high but isoprene emissions are still relatively low. During that time observed methanol concentrations account for on average 20% of the total CO and HCHO production rates as simulated by GEOS-Chem, compared to 12% later in the summer and 12% on an annual average basis. The biased seasonality in the model means that the photochemical role for methanol early in the growing season is presently underestimated.

2.1 Introduction

Methanol (CH_3OH) is one of the most abundant non-methane organic gases in the atmosphere, with concentrations ranging from hundreds of parts per trillion (pptv) in the remote troposphere to tens of parts per billion (ppbv) near surface sources (Singh et al., 1995; Karl et al., 2003; Millet et al., 2004; Singh et al., 2004; Schade and Goldstein, 2006; Jordan et al., 2009). It affects background and boundary layer photochemistry, and is an important source of carbon monoxide (CO) and formaldehyde (HCHO) (Riemer et al., 1998; Tie et al., 2003; Millet et al., 2006; Duncan et al., 2007; Choi et al., 2010). Here we present over one full year of methanol concentration measurements from a tall tower observatory in the US Upper Midwest, and interpret the data in terms of the information they provide on seasonal methanol sources and natural versus anthropogenic contributions.

Estimates of the global methanol source range from 75 to 350 Tg yr^{-1} (Singh et al., 2000; Galbally and Kirstine, 2002; Tie et al., 2003; Singh et al., 2004; Jacob et al., 2005; Millet et al., 2008; Stavrakou et al., 2011), with the largest fluxes from terrestrial plant growth (MacDonald and Fall, 1993; Fall and Benson, 1996; Singh et al., 2000; Karl et al., 2003; Harley et al., 2007; Folkers et al., 2008; Stavrakou et al., 2011). Other methanol sources include emissions from decaying plant matter (Warneke et al., 1999), biomass and biofuel burning (Holzinger et al., 1999; Andreae and Merlet, 2001), urban and industrial activities (de Gouw et al., 2005), and atmospheric production (mostly from methane oxidation) (Madronich and Calvert, 1990; Tyndall et al., 2001). The marine biosphere appears to be a large gross source but an even larger gross sink of atmospheric methanol, so that overall it acts as a net sink (Singh et al., 1995; Heikes et al., 2002; Williams et al., 2004; Millet et al., 2008; Stavrakou et al., 2011). Gas-phase oxidation by OH is the other major methanol sink with deposition playing a smaller but still significant role (Atkinson et al., 2006; Karl et al., 2010). The overall atmospheric lifetime for methanol is an estimated 5-12 days (Heikes et al., 2002; Tie et al., 2003; Singh et al., 2004; Stavrakou et al., 2011).

The atmospheric methanol budget includes substantial uncertainties, most notably in terms of the magnitude and distribution of biogenic emissions which are large but remain poorly constrained. This in part reflects the scarcity of long-term measurements to constrain methanol emission fluxes and their seasonal variability.

In this paper we report atmospheric methanol measurements made using a proton transfer reaction mass spectrometer (PTR-MS) over one year (01/2010-02/2011) at the University of Minnesota tall tower Trace Gas Observatory (KCMP tall tower), a 244 m AmeriFlux tall tower in the US Upper Midwest (Figure 2.1). Measurements are made at a sampling height of 185 m above ground level, providing a high-resolution signal with regional-scale footprint. The tower is located near the intersection of the major North American ecosystems (eastern deciduous forest, northern coniferous forest, agriculture, and western prairie), and is at times downwind of the Twin Cities metropolitan area (2010 population: 3.3 M), thus affording information on emissions of methanol and other reactive gases from some of the most important US landscapes as well as from anthropogenic sources. We apply the tall tower methanol observations with a suite of other chemical measurements, and in combination with a global 3-D chemical transport model (GEOS-Chem), to better understand seasonal methanol sources, natural versus anthropogenic contributions, and the resulting impact on atmospheric formaldehyde and CO.

2.2 Methods

2.2.1 Field site description

The University of Minnesota tall tower Trace Gas Observatory is a Minnesota Public Radio communications tower (KCMP 89.3 FM, 44.689°N, 93.073°W; 244 m height, 534 m above sea level), located approximately 25 km south of Minneapolis-St. Paul, MN, US (Figure 2.1). Land cover within a 50 km radius of the tall tower consists of approximately 26% crops, 18% grassland, 18% woodland, 27% developed land, 6% wetland, and 5% water (Corcoran, 2009). May through October is the freeze-free growing season near the site with a 30-year normal (arithmetic mean) temperature of 16.6°C (min 11.2°C, max 23.6°C). The 30-year normal annual precipitation is 88 cm, about 70% of which occurs

between May and October each year (Corcoran, 2009). Winter is cold (November to January 30-year mean -8.2°C, min -12.2°C, max -3.3°C) and the snow cover period can span November to March (Corcoran, 2009; NOAA-MRCC, 2011).

The tower was instrumented with a variety of micrometeorological instruments in April 2007, and is part of the AmeriFlux network (Sitename KCMP tall tower) (Griffis et al., 2010). A three-dimensional sonic anemometer-thermometer (CSAT3, Campbell Scientific Inc., USA) installed near the air sample inlet measures the three components of wind speed and temperature at 10 Hz for eddy flux measurements of CO_2, H_2O, and sensible heat. A detailed description of meteorological measurements at the site is given by Griffis et al. (2010).

Figure 2.2 shows the seasonal wind speed and direction observed during 2010 at the KCMP tall tower. Mean wind speeds for each season ranged between 5.5 and 7.5 m s^{-1}. Winds during spring were most commonly from south to southeast, while in the summer southerly and north-westerly winds were most frequent. In the autumn and winter, winds were predominantly from the northwest. The footprint sampled by the KCMP tall tower therefore varies through the year, due to these shifting wind patterns (as well as seasonal changes in boundary layer mixing and photochemical lifetimes).

2.2.2 Volatile organic compound (VOC) measurements

We measure methanol and an ensemble of other VOCs (including isoprene and its first-generation oxidation products methyl vinyl ketone and methacrolein; acetone; acetonitrile; and C_6-C_9 aromatics) at the KCMP tall tower using PTR-MS (HS-PTR-MS, Ionicon Analytik, Austria). In this technique, air flows continuously through a drift tube reaction chamber containing H_3O^+ ions produced by hollow cathode discharge. VOCs with a proton affinity higher than that of water (>165.2 kcal/mol) are ionized via proton-transfer reaction, and subsequently separated and detected by a quadrupole mass spectrometer with a secondary electron multiplier (Inficon, Liechtenstein) (Lindinger et al., 1998; de Gouw and Warneke, 2007).

The PTR-MS is maintained in an air-conditioned communications building at the base of the tower and was deployed to the site in July 2009. All sampling surfaces are composed of Perfluoroalkoxy (PFA) Teflon tubing to minimize VOC adsorption during measurement (de Gouw and Warneke, 2007; Schnitzhofer et al., 2009) and kept at ambient temperature, except the final ~1 m of the inlet line, which is passivated stainless steel (Silcosteel, Restek Corp., USA) heated to 60°C. A continuous 0.95 cm × 1.27 cm (I.D. × O.D.) sampling line (PFA, Jensen Inert Products, USA) extends from there up the tower to the inlet 185 m above ground, with an inline filter (90 mm PFA filter holder; 30-60 μm PTFE filter membrane, Savillex Corp., USA) installed to remove coarse particulates. A sampling pump pulls air down from the inlet at ~12 standard l m^{-1}, with the line pressure maintained at ~900 hPa. The resulting residence time for air in the line is approximately 2 minutes under normal sampling conditions. We performed a series of tests to thoroughly investigate any potential VOC wall loss or interference in the 185 m PFA inlet line. Laboratory experiments showed no detectable effect from the PFA inlet line for any of the reported compounds, consistent with results from another recent study (Schnitzhofer et al., 2009).

During measurement, the PTR-MS steps continuously through a series of 15 protonated VOC masses (including m/z 33 for methanol), with 2-20 s dwell time on each. Additional masses are monitored for diagnostic purposes at 200 ms dwell time each (e.g., H_3O^+, H_3O^+ (H_2O)), for a total measurement cycle of 26 s (October 2009 to July 2010) or 170 s (after August 2010). Drift tube pressure is maintained at 2.0 to 2.3 mbar, voltage at 600 V, and temperature at 60°C.

For all species there is a nonzero background signal because of impurities in the system and/or the presence of unwanted ions from the ion source (de Gouw et al., 2003), so regular background checks under ambient humidity are performed every 2-5 hours. Background signals are monitored for 5-10 measurement cycles by passing ambient air flow through a 0.95 cm × 1.27 cm (I.D. × O.D.) stainless steel tube filled with platinum bead catalyst (3 mm in diameter; Shimadzu Corp., Japan) and heated to 450°C. After

subtracting the interpolated background signals, the raw data are post-processed following de Gouw et al. (2003) to account for humidity effects.

The PTR-MS is calibrated by dynamic dilution of multi-component standards (AiR Environmental Inc., USA; stated accuracy ±5%) into zero air (generated as above). The standard cylinders were originally filled December 2008 and were re-analyzed in May 2011. VOC concentrations in the standards range from tens to hundreds of ppbv depending on the compound (202 ppbv for methanol). Calibration curves were performed automatically every 23 hours through August 2010; this was subsequently decreased to 47 hours because of the observed instrument stability. Under most conditions, the R^2 values for 6-point calibration curves are >0.995 for reported compounds, with the relative standard deviation of residuals <7%. Detection limits, defined as 3× the precision, are ~220 pptv for methanol (5 s dwell time), ~18 pptv for benzene (10 s dwell time), and ~30 pptv for toluene (10 s dwell time). Typical sensitivities during calibration are ~10.9 ncps/ppbv for methanol, ~10.2 ncps/ppbv for benzene, and ~13.2 ncps/ppbv for toluene for a drift tube pressure of 2.2 mbar and a drift tube voltage of 600 V. The overall uncertainty of measurement for methanol, based on quadrature addition of the individual error sources (flow controllers, standard accuracy, calibration fit, standard error of the 30-minute averages, etc.), is estimated at 10% on average (and in nearly all cases <20%).

All analyses presented here were performed using the open-source tools R (www.r-project.org) and openair (www.openair-project.org).

2.2.3 CO measurements

We apply concurrent CO measurements at the KCMP tall tower in our interpretation of the methanol data. CO (and H_2) are measured by gas chromatography (GC) with a reducing compound photometer (Peak Performer 1; Peak Laboratories LLC., USA). CO and H_2 eluting from the GC column (Unibeads 1S and MS 13X) pass directly into a heated mercuric oxide bed (265°C). During the process, mercury vapour is liberated and subsequently measured via UV light absorption in the photometer cell. Compressed

medical grade air is used as carrier gas. Multi-point calibrations are carried out daily by dynamic dilution of a ppmv-level standard (Scott Specialty Gases, USA; stated accuracy ±2%) into zero air generated by passing ambient air through a Sofnocat catalyst (Molecular Products Inc., USA) bed heated to 60°C. Under normal conditions, the R^2 values for 6-point calibration curves are >0.999 for both CO and H_2, with the relative standard deviation of residuals <3%. The detection limits for CO and H_2 are 300 and 800 pptv respectively for 3 minute measurements.

2.2.4 GEOS-Chem chemical transport model

We use the GEOS-Chem 3-D model of atmospheric chemistry (Bey et al., 2001) as a tool to interpret the tall tower observations in terms of constraints on methanol source types. GEOS-Chem (v8, http://www.geos-chem.org) is a global Eulerian chemical transport model driven by assimilated meteorological observations from the NASA Goddard Earth Observing System (GEOS-5). The meteorological fields have 0.5°×0.667° horizontal resolution and 72 vertical layers. For our work here we reduce the spatial resolution to 2°×2.5° and 47 layers, of which 14 are below 2 km altitude, and use a 15-minute transport timestep. For methanol, we apply here the simulation implemented in GEOS-Chem by Millet et al. (2008), with updates outlined below, while for CO and other tracers we apply the full-chemistry simulation described in Millet et al. (2010).

Biogenic emissions of methanol and other VOCs are computed online in GEOS-Chem using the Model of Emissions of Gases and Aerosols from Nature (MEGANv2.0; Guenther et al., 2006). This is change over the earlier work by Millet et al. (2008), which used a simple net primary productivity (NPP) based parameterization for estimating emission. Here, fluxes are estimated for each model grid square as a sum of contributions from four plant functional types (PFTs: broadleaf trees, needleleaf trees, shrubs, and herbaceous plants [crops + grasslands]):

$$E = \gamma \sum_{i=1}^{4} \varepsilon_i \chi_i \qquad (2.1)$$

where ε_i is the canopy emission factor for PFT i with fractional coverage χ_i. Here we use ε_i= 800 μg m^{-2} h^{-1} for the four PFTs. The overall activity factor γ is calculated from a set of individual activity factors accounting for the effects of temperature, photosynthetic photon flux density (PPFD), leaf age, and leaf area index (LAI) on emissions. Activity factors for LAI, PPFD and leaf age are computed as described by Stavrakou et al. (2011) and Guenther et al. (2006), but using a light-dependent fraction of 0.75 and relative emission rates of 3.0, 2.6, 0.85, and 1.0 for new, young, mature, and old leaves. Leaf age fractions are parameterized based on monthly changes in leaf area index as described by Guenther et al. (2006). The higher emission rate for old relative to mature leaves represents the methanol flux from dead and decaying foliage (Warneke et al., 1999). The temperature dependence of methanol emission is modelled using an exponential function,

$$\gamma_T = \exp\left[\beta(T - 303)\right] \tag{2.2}$$

with β = 0.08 and T the surface air temperature (K). The global annual flux of methanol from terrestrial plants for this simulation is 95 Tg in 2010. This is significantly lower than the base-case simulation presented by Millet et al. (2008) using the NPP-based parameterization of biogenic emissions (145 Tg/y), and comparable to their optimized estimates based on a reduced biogenic source (72 – 89 Tg/y).

Anthropogenic emissions over the US are from the US EPA NEI-99 (EPA, 1999), updated by Hudman et al. (2007; 2008) to account for recent CO and NO_x emission reductions. The anthropogenic methanol flux is estimated based on a methanol:CO molar emission ratio of 0.012 (Goldan et al., 1995; de Gouw et al, 2005; Millet et al., 2005; Warneke et al., 2007). Methanol emissions from fires are from the Global Fire Emissions Database version 2 (GFEDv2, van der Werf et al., 2006) for the year 2008 (the most recent year for which these emissions are available) and measured species:species pyrogenic emission ratios (Andreae and Merlet, 2001; Andreae, unpublished data, 2006). Other methanol sources (biofuel burning, photochemical production, gross ocean emission) and sinks (oxidation by OH, gross ocean uptake) are implemented as described in our earlier work (Millet et al., 2008).

GEOS-Chem is not necessarily expected to fully resolve the fine-scale concentration fluctuations observed at the KCMP tall tower due to the 2°×2.5° model resolution. However, as we will show it does provide a useful way to leverage the observations in testing some basic assumptions in terms of how methanol sources are represented in current models.

2.3 Results and discussion

2.3.1 Seasonality of methanol abundance and emissions in the US Upper Midwest

Figure 2.3 shows hourly mean methanol mixing ratios observed from January 2010 through February 2011 at the KCMP tall tower. Also shown are concurrent measurements of benzene, toluene, CO, and air temperature. For all compounds statistical outliers (>0.98 quantile for each month) have been removed prior to plotting. Table 2.1 shows the corresponding seasonal statistics for methanol along with data from related sites where measurements covered multiple seasons.

Methanol is the most abundant VOC measured at the KCMP tall tower, with a 2010 annual mean mixing ratio of 3.8 ppbv (median 3.0 ppbv). The highest seasonal mixing ratios of methanol are observed during summer, reflecting biogenic emissions in the warm season. Lowest concentrations are seen during winter; spring and autumn show intermediate levels of similar magnitude (Table 2.1). This seasonality is broadly consistent with the few other in-situ observations spanning a full annual cycle (Table 2.1; Schade and Goldstein, 2006; Jordan et al., 2009; Lappalainen et al., 2009).

We also see in Figure 2.3 some wintertime events with strongly elevated concentrations of methanol (as well as of benzene, toluene, and CO). These reflect local anthropogenic emissions within the shallow wintertime mixed layer, transported from the Twin Cities by northwesterly winds (predominant at that time of year).

Prior methanol observations in the US Midwest are sparse (Table 2.1). They include urban measurements in Pittsburgh PA (on average ~1.6-2.4× higher than observed at the KCMP tall tower) (Millet et al., 2005) and measurements over a mixed hardwood forest in northern Michigan (~1.2-2.0× higher than KCMP) (Karl et al., 2003). Table 2.1 shows that the methanol concentrations at the KCMP tall tower are generally in the range observed at rural sites elsewhere in the US and abroad.

Figure 2.3 also shows the methanol concentrations simulated by GEOS-Chem at the KCMP tall tower (red). The model consistently underestimates the observed concentrations year-round, with ~35% low bias during summer. This can be compared to other recent findings by Millet et al. (2008) and Stavrakou et al. (2011). Using an NPP-based parameterization of biogenic emissions, and after scaling down this biogenic flux to account for a source overestimate, Millet et al. (2008) found that their simulation still had a slight high bias in the eastern US and a low bias in the west. Likewise, on the basis of satellite observations from the IASI sensor, Stavrakou et al. (2011) found that MEGAN overpredicts emissions in the eastern US while underpredicting in the west. More work is needed to better quantify methanol emission rates in different ecosystems and regions, but the observations reported here suggest a source underestimate for the US Upper Midwest.

The seasonality of methanol concentrations as seen in Figure 2.3 is clearly distinct from that of CO, benzene, and toluene, which are predominantly emitted from anthropogenic sources (CO is also produced in the atmosphere from VOC oxidation, as we discuss later). Mixing ratios for these species are low in the summer and peak during winter, reflecting the seasonal change in OH radical concentrations. Below (Sect. 2.3.2) we will use these anthropogenic compounds as tracers to evaluate the relative importance of biogenic versus anthropogenic methanol sources for the region sampled by the KCMP tall tower.

Current understanding of the seasonality of methanol emissions is based on the premise that pectin biosynthesis during plant and leaf growth is a major source of atmospheric

methanol, resulting in higher emissions from new and young leaves in spring and early summer as compared to mature and old leaves during later summer and autumn (MacDonald and Fall, 1993; Fall and Benson, 1996; Galbally and Kirstine, 2002; Fall, 2003; Karl et al., 2003). Long-term measurements from the KCMP tall tower, with its source footprint influenced by multiple PFTs, provide an opportunity to test how well this seasonal dependence is represented in current models.

Figure 2.4 shows the normalized seasonality in methanol abundance observed at the KCMP tall tower (black) compared to that simulated by GEOS-Chem (red). The simulated seasonality is generally similar to the observations, peaking in summer and with a winter minimum. However, the modeled seasonal amplitude is stronger than observed (simulated summer:winter ratio of 3 versus an observed value of 2). As we discuss later, this in part reflects a model underestimate of the anthropogenic methanol source for this region.

As Figure 2.4 shows, the onset of biogenic methanol emissions is well-captured by the model, with measured and simulated concentrations rising in parallel during mid-April and May, and in concert with increasing regional leaf area. However, the seasonal peak in the model is phase-shifted relative to the observations, occurring substantially later in the summer (second week of August versus mid-July in the observations). Later (Sect. 2.3.3) we assess how errors in the assimilated temperatures used to drive GEOS-Chem and MEGAN affect the model:measurement comparisons, but the temperature bias is small and cannot explain this seasonality offset. It appears likely that MEGAN is underestimating the relative methanol emission rate for younger versus older leaves, at least for this part of North America.

2.3.2 Anthropogenic versus biogenic sources of methanol

In this section, we apply the KCMP tall tower measurements to evaluate the year-round importance of anthropogenic methanol emissions in the US Upper Midwest. Globally, anthropogenic methanol emissions are uncertain (2-11 Tg yr^{-1}) and are thought to make

up only a small fraction of the total flux (2-5%; Singh et al., 2000; Galbally and Kirstine, 2002; Heikes et al., 2002; Jacob et al., 2005; Millet et al., 2008; Stavrakou et al., 2011). On a regional scale, and in winter, the contribution from urban and industrial sources can be more substantial.

In winter, methanol concentrations at the KCMP tall tower are well-correlated with CO, benzene, and toluene (R=0.67, 0.54, and 0.65, respectively during December-February), providing a fingerprint of regional anthropogenic emissions in the absence of any significant biogenic sources (or of photochemical production in the case of CO). The corresponding methanol:tracer major axis slopes are 0.034 (0.032-0.035) ppbv/ppbv for CO, 21.3 (20.2-22.4) ppbv/ppbv for benzene, and 26.0 (24.2-27.9) ppbv/ppbv for toluene (values in parentheses indicate 95% confidence intervals, CI). For this analysis we remove data above the 0.8 quantile to ensure a regionally representative signal, and subtract a 7-day running 0.1 quantile to eliminate any influence from changing atmospheric background concentrations. No statistical difference in the slopes is seen for weekdays versus weekends, and no clear enhancements of acetonitrile (a biomass burning tracer) were observed during winter. We therefore treat the observed methanol:tracer enhancement ratios as regional urban emission ratios, including contributions from fossil fuel combustion, industrial activity, and solvent use.

The observed wintertime methanol:CO slope can be compared to previously reported methanol:CO enhancement ratios which range from 0.004 to 0.056 ppbv/ppbv (Goldan et al., 1995; Singh et al., 1995; Salisbury et al., 2003; Jacob et al., 2005; Warneke et al., 2007; and references therein). The wintertime methanol:CO enhancement ratio observed at the KCMP tall tower is a factor of 2.8 higher than the global emission ratio employed in GEOS-Chem (0.012 ppbv/ppbv; Millet et al., 2008), indicating a significantly larger anthropogenic methanol flux for this area.

We apply here the observed tracer-tracer correlations to diagnose the anthropogenic methanol contribution f_{ANTH} throughout the year as:

$$f_{ANTH} = \frac{E_X [X]_t}{[CH_3OH]_t} \quad (2.3)$$

where E_X is the methanol enhancement ratio relative to tracer X (CO, benzene, or toluene) derived from the wintertime data, $[X]_t$ is the observed enhancement of X at time t, and $[CH_3OH]_t$ is the observed methanol abundance at time t. Potential biases in this method can arise from the assumption of a constant emission ratio, or because of differing atmospheric lifetimes for the compound of interest and the tracer. The secondary CO source from VOC oxidation (Hudman et al., 2008) can also complicate interpretation. We therefore evaluate the robustness of the approach in two ways. First, we apply it to the CO and methanol concentrations simulated by GEOS-Chem and compare the result with the actual anthropogenic methanol abundance in the model, which is known. Second, we assess the consistency of the findings using multiple anthropogenic tracers (CO, benzene, and toluene) in the observations. These analyses provide a means of estimating the uncertainty in the results.

Figure 2.5 (top panel) shows the source tracer approach applied to simulated methanol and CO concentrations from GEOS-Chem. The anthropogenic fraction f_{ANTH} estimated using the methanol:CO correlation agrees well with the actual model value: major axis regression of the calculated versus actual model f_{ANTH} yields a slope of 0.95 (95% CI: 0.80-1.09) with R = 0.83 (Figure 2.6). Likewise, applying CO, benzene and toluene as tracers to estimate f_{ANTH} in the observations gives consistent results to within ±30% (Figure 2.6). Both tests thus provide support for the use of this method in interpreting the observations.

Figure 2.5 (middle panel) shows the year-round anthropogenic contribution to the observed methanol abundance at the KCMP tall tower estimated on the basis of measured CO (black), benzene (red), and toluene (blue). In all cases we see a pronounced and consistent seasonal cycle, where regional anthropogenic sources account for approximately 10% of observed levels during summer, and up to 70% (on average 40%) during winter. The seasonality is driven by the changing importance of biogenic

emissions, rather than by any strong variation in the absolute anthropogenic flux itself: the bottom panel of Figure 2.5 shows that the weekly median anthropogenic contribution is between 0.2-1.5 ppbv year-round. The source tracer approach does not provide a straightforward way to parse the residual, non-anthropogenic methanol abundance: biogenic tracers, such as isoprene, tend to be short-lived, and emissions may not correlate particularly well with those of methanol. In the GEOS-Chem simulation the corresponding non-anthropogenic fraction is almost exclusively biogenic during summer (with nearly 80% are from crops and grasslands), and during winter represents a mixture of transported biogenic emissions, biomass and biofuel burning, and photochemical production.

We repeated this analysis with a filter applied (30° < wind direction < 300°) to exclude air masses transported directly from Minneapolis-St. Paul; this resulted in only minor changes to the calculated anthropogenic component (to approximately 13% of the total in summer and 44% in winter).

2.3.3 Temperature control on methanol emissions

Biogenic methanol emissions increase exponentially with temperature (Harley et al., 2007; Folkers et al., 2008). In this section, we use the tall tower measurements during summer, when (as we have shown above) the land biosphere is the dominant source, to test the temperature-flux relationship used in present models.

Figure 2.7 shows daytime summer (June-August, 07:00-18:00 LST) methanol concentrations as a function of temperature. A wind direction filter (30° < wind direction < 300°) is applied to exclude urban impacts from Minneapolis-St. Paul. An exponential fit to the observations in Figure 2.7 yields a coefficient of 0.087 (95% CI: 0.082-0.094), in the range of previously published values (0.068-0.094) (Riemer et al., 1998; Schade and Goldstein, 2006; Lappalainen et al., 2009). The observed coefficient is also statistically consistent with the corresponding value from a fit of the simulated methanol abundance to the assimilated temperature used to drive GEOS-Chem (0.083, 95% CI:

0.078-0.088), and with the β value used in the emission algorithm (0.08; Eq. 2.2). We conclude that the model biogenic temperature response is accurate to within the constraints provided by the KCMP tall tower observations.

We analyzed the anthropogenic tracers CO, benzene, and toluene in a similar manner, and found no positive correlation with temperature ($R \leq 0.1$), so that the strong observed methanol:temperature correlation is mainly providing information relevant to the biogenic source, rather than vertical mixing or evaporative emissions.

The fact that the simulated methanol concentrations are biased low by ~35% in the summer compared to the observations (Figure 2.3) thus suggests that some emission parameters, other than the temperature dependence are not adequately represented for this region in GEOS-Chem and MEGANv2.0. The GEOS-5 temperatures used in GEOS-Chem have a slight low bias (on average -0.9°C) compared to the observations, but we find that correcting this would increase model concentrations by only ~10%, significantly less than the model-measurement mismatch.

2.3.4 Methanol as a source of HCHO and CO

HCHO and CO are produced sequentially during the oxidation of methanol by OH and with essentially quantitative yield. The production rate of HCHO (P_{HCHO}) and CO (P_{CO}) from methanol oxidation is:

$$P_{CO} \approx P_{HCHO} = k_{OH} Y [OH][CH_3OH] \quad (2.4)$$

with k_{OH} the rate constant for reaction of methanol with OH (Atkinson et al., 2006) and Y the HCHO yield (1.0). The production rate of CO from methanol is essentially equivalent to the production rate of HCHO, since the HCHO lifetime is ~10× shorter than that of methanol (Atkinson et al., 2006), and depositional sinks for HCHO are small (Dufour et al., 2009).

Figure 2.8 shows the CO and HCHO production rates computed from the methanol measurements at the KCMP tall tower. We plot these also as a fraction of the total CO and HCHO production rates simulated by GEOS-Chem (right panel), to gauge methanol's importance as a source of these two important compounds in the US Upper Midwest (OH concentrations in Eq. 2.4 are likewise taken from the model).

We see from Figure 2.8 that P_{HCHO} and P_{CO} estimated from the methanol observations at the KCMP tall tower range from 1.4×10^4 to 8.1×10^5 molec cm^{-3} s^{-1}, with an annual mean of 2.3×10^5 molec cm^{-3} s^{-1}. Observed methanol concentrations thus account for between 4 and 25%, and on average 12%, of the total CO and HCHO production rates as simulated by the GEOS-Chem model. Methanol's contribution in late summer (~12%) is comparable to that seen at Blodgett Forest Research Station in California (13-18% during daytime in late summer) (Choi et al., 2010). At the KCMP tall tower, the highest fractional contribution to tropospheric HCHO and CO (~20%) occurs during April, May, and June, at a time when methanol emissions and concentrations are high, but prior to the seasonal peak in isoprene emissions later in the summer. Thus the seasonal phase shift for methanol compared to isoprene manifests in terms of a pronounced photochemical role early in the growing season. This role is underestimated in the model because the simulated seasonal peak occurs too late in the summer.

2.4 Conclusions

We applied measurements of a suite of atmospheric VOCs and CO over one year (01/2010-02/2011) from the KCMP tall tower in the US Upper Midwest to test our understanding of methanol sources and seasonal impacts as represented in a current chemical transport model.

Measured methanol concentrations at the KCMP tall tower ranged from 0.1 ppbv to 25 ppbv with an annual mean of 3.8 ppbv. This is at the low end of the sparse measurements previously reported for the US Midwest, and in the range observed at rural sites elsewhere. Methanol concentrations observed at the KCMP tall tower exhibited a strong

seasonal pattern driven by biogenic emissions, with concentrations highest during summer and lowest during winter. The seasonality simulated by GEOS-Chem (driven by MEGANv2.0) is generally similar to the observations, but the seasonal peak occurs about 1 month later than is observed. This suggests a model underestimate of the relative methanol emission for younger versus older leaves in this region.

We examined the year-round importance of anthropogenic methanol emissions in the US Upper Midwest using a source tracer approach. This method was first validated by applying it to the GEOS-Chem output and comparing the results to the known anthropogenic methanol in the model, and by employing multiple observed anthropogenic tracers (CO, benzene, and toluene). Anthropogenic methanol sources accounted for approximately 10% of the total observed abundance during summer, and up to 70% during winter. We attribute the remainder to predominantly biogenic emissions during summer and to a mixture of sources during winter.

Biogenic methanol emissions increase exponentially with temperature, and an exponential fit of summer daytime methanol concentrations to temperature at the KCMP tall tower yields a regression coefficient of 0.087 (95% CI: 0.082-0.094), statistically consistent with the value from a corresponding fit using the simulated methanol abundance (0.083, 95% CI: 0.078-0.088). We conclude that the temperature dependence of emissions employed for methanol in MEGANv2.0 is accurate to within the constraints provided by our data. However, the simulated methanol concentrations are biased low by on average 35% during summer, suggesting that some other emission parameters (such as the base emission factors) are not accurately represented for this region. A small bias (on average -0.9°C) in the assimilated GEOS-5 temperatures used in GEOS-Chem is insufficient to correct the discrepancy.

Finally, we estimated the CO and HCHO production rates from the methanol measurements and evaluated methanol's importance as a precursor of these two key compounds. Observed methanol concentrations accounted for on average 12% (and between 4% and 25%) of the total CO and HCHO production rates as simulated by the

GEOS-Chem model, with the highest seasonal contribution (20%) during spring and early summer. At this time, methanol emissions and concentrations are high, while regional isoprene emissions are still relatively low. The biased seasonality in the model means that the photochemical role of methanol in the early growing season is not adequately accounted for.

The measurements presented here provide new constraints on the seasonality of natural and anthropogenic contributions to atmospheric methanol abundance. We plan in the future to apply these data in a high-resolution inverse analysis to quantify the impact from different plant types on concentrations of methanol and other VOCs for this region. In the GEOS-Chem simulation, methanol from crops and grasslands account for nearly 80% of the total abundance at the KCMP tall tower in the summer. Better information on seasonal fluxes from crops and grasslands is thus key to improving simulations of atmospheric composition for the central US.

Table 2.1. Seasonality of atmospheric methanol abundance (ppbv) observed at the KCMP tall tower in the US Upper Midwest and comparison with other sites.

		spring[1]	summer[1]	autumn[1]	winter[1]	land cover	measurement height
KCMP tall tower, MN, US (2010-2011; this study)	mean	4.0	7.0	3.2	2.1	mix	185 m
	median	3.2	6.6	2.8	1.6		
	10^{th} -90^{th} percentiles	1.8-7.6	3.9-10.3	1.1-5.9	0.8-3.8		
Pittsburgh, PA, US (2002)[2]	median		10.7		3.8	urban	surface
UMBS, MI, US (2001/2002) [3]	mean	8	10	4		mixed forest	34 m
UC Berkeley BFRS, CA, US (2000-2001)[4]	median		10.9		2.0	needleleaf	12 m
Thompson Farm, NH, US (2004-2007)[5]	median	1.3	2.7	1.1	1.0	crop and mix forest	12 m

1 Seasons here are: spring (March - May), summer (June - August), autumn (September - November), winter (December - February)

2 Pittsburgh, PA, USA; Millet et al. (2005)

3 University of Michigan Biological Station, MI, USA; Karl et al. (2003)

4 UC Berkeley Blodgett Forest Research Station, CA, USA; Schade and Goldstein (2006)

Zurich, Switzerland (2005-2006)[6]	mean	2.2	3.2	1.1	1.2	urban	surface
SMEAR-II, Finland (2006-2007)[7]	day-time median	~0.5	~2	~1	~0.4	needleleaf	14 m

5 Thompson Farm, NH, USA; Jordan et al. (2009)

6 Zurich, Switzerland; Legreid et al. (2007)

7 SMEAR-II, Hyytiälä, Finland; Lappalainen et al. (2009)

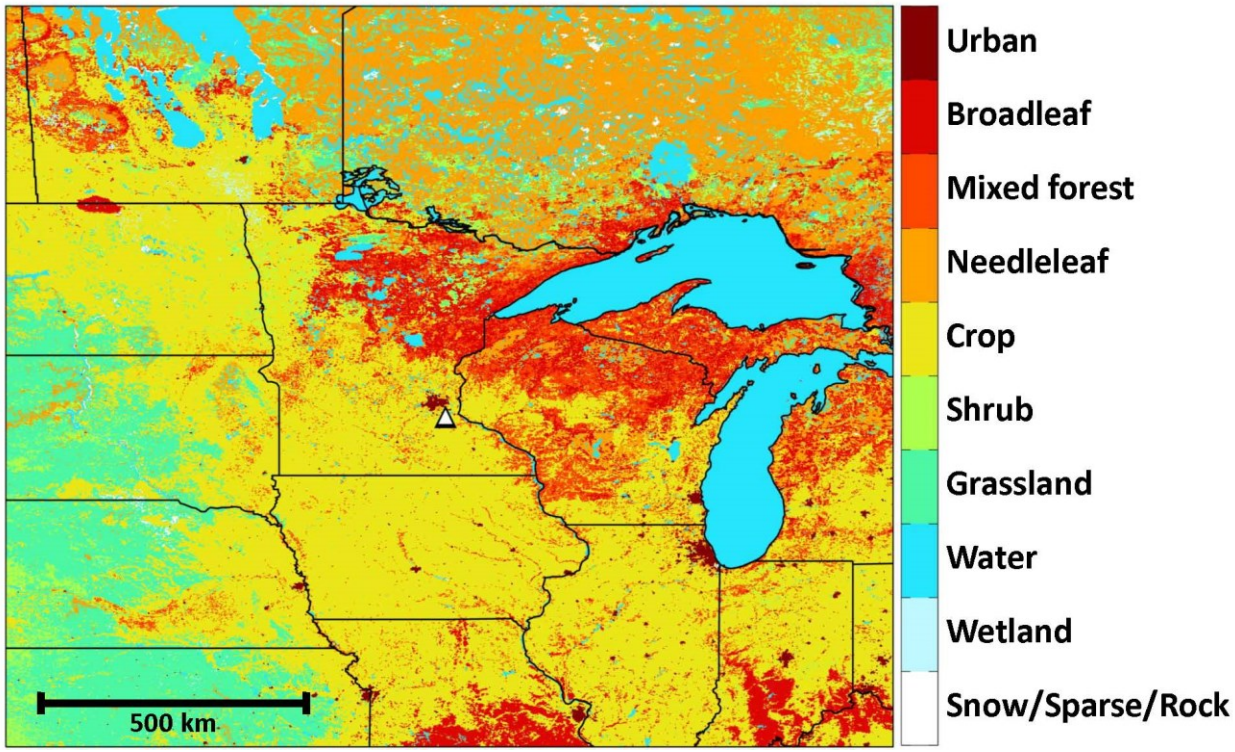

Figure 2.1 The KCMP tall tower (white triangle) in Rosemount, MN is located in the US Upper Midwest near the intersection of the main North American ecosystems. The tower is approximately 25 km south of the Minneapolis-St. Paul metropolitan area.

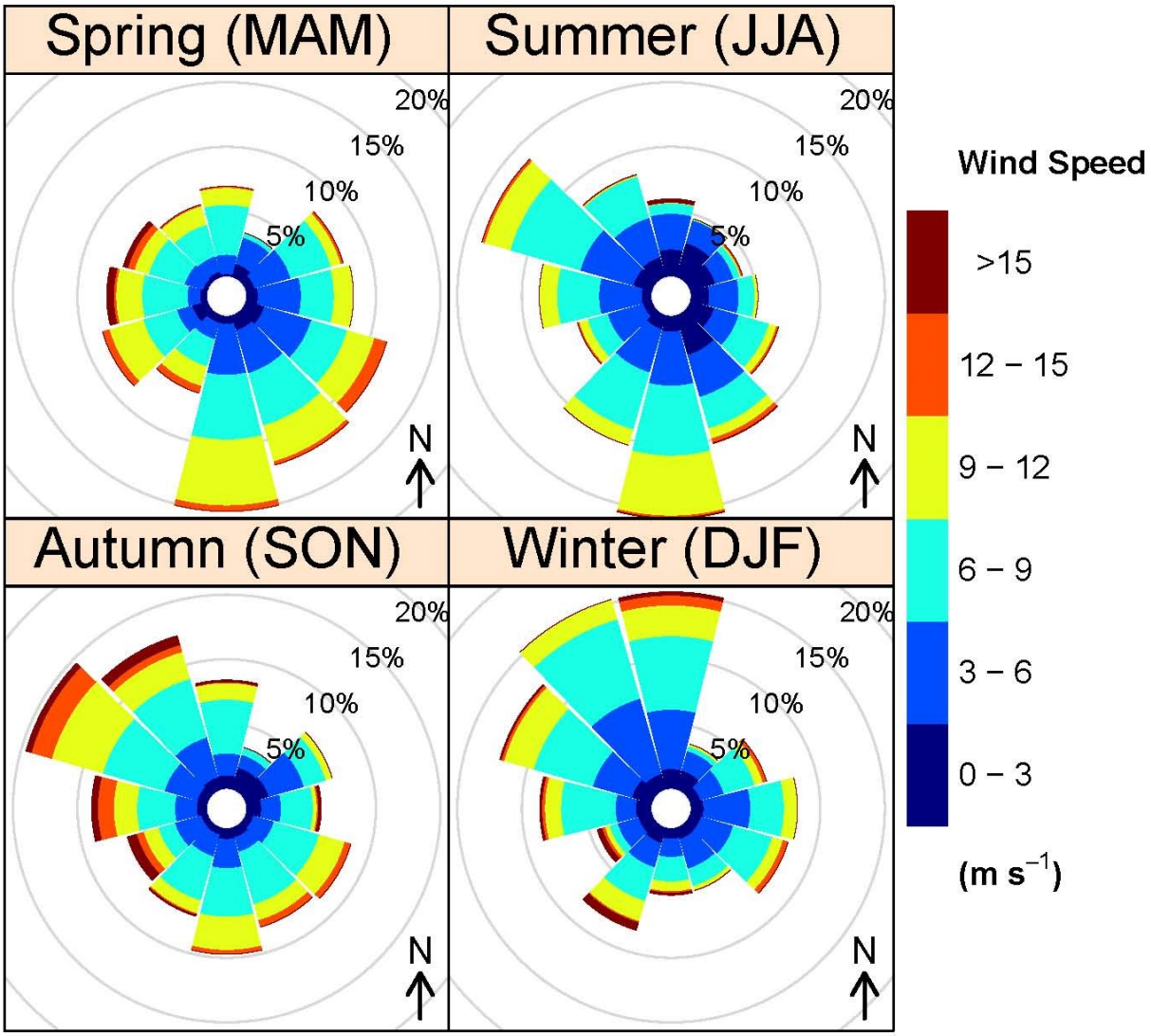

Figure 2.2. Wind rose plots showing wind speed as a function of direction during 2010 at the KCMP tall tower. MAM: March, April, May; JJA: June, July, August; SON: September, October, November; DJF: December, January, February.

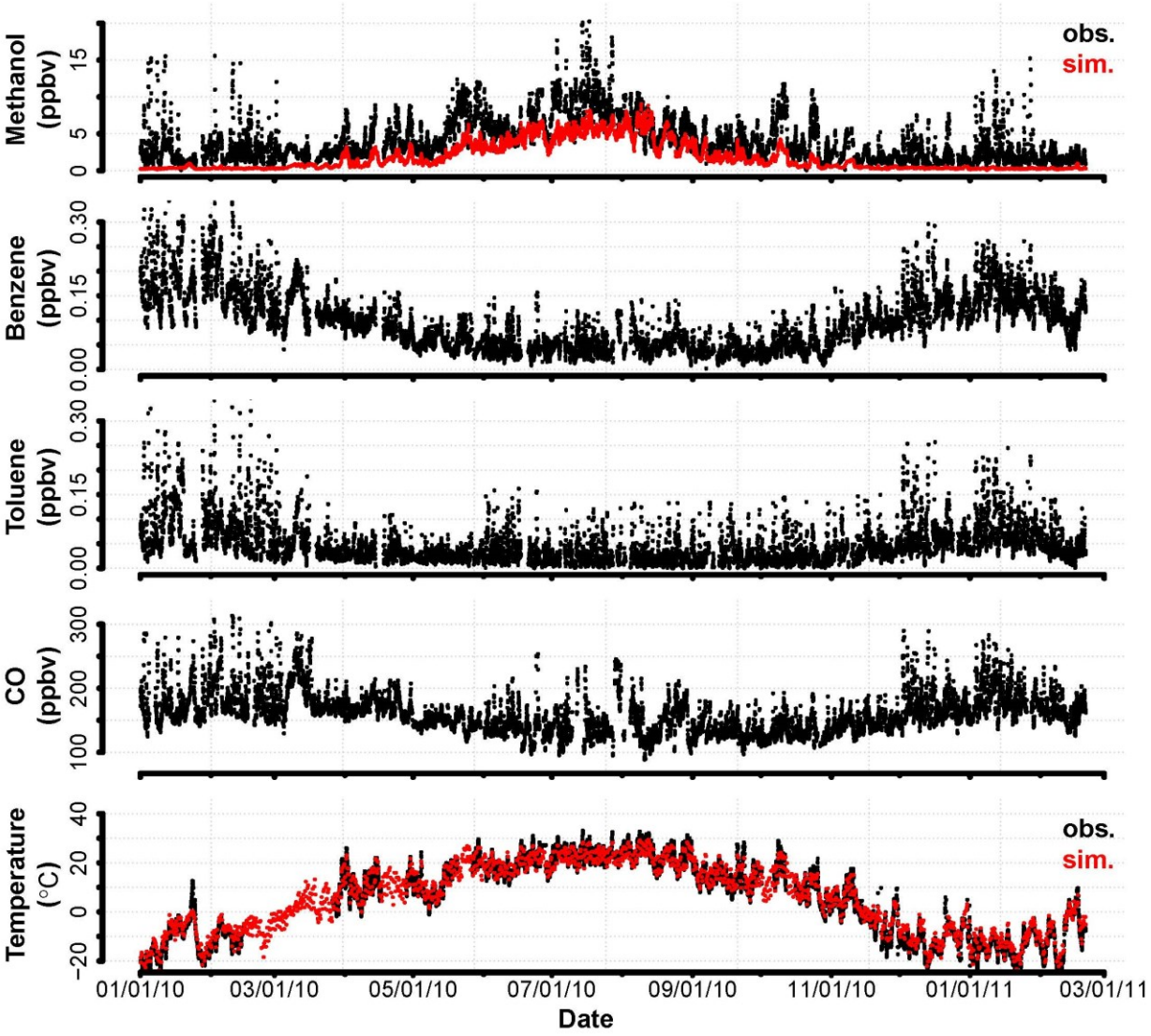

Figure 2.3. Annual cycle in methanol, benzene, toluene, CO and air temperatures observed at the KCMP tall tower from January 2010 through February 2011 (black). Methanol concentrations simulated by GEOS-Chem are shown in red, as are the assimilated temperature used to drive the model. All data points are 1-hour means. For all compounds statistical outliers (>0.98 quantile for each month) have been removed prior to plotting.

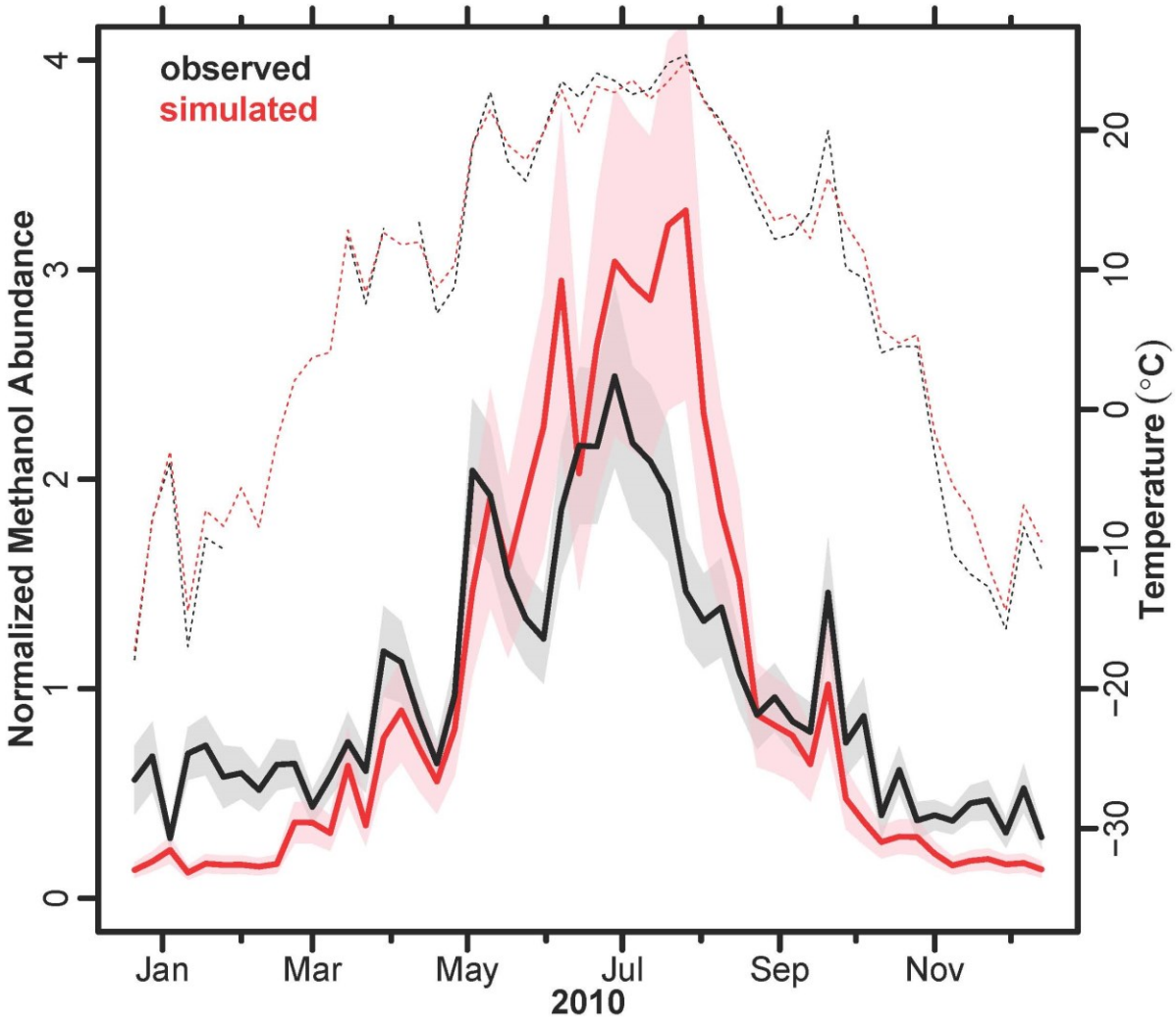

Figure 2.4. Seasonality of atmospheric methanol abundance in the US Upper Midwest. Weekly medians (normalized to the annual average) observed at the KCMP tall tower (solid black line) are compared to the corresponding values simulated by GEOS-Chem (solid red line). Shaded areas show the 95% confidence intervals. Dashed lines show the weekly median air temperatures measured at the site (black) and the assimilated values used to drive GEOS-Chem (red).

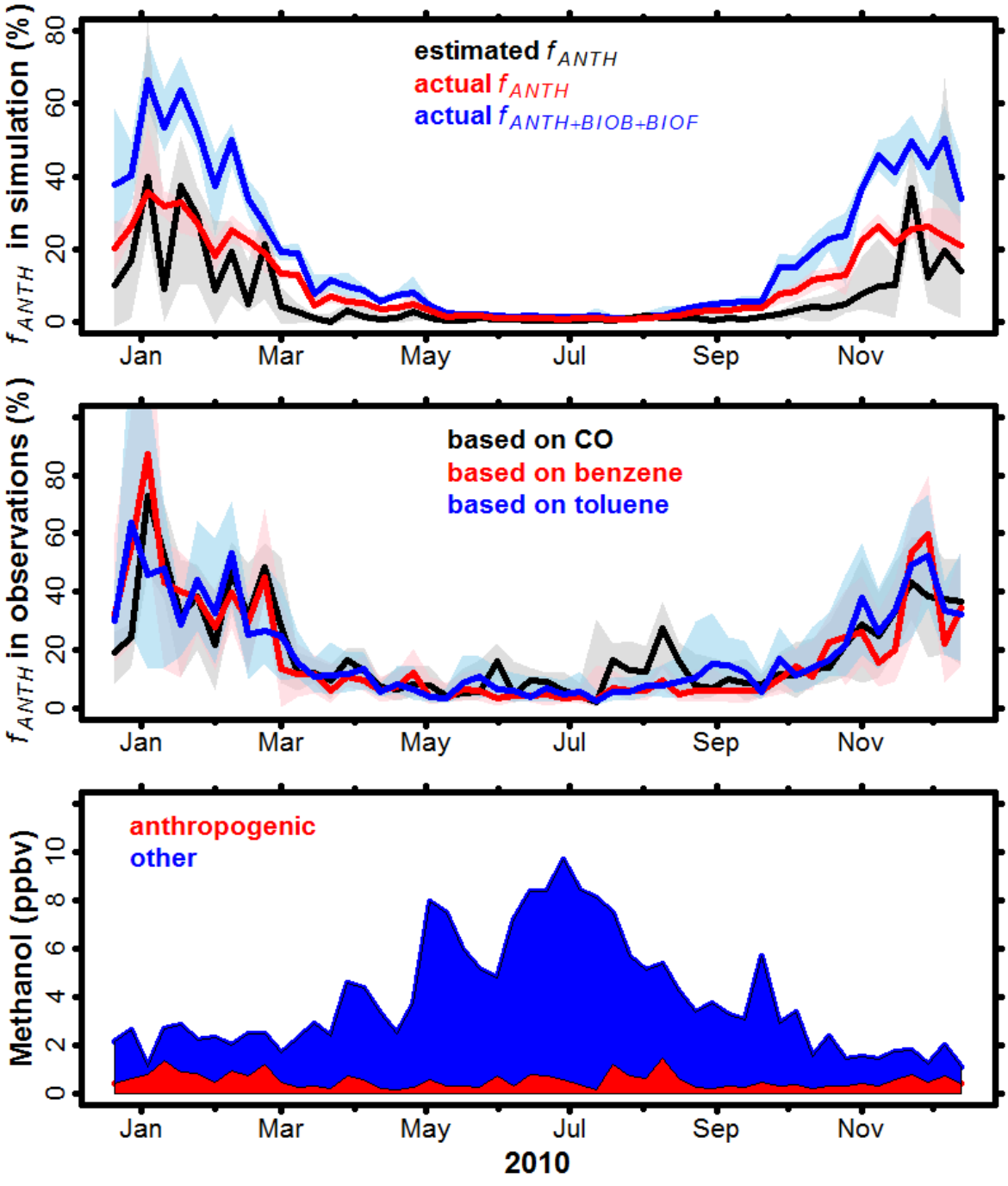

Figure 2.5. Source-tracer approach to estimate the anthropogenic contribution to methanol abundance at the KCMP tall tower.

Top panel: seasonal contribution of anthropogenic sources to simulated methanol abundance in GEOS-Chem. The black line shows the weekly median anthropogenic contribution estimated from the methanol:CO correlation as a test of the same approach applied to the observations. Also shown are the actual model contributions from anthropogenic emissions (red line) and from anthropogenic emissions + biomass and biofuel burning (blue line). Shaded areas show the interquartile range in each case.

Middle panel: seasonal anthropogenic contribution to methanol abundance at the KCMP tall tower estimated using different anthropogenic tracers (black: CO; red: benzene; blue: toluene). The shaded areas represent the interquartile range about the weekly median.

Bottom panel: stack plot of seasonal anthropogenic methanol concentrations (red) at the KCMP tall tower estimated using CO as the anthropogenic tracer (weekly median values). The blue area shows the cumulative contribution to the observed methanol abundance from other sources, including regional and transported biogenic emissions, photochemical production, fires, etc.

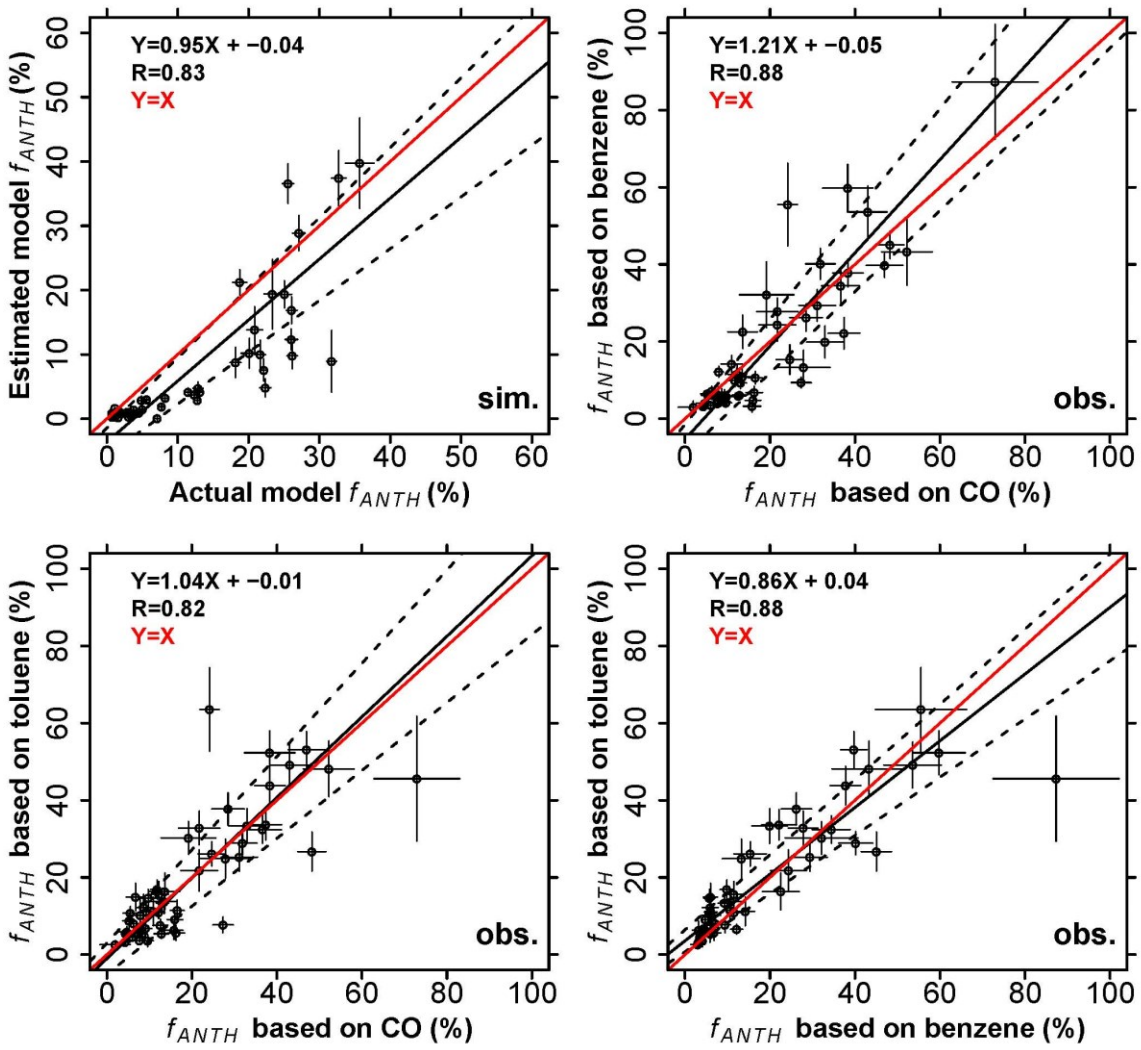

Figure 2.6. Top left panel: weekly anthropogenic methanol contribution in the model, estimated using the methanol:CO correlation, compared to the actual model values. The other panels compare the anthropogenic methanol contribution in the observations estimated using the different source tracers (CO, benzene, and toluene). Black solid lines show the best fit (major axis regression), with regression parameters given inset. Black dashed lines show the 95% confidence interval for the best fit line. The 1:1 line is shown in red. Error bars show the 95% confidence interval for each weekly median.

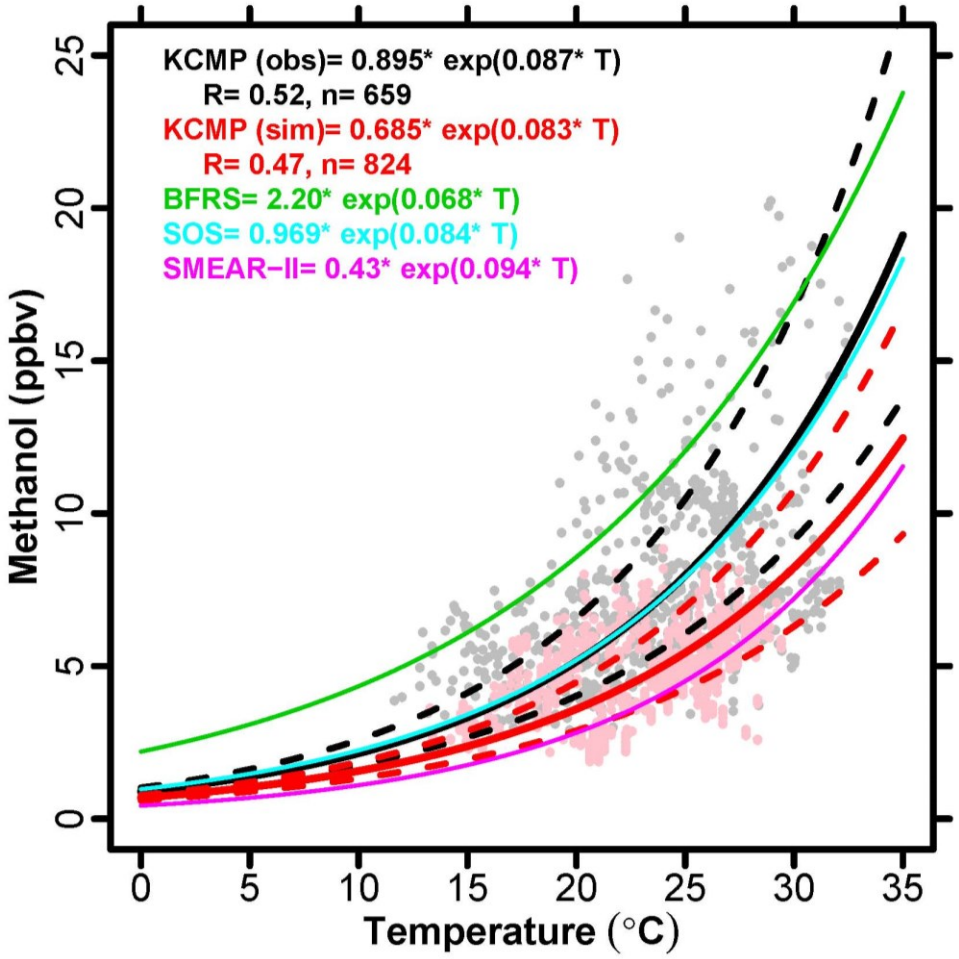

Figure 2.7. Methanol concentrations (ppbv) versus temperature (°C). Shown are observed (black) and simulated (red) methanol concentrations at the KCMP tall tower during daytime in summer (June-August; 07:00-18:00 LST). Solid lines (black and red) show an exponential fit (major axis regression) to the observations and model output, with regression parameters given inset and 95% confidence intervals shown by the dashed lines. Also shown are the corresponding exponential fits derived from previous studies in California US (BFRS, Schade and Goldstein, 2006); Tennessee US (SOS, Riemer et al., 1998); and Hyytiälä Finland (SMEAR-II, Lappalainen et al., 2009).

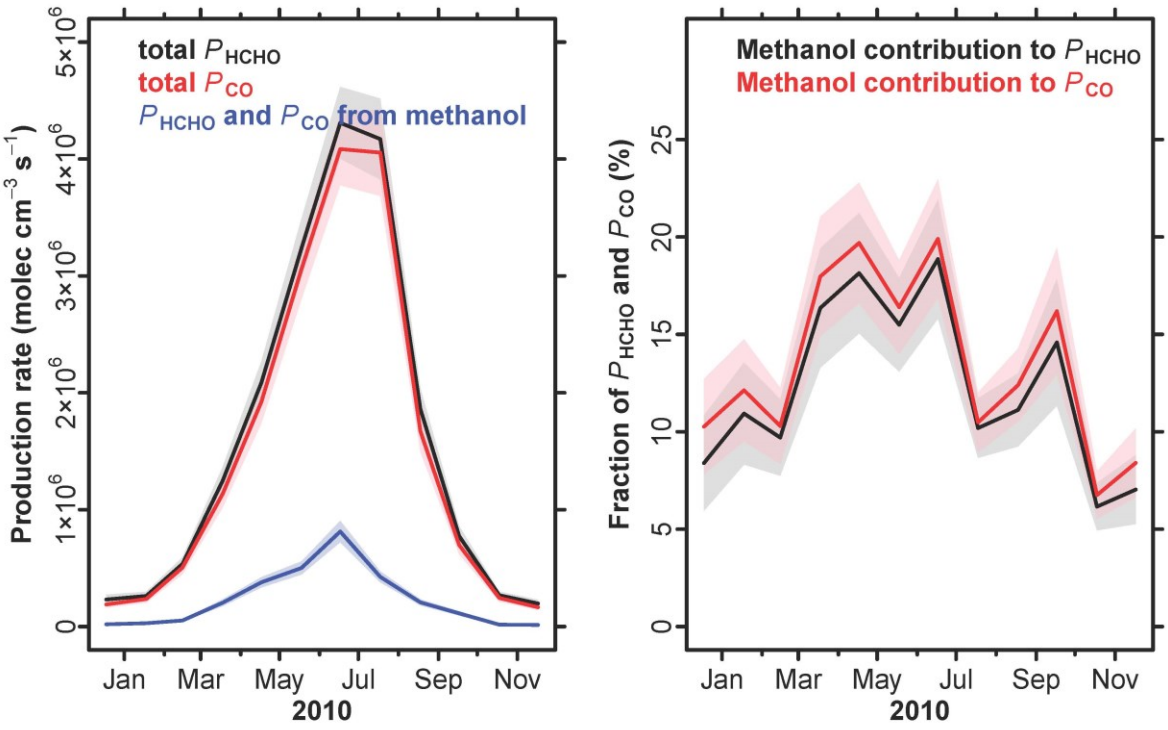

Figure 2.8. Monthly mean methanol contribution to the production rate of HCHO and CO at the KCMP tall tower, estimated as described in the text. Left panel: monthly mean production rates of HCHO and CO calculated from observed methanol concentrations at the KCMP tall tower (blue) compared to the total production rates of HCHO (black) and CO (red) simulated by GEOS-Chem. Right panel: monthly CO and HCHO production rates computed from the methanol measurements at the KCMP tall tower plotted as a fraction of the total production rates simulated by GEOS-Chem. Shaded areas show the 95% confidence intervals.

3 North American acetone sources determined from tall tower measurements and inverse modelling

Abstract

We apply a full year of continuous atmospheric acetone measurements from the University of Minnesota tall tower Trace Gas Observatory (KCMP tall tower; 244 m a.g.l.), with a 0.5° × 0.667° GEOS-Chem nested grid simulation to develop quantitative new constraints on seasonal acetone sources over North America. Biogenic acetone emissions in the model are computed based on the MEGANv2.1 inventory. An inverse analysis of the tall tower observations implies a 37% underestimate of emissions from broadleaf trees, shrubs, and herbaceous plants, and an offsetting 40% overestimate of emissions from needleleaf trees plus secondary production from biogenic precursors. The overall result is a small (16%) model underestimate of the total primary + secondary biogenic acetone source in North America. Our analysis shows that North American primary + secondary anthropogenic acetone sources in the model (based on the EPA NEI 2005 inventory) are accurate to within approximately 20%. An optimized GEOS-Chem simulation incorporating the above findings captures 70% of the variance (R = 0.83) in the hourly measurements at the KCMP tall tower, with minimal bias. The resulting North American acetone source is 10.9 Tg a^{-1}, including both primary emissions (5.5 Tg a^{-1}) and secondary production (5.5 Tg a^{-1}), and with roughly equal contributions from anthropogenic and biogenic sources. The North American acetone source alone is nearly as large as the total continental volatile organic compound (VOC) source from fossil fuel combustion. Using our optimized source estimates as a baseline, we evaluate the sensitivity of atmospheric acetone and peroxyacetyl nitrate (PAN) to shifts in natural and anthropogenic acetone sources over North America. Increased biogenic acetone emissions due to surface warming are likely to provide a significant offset to any future decrease in anthropogenic acetone emissions, particularly during summer.

3.1 Introduction

Acetone ($CH_3C(O)CH_3$) is the simplest ketone and one of the most abundant volatile organic compounds (VOCs) in the atmosphere, with typical mixing ratios ranging from a few hundred parts per trillion (pptv) to several parts per billion (ppbv) or more (Chatfield et al., 1987; Singh et al., 1995; Arnold et al., 1997; Riemer et al., 1998; Goldstein and Schade, 2000; Karl et al., 2003; Lewis et al., 2005; Aiello and McLaren, 2009; Gao et al., 2013). It affects atmospheric chemistry as an important source of hydrogen oxide radicals (HO_x = OH + HO_2) in the upper troposphere (Jaeglé et al., 1997; McKeen et al., 1997; Wennberg et al., 1998; Folkins and Chatfield, 2000; Jaeglé et al., 2001; Arnold et al., 2005), and as a precursor of peroxyacetyl nitrate (PAN, $CH_3C(O)OONO_2$), which is a key reservoir for nitrogen oxides (NO_x = NO + NO_2) (Singh and Hanst, 1981; Singh et al., 1994; Singh et al., 1995; Arnold et al., 1997). Estimates of the global acetone source vary widely (40-200 Tg a^{-1}; Singh et al., 2000; Potter et al., 2003; Singh et al., 2004; Arnold et al., 2005; Folberth et al., 2006; Elias et al., 2011; Fischer et al., 2012). Here we present a full year of continuous atmospheric acetone measurements from a tall tower observatory in the US Upper Midwest, and apply a nested chemical transport model (GEOS-Chem CTM) in an inverse analysis to develop quantitative new constraints on seasonal acetone sources over North America.

Acetone is emitted by terrestrial vegetation as a by-product of plant metabolic processes such as cyanogenesis and acetoacetate decarboxylation (Fall, 2003; Jardine et al., 2010), and during plant decay (de Gouw et al., 1999; Warneke et al., 1999). Recent estimates of the resulting biogenic flux to the atmosphere have ranged between 20 and 194 Tg a^{-1} (Singh et al., 2000; Jacob et al., 2002; Potter et al., 2003; Singh et al., 2004; Arnold et al., 2005; Lathière et al., 2006; Elias et al., 2011; Fischer et al., 2012; Guenther et al., 2012). The other principal source of atmospheric acetone is thought to be photochemical oxidation of precursor VOCs, including the predominantly anthropogenic 2-methyl alkanes (propane, isobutane, isopentane) as well as the biogenic 2-methyl-3-buten-2-ol (MBO) and monoterpenes (Alvarado et al., 1999; Reissell et al., 1999). Other terrestrial

sources include biomass burning (Simpson et al., 2011) and direct anthropogenic emissions (Goldan et al., 1995; Goldstein and Schade, 2000; de Gouw et al., 2005). Globally, the oceans appear to be both a gross source and a gross sink for atmospheric acetone (Fischer et al., 2012); however, the magnitude and variability of the corresponding net flux is quite uncertain (de Reus et al., 2003; Williams et al., 2004; Lewis et al., 2005; Marandino et al., 2005; Sinha et al., 2007; Taddei et al., 2009; Fischer et al., 2012; Read et al., 2012; Sjostedt et al., 2012). Along with gross oceanic uptake, sinks of atmospheric acetone include photochemical oxidation by OH, photolysis, and deposition to land (Chatfield et al., 1987; McKeen et al., 1997; Gierczak et al., 1998; Blitz et al., 2004; Karl et al., 2010). The mean tropospheric lifetime of acetone is estimated to be between 14 and 35 days (Jacob et al., 2002; Arnold et al., 2005; Fischer et al., 2012).

The most recent laboratory study of the temperature-dependent quantum yields for acetone photolysis (Blitz et al., 2004) led to a significant change in our understanding of the atmospheric budget of acetone. Specifically, Blitz et al. (2004) measured the quantum yields to be substantially lower than previously reported. Those findings imply an increased acetone lifetime, and reverse the relative importance of photolysis and OH oxidation as acetone sinks (Fischer et al., 2012). They also modify the importance of acetone as a precursor of HO_x and PAN (Arnold et al., 2005), leading to less PAN in the Northern Hemisphere (especially in the upper troposphere), but more PAN in parts of the Southern Hemisphere.

In this work, we employ the GEOS-Chem CTM and one year of continuous acetone measurements from the University of Minnesota tall tower Trace Gas Observatory (KCMP tall tower) in a Bayesian inverse framework to develop new top-down constraints on natural and anthropogenic acetone sources in North America. The tall tower measurements provide a high-resolution and long-term atmospheric dataset with a regional to continental-scale footprint that is influenced by a range of biogenic and

anthropogenic sources (Hu et al., 2011). We then use these updated source estimates to investigate the impact of North American acetone sources on atmospheric PAN, and the sensitivity of atmospheric acetone and PAN to shifts in biogenic and anthropogenic acetone sources.

3.2 Methods

3.2.1 Field site and PTR-MS measurements

The University of Minnesota tall tower Trace Gas Observatory is a 244 m Minnesota Public Radio communications tower at Rosemount, MN (KCMP 89.3 FM, 44.689°N, 93.073°W; tower base is 290 m above sea level), located 28 km south of downtown St. Paul, MN, US. A detailed description of the site is given elsewhere (Griffis et al., 2010; Hu et al., 2011).

Acetone (protonated *m*/*z* 59) and a suite of other VOCs (including methanol, isoprene and its first-generation oxidation products, acetonitrile, and C_6-C_9 aromatics) were measured at the KCMP tall tower using a PTR-MS (proton transfer reaction mass spectrometer, Ionicon Analytic GmbH, Austria) between July 2009 and August 2012. The PTR-MS is housed in a climate-controlled communications building at the base of the tower. A continuous length of perfluoroalkoxy (PFA) sampling line (0.95 cm ID × 1.27 cm OD, Jensen Inert Products, USA) is mounted on the tower, with an inlet and inline filter (90 mm PFA filter holder; 30-60 μm PTFE filter membrane, Savillex Corp., USA) installed at 185 m elevation. A sampling pump pulls air down from the inlet at ~12 standard liters per minute (l min^{-1}), so that the residence time for air in the line is approximately 2 minutes under normal sampling conditions. A series of laboratory experiments showed no detectable effect from the long PFA inlet line on the measured acetone mixing ratios.

A detailed discussion of the measurement approach is provided by Hu et al (2011). The PTR-MS is calibrated every 23 h (prior to August 2010) or 47 h (subsequently) by

dynamic dilution of multi-component standards (Apel-Riemer Environmental Inc., USA) into a stream of catalytically generated zero air. The acetone standard was originally filled in December 2008 (nominal mixing ratio 152.6 ppbv, stated accuracy ±5%), and recertified in January 2012 (152.9 ppbv). Under most conditions, the R^2 values for 6-point calibration curves are > 0.99 for acetone, with the relative standard deviation of residuals < 7%. The detection limit, defined as 3× the measurement precision, is ~30 pptv for acetone (at 10 s dwell time). Typical sensitivity during calibration is 18 ncps $ppbv^{-1}$ for a drift tube pressure of 2.2 mbar and a drift tube voltage of 600 V. The overall uncertainty of measurement for acetone, based on quadrature addition of the individual error sources (flow controllers, standard accuracy, calibration fit, standard error of the 30 min average, etc.), averages approximately 10% (and in nearly all cases is < 20%).

3.2.2 GC-MS/FID measurements

We also collected a series of cartridge samples at the tall tower to test the specificity of the PTR-MS measurements for acetone and other compounds. A total of 25 standard samples and 100 ambient samples were periodically collected between winter 2010 and summer 2012 for subsequent quantification by gas chromatography with mass selective and flame ionization detectors (GC-MS/FID) at the Institute of Arctic and Alpine Research, University of Colorado at Boulder.

Sample air was first scrubbed for ozone using sodium-thiosulfate coated glass fiber filters (Pollmann et al., 2005). The air was then dried to a dew point of -25°C by flowing it through a Peltier-cooled stainless steel trap. Analytes were subsequently trapped on dual-bed adsorbent cartridges made of glass tubing (0.64 cm OD × 9.00 cm length) and filled with 0.15 mg Carboxen 1016 and 0.15 mg Carboxen 1000 solid adsorbents. The adsorbent tubes were cooled to 10°C during sampling using a custom-made autosampler similar to the one described in Helmig et al. (2004). Cartridges were stored in a freezer at -18°C between sampling and analysis. A Perkin Elmer ATD-400 automated desorption unit was used for thermal desorption, with analytes then pre-focused on a dual-bed

microtrap filled with Carboxen 1016 and Carboxen 1000 adsorbents. Gas chromatography separation was achieved on a 0.32 mm ID × 60 m length × 1.8 μm film thickness DB-624 capillary column (Agilent, USA). The column flow was split for dual detection by electron impact mass spectrometry (Agilent MSD 5972, USA), in selected ion monitoring mode, and by flame ionization detection. Acetone was quantified from its m/z = 43 and 58 mass fragment signals. Quantification was achieved after establishing response curves from analysis of a minimum of 5 calibration samples that were prepared by dynamic dilution of a ~ 500 ppbv standard (Apel-Riemer Environmental Inc., USA).

All standard intercomparisons between the UMN and CU cylinders agreed to within 10% for acetone, with no evidence of mixing ratio drift in the standard cylinders. Ambient intercomparisons (n = 85) between the PTR-MS and cartridge+GC-MS/FID systems showed good agreement for acetone: slope = 1.01 (95% confidence interval, CI: 0.92 – 1.11), intercept = -0.07 ppbv (95% CI: -0.21 - 0.05), R = 0.92. The fact that the slope and intercept are not significantly different from 1.0 and 0.0, respectively, confirms that the PTR-MS acetone measurements (at m/z 59) are robust, and that any interference (e.g., propanal) is minor, which is consistent with conclusions from previous studies (de Gouw et al, 2003; de Gouw and Warneke, 2007).

3.2.3 GEOS-Chem chemical transport model

We use the GEOS-Chem CTM version 9.1.3 to interpret the tall tower acetone observations. GEOS-Chem (www.geos-chem.org) is a global Eulerian chemical transport model driven by NASA Goddard Earth Observing System (GEOS-5.2.0) assimilated meteorological fields. In this work, we employ a GEOS-Chem nested simulation (Wang et al., 2004; Chen et al., 2009; Zhang et al., 2011; van Donkelaar et al., 2012) over North America for 2010. The nested domain covers 10 to 70°N and 140 to 40°W (Figure 3.1), with 0.5° × 0.667° horizontal resolution and 47 model layers in the vertical extending up to 0.01 hPa (14 layers are below 2 km altitude). Model transport occurs on a 10 min time step. Boundary layer mixing in GEOS-Chem uses the non-local scheme of Lin and McElroy (2010).

GEOS-Chem includes detailed HO_x-NO_x-VOC-ozone chemistry coupled to aerosols (Bey et al., 2001; Mao et al., 2010; Fischer et al., 2012). Photolysis frequencies are computed based on the Fast-JX scheme as implemented in GEOS-Chem by Mao et al. (2010), with updated quantum yields for acetone photodissociation from Blitz et al. (2004) and accounting for the effect of aerosol extinction on photolysis rates (Martin et al., 2003). A one year spin-up for 2009 is used to remove the effects of initial conditions. Lateral boundary conditions for all species at each vertical layer are based on 3-hourly output from year-long global simulations carried out at 4° × 5° resolution (Wang et al., 2004; Chen et al., 2009; Zhang et al., 2011; van Donkelaar et al., 2012).

Biogenic emission of VOCs including acetone and its biogenic precursors (monoterpenes and MBO) are computed online in GEOS-Chem using MEGANv2.1 (Model of Emissions of Gases and Aerosols from Nature; Guenther et al., 2012). Fluxes are calculated for each model grid square as a sum of contributions from four plant functional types (PFTs: broadleaf trees, needleaf trees, shrubs, and herbaceous plants [crops + grasslands]):

$$E = \gamma \sum_{i=1}^{4} \varepsilon_i \chi_i \qquad (3.1)$$

where ε_i is the canopy emission factor for PFT i with fractional coverage χ_i. The canopy emission factors (ε) for acetone are 240 μg m^{-2} h^{-1} for broadleaf trees, needleleaf trees, and shrubs, and 80 μg m^{-2} h^{-1} for herbaceous plants (Guenther et al., 2012). The non-dimensional activity factor γ scales the emissions according to local environmental conditions (leaf age, surface temperature, light, leaf area index) according to Guenther et al. (2012), assuming a light-dependent fraction of 0.2 for acetone emissions (i.e. 20% of the emissions are influenced by light). The temperature dependence of acetone emissions is simulated using an exponential β coefficient of 0.10. The MEGANv2.1 acetone emission factors and light and temperature dependencies have been established based on a limited set of enclosure and above canopy eddy flux measurements (e.g., Macdonald

and Fall, 1993b; Janson et al., 1999; Baker et al., 2001; Schade and Goldstein, 2001; Karl et al., 2002; Karl et al., 2004), and are highly uncertain. Part of our objective here is to apply the KCMP tall tower data to evaluate and better constrain the simulated biogenic acetone flux.

Photochemical acetone production from oxidation of biogenic monoterpenes and MBO is computed based on MEGANv2.1 emissions of those species (Guenther et al., 2012) and fixed average molar acetone yields (0.12 for monoterpenes, 0.60 for MBO), following earlier work (Jacob et al., 2002; Fischer et al., 2012). The resulting a priori terrestrial North American biogenic acetone source over the domain of Figure 3.1 is 4.8 Tg in 2010 (76% primary, 24% secondary), which is approximately 13% of the global terrestrial biogenic acetone source (Fischer et al., 2012).

Direct anthropogenic emissions of acetone and its alkane precursors over North America are derived from the US EPA National Emission Inventory for 2005, NEI 2005 (EPA, 2005). The total a priori North American anthropogenic acetone source in the model is then 4.9 Tg a^{-1} (12% primary, 88% secondary) within the domain of Figure 3.1. The total anthropogenic acetone source is thus similar to the total biogenic source over the region, and accounts for approximately 19% of the global anthropogenic acetone source for 2010. Biomass burning emissions of acetone and isoalkanes are computed based on the monthly GFED3 inventory (Global Fire Emissions Database version 3) (van der Werf et al., 2010) and measured species:species pyrogenic emission ratios (Andreae and Merlet, 2001), giving a total North American acetone source from fires of 0.1 Tg for 2010.

Acetone sinks (including oxidization by OH, photolysis, and deposition) and bidirectional oceanic exchange are computed following Fischer et al. (2012). We use a rate constant $k = 3.28 \times 10^{-11}\exp[-200/T]$ for the oxidation of acetone by OH (Sander et al., 2011) and absorption cross-sections and photolysis quantum yields from Blitz et al. (2004). Dry deposition is computed assuming a constant deposition velocity of 0.1 cm s^{-1} for ice-free land (Jacob et al., 2002; Fischer et al., 2012).

3.3 Results and analysis

3.3.1 Acetone abundance in the US Upper Midwest and its relationship with methanol

Figure 3.2 shows hourly mean acetone mixing ratios measured from January 2010 through February 2011 at the KCMP tall tower. Statistical outliers (> 0.98 quantile for each month) have been removed prior to plotting. We also show in Figure 3.2 concurrent measurements of methanol. Hu et al. (2011) showed that atmospheric methanol in this region is predominately (nearly 90%) biogenic during summer, with a mixture of contributing sources (including 40% from anthropogenic emissions) during winter.

The 2010 annual mean acetone mixing ratio at the KCMP tall tower is 1.2 ppbv (median 1.0 ppbv), with strong seasonal changes. As with methanol, the lowest observed acetone mixing ratios occur during winter, with a December-February mean of 0.6 ppbv (Table 3.1). Mixing ratios are highest during summer, driven by biogenic emissions and enhanced photochemical production at that time of year (June-August mean 2.1 ppbv; Table 3.1). However, while methanol mixing ratios peak during early summer (mid-July), the seasonal peak for acetone occurs later in the season (mid-August). This seasonal offset arises from the differing source characteristics for the two compounds. Methanol is thought to be produced in plants mainly as a by-product of pectin demethylation during plant and leaf growth, leading to peak mixing ratios early in the growing season (MacDonald and Fall, 1993a; Fall and Benson, 1996; Hu et al., 2011; Wells et al., 2012). While biogenic emissions of acetone clearly drive the observed seasonality for this compound as well (as shown later in Section 3.3.5), these emissions are thought to be related to a number of different biological pathways (Macdonald and Fall, 1993b; Fall, 2003; Jardine et al., 2010), and no clear dependence on leaf age has been observed (Karl et al., 2003). Unlike methanol, which has a diffuse secondary source mainly from the oxidation of methane (Jacob et al., 2005; Millet et al., 2008), acetone also has a strong photochemical source from biogenic and anthropogenic precursor VOCs (Goldstein and Schade, 2000; de Gouw et al., 2005).

Based on the acetone:methanol correlation (R = 0.83, n = 6637 for year-2010), and the fact that methanol is mainly biogenic during summer, we initially tried to estimate the importance of biogenic acetone sources at the KCMP tall tower using methanol as a biogenic tracer. However, the distinct seasonal trajectories for the two compounds complicate such an analysis. We see in Figure 3.3 that the differing source characteristics drive seasonal shifts in the strength of the acetone:methanol correlation, with the highest correlation occurring during spring and autumn, and the lowest during winter and summer. Also, the measured acetone vs. methanol regression slopes are relatively consistent year-round at the KCMP tall tower (0.20 - 0.31; mean 0.25), suggesting that, while in the annual sum methanol sources are mainly natural, the effective acetone:methanol ratios for biogenic and anthropogenic sources are quite similar. This makes it difficult to effectively segregate acetone sources based on this correlation. During winter, biogenic emissions are negligible for both compounds, and the slope at this time can be interpreted as the mean anthropogenic acetone:methanol emission ratio (95% CI: 0.19 – 0.23; Figure 3.3). This is nearly identical to the slope during summer (95% CI: 0.19 - 0.22; Figure 3.3), when biogenic emissions are the predominant source of methanol (Hu et al., 2011) and account for approximately half the acetone abundance (as shown later).

3.3.2 Inverse analysis

In this section, we use a Bayesian optimization approach to interpret the KCMP tall tower observations in terms of the information they provide on North American acetone sources. The method derives the optimal set of acetone sources most consistent with observational constraints (i.e., the tall tower acetone measurements) and with prior knowledge (i.e., the a priori primary and secondary sources described in Section 3.2.3) by minimizing the cost function $J(\boldsymbol{x})$ (Rodgers, 2000):

$$J(\mathbf{x}) = (\mathbf{x} - \mathbf{x}_a)^T \mathbf{S}_a^{-1} (\mathbf{x} - \mathbf{x}_a) + (\mathbf{Kx} - \mathbf{y})^T \mathbf{S}_\Sigma^{-1} (\mathbf{Kx} - \mathbf{y}) \quad (3.2)$$

The first term on the right hand side of the equation represents the error-weighted misfit between the sources being optimized ($\boldsymbol{x}$) and their initial guess values ($\boldsymbol{x}_a$), while the second term represents the error-weighted misfit between the predicted ($\mathbf{K}\boldsymbol{x}$) and observed ($\boldsymbol{y}$) acetone mixing ratios. $\mathbf{S}_a$ and $\mathbf{S}_\Sigma$ are the a priori and observational error covariance matrices, respectively (Heald et al., 2004).

We construct the Jacobian matrix $\mathbf{K}$ by perturbing each model source individually (excluding gross ocean emissions) by 10%, rerunning the model, and calculating the resulting change in acetone mixing ratios at the KCMP tall tower. These sensitivities were derived with respect to eight distinct acetone sources within the North American domain of Figure 3.1: biogenic emissions from broadleaf trees, needleleaf trees, shrubs, and herbaceous plants; secondary production from biogenic precursors; primary anthropogenic emissions; secondary production from anthropogenic precursors; and biomass burning. We also derive the sensitivity with respect to sources outside North America, manifested as the boundary conditions for the nested model domain. We verified the assumption of a linear relationship between acetone sources and mixing ratios by comparing the scaled sum of all sensitivities from the perturbed simulations to the baseline total acetone mixing ratios simulated at the KCMP tall tower (R = 1.00, slope = 1.00, n = 8737).

We estimate the errors in the prior source terms at 100%, and assume they are uncorrelated, so that the resulting a priori error covariance matrix $\mathbf{S}_a$ is diagonal. The observational error covariance matrix $\mathbf{S}_\Sigma$ is constructed by combining the measurement error ($\mathbf{S}_{meas}$) and the model error ($\mathbf{S}_{mod}$), assuming they are uncorrelated so that $\mathbf{S}_\Sigma$ is also diagonal. We estimate the measurement uncertainty at 30 pptv +10% (Section 3.3.2). The forward model uncertainty includes representation error, transport error, and any error due to other model processes that are not included in the state vector $\boldsymbol{x}$ being optimized (Palmer et al., 2003; Heald et al., 2004). Representation error, describing the mismatch between model and observations due to subgrid-scale variability (Palmer et al., 2003),

can be assumed to be negligible for this analysis due to the large footprint of the KCMP tall tower (sampling height at 185 m a.g.l.) combined with the high resolution of the nested model simulation (0.5° × 0.667°). A dominant contributor to model transport uncertainty is the simulated boundary layer depth. Here we assess that error by comparing the GEOS-5.2.0 mixing depths at the KCMP tall tower with nearby radiosonde data (NOAA NCDC Station Minneapolis, ID 72649, 44.85°N, 93.57°W, approximately 40 km northwest of the KCMP tall tower). We find that the GEOS mixing depths in 2010 are generally consistent with the observations to better than 20% (slope = 0.90, $R = 0.78$, $n = 353$). We thus employ a forward model uncertainty of 20%. Later, we examine the degree to which our inversion results depend on the above assumptions used to construct $\mathbf{S}_a$ and $\mathbf{S}_\Sigma$.

Our initial analyses employed the above ensemble of nine source types as state vector for the inverse calculation. We find, however, that biomass burning has only a minor impact on simulated acetone mixing ratios at the KCMP tall tower (up to 8% for specific events in spring, but < 1% for the rest of 2010), so we do not attempt to constrain that source. We also merge needleleaf tree emissions and secondary biogenic production into a single acetone source category in the following analysis, since the two are highly correlated in the model ($R = 0.97$, $n = 6637$). We then performed a series of tests to examine how well the remaining seven source types can be resolved based on the KCMP tall tower observations. First, we inspected the averaging kernel matrix and the singular value of the prewhitened Jacobian for the system (Palmer et al., 2003; Heald et al., 2004). However, we found that both methods provided an overly-optimistic measure of the resolving power of the KCMP dataset, based on the fact that the resulting state vector combinations led to unrealistic and non-physical solutions.

We instead employ a pseudo-observation analysis to aid in identifying an appropriate combination of elements to include in the state vector. A synthetic dataset was created by reducing all model acetone sources by 50%, with random measurement and model noise then applied to the simulated mixing ratios (normally distributed with zero mean and

standard deviation equal to 21% of the simulated value). We then tested different state vector combinations in the inverse analysis in terms of their ability to return a posteriori scale factors approaching the true value of 0.5. In this way, we selected a four-element state vector, composed of 1) acetone emissions from broadleaf trees, shrubs, and herbaceous plants (BT+SH+HB), 2) emissions from needleleaf trees plus secondary production from biogenic precursors (NT+BIOG2), 3) primary and secondary anthropogenic acetone sources (ANTH), and 4) sources outside North America / long-range transport (BOUNDARY). The corresponding scale factors in the pseudo-observations test for those source combinations were 0.54, 0.57, 0.50, and 0.37, respectively. Based on this analysis, we can expect inversion of the KCMP observations to resolve these North American source categories to better than 20%, with a slightly higher error for the boundary condition.

3.3.3 Optimized North American acetone sources

Figure 3.4 shows the a posteriori scale factors for our four North American acetone source categories: acetone emissions from broadleaf trees + shrubs + herbaceous plants (BT+SH+HB), emissions from needleleaf trees + secondary production from biogenic precursors (NT+BIOG2), primary + secondary anthropogenic acetone sources (ANTH), and long-range transport associated with sources outside North America (BOUNDARY). The results imply a 37% model underestimate (a posteriori scale factor, SF = 1.37; 95% CI = 1.22 – 1.52) of acetone emissions from broadleaf trees, shrubs, and herbaceous plants, and a 40% overestimate (SF = 0.60; 95% CI = 0.45 – 0.79) of emissions from needleleaf trees plus secondary production from biogenic precursors. Confidence intervals are derived as described later in Section 3.3.4. Overall, this corresponds to a 16% underestimate of the total North American biogenic acetone source (including primary and secondary contributions) in the a priori model.

These opposing changes to the prior source estimates for the broadleaf tree + shrub + herbaceous plant category and the needleleaf tree + secondary biogenic production category probably reflect a misrepresentation of the associated canopy emission factors in

MEGAN. Errors in land cover or in the MEGAN activity factors that scale emissions according to environmental conditions could also be responsible. However, Guenther et al. (2012) found that specification of emission factors for various land cover types represents the largest contributor to the overall emission estimate uncertainty for biogenic VOCs.

Another possible explanation would be errors in the meteorological fields used to drive GEOS-Chem and MEGAN, but this appears less likely. In our previous work we found that the GEOS-5 surface air temperatures agree well with the observed values at KCMP tall tower (average bias -0.9 °C, Hu et al., 2011). Likewise, the simulated mixing depths appear consistent with radiosonde observations (Section 3.3.2). In addition, any model bias in temperature, light, or other environmental parameter would likely affect biogenic emissions from all plant types in the same direction (unless the bias happened to be correlated with the PFT distributions), whereas we find an increase for one source category versus a decrease for the other. However, because of the way source categories are combined in the state vector, we can't rule out the possibility of an underestimate of direct acetone emission across all PFTs, combined with an overestimate of secondary biogenic production.

We find that the simulated North American anthropogenic acetone source (computed based on EPA's NEI 2005) is accurate to within the constraints provided by the KCMP tall tower observations (SF = 1.11; 95% CI = 0.94 – 1.26). The optimization is not capable of resolving the relative importance of primary versus secondary anthropogenic sources of atmospheric acetone, as these are highly correlated (model R = 0.68 at the KCMP tall tower). However, as we show later (Section 3.3.5), the secondary anthropogenic acetone source in the model predominates over primary emissions, so that the a posteriori scale factor for the total anthropogenic source is mainly weighted towards this secondary fraction.

We also infer a 40% underestimate (SF = 1.40; 95% CI = 1.31 – 1.54) of the acetone boundary condition for our North American domain (Figure 3.1). This could be due to a

number of upstream acetone source or sink processes, including an underestimate of emissions elsewhere in the world, a misdiagnosis of the air-ocean flux, or an underestimate of the acetone lifetime. However, given the atmospheric lifetime for acetone (32 days against photochemical loss and land uptake; Fischer et al., 2012), we don't expect our derived constraints on North American sources to be particularly sensitive to uncertainty in model OH or deposition; any such error would mainly manifest as a problem with the boundary conditions and be corrected by the corresponding scale factor.

Figure 3.5 shows that the resulting optimized simulation captures 70% of the variance in the 2010 hourly measurements at the KCMP tall tower, with minimal bias (R = 0.83, slope = 1.03). Model:measurement slopes for individual seasons are all within 20% of unity. However, the winter comparison reveals two populations (red dots in Figure 3.5), with most of the simulated values lower than the observations. This bifurcation is due to the fact that our sampling height (185 m) is close to the mixing depth in winter. At times, the GEOS mixing depths are slightly lower than our sampling height while the actual mixing depths are above it, so that the model is sampling the free troposphere while the actual measurements are within the boundary layer. We examine this point in more detail later to see how it affects our inversion results (Section 2.3.4; Figure 3.4).

We thus estimate the total acetone source from North America at 10.9 Tg for 2010 (excluding gross oceanic emission; Table 3.2), which is consistent with the a priori model source (9.7 Tg) to within uncertainty. Including both primary (3.0 TgC biogenic; 0.4 TgC anthropogenic) and secondary (0.4 TgC biogenic; 3.0 TgC anthropogenic) contributions, the continental acetone source is then nearly as large as the sum of all direct fossil fuel VOC emissions from North America (6.8 TgC versus 9.2 TgC). Annually, we find that direct biogenic emissions (44%) and secondary production from anthropogenic precursors (44%) are the predominant North American acetone sources in the optimized simulation, followed by secondary production from biogenic precursors (6%), primary anthropogenic emissions (6%), and a minor biomass burning source (< 1%).

3.3.4 Uncertainty analysis

We carried out a series of sensitivity tests to quantify the uncertainty in our acetone source estimates. These included various modifications to the error covariance matrices $\mathbf{S}_a$ and $\mathbf{S}_\Sigma$ (halving and doubling $\mathbf{S}_a$, $\mathbf{S}_{mod}$, and $\mathbf{S}_{meas}$; setting $\mathbf{S}_{meas}$ to a fixed value of 10% or 0), along with a series of test inversions designed to assess the impact of model transport uncertainty (using only daytime data; only nighttime data; and excluding each season). Finally, we applied a bootstrap analysis to resample (> 1000 times) our hourly observations for each of the above sensitivity analyses in order to obtain confidence intervals for the resulting a posteriori scale factors. The final uncertainties for the a posteriori estimates are taken as the 5-95% probability range across all sensitivity inversions, and are shown in Figure 3.4.

3.3.5 Source apportionment for acetone in the US Upper Midwest

Our optimized (a posteriori) acetone simulation is able to capture much of the observed variability in acetone mixing ratios at the KCMP tall tower throughout the year, and we therefore apply it to interpret the tall tower observations in terms of the seasonal importance of different acetone sources for this region.

On a yearly basis, North American biogenic sources, North American anthropogenic sources, and long-range transport (i.e., from outside the North American domain of Figure 3.1) make similar contributions to acetone levels in the US Upper Midwest (32%, 32%, 36%, respectively), though with differing seasonality. Figure 3.6 (top panel) shows that the weekly mean acetone contribution from long-range transport is approximately 0.5 ppbv year-round, with no major seasonal variation. North American anthropogenic sources, predominantly secondary in origin, are of comparable importance in the annual mean (0.4 ppbv), but with episodic enhancements during winter and spring. The relatively weak seasonality seen for the secondary anthropogenic and long-range transport contributions likely reflects a compensation between an increased photochemical production rate in the summer and a longer acetone lifetime in the winter.

The bottom panel of Figure 3.6 shows that, during winter, acetone in the US Upper Midwest arises mainly from sources outside North America (50%) and from anthropogenic sources within North America (45%). Biogenic sources become important starting in April, and exceed the sum of anthropogenic sources plus long-range transport from May through the middle of September. During summer, North American anthropogenic sources (20%) and long-range transport (19%) play relatively modest roles; biogenic sources predominate (47% primary; 14% secondary; Figure 3.6). Among biogenic sources, crop and grassland emissions are most important, accounting for a third of the total biogenic acetone at the KCMP tall tower during the growing season, followed by secondary biogenic production (24%), emissions from needleleaf trees (16%), broadleaf trees (14%), and shrubs (13%). As we see in Figure 3.6, the strong observed seasonality in atmospheric acetone is mainly driven by the changing importance of biogenic emissions.

3.3.6 Sensitivity of acetone and PAN to shifts in North American acetone sources

Acetone photolysis is a significant source of PAN, especially in the mid- and upper troposphere (Singh et al., 1994):

$$CH_3C(O)CH_3 + h\nu + 2O_2 \rightarrow CH_3C(O)O_2 + CH_3O_2 \quad (3.3)$$

$$CH_3C(O)O_2 + NO_2 + M \rightleftharpoons CH_3C(O)O_2NO_2 + M \quad (3.4)$$

Acetone sources thus affect the partitioning and long-range transport of atmospheric reactive nitrogen. However, the updated quantum yields for acetone photodissociation lead to lower predicted photolysis rates throughout the troposphere, and especially in the cold upper troposphere (Blitz et al., 2004; Arnold et al., 2005). In this section, we

examine the sensitivity of atmospheric PAN to changes in North American acetone sources, using our optimized acetone budget as a baseline.

To assess this sensitivity, we carry out a perturbation analysis in which North American (primary + secondary) acetone biogenic sources are increased by 35% (+35% BIOG). This is similar, for example, to the acetone emission increase expected for a 3°C surface warming based on the MEGANv2.1 temperature dependence of emissions (β = 0.10; Guenther et al., 2012). We also carry out a second perturbation analysis in which anthropogenic acetone sources from North America are reduced by the same fraction (-35% ANTH; again including both primary and secondary components). A final sensitivity simulation examines the combined effect of the biogenic (+35% BIOG) and anthropogenic (-35% ANTH) perturbations (COMBO). For all scenarios, the acetone sources outside North America are unchanged.

Figure 3.7 shows the August changes to atmospheric acetone and PAN in the mid-troposphere and at the surface resulting from these source perturbations. For the -35% ANTH scenario, atmospheric acetone decreases by up to 9% at 700 hPa and 20% at the surface. This leads to a modest shift in the partitioning of reactive nitrogen, with PAN decreasing by up to 4%. On the other hand, the increased biogenic source in the +35% BIOG scenario leads to an atmospheric acetone increase of up to 16% at 700 hPa and 30% at the surface, along with a PAN increase of up to 7%. For the COMBO scenario, the biogenic flux increase thus more than offsets the 35% decrease to the anthropogenic source. The net effect during August is a widespread acetone increase in surface air and at 700 hPa (up to 29% and 11%, respectively) over North America (Figure 3.7), with a small net PAN increase of up to 3%.

The top and middle panels of Figure 3.8 show the seasonality of these simulated changes in acetone and PAN mixing ratios at 700 hPa over North America. For the COMBO scenario, we see acetone and PAN increases from May through October, and decreases

during the colder months. The largest net change occurring during summer is relatively small (a few pptv), but positive. Any future decrease in anthropogenic acetone emissions is thus likely to be significantly offset by increased biogenic acetone emissions due to surface warming. Such warming would also affect other parameters, such as the PAN lifetime: these perturbation analyses thus represent the partial derivatives of atmospheric acetone and PAN with respect to biogenic and anthropogenic acetone source changes within North America.

Finally, we derive the PAN fraction at 700 hPa over North America resulting from domestic acetone sources (bottom panel in Figure 3.8), based on the scaled response to the perturbations above. During summer, North American acetone sources contribute only up to 6% of the total PAN abundance at 700 hPa formed over this region (biogenic: 4%; anthropogenic: 2%). During winter, North American acetone sources (mainly anthropogenic) account for less than 2% of the PAN abundance in this part of the free troposphere.

3.4 Conclusions

We developed new constraints on natural and anthropogenic acetone sources over North America based on inverse modeling of a full year (January 2010 – February 2011) of continuous atmospheric acetone measurements from the University of Minnesota tall tower Trace Gas Observatory (KCMP tall tower). We then used this information to evaluate the sensitivity of atmospheric acetone and peroxyacetyl nitrate (PAN) with respect to changes in North American biogenic and anthropogenic acetone sources.

Acetone mixing ratios measured at the KCMP tall tower ranged from 0.1 ppbv to 4.1 ppbv, with an annual mean of 1.2 ppbv (median 1.0 ppbv); mixing ratios were in general lower during winter, and higher in summer. Atmospheric acetone at the KCMP tall tower is well correlated with methanol (R = 0.83 for the full year, n = 6637), consistent with

observations elsewhere (Goldan et al., 1995; Riemer et al., 1998; Salisbury et al., 2003; Singh et al., 2004; Schade and Goldstein, 2006). However, due to the different mechanisms driving plant emissions of these two compounds, the seasonal peak for acetone occurs roughly one month later than that for methanol (mid-August versus mid-July). This degrades the correlation between the two compounds during summer. We found the acetone:methanol slope to be relatively consistent through all seasons (between 0.20 and 0.31) at the tall tower, implying similar acetone:methanol ratios for both biogenic and anthropogenic sources.

We applied the KCMP tall tower observations in a Bayesian optimization approach to develop new top-down acetone source estimates for North America. We found that the a priori model (GEOS-Chem, driven by the MEGANv2.1 biogenic inventory) underestimates acetone emissions from broadleaf trees + shrubs + herbaceous plants by 37%, while overestimating needleleaf tree emissions + secondary production from biogenic precursors by 40%. The overall result is a small (16%) model underestimate of the total primary + secondary biogenic acetone source over North America. Estimated North American primary + secondary anthropogenic acetone sources, computed in the model based on EPA's NEI 2005 inventory, are accurate to within approximately 20%. An optimized GEOS-Chem simulation incorporating the above findings captured 70% of the variance (R = 0.83) in the hourly measurements at the KCMP tall tower over the full year. The resulting North American acetone source is 10.9 Tg a^{-1}, with roughly equal contributions from anthropogenic and biogenic sources. The acetone source alone is then comparable to (~75%) the total direct VOC source from North American fossil fuel combustion.

We find during winter that acetone in the US Upper Midwest arises mainly from sources outside North America (50%), with primary (15%) and secondary (29%) anthropogenic sources within North America also important. During summer, North American biogenic sources predominate (47% primary; 14% secondary), with anthropogenic sources (20%)

and long-range transport (19%) playing more modest roles. On a yearly basis, domestic biogenic, domestic anthropogenic and transported acetone sources are of similar importance, but with differing seasonality.

We then applied our optimized source estimates to gauge the sensitivity of the atmospheric acetone and PAN abundance over North America to shifts in biogenic and anthropogenic acetone sources. A 35% increase to modeled primary + secondary biogenic acetone sources over North America (which is a conservative estimate of the warming-driven emission enhancement to be expected over the 21th century) increases model acetone and PAN mixing ratios by up to 29% and 7%, respectively. This increase would more than offset a comparable relative decrease (-35%) in the anthropogenic acetone source due to future emission controls.

Table 3.1. Seasonal acetone mixing ratios measured at the KCMP tall tower.

	Statistic	Value (ppbv)
spring[1]	mean	1.3
	median (10^{th}-90^{th} percentiles)	1.2 (0.7-2.0)
summer[2]	mean	2.1
	median (10^{th}-90^{th} percentiles)	2.1 (1.4-2.8)
autumn[3]	mean	1.1
	median (10^{th}-90^{th} percentiles)	1.0 (0.5-1.9)
winter[4]	mean	0.6
	median (10^{th}-90^{th} percentiles)	0.6 (0.4-0.9)

[1]Spring: March-May. [2]Summer: June-August. [3]Autumn: September-November. [4]Winter: December-February.

Table 3.2. North American[1] acetone sources (Tg a^{-1}): A priori forward model sources and a posteriori sources optimized based on the KCMP tall tower measurements. 95% confidence intervals for the optimized posteriori sources are provided in parentheses.

	Biogenic[2]	Anthropogenic[2]	Biomass burning	NA Total[3]	Cost Function Reduction[4]
A priori	4.8	4.9	0.06	9.7	-
A posteriori	5.5 (4.7-6.5)	5.4 (4.5 - 6.0)	0.06	10.9 (9.2 – 12.5)	1.37

[1]North America is defined here as the domain from 13 to 70°N and 140 to 50°W. [2]Including both primary emissions and secondary photochemical production. [3]Total North American acetone source, excluding ocean exchange. [4]$J_{initial}/J_{final}$.

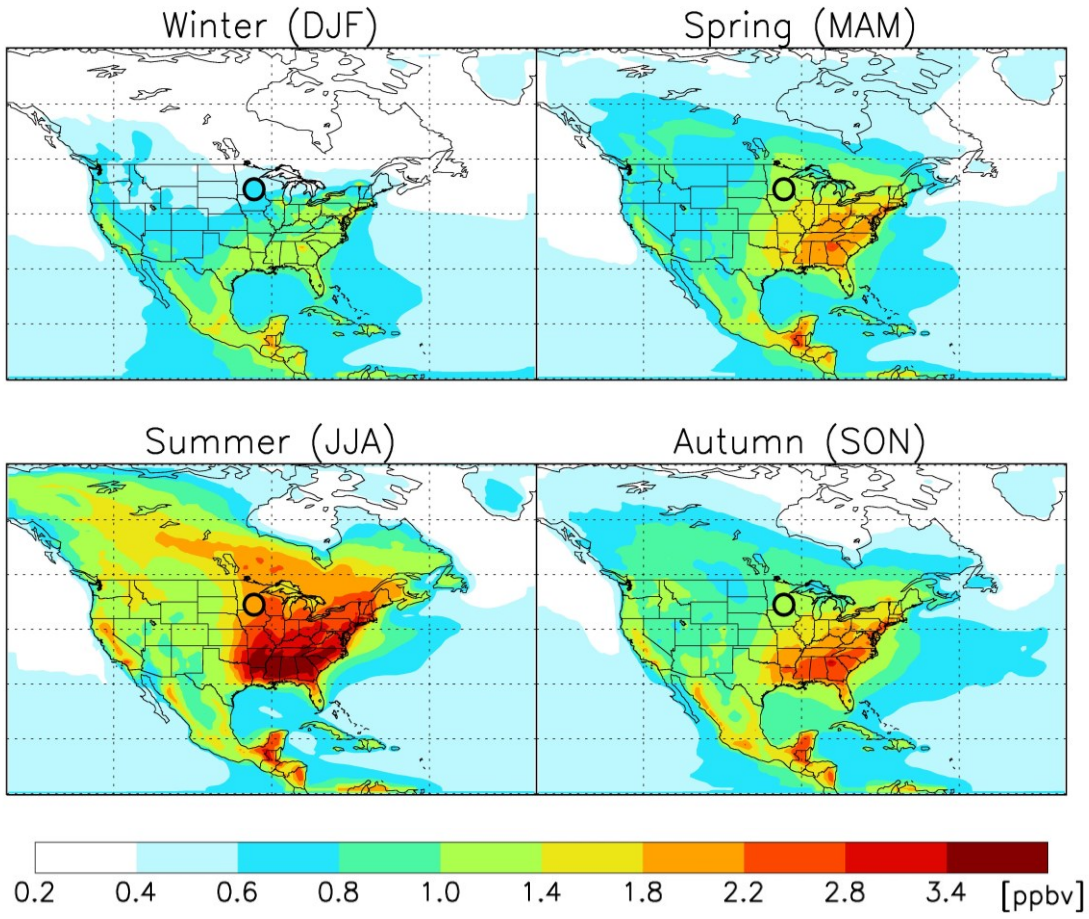

Figure 3.1. Surface acetone mixing ratios over the nested North American domain (10-70°N; 140-40°W) in the GEOS-Chem a priori simulation for the year 2010. A sub-domain (13-70°N; 140-50°W) is used in the paper for computing North American source magnitudes. Measured mixing ratios at the KCMP tall tower (44.689°N, 93.073°W) are indicated by the filled circle on the same color scale.

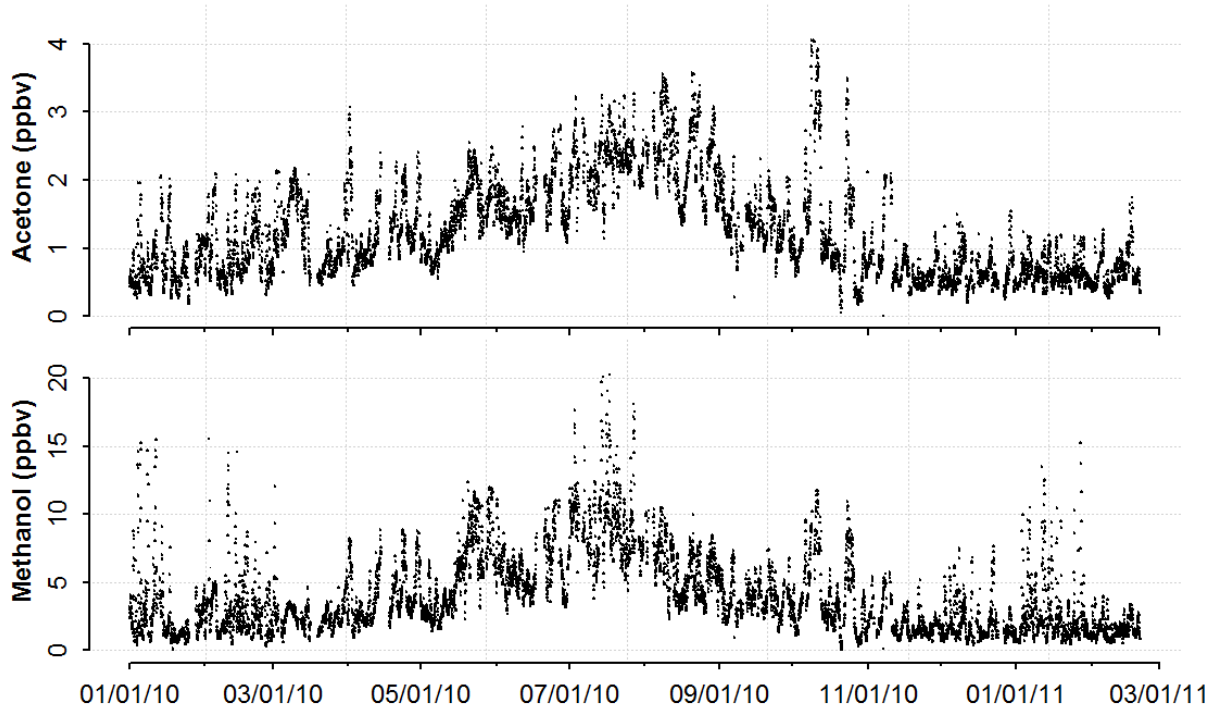

Figure 3.2. Annual cycle in atmospheric acetone and methanol observed at the KCMP tall tower from January 2010 through February 2011. All data points are 1 h averages. Statistical outliers (> 0.98 quantile for each month) have been removed prior to plotting.

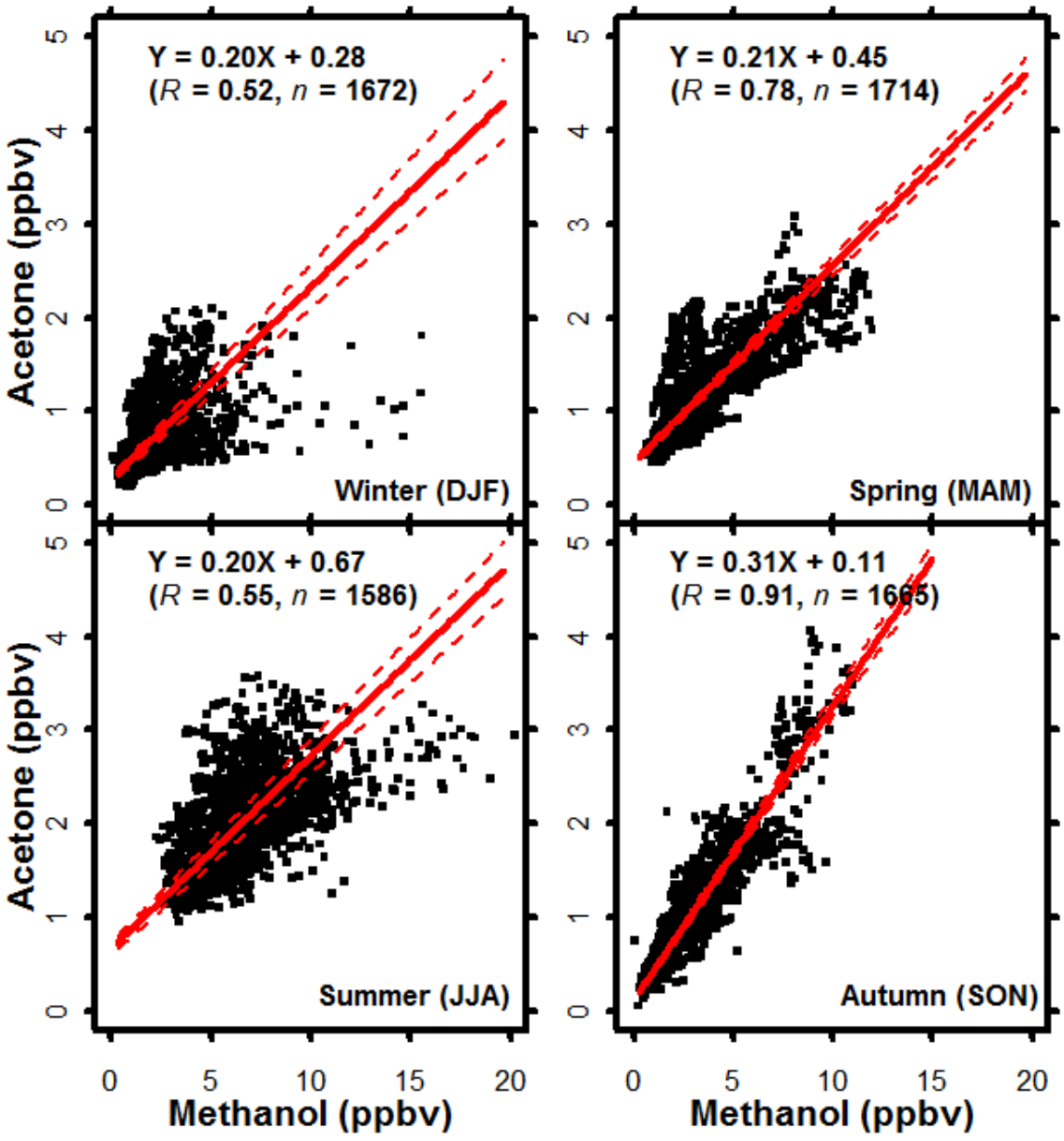

Figure 3.3. Seasonal linear correlation (major axis regression) between atmospheric acetone and methanol mixing ratios observed at the KCMP tall tower in 2010. Red dashed lines show the 95% confidence interval for the best fit line (red solid line). Data points are 1 h means.

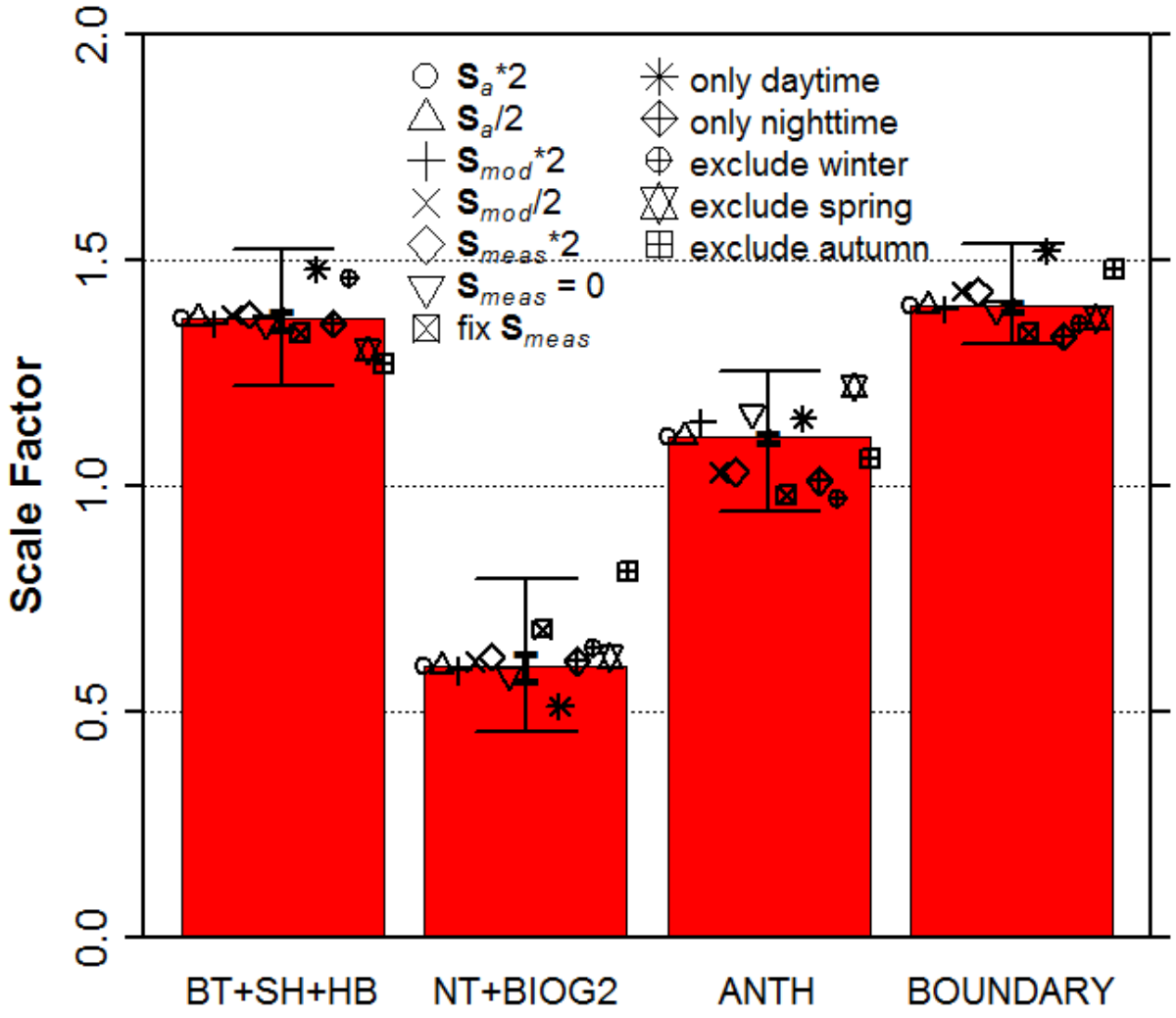

Figure 3.4. A posteriori scale factors for North American acetone sources computed on the basis of the KCMP tall tower measurements: BT+SH+HB, broadleaf trees + shrubs + herbaceous plants; NT+BIOG2, needleleaf trees + photochemical production from biogenic precursors; ANTH, primary + secondary anthropogenic sources; BOUNDARY, acetone boundary condition/long-range transport. Also shown is the range of scale factors derived from an ensemble of sensitivity calculations (see text). Thin error bars show 95% confidence intervals derived from a bootstrap analysis as described in the text. Thick error bars show the a posteriori errors from the inversion analysis. A priori scale factors are one in all cases.

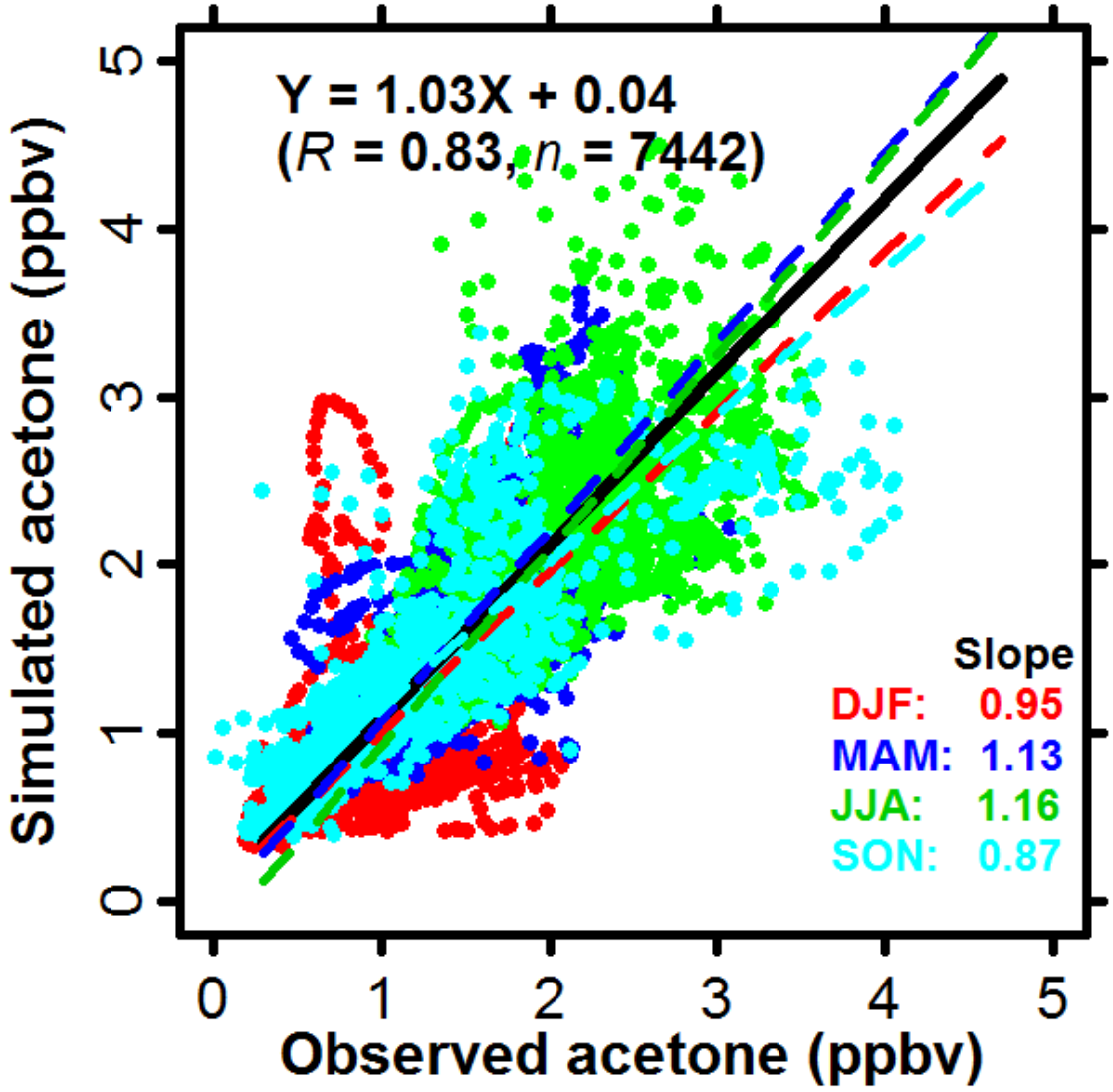

Figure 3.5. Atmospheric acetone mixing ratios from the optimized GEOS-Chem simulation compared to observations at the KCMP tall tower in 2010, colored by season. Data points are 1 h mean values.

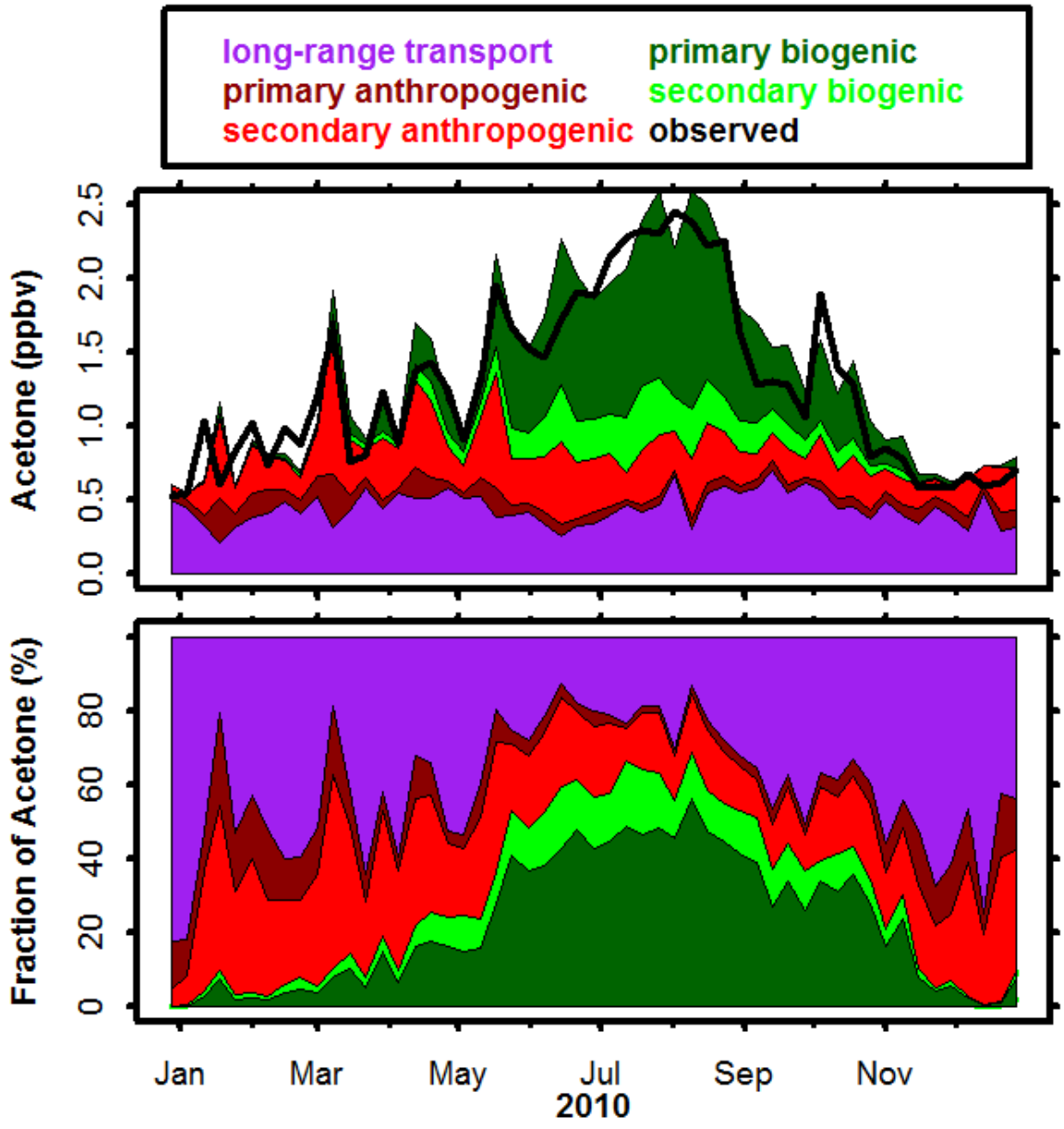

Figure 3.6. Top panel: stack plot of the seasonal acetone mixing ratios from various sources in the optimized GEOS-Chem simulation at the KCMP tall tower. Also shown are the observed acetone mixing ratios at the tall tower (black line). Bottom panel: Fractional contribution of these sources to the total modeled acetone abundance in the optimized simulation.

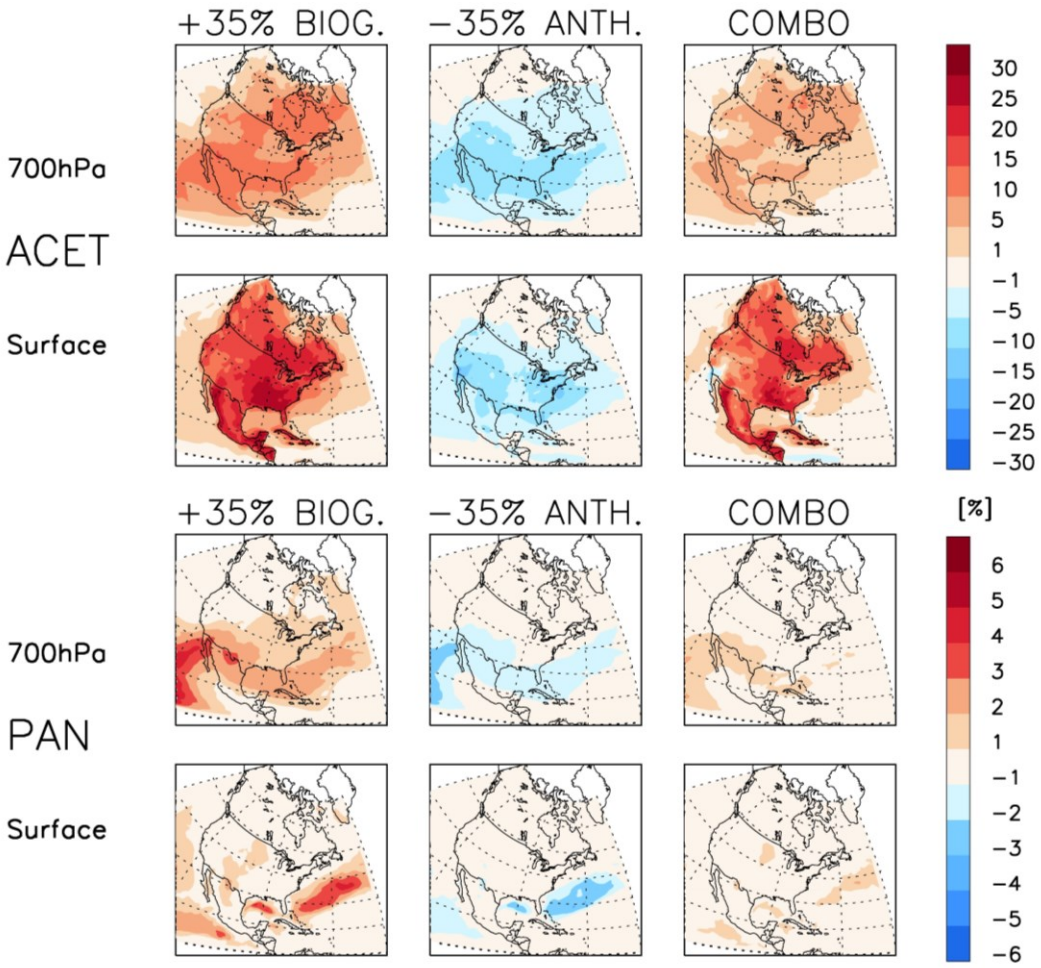

Figure 3.7. Sensitivity of atmospheric acetone and PAN to biogenic and anthropogenic source changes in North America during August. Shown are the percent changes due to a 35% increase in primary + secondary biogenic acetone sources (+35% BIOG), a 35% decrease in primary + secondary anthropogenic sources (-35% ANTH), and the combined effect of the two (COMBO). Note differing color bars for acetone and PAN.

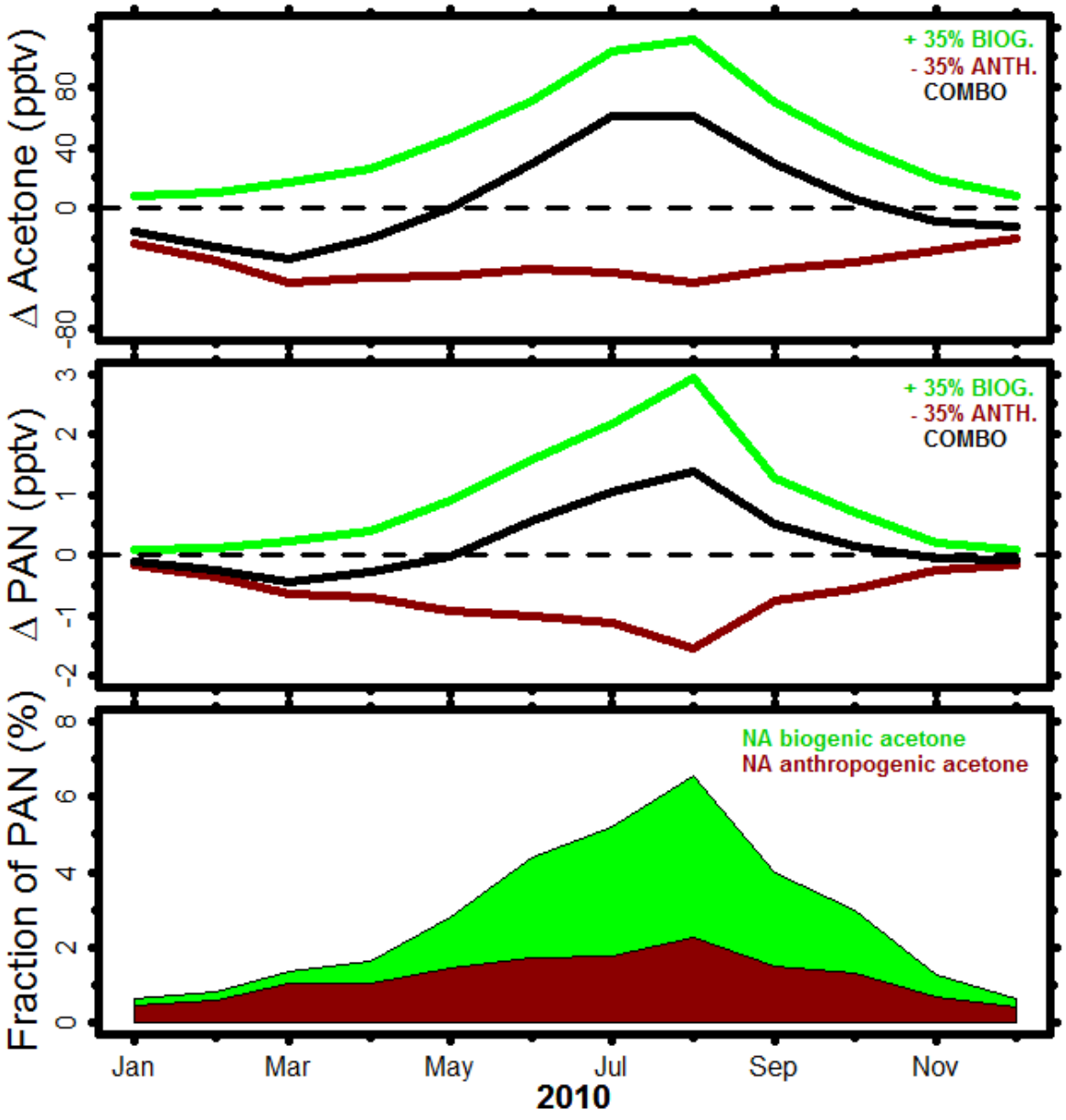

Figure 3.8. Simulated change (pptv) in seasonal acetone (top panel) and PAN (middle panel) mixing ratios at 700 hPa for the sensitivity runs shown in Figure 3.7. The bottom panel shows the fractional contribution of biogenic and anthropogenic acetone sources in North America to the simulated PAN abundance. Values shown represent an average over continental North America.

4 Isoprene emissions and impacts over an ecological transition region in the US Upper Midwest

Abstract

In this paper we present a full year of continuous in-situ measurements of isoprene and its oxidation products methyl vinyl ketone and methacrolein (MVK+MACR) by proton-transfer-reaction mass spectrometry (PTR-MS) from a 244 m tall tower in the US Upper Midwest (KCMP tall tower). The tower is located at an ecological transition between isoprene-emitting deciduous forest to the north and east, and predominantly non-isoprene-emitting agricultural landscapes to the west and south. Based on independent cartridge measurements and a source-tracer analysis, we estimate that anthropogenic interferences (or anthropogenic isoprene) contribute on average 20% of the observed PTR-MS m/z 69 signal during daytime in summer at the KCMP tall tower (and up to 80% at night). Interferences for MVK+MACR at m/z 71 are small (7%). After removing these interferences, the observed isoprene and MVK+MACR mixing ratios show pronounced seasonal cycles, reaching maxima of 2540 pptv (isoprene) and 2790 pptv (MVK+MACR) during summer. The KCMP tall tower is impacted both by nearby isoprene sources (with transport time within an isoprene lifetime) and more distant regional isoprene sources (with transport time exceeding an isoprene lifetime), as indicated by daytime enhancements of isoprene (but little MVK+MACR) under southwest winds, and enhancements of MVK+MACR (but little isoprene) under other directions. We find that the GEOS-Chem chemical transport model driven with the MEGANv2.1 biogenic inventory can reproduce the observed isoprene mixing ratios to winthin model uncertainty once improved land cover and temperature estimates are implemented in the model. However, a model low bias in MVK+MACR of (25% - 66%) cannot be resolved, even across diverse model assumptions for chemistry, atmospheric mixing, and land cover. This suggests that, while isoprene emissions in the immediate vicinity of the KCMP tall tower are adequately captured, the model is still

underestimating emissions across the broader region. Using the loss of HO_x radicals relative to the loss of NO_x radicals (L_{HOx}/L_{NOx}) in the model as an indicator, we find that this region experiences a strong seasonal shift between VOC-limited chemistry in the spring and fall and NOx-limited or transitional chemistry in the summer, and that this transition is driven by the temporal and spatial distribution of isoprene emissions. Isoprene's role in causing these chemical shifts is likely underestimated for this area due to the underprediction of regional isoprene fluxes.

4.1 Introduction

Biogenic volatile organic compounds (BVOCs) play a major role in atmospheric chemistry and climate. They are precursors of ozone and of secondary organic aerosol, and modulate the troposphere's oxidizing potential and thus the lifetime of methane and other greenhouse gases and pollutants. Of the more than 1000 VOCs that have been measured in the atmosphere (Goldstein and Galbally, 2007), the estimated global emissions of isoprene (2-methyl-1,3-butadiene, C_5H_8) are: *i*) believed to account for some ~50% of the total BVOC flux each year (Guenther et al., 2006); *ii*) comparable to those of methane (Chen and Prinn, 2006); and *iii*) several times larger than those of all anthropogenic VOCs combined (Chapter 5).

Isoprene is produced enzymatically in the foliage of terrestrial plants, and the resulting emissions can count for 0.1-3% of annual net photosynthetic uptake for certain plant species (Sharkey et al., 1996; Goldstein et al., 1998). Isoprene emission may have evolved in plants as a mechanism for coping with heat stress (Sasaki et al., 2007; Sharkey et al., 2008), although other adaptive benefits have also been proposed (Monson et al., 2013). Emissions vary between species and depend strongly on temperature and light, as well as on other environmental and ecological factors such as soil moisture, phenology, nutrient availability, and atmospheric CO_2 concentration (e.g., Sharkey et al., 1991; Goldstein et al., 1998; Harley et al., 1999; Guenther et al., 2012; Monson et al., 2012). Isoprene is highly reactive in the atmosphere, with a lifetime against oxidation by the

hydroxyl radical (OH) of less than 1 hour during daytime in summer (82 min at [OH] = 2×10^6 molecules cm^{-3}) and first-generation oxidation products that can include methyl vinyl ketone (MVK), methacrolein (MACR), formaldehyde (HCHO), hydroxyhydroperoxides, and hydroperoxyaldehydes (Pierotti et al., 1990; Montzka et al., 1993; Warneke et al., 2001; Paulot et al., 2009a; Crounse et al., 2011).

Global isoprene emissions are currently estimated at 350-800 Tg y^{-1} (Arneth et al., 2008; Guenther et al., 2012). Bottom-up emission uncertainties are typically estimated at a factor of 2 or more, based on top-down information from satellite (Palmer et al., 2003; Shim et al., 2005; Fu et al., 2007; Millet et al., 2008; Barkley et al., 2011; Marais et al., 2012) and aircraft observations (Karl et al., 2007; Warneke et al., 2010). Errors on local-to-regional scales are often even larger (Guenther et al., 2006; Guenther et al., 2012). Predicated isoprene fluxes are highly dependent on model inputs such as weather, leaf area index (LAI), and land cover (Sharkey et al., 1996; Arneth et al., 2008), and as a result it is often a major challenge to discern whether discrepancies between an emission inventory and observations arise from unrealistic inputs used to drive the emission models or from the emission model algorithms themselves (Lamb et al., 1987; Guenther et al., 2012).

Prior evaluations of isoprene emission estimates over North America have led to seemingly inconsistent conclusions. For example, the total North American isoprene flux derived from formaldehyde column measurements from three different satellite sensors (OMI, GOME and SCIAMACHY) was found to be 4-40% lower than predicted by MEGAN2 (Model of Emissions of Gases and Aerosols from Nature version 2; Palmer et al., 2006; Millet et al., 2008; Stavrakou et al., 2009); with a somewhat larger bias over the US Upper Midwest (~70%; Millet et al., 2008). A subsequent analysis of airborne measurements suggested that MEGAN2 overpredicts isoprene emissions over the eastern United States and Texas by up to a factor of 2 (Warneke et al., 2010). On the other hand, Müller et al (2008) found that isoprene emissions predicted on the basis of MEGAN2 and

a detailed canopy environment model were 40% too low compared to in-situ flux measurements at Harvard Forest in central Massachusetts, USA (Müller et al., 2008), a site with 60-70% broadleaf deciduous tree coverage (Goldstein et al., 1998). However, the above studies employed divergent meteorological and land cover datasets, and differed also in their implementation of MEGAN within the overarching chemical transport model – CTM (e.g., parameterization of the forest canopy). Collective interpretation of such studies in terms of broader implications for emission models such as MEGAN therefore requires careful consideration of how the overall CTM framework and driving variables affect the emission estimates.

In this study, we present a full year of continuous in-situ concentration measurements of isoprene and its oxidation products (MVK+MACR) from a tall tower in the US Upper Midwest (KCMP tall tower). The site is ~25 km south of the Twin Cities of Minneapolis and St. Paul, and lies at the ecological transition between high-isoprene-emitting eastern deciduous forest to the north and east, and predominantly non-isoprene-emitting agricultural landscapes to the west and south. We interpret this dataset with a 0.5° × 0.667° nested version of the GEOS-Chem CTM in terms of its implications for present understanding of isoprene emissions and chemical impact in this region. We further investigate the role of isoprene in driving a seasonal shift between NO_x- and VOC-limited photochemistry during the spring and fall in this part of the US Upper Midwest.

4.2 Methods

4.2.1 KCMP tall tower

Figure 4.1 shows the fractional distributions of four major plant function types (PFTs) in the US Upper Midwest (Oleson et al., 2010), along with annual isoprene and NO_x emissions for this region computed as described in Section 4.2.3. As we see, the KCMP tall tower (as well as the nearby Twin Cities of Minneapolis and St. Paul) is situated on a strong isoprene emission gradient between the deciduous forests to the northeast and the

mainly agricultural areas to the southwest. The tower is also at times downwind of the Twin Cities metropolitan areas (2010 population: 3.3M; U.S. Census Bureau, 2010), and thus is periodically impacted by urban pollution outflows. The tower location thus provides a unique natural laboratory to study interacting biogenic and anthropogenic processes. A detailed description of the KCMP tall tower and of the meteorological measurements at the site is given in earlier papers (Griffis et al., 2010; Hu et al., 2011).

4.2.2 PTR-MS and cartridge-GC-MS/FID measurements at the KCMP tall tower

Isoprene (protonated m/z 69), its oxidation products MVK+MACR (protonated m/z 71), and a suite of other VOCs (including methanol, acetone, acetonitrile, and C_6-C_9 aromatic compounds) were measured using a high-sensitivity proton transfer reaction mass spectrometer (PTR-MS, Ionicon Analytic GmbH, Austria) between July 2009 and August 2012 at the KCMP tall tower. Measurements were made every ~3 minutes with ambient air sampled via perfluoroalkoxy tubing at 185 m above ground level, thus providing a highly temporally resolved signal that is more regionally representative than is obtainable with measurement near the surface (Hu et al., 2011; Hu et al., 2013; Kim et al., 2013). The PTR-MS was automatically calibrated in-situ every 23 h or every 47 h (before or after August 2010, respectively), by dynamic dilution of multi-component standards (Apel-Riemer, Inc., USA) into zero air generated by passing ambient air through a heated platinum bead catalyst (450°C; Shimadzu Corp., Japan). Instrument background levels were checked every ~2 h by measuring zero air as described above.

In parallel with the PTR-MS measurements, a series of cartridge samples were collected at the KCMP tall tower to test both the specificity of the PTR-MS measurements and the stability of the VOC standards used for PTR-MS calibration (Hu et al., 2013). A total of 100 ambient samples (plus 25 calibration gas samples for standard intercomparison) were collected using a custom-built auto-sampler (Helmig et al., 2004) between December

2010 and August 2012. All cartridge samples were subsequently analyzed by gas chromatography with mass selective and flame ionization detectors (GC-MS/FID) at the Institute of Arctic and Alpine Research (INSTAAR), University of Colorado at Boulder. A detailed description of the cartridge sampling and quantification system used in this work is provided by Hu et al. (2013) and Helmig et al. (2004).

The pre-mixed VOC standard cylinders used for PTR-MS calibration were originally filled in December 2008 to nominal mixing ratios of 50 ppbv for isoprene, 150 ppbv for MVK, and 178 ppbv for MACR. The cylinders were recertified in January 2012, at which time isoprene was nearly unchanged at 53 ppbv, but MVK and MACR had decreased by 90% and 35%, respectively (to 14 ppbv for MVK and 112 ppbv for MACR). These results were confirmed by cartridge samples collected from December 2010 through July 2011. Cartridge measurements of calibration standards over this time period indicate that relative to the INSTAAR standards: *i*) the isoprene mixing ratio was stable and consistent with the original certification (51 ppbv as measured by cartridge+GC-MS/FID); *ii*) the MACR mixing ratios was stable but 37% lower than the original certification (and consistent with the January 2012 recertification); *iii*) the MVK mixing ratio was not stable but rather appeared to be drifting lower with time (Table 1). We thus restrict the present analysis to the time period from January 2011 to December 2011. Calibrations for MVK+MACR are based on the recertified MACR standard (112 ppbv) and follow the approach of de Gouw et al (2003) to calculate a weighted instrument response factor for the sum of MVK and MACR based on the measured MACR sensitivity and its typical sensitivity and abundance relative to MVK (Stroud et al., 2001; de Gouw et al., 2003). The resulting detection limits are 38 pptv for isoprene and 21 pptv for MVK+MACR. Estimated uncertainties for the hourly isoprene and MVK+MACR measurements used in this study are $\leq$ 15% on average (and in nearly all cases are <40%); standard errors associated with the 1-hour averaging windows made the largest contribution to this (~2/3), followed by the various sources of instrumental error (e.g., mass flow measurement, calibration factors and fit). All VOC data presented here, along with

concurrent measurements of other VOCs and CO from the KCMP tall tower, are publicly available at www.atmoschem.umn.edu/data.

4.2.3 GEOS-Chem chemical transport model

We use a nested-grid version of the GEOS-Chem CTM (version 9.1.3) to simulate isoprene and MVK+MACR mixing ratios at the KCMP tower. The model is driven by GEOS-5.2 assimilated meteorological data from the NASA Goddard Modeling and Analysis Office, with 0.5° × 0.667° horizontal resolution over North America (10°-70°N and 140°-40°W), 47 vertical layers extending from Earth's surface to 0.01 hPa, and timesteps of 10 min (transport, convection) and 20 min (emissions, chemistry; Bey et al., 2001). A global 4° × 5° simulation is used to generate the lateral boundary conditions (for all species, at each vertical layer, every 3 hours) required for the nested grid runs (Wang et al., 2004; Chen et al., 2009; Zhang et al., 2011; van Donkelaar et al., 2012). A one year spin-up for 2010 is used to initialize the simulation for 2011, the period of this study. A detailed description of the GEOS-Chem CTM can be found at www.geos-chem.org.

In particular, for this work we use the Emissions Database for Global Atmospheric Research (EDGAR) monthly inventory for global CO, NO_x, and SO_2 emissions (Olivier and Berdowski, 2001). Global anthropogenic VOC emissions are from the REanalysis of the TROpospheric chemical composition (RETRO) inventory (Schultz et al., 2007), which is implemented in GEOS-Chem as described in Chapter 5. Anthropogenic emissions (CO, NO_x, SO_x, NH_3, and VOCs) over the U.S. are taken from the EPA's National Emission Inventory for 2005 (NEI05; EPA, 2005). Biomass burning emissions are computed based on the monthly GFED3 inventory (Global Fire Emission Database version 3; van der Werf et al., 2010) and measured species: species open fire emission ratios (Andreae and Merlet, 2001).

For this work, we implement the latest version of the Model of Emissions of Gases and Aerosols from Nature (MEGANv2.1; Guenther et al., 2012) within GEOS-Chem to calculate biogenic emissions of isoprene and other VOCs. MEGANv2.1 computes emissions for each model grid cell based on the fractional coverage of 15 plant function types and their corresponding base emission factors for VOCs under standard conditions (air temperature = 303 K, photosynthetic active radiation [PAR] = 1500 μmol m^{-2} s^{-1}, and leaf area index [LAI] = 5). Deviations from these standard conditions are accounted for using a set of non-dimensional activity factors (Guenther et al., 2012). PAR (diffuse and direct) and 2 m air temperature from the GEOS-5.2 assimilation system, and monthly mean LAI derived from MODIS observations (Myneni et al., 2007; LAI of year-2008 for all ensuing years) are employed to calculate the activity factors for solar radiation, temperature, LAI, and leaf age (γ_{PAR}, γ_T, γ_{LAI}, and γ_{age}). Compounds undergoing bidirectional exchange (formaldehyde, acetaldehyde, ethanol, formic acid, acetic acid) are treated as described by Millet et al. (2010) and Guenther et al. (2012). We do not include here any soil moisture effect on isoprene emissions.

Later, we compare the γ_T values computed in the model to those calculated with the surface air temperature observed at the KCMP tall tower to quantify the extent to which errors in the GEOS-5.2 assimilated temperature fields bias the simulated isoprene (and MVK+MACR) mixing ratios. The temperature activity factor for isoprene is calculated according to (Guenther et al. 2012):

$$\gamma_T = E_{opt} \left[200 \frac{\exp(C_{T1}\, x)}{200 - C_{T1}\,(1 - \exp(200\, x))} \right] \qquad (4.1a)$$

where

$$x = \frac{\left[\left(\frac{1}{T_{opt}}\right) - \frac{1}{T}\right]}{0.00831} \quad (4.1b)$$

$$T_{opt} = 313 + (0.6\,(T_{240} - 297)) \quad (4.1c)$$

$$E_{opt} = C_{eo} \times \exp\left(0.08\,(T_{240} - 297)\right) \quad (4.1d)$$

In equations 1a-1d, T is the (2 m) surface air temperature, which is assumed equivalent to the leaf temperature over forests, and T_{240} is the average surface air temperature over the past 240 h. C_{TI} and C_{eo} are both VOC-dependent empirical coefficients, and are set equal to 95 and 2, respectively, in the case of isoprene.

Our implementation of MEGANv2.1 within GEOS-Chem uses the PCEEA canopy environment parameterization described in Guenther et al. (2006), and (as a default) PFT distributions from version 4 of the Community Land Model (CLM4; native spatial resolution 0.47°× 0.63°; Oleson et al., 2010). For the present work, we also use a second land cover database for the region surrounding the KCMP tall tower, from the 2007 US Department of Agriculture National Agricultural Statistics Service Cropland Data layer product (native spatial resolution of 30 m× 30 m; USDA-NASS, 2007). Land cover differences between CLM4 and USDA-NASS are substantial over this transitional region between high isoprene-emitters (broadleaf trees with base emissions of 10^4 μg m^{-2} h^{-1}) and non -emitter (crops with base emissions of 10^0 μg m^{-2} h^{-1}) (Figure 4.1; Table 4.2). For example, broadleaf tree coverage within the model grid cell containing our tall tower is 12.2% according to the USDA-NASS dataset, but only 5.1% according to CLM4. This leads to a twofold difference in the derived annual emission factor for isoprene in the two cases (1430 μg m^{-2} h^{-1} for USDA-NASS versus 770 μg m^{-2} h^{-1} for CLM4; Table 4.2). Later, we will assess how these differences affect the interpretation of our results.

The GEOS-Chem chemical mechanism includes detailed HO_x-NO_x-VOC-ozone chemistry coupled to aerosols, employing the most recent JPL/IUPAC recommendations as described by Mao et al., 2010. Isoprene oxidation in GEOS-Chem v9.1.3 follows the scheme of Paulot et al. (2009a; 2009b) for high-NO_x and low-NO_x conditions, respectively. Dry deposition is computed with a resistance-in-series model (Wesely, 1989), with reactive uptake for oxygenated VOCs prescribed according to Karl et al., 2010.

4.3 Specificity of PTR-MS measurements for isoprene (m/z 69) and MVK+MACR (m/z 71)

Several previous studies have pointed out that isoprene measurements by quadrupole PTR-MS at m/z 69 can be subject to interferences from *i*) other biogenic VOCs such as 2-methyl-3-butene-2-ol (232 MBO; de Gouw and Warneke, 2007; Karl et al., 2012); *ii*) furan in biomass burning plumes (Christian et al., 2004); and *iii*) a variety of alkenes and cycloalkanes in urban air and oil/gas extraction areas (de Gouw et al., 2003; Warneke et al., 2014). There is also known to be a small anthropogenic source of isoprene and MVK+MACR associated with tailpipe emissions (e.g., McLaren et al., 1996; Borbon et al., 2001; Park et al., 2011; Wang et al., 2013). In addition, some recent work indicates that isoprene peroxides can be detected along with MKV+MACR at m/z 71, which would complicate the interpretation of measurements at this mass (Liu et al., 2013). However, given the significant NO_x levels for the region of our study (Section 4.6), we do not expect a major contribution from such species.

We employ here two independent approaches to quantify the contribution from interferences and anthropogenic emissions to the tall tower isoprene and MVK+MACR measurements. First, ambient PTR-MS observations are compared with concurrent speciated measurements by cartridge-GC-MS/FID. Figure 4.2 shows that the two measurements agree to within their combined uncertainties (~20%), for both isoprene and MVK+MACR, and for both daytime and nighttime measurements.

In the second approach, we use the source tracer technique described by Hu et al. (2011), which had an estimated uncertainty of ±30% when applied to methanol. Here we use C_8 and C_9 aromatic VOCs as anthropogenic tracers, since their atmospheric lifetimes are comparable to those of isoprene and MVK+MACR (i.e., on the order of hours). We employ wintertime (December - February) measurements to derive anthropogenic enhancement ratios for isoprene and MVK+MACR relative to C_8 aromatics and C_9 aromatics (Table 3), under the assumption that biogenic influences at this time are negligible. We then assume that the same enhancement ratios can be employed year-round to quantify the non-biogenic signal at m/z 69 and m/z 71.

Figure 4.3 shows the resulting year-round anthropogenic contributions to the measured m/z 69 and m/z 71 signals at the KCMP tall tower, as well as their summertime diurnal cycles. Applying either C_8 or C_9 aromatics as the anthropogenic tracer yields results that in general agree to within 10%.

Based on this approach, we find that the non-biogenic contribution to the m/z 69 signal measured at the KCMP tall tower averages 22% (95% confidence interval: 18%-26%) during summer daytime (June – August, 10:00-17:00 CST), and 31% over the whole summer (Figure 4.3). It contributes up to 80% of the observed m/z 69 signal during the night and early morning, when anthropogenic emissions can accumulate in the shallow boundary layer. The absolute anthropogenic contribution is consistently between 30-46 pptv, close to the PTR-MS detection limit for isoprene (38 pptv). The anthropogenic contribution to the m/z 71 signal abundance is smaller (19-26 pptv): amounting to only 7% of the total during summer daytime and 8% over the whole summer (Figure 4.3).

The comparisons between the PTR-MS and the cartridge-GC-MS/FID measurements of isoprene and MVK+MACR shown in Figure 4.2 do not show any evidence of a high bias for the PTR-MS, even during nighttime. This suggests that the non-biogenic component inferred above may be predominately due to anthropogenic isoprene (and MVK+MACR)

as opposed to interfering isobaric compounds. In the following sections, we subtract the anthropogenic contributions to the observed m/z 69 and m/z 71 signals, and treat the residuals as biogenic isoprene and MVK+MACR, respectively.

4.4 Isoprene and its oxidation products in the US Upper Midwest

Figure 4.4 shows daytime average (10:00-17:00 CST) isoprene and MVK+MACR mixing ratios, and surface air temperature measured at the KCMP tall tower during 2011. Figure 4.5 plots the daytime average measurements of isoprene, MVK+MACR, ratio of isoprene/(MVK+MACR), and the calculated gamma γ_T based on the equation (4.1) for the growing season only.

Pronounced seasonal cycles are seen for isoprene and MVK+MACR, with elevated mixing ratios during the May-September growing season, that reached maxima of 2540 pptv (isoprene) and 2790 pptv (MVK+MACR). Onset of isoprene emission began around May 30 (day of year 251) in the vicinity of the KCMP tall tower, when the average daytime air temperature reached 27 °C; for the most part it then remained above 20 °C throughout the ensuing summer. The observed mixing ratios of isoprene and its oxidation products then decreased rapidly in mid-September once daytime temperature dropped below 20 °C (at which point γ_T dropped to almost zero; Figure 4.5). This timing of the annual cycle course is consistent with that observed at Harvard forest (June 1 to September 7), a site at a similar latitude as our tower, reflecting the concurrent drivers of plant phenology and associated temperature changes on the seasonal course of isoprene emissions (e.g., Goldstein et al., 1998)

Figure 4.6 shows the average summertime diurnal cycles for isoprene, MVK+MACR, the isoprene/(MVK+MACR) ratio, C_8 aromatics, and surface air temperature as a function of wind direction at the KCMP tall tower. A noteable feature in these polar annulus plots is that elevated isoprene and MVK+MACR mixing ratios are frequently observed at night

with winds from the northeast and east. Mixing ratios for athropogenic tracers such as the C_8 aromatics are also enhanced at night in the shallow nocturnal boundary layer (Figure 4.6), but these exhibit a different diurnal cycle tied to morning and evening rush hours, and are most strongly associated with a distinct wind direction (i.e., winds from the north transporting pollution from the Twin Cities). The fact that the nighttime enhancements of MVK+MACR originate from a wider swath of wind direction and persist for longer periods of time than those of isoprene imply that they are result from biogenic sources somewhat distant from the tall tower. This is consistent with the extensive broadleaf tree cover to the north and east of the KCMP tall tower (Figure 4.1). Such transport of isoprene and its oxidation products into the Twin Cities area at night will drive nighttime chemistry involving NO_3 and O_3 and likely the formation of gas- and aerosol-phase nitrates (Brown et al., 2013).

We see in Figure 4.6 that hot conditions and daytime isoprene enhancements tend to be associated with winds from the southwest, indicating nearby emissions in this direction. Under these conditions, the isoprene/(MVK+MACR) ratio is relatively high ($\geq$ 1), indicating an approximate transport time less than one isoprene lifetime (e.g., < 27 km at an assuming average wind speed of 5 m/s and an 82 min isoprene lifetime). On the other hand, the mean isoprene/(MVK+MACR) ratio from other wind directions (170°-280°) is only 0.30 (Figure 4.5 and left panel of Figure 4.7), indicating more regional aged emission with aggregate effective transport of ~50 km.

4.5 Model underprediction of regional isoprene emissions

Initial model:observation comparisons revealed a dramatic low model bias when using CLM4 land cover to drive biogenic emissions in MEGANv2.1: a factor of 6.0 for isoprene, and 5.4 for MVK+MACR during daytime (10:00-17:00 CST) in summer 2011. When using the higher-resolution USDA NASS land cover, these model biases are reduced by one-half to one-third (to factors of 2.7 and 3.5, respectively). The simulated isoprene emissions are thus extremely sensitive to the selection of land cover for this

region: in this transitional landscape with ~5-15% broadleaf tree cover, a small absolute error in the estimated PFT fractions can lead to a large discrepancy in the simulated isoprene emissions and abundance (Figure 4.1 and Table 4.2).

In addition, Figure 4.1 shows that the KCMP tall tower is located near the intersection of four model grid cells, with the adjoining three cells having more than twice the broadleaf tree coverage of the cell containing the tower (>11% versus 5%) according to CLM4 (Figure 4.1). This type of representation error is dependent on the model resolution, and is a particular issue for short-lived tracers such as isoprene and MVK+MACR. To minimize its effect here, we use inverse distance-weighted mixing ratios for the model:observation comparisons below. Specifically (and unless indicated otherwise), the simulated mixing ratios at the tall tower are taken as the mean from the four intersecting grid cells, with each value weighted by the inverse distance between the center of that grid cell and the tall tower. The average low biases in the base model for summer daytime are then reduced to factors of 2.4 (1.8 when using NASS) for isoprene and 2.6 (2.3 when using NASS) for MVK+MACR relative to the KCMP tall tower observations.

Figure 4.4 shows the resulting simulated isoprene and MVK+MACR mixing ratios in the base simulations using CLM4 vegetation cover (red; daily 10:00-17:00 CST averages), along with the assimilated surface air temperature that is used to compute the BVOC fluxes within MEGANv2.1. We see that the base model captures the seasonal cycle for isoprene and its oxidation products, including the timing of the onset and shutdown of isoprene fluxes in the spring and fall. For most of the growing season, there is little bias in the modeled isoprene mixing ratios (Figure 4.5). However, the model cannot reproduce the periodic large enhancements seen in the observations; the low model bias during these events is associated with a corresponding low bias in the GEOS-5.2 temperature (and therefore γ_T; Eq. 4.1) that manifests during these same periods (Figure 4.5). On the other hand, the low bias in the simulated MVK+MACR mixing ratios shows little to no correlation with γ_T (Figure 4.5).

We next compare the hourly simulated and observed isoprene and MVK+MACR mixing ratios as a function of wind direction (Figure 4.8). When the wind is not out of the southwest (wind directions other than 170°-280°), the simulated isoprene mixing ratios show only a small bias compared to the observations (-18%; 95% confidence interval: 10%-26%), which can be explained by a similar bias level in the assimilated temperatures used in GEOS-Chem: the simulated γ_T values are 18% (95% CI: 15%-22%) too low based on the observed surface temperatures at the KCMP tall tower. On the other hand, when the wind is out of the southwest (170°-280°; black), the simulated isoprene mixing ratios show a significant low bias compared to the observations (-70%; 95% CI: 64%-73%). The low bias in the assimilated temperatures (-40% under these conditions; 95% CI: 35%-45%) is a main driver of this discrepancy. In addition, as discussed in Section 4.4, there is clearly a distinct source region to the southwest of our tall tower that is within one isoprene e-folding distance (and therefore within one model grid cell), This type of near-field effect cannot be captured at the ~ 50 km × 50 km resolution of our simulation (Figure 4.7).

Model:observation comparisons for MVK+MACR are more stable than is the case for isoprene, and do not vary significantly with wind direction: on average, the simulated MVK+MACR mixing ratios are 61% (56%-67%) lower than the KCMP tall tower observations. Below, we test the robustness of the above comparisons to a variety of model assumptions, and assess what conclusions can be drawn regarding the emissions and impact of isoprene in this region.

To this end, we repeat the above model:observation comparisons while varying key model parameters to test how the results vary under differing model treatments for chemistry (including versus excluding bromine chemistry; varying the reactive uptake coefficients for HO_2 on aqueous aerosol), land cover (CLM4 versus USDA-NASS), boundary layer mixing (local versus nonlocal schemes; Lin and McElroy, 2010), and varying NO_x and isoprene emissions (Figure 4.9). We exclude for this purpose periods

with southwesterly winds due to the associated bias in the assimilated surface temperature.

We find that the isoprene bias in the model is not significant when one considers the sensitivity of the simulated mixing ratios to the various model assumptions (Figure 4.9): model:observation slopes range from 0.42 – 1.53 across different configurations for chemistry, mixing, and land cover. On the other hand, model biases for MVK+MACR (25%-66%) are larger than those for isoprene, and are robust across our ensemble of sensitivity runs (Figure 4.9). Because MVK and MACR are *i*) longer-lived than isoprene, *ii*) produced throughout the atmospheric mixing layer rather than emitted at the surface, and *iii*) somewhat chemically buffered (their source as well as their main sink is photochemical), their simulated abundance is much less sensitive to specific model assumptions regarding mixing, chemistry, and fine-scale land cover.

Taken as a whole, the above findings (persistent low model bias for MVK+MACR but not for isoprene) suggest a general underestimate of isoprene emissions in the broader region, but not necessarily in the immediate vicinity of the tower. This is consistent with the fact that the predominant isoprene emitters are concentrated 50 km or more from the tower (Figure 4.1) and with the aged nature of the biogenic mixture reaching the site (Section 4.4). An alternative explanation for the low model MVK+MACR would be an OH overestimate for this area. Arguing against the latter as the sole explanation is the fact that a sensitivity run with NO_x emissions decreased by 50% did not come close to resolving the discrepancy (Figure 4.9). This suggests that a major bias in model OH would be required to reconcile the observed and simulated MVK+MACR abundance, and this type of bias is not evident from a previous analysis of benzene:toluene ratios at this site (Chapter 5).

4.6 Seasonal NO_x-VOC photochemical transition as controlled by isoprene emissions

It is well known that isoprene and other biogenic VOCs plays a key role in ozone formation (e.g., National Research Council, 1991; Jacob et al., 1995; Fiore et al., 2005). Here we use the GEOS-Chem simulation driven by USDA NASS land cover, which shows reasonable agreement with the KCMP tall tower isoprene observations (though still underestimating MVK+MACR; Figure 4.9), to examine the role of isoprene emissions in shifting between NO_x- and VOC-limited chemical regimes during the vernal and autumnal seasonal transitions in the US Upper Midwest.

The sensitivity of ozone production to isoprene emissions depends on NO_x (e.g., Fiore et al., 2005), which was not measured at the KCMP tall tower. However, we find that the simulated summer daytime NO_2 mixing ratios (computed from the four intersecting grid cells in the same way as for isoprene and MVK+MACR) based on NEI05 emissions are comparable to those measured at a nearby EPA monitoring site (Site Number 423, ~6 km north of the tall tower; EPA, 2011), particularly when one considers the known tendency of this type of analyzer (chemiluminescence with molybdenum converter) to overestimate NO_2 (Dunlea et al., 2007; Steinbacher et al., 2007; Lamsal et al., 2008; Boersma et al., 2009): the corresponding NO_2 mixing ratios are 1.5 ± 0.7 ppbv in the model versus 2.2 ± 3.0 ppbv as reported by the EPA (mean ± standard deviation).

We use loss of HO_x radicals via self-reaction (L_{HOx}, where $HO_x = OH + HO_2 + \Sigma RO_2$) relative to the loss of NO_x radicals (L_{NOx}, where where $NO_x = NO + NO_2 + NO_3 + HONO$) as an indicator for NO_x- versus VOC-limited O_3 chemistry (Sillman et al., 1990; Kleinman, 1994). The transition between NO_x-and-VOC-limited regimes can be defined as the point when $L_{HOx}/L_{NOx} = 1$ (Duncan et al., 2010). When $L_{HOx}/L_{NOx} > 1$, HO_x radicals tend to react with themselves rather than with NO_x, so that peroxide formation is the main HO_x sink. Under this condition, production of O_3 is limited by the availability of atmospheric NO_x, but is insensitive to moderate changes in VOC abundance (the so

called NO_x-limited regime). When $L_{HOx}/L_{NOx} < 1$, loss of atmospheric HO_x occurs predominantly through reaction with NO_x, and O_3 production becomes linearly dependent on the VOC abundance but inversely proportional to NO_x (the so called VOC-limited regime).

Figure 4.10 shows the simulated monthly mean (daytime 10:00-17:00 CST) L_{HOx}/L_{NOx} ratios and isoprene emissions in the region surrounding the tall tower from April to September 2011. As temperatures rise during summer, isoprene fluxes increase (Figure 4.4, 4.10), and drive a pronounced seasonal shift from a springtime VOC-limited regime ($L_{HOx}/L_{NOx} < 1$) to summertime NO_x-limited conditions ($L_{HOx}/L_{NOx} \geq 1$) towards the northeast and transitional conditions ($L_{HOx}/L_{NOx} \sim 1$) elsewhere in this region. This is then followed by a general switch back to VOC-limited conditions in fall, when air temperature drops, leaves begin to senesce, and isoprene emissions decrease dramatically (Figure 4.4, 4.10). We also see significant spatial gradients in these chemical regime shifts, reflecting the heterogeneous land cover and isoprene fluxes in this transitional region (Figure 4.1, 4.10). The underestimated isoprene fluxes for this area indicated by the low model bias in MVK+MACR (Section 4.5) would imply a more NO_x-limited situation than is portrayed in Figure 4.10. However, regardless of the changing seasons, the Twin Cities urban core remains VOC-limited in the model due to high local NO_x emissions.

Previously, Jacob et al. (1995) has suggested that the seasonal transition from NO_x-limited to VOCs- limited regime should occur during September in the eastern United States. We here show that such seasonal photochemical regime transition also exists in the US Upper Midwest. Furthermore, we see here the NO_x- and VOC-limited chemical regimes can vary not only seasonally (from summer to fall, and from spring to summer) but also spatially, as controlled by the timing and the spatial distribution of isoprene emissions. We expect this to be a general phenomenon in other regions as well, especially in those locations where isoprene emissions show considerable spatial variability. The

seasonal and spatial transition for photochemical regimes have important implications for designing effective O_3 control strategies for different regions and for different seasons. NO_x emission controls will become increasingly effective for controlling ozone in this region, as the domestic NO_x emissions are declining (e.g., McDonald et al., 2013; de Gouw et al., 2014).

4.7 Conclusions

We presented a full year of continuous in-situ measurements of isoprene and its oxidation products (MVK+MACR) from the KCMP tall tower, a site lying at the ecological transition between isoprene-emitting deciduous forest to the north and east and predominantly non-isoprene-emitting agricultural landscapes to the west and south. Based on an intercomparison with cartridge measurements and a source-tracer analysis, we find that anthropogenic compounds (likely isoprene itself) make a non-negligible contribution to the m/z 69 signal measured by PTR-MS at this site (20% during summer daytime). Conversely, the anthropogenic contribution to the MVK+MACR signal at m/z 71 is small (7% during summer). We find isoprene mixing ratios simulate by the GEOS-Chem CTM model on the MEGANv2.1 biogenic inventory have no significant bias compared to the tall tower observations once model uncertainties related to chemistry, atmospheric mixing, and land cover are taken into count. On the other hand, a persistent low model bias (25-66%) in MVK+MACR across a variety of model assumptions and configurations suggests that isoprene emissions in the broader region (but not necessarily in the immediate vicinity of the tall tower) are underestimated. This inference is consistent with the fact that the predominate isoprene emitters are concentrated 50 km or more from the tower, and also with the photochemically aged nature of the biogenic mixture that reaches the tower.

We find that isoprene fluxes drive a widespread seasonal shift in this region between VOC-limited chemistry during spring and fall, and NO_x-limited or transitional conditions during summer. There are major gradients in these shifts, reflecting heterogeneous land

cover and isoprene fluxes in this transitional region. The chemical role that isoprene plays in this area is likely still underestimated in the model due to the inferred underprediction of emissions. Based on our model simulations, much of the region surrounding the Twin Cities (outside of the consistently VOC-limited urban core itself) is close to transition between NO_x- and VOC-limited conditions during summer. Continued NO_x emission reductions should therefore become more effective at controlling ozone as this area shifts to a more NO_x-limited regime.

The 0.5°×0.667° nested GEOS-Chem model and the MEGANv2.1 biogenic inventory demonstrate significant skill at simulating the abundance of isoprene and its oxidation products MVK+MACR, despite their short atmospheric lifetimes. However, appreciable uncertainties remain due to model resolution limitations as well as errors in land cover and meteorological input data. BVOC emission estimates have improved dramatically since the first inventories were developed 2-3 decades ago (e.g., Lamb et al., 1987; Müller, 1992; Guenther et al., 1995). At this point, development of high resolution, validated land cover data and more accurate meteorological fields is a key need for additional future improvement. Observational studies exploiting aircraft eddy covariance measurements, tall tower platforms, and satellite measurements are also needed to provide regional-scale constraints on isoprene fluxes and the subsequent atmospheric effects.

Table 4.1. Mixing ratios of the VOC calibration standards over the course of the study period relative to the original certified values.

Units: ppbv

	Original	Cartridge-GC-MS/FID				Reanalysis
Date	12/2008	12/2010	04/2011	04/2011	07/2011	01/2012
Isoprene	50	+4%	+0%	+2%	+2%	+6%
MACR	178	-35%	-37%	-37%	-	-37%
MVK	150	-87%	-87%	-86%	-91%	-91%

Table 4.2. Fractional coverage of plant function types (PFTs) for the GEOS-Chem model grid cell containing the KCMP tall tower, according to the CLM4 (Oleson et al., 2010) and USDA NASS (USDA-NASS, 2007) land cover datasets. Also shown is the isoprene base emission factor for each PFTs according to MEGANv2.1 (Guenther et al., 2012).

	Barren	Crop	Developed	Deciduous	Evergreen	Shrub	Grass	Sum	AEF[1]
EF[2] ($ug/m^2/h$)	0	1	0	10000	600	4000	800	%	($ug/m^2/h$)
USDA NASS (%)	0.18	50.49	15.52	12.19	0.04	1	20.61	100	1425
CLM4 (%)	0.03	58.81	-	5.14	0.64	-	31.30	95.92	769

[1] AEF: annual emission factor calculated as the sum of products of the PFT fractional coverage and the corresponding emission factor.

[2] EF: isoprene base emission factor.

Table 4.3. Correlation between C_8-C_9 aromatics and observed signals at m/z 69 and m/z 71 during winter (December-February)

	C_8 aromatics		C_9 aromatics		
	Slope	*R*	Slope	*R*	N
Isoprene (m/z 69)	0.33	0.82	0.89	0.79	1590
MVK+MACR (m/z 71)	0.22	0.69	0.59	0.67	1590

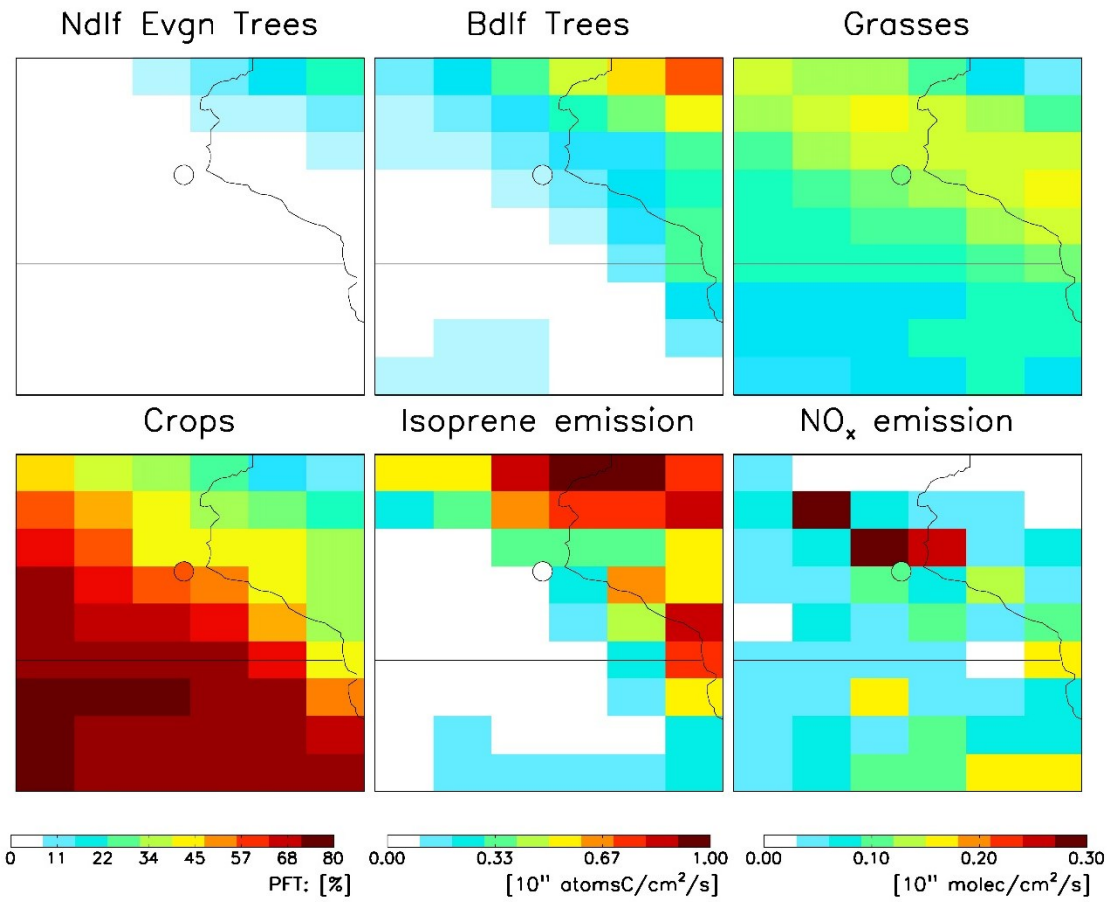

Figure 4.1. Fractional distribution of major plant functional types in the US Upper Midwest, according to CLM4 (year-2005; Oleson et al., 2010). Ndlf Evgn Trees: needleleaf evergreen trees; Bdlf Trees: broadleaf trees; grasses, and crops. Also shown are the simulated isoprene emissions and NO_x emissions (summer mean) for 2011. See text for details. The location of the KCMP tall tower is indicated by the filled circle.

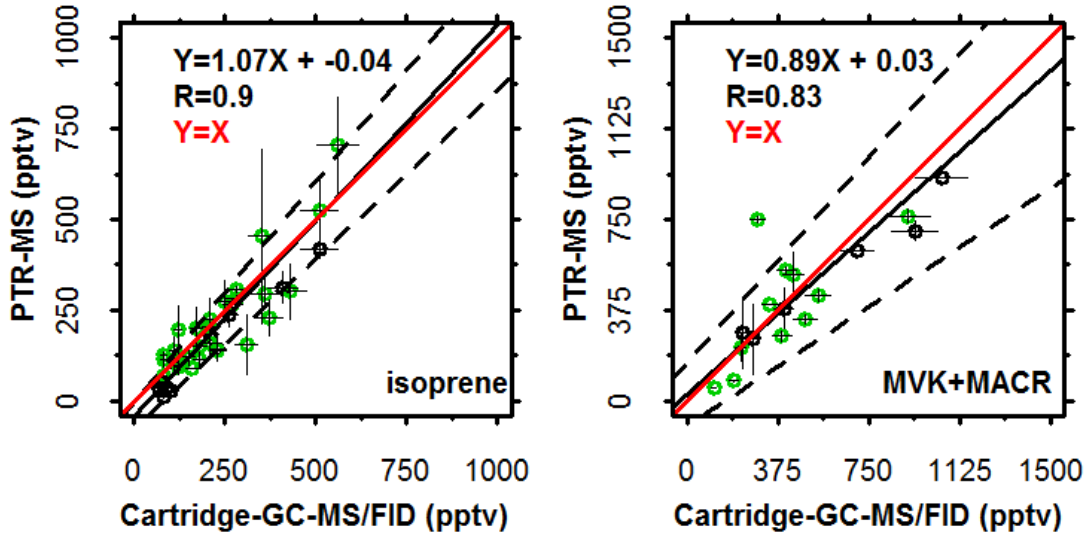

Figure 4.2. Intercomparison between PTR-MS and cartridge-GC-MS/FID measurements at the KCMP tall tower. Left panel: PTR-MS measurements at m/z 69 versus isoprene as measured by cartridge-GC-MS/FID (December 2010 to August 2012). Right panel: PTR-MS measurements at m/z 71 versus MVK+MACR as measured by cartridge-GC-MS/FID (July-August 2012). Data points are colored to indicate daytime (green dots) versus nighttime (black dots) measurements. Black solid lines show the best fit from a major axis regression, with parameters given inset. Dashed lines show the 95% confidence interval for the best fit. The 1:1 line is shown in red. Error bars indicate the 95% confidence interval for each measurement.

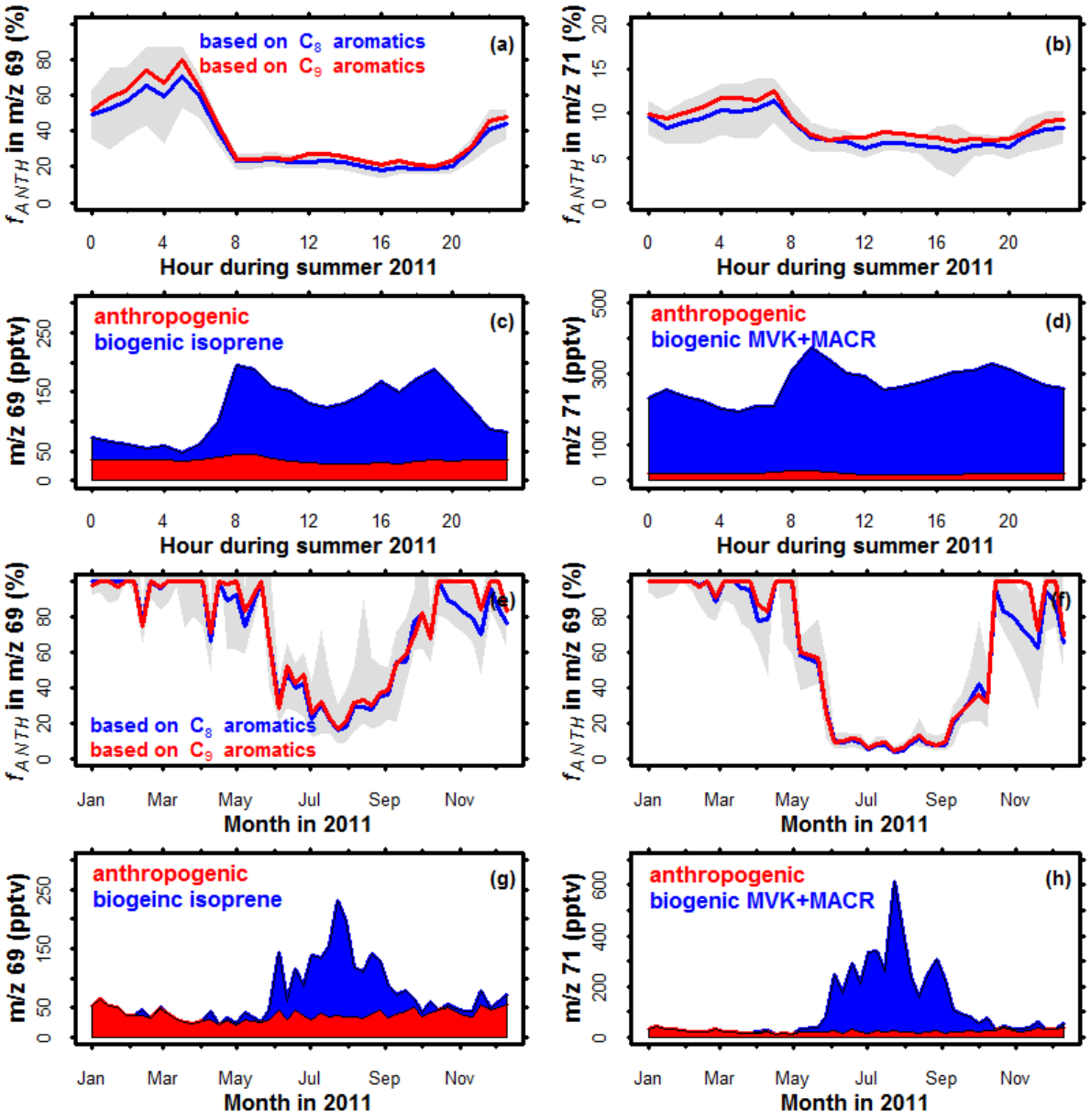

Figure 4.3. Anthropogenic and biogenic contributions to the m/z 69 and m/z 71 signals measured by PTR-MS at the KCMP tall tower during 2011. 1st row: diurnal contributions (hourly median) of anthropogenic sources to the m/z 69 and m/z 71 signals during summer 2011, estimated using different anthropogenic tracers (blue: C_8 aromatics; red:

C_9 aromatics). Shaded areas represent the 95% confidence interval of estimates using C_8 aromatics. 2nd row: stack plots of the diurnal biogenic and anthropogenic contributions to the m/z 69 and m/z 71 signal during summer 2011, estimated using C_8 aromatics as the anthropogenic tracer (hourly median). 3rd and 4th rows: same as the 1st and 2nd rows, except showing the seasonal anthropogenic and biogenic contributions (based on weekly medians).

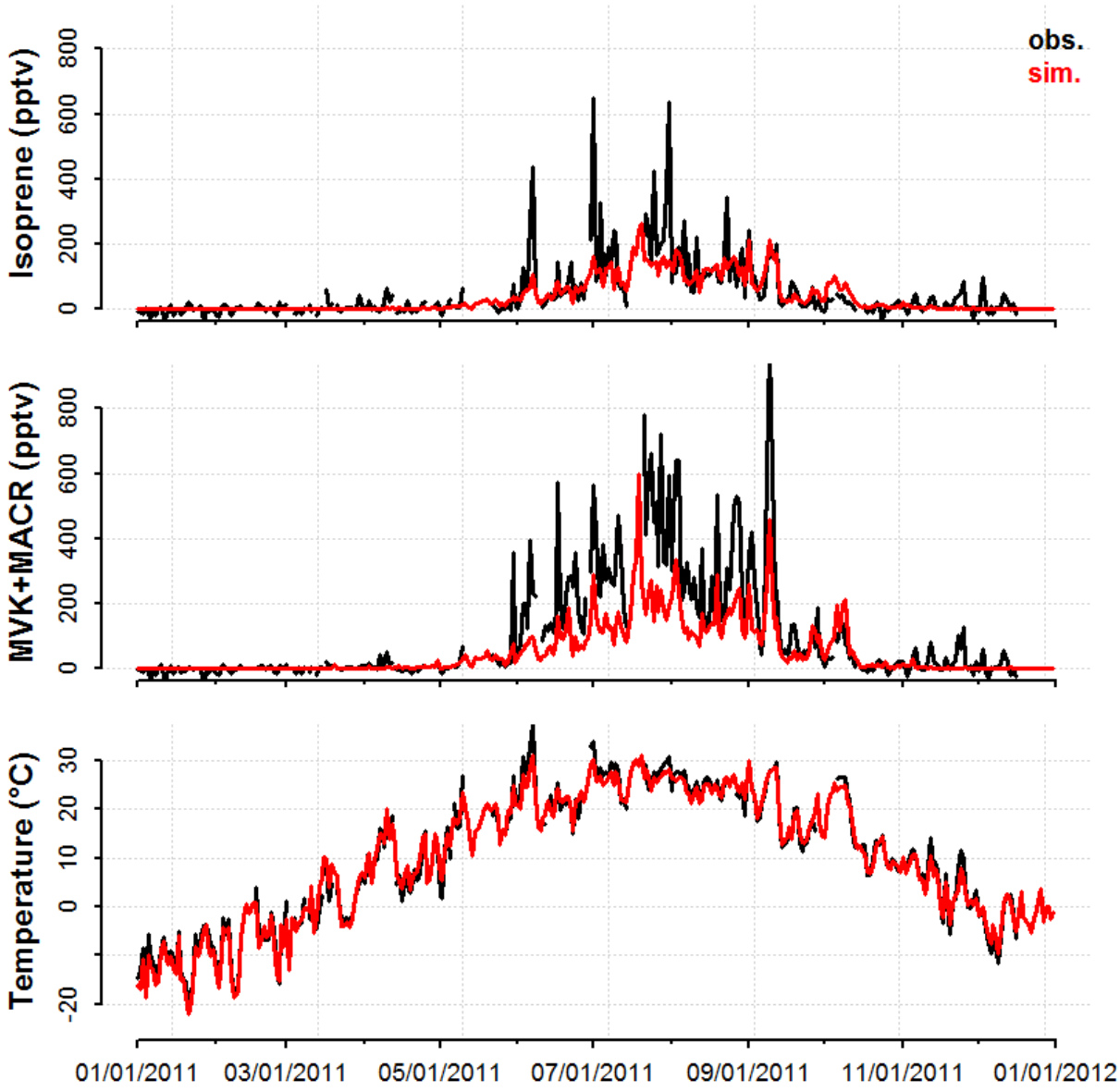

Figure 4.4. Annual cycle of biogenic isoprene and MVK+MACR mixing ratios and air temperature measured at the KCMP tall tower in 2011 (black; daytime averages for 10:00-17:00 CST). Anthropogenic contributions to the m/z 69 and m/z 71 signals have been removed as described in the text. Also shown are the isoprene and MVK+MACR mixing ratios simulated by GEOS-Chem (using CLM4 vegetation), and the assimilated 2 m air temperatures used to drive the model (red).

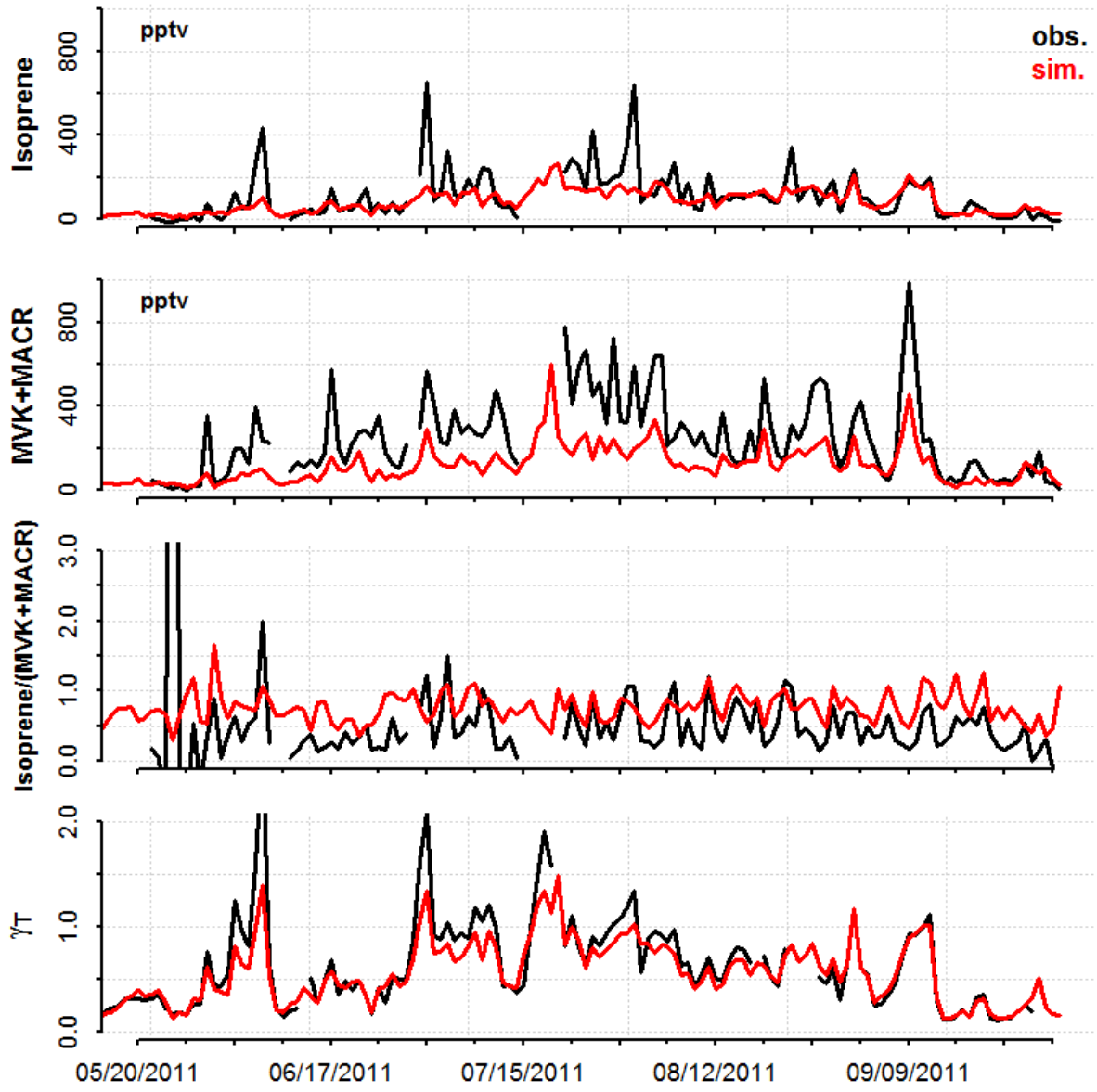

Figure 4.5. Daytime (10:00 - 17:00 CST) average isoprene, MVK+MACR, isoprene/(MVK+MACR), and γ_T values at the KCMP tall tower during the growing season (May 20, 2011 to September 31, 2011). Measurements (in black) are compared to the corresponding simulated values from GEOS-Chem using CLM4 land cover (in red).

Anthropogenic contributions to the measured isoprene and MVK+MACR mixing ratios have been removed as described in the text.

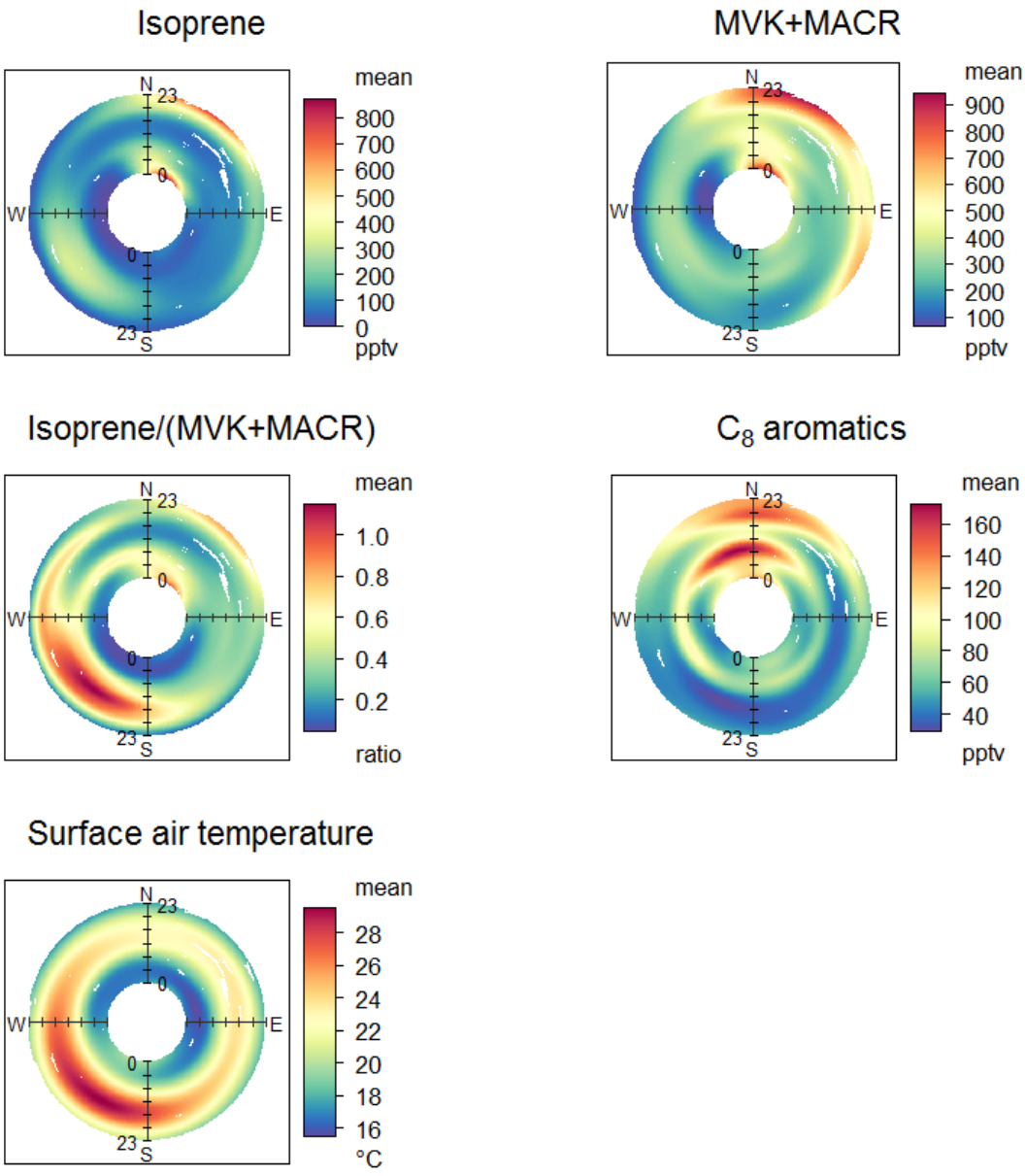

Figure 4.6. Diurnal cycle as a function of wind direction for isoprene, MVK+MACR, the isoprene/(MVK+MACR) ratio, C_8 aromatics, and surface air temperature as measured during summer 2011 at the KCMP tall tower. Plots mad using the open source R package openair (Carslaw and Ropkins, 2012).

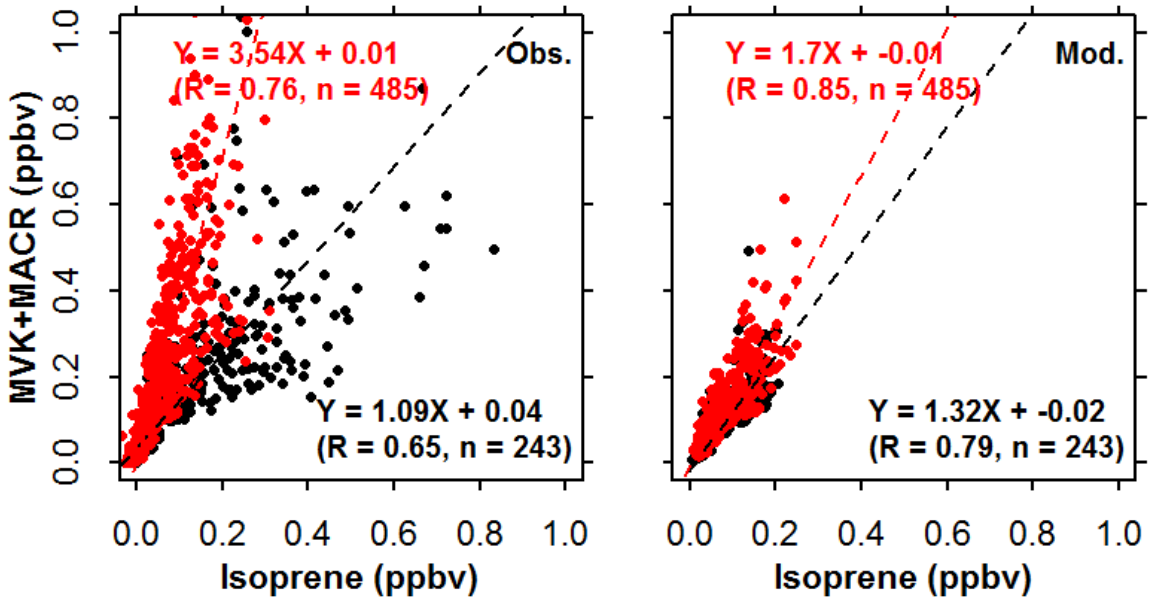

Figure 4.7. Correlation between MVK+MACR and isoprene mixing ratios during summer daytime (10:00-17:00 CST) as measured at the KCMP tall tower (left) and simulated by GEOS-Chem using CLM4 land cover (right). Data are colored according wind direction: black dots indicate southwesterly wind (170°- 280°) and red dots indicate all other wind directions, Dotted lines show the major axis regression best fit lines for the corresponding data subsets, with parameters given inset.

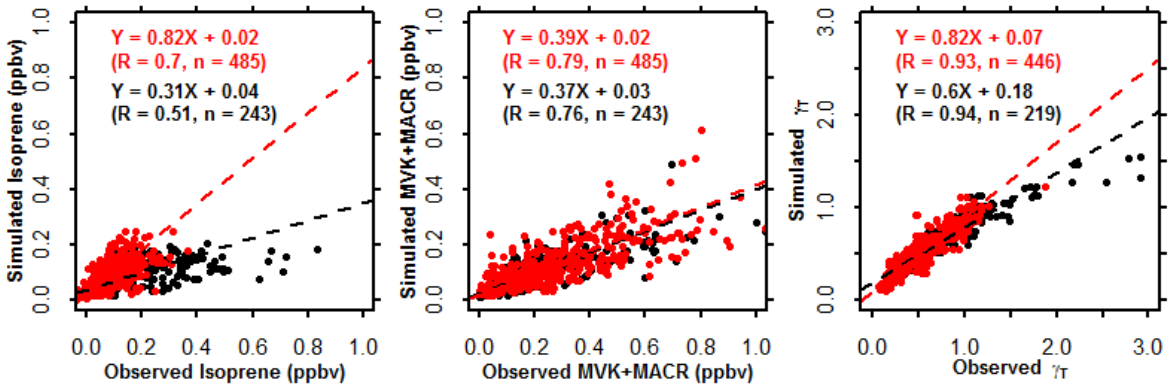

Figure 4.8. Model:measurement comparisons at the KCMP tall tower during summer daytime (10:00-17:00 CST). Measured mixing ratios of isoprene and MVK+MACR, and γ_T values computed based on the observed temperatures, are compared to the simulated values from GEOS-Chem using CLM4 land cover. Data are colored by wind direction, with black dots indicating southwesterly winds (170°- 280°) and red dots indicating all other wind directions. Dotted lines show the major axis regression best fits for the corresponding data subsets, with parameters given inset.

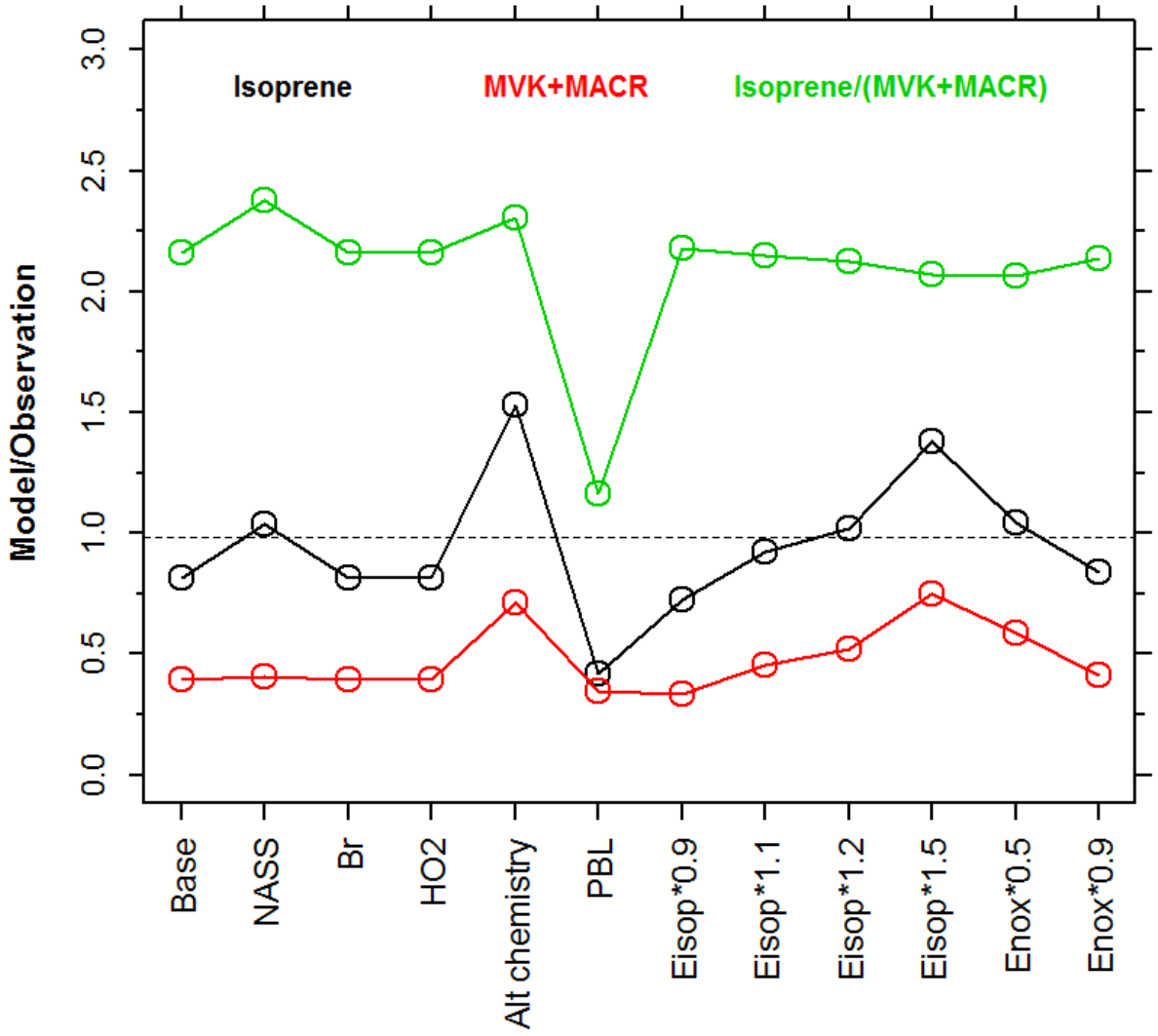

Figure 4.9. Model/measurement agreement for isoprene (black), MVK+MACR (red), and the isoprene/(MVK+MACR) ratio (green) across an ensemble of sensitivity simulations using GEOS-Chem and MEGANv2.1. Values shown are model:measurement slopes from a major axis regressions (in the case of isoprene and MVK+MACR) or the median mdoel:measurement ratio (in the case of isoprene/(MVK+MACR)) for daytime (10:00 – 17:00 CST) during the 2011 growing season. Periods with southwesterly winds have

been excluded (see text). The black dotted line shows the average model/measurement ratio for γ_T over the same time interval. *Base*: simulation using CLM4 vegetation, with the model values taken as an inverse distance-weighted mean of the 4 intersecting grid cells as described in Section 4.5. *NASS*: same as *Base* except using USDA NASS land cover (USDA-NASS, 2007). *Br*: same as *Base*, except including bromine chemistry, which modifies the model oxidant fields (Parrella et al., 2012). *HO2*: same as *Base*, except using a reactive uptake coefficient for HO_2 on aqueous aerosols of 0.4 rather than 0.2 (Mao et al., 2013). *Alt chemistry*: previous model representation of isoprene chemistry (Palmer et al., 2006; Millet et al., 2008). *PBL*: using a local rather than a non-local scheme for boundary layer mixing in the model (Lin and McElroy, 2010). *Eisop*x.x*: isoprene emissions multiplied by a factor of x.x. *Enox*x.x*: NO_x emissions multiplied by x.x.

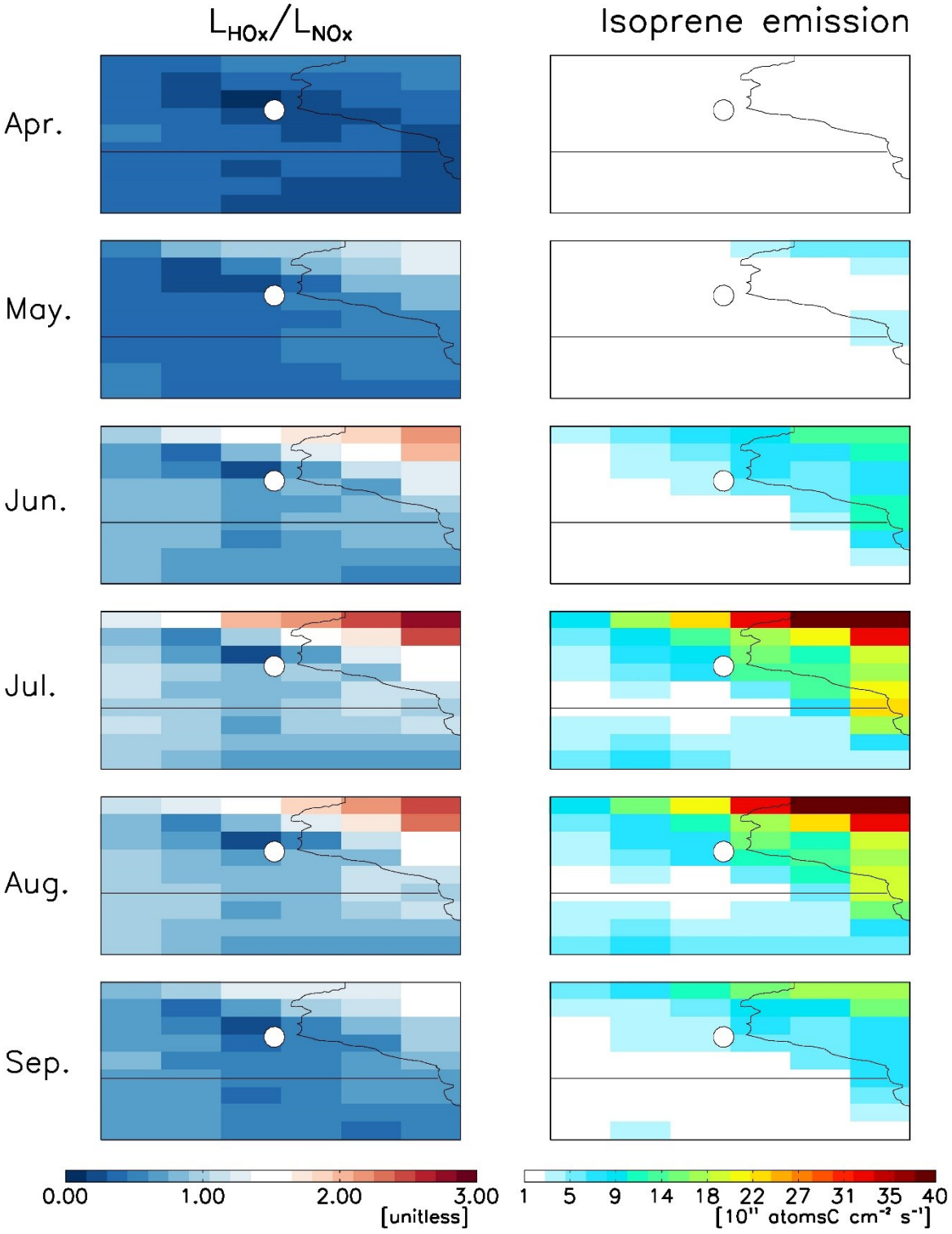
L_{HOx}/L_{NOx}
Isoprene emission
Apr.
May.
Jun.
Jul.
Aug.
Sep.
0.00
1.00
2.00
3.00
[unitless]
1
5
9
14
18
22
27
31
35
40
[10^{11} atomsC cm^{-2} s^{-1}]

Figure 4.10. Seasonal evolution of NO_x- versus VOC-limited ozone chemistry in the region surrounding the KCMP tall tower, as simulated by GEOS-Chem. Plotted are the monthly mean daytime (10:00-17:00 CST) L_{HOx} /L_{NOx} ratios and isoprene emissions based on the USDA NASS land over dataset (USDA-NASS, 2007). See text for details.

5 Emissions of C_6-C_8 aromatic compounds in the United States: Constraints from tall tower and aircraft measurements

Abstract

We present two full years (2010-2011) of continuous C_6 (benzene), C_7 (toluene) and C_8 (ethylbenzene + m-, o-, and p-xylene) aromatic compounds measurements by PTR-MS at the University of Minnesota tall tower Tracer Gas Observatory (KCMP tall tower, 244 m a.g.l.). We employ a 0.5° ×0.667° GEOS-Chem nested grid simulation in a Bayesian inverse framework to interpret the tall tower data in terms of the constraints they provide on emission sources of C_6-C_8 aromatics. We then apply independent measurements from six recent aircraft campaigns across the contiguous US to assess the degree to which our findings appear to be nationally representative. Based on the tall tower data we find that the RETRO (REanalysis of the TROpospheric chemical composition) global emission inventory, constructed for year-2000, significantly overestimates US aromatic emissions by as factors of 2.0 [1.4-3.5], 4.5 [3.3-7.1], and 2.4 [1.5-5.0] for benzene, toluene, and C_8 aromatics during 2010-2011. Likewise, the US EPA's NEI08, scaled to 2010 and 2011, overestimates the toluene flux by a factor of 3.1 [2.3-4.9], reflecting an inventory bias in non-road emissions in the inventory and a lumped speciation in our implementation. Our annual top-down emission estimates for benzene and C_8 aromatics derived from the tall tower measurements agree with the bottom-up values from the EPA's NEI08, as does the inferred contribution from non-road sources. However, the NEI08 appears to underestimate on-road emissions of these compounds by a factor of 2 during the warm season (April – October). We find also that C_6-C_8 aromatic sources upwind of North America, manifested as the boundary condition for the nested model domain, are more than double the prior estimate. This may reflect a substantial underestimate of aromatic sources in East Asia (by a factor >2 relative to RETRO). Long-range transport exerts an important influence on the abundance of aromatics over the US: up to 60% of observed benzene mixing ratios (up to 20% for toluene and 15% for C_8 aromatics) during winter in

the US Upper Midwest can be attributed to sources outside North America. Independent aircraft measurements suggest that the inventory biases found here for C_6-C_8 aromatics based on data in the Upper Midwest also apply to other parts of the contiguous US, with notable exceptions for toluene in California and Houston, Texas; there, the prior bottom-up estimate appears to be more accurate. Our best-estimates for aromatic emissions are 206 GgC for benzene, 310 GgC for toluene, and 822 GgC for C_8 aromatic compounds over the contiguous US for 2011.

5.1 Introduction

Aromatic volatile organic compounds (VOCs) such as benzene (C_6H_6), toluene (C_7H_8), xylenes (C_8H_{10}; including o-, m-, p- isomers), and ethylbenzene (also C_8H_{10}) are ubiquitous in the atmosphere and are important anthropogenic precursors of secondary organic aerosol (Johnson et al., 2005; Martín-Reviejo and Wirtz, 2005; Ng et al., 2007; Henze et al., 2008), peroxy acetyl nitrate (PAN) (Liu et al., 2010), and, to a lesser degree, ground-level ozone (Xue et al., 2013; Jaars et al., 2014). These aromatic VOCs (so-called BTEX compounds) are categorized as hazardous air pollutants (HAPs) under the US Clean Air Act Amendments of 1990 (EPA, 1990), as they are known or suspected to cause serious health effects. For instance, benzene is classified as a Group 1 carcinogen by the International Agency for Research on Cancer (Baan et al., 2009). Despite their importance, emissions of aromatic compounds remain poorly quantified. In this work, we present two years of continuous aromatic VOC measurements from a tall tower in the Upper Midwest of the United States. We apply a nested chemical transport model (GEOS-Chem CTM) to interpret these data along with an ensemble of recent aircraft observations, in terms of the constraints they imply for US sources of C_6-C_8 aromatic compounds.

Atmospheric C_6-C_8 aromatic compounds mainly originate from primary anthropogenic sources, including vehicular emissions (on-road and off-road) associated with the incomplete combustion and evaporation of fuel, stationary sources such as industrial

surface coating and solvent use, gas stations, refineries, power plants, and waste treatment facilities (Singh et al., 1985; Kaiser et al., 1992; Harley et al., 2006; Karl et al., 2009), and from biomass burning (Andreae and Merlet, 2001). The atmospheric removal of C_6-C_8 aromatic compounds is almost exclusively through oxidation by OH, resulting in atmospheric lifetimes of about 10 days for benzene, 2 days for toluene, and 1 day or less for ethylbenzene and xylenes (at OH = 10^6 molec cm^{-3}) (IUPAC, 2013).

Recent top-down studies imply the presence of large uncertainties in current bottom-up emission estimates for C_6-C_8 aromatic compounds. For instance, Fortin et al. (2005) applied ambient benzene:acetylene ratios from a variety to field experiments to infer a 56% drop in US benzene emissions between 1994 and 2003. This finding contradicted available bottom-up information from the EPA's National Emission Inventory (NEI99), which predicted benzene:acetylene emission ratios 3-4× higher than could be reconciled with atmospheric data (Parrish, 2006). Evidence from tall tower, automobile (Pétron et al., 2012), and aircraft-based observations (Pétron et al., 2014) suggested that benzene sources from oil and gas operations in northeastern Colorado are underestimated in the state emission inventory (Bar-Ilan et al., 2008; CDPHE, 2008) by at least as a factor of 6, though likely with much greater uncertainty as argued by Levi, 2012; Levi, 2013. On the other hand, Warneke et al (2007) found that their model simulation for 2004 based on the EPA's NEI99 inventory overpredicted toluene mixing ratios in the New England area by a factor of 3, suggesting a large emission overestimate for that compound. A recent top-down estimate for East Asian aromatic emissions is about 6 times larger than predicted by current bottom-up inventories (Liu et al., 2012); if true, this would imply that long-range transport is a more substantial source of aromatics VOCs over the US than is presently thought, at least in the case of benzene with its longer atmospheric lifetime.

In this study, we aim to develop an improved understanding of aromatic VOC emissions in the United States. We combine 2 years of continuous in-situ observations from a tall tower in the US Upper Midwest (KCMP tall tower) with a 0.5° × 0.667° nested version

of the GEOS-Chem CTM in an inverse framework to derive optimized emission estimates for C_6 (benzene), C_7 (toluene) and C_8 (ethylbenzene + m-, o-, and p-xylene) aromatic compounds. We then apply independent measurements from six recent aircraft campaigns across the contiguous US to assess the degree to which our findings appear to be nationally representative.

5.2 Methods

5.2.1 KCMP tall tower measurements

The KCMP tall tower (44.6886°N, 93.0728°W; 244 m height) is in a rural location, 29 km south of downtown St. Paul, MN, US. Measurements at the tower were initialized in April 2007, and subsequent studies have employed data from this site to advance our understanding of land-atmosphere interactions and surface fluxes of greenhouse gases and reactive trace species, such as carbon dioxide (Griffis et al., 2010), nitrous oxide (Griffis et al., 2013), methane (Zhang et al., 2013), methanol (Hu et al., 2011; Wells et al., 2012), acetone (Hu et al., 2013), and carbon monoxide (Kim et al., 2013).

We used a high-sensitivity proton transfer reaction mass spectrometer (PTR-MS, Ionicon Analytik, Austria) to measure a suite of VOCs including C_6-C_8 aromatic compounds, every ~3 minutes between July 2009 and August 2012. Measurements were made at a sampling height of 185 m above ground level, thus providing a temporally resolved dataset with a large-scale footprint (Hu et al., 2011; Hu et al., 2013; Kim et al., 2013). The PTR-MS was calibrated automatically using a 6-point standard curve every 23 h or every 47 h (before or after August 2010, respectively), generated by dynamic dilution of multi-component standards into zero air. The latter was created by passing ambient air through a heated platinum bead catalyst (450°C; Shimadzu Corp., Japan). The VOC standard cylinders were originally filled in December 2008 (Apel-Riemer, Inc., USA) and were recalibrated in November 2013 (33 ppbv for benzene, 35 ppbv for toluene, and 50 ppbv for p-xylene) using a custom-built permeation system employing a heated catalyst

and a CO_2 sensor (LI-840A, Li-COR Environmental, USA) to quantify the VOC concentration in the calibration stream (Veres et al., 2010). The PTR-MS measures all C_8 aromatic compounds at m/z 107; here we use the approach of de Gouw et al (2003) to calculate a weighted calibration factor for the sum of C_8 aromatics based on the measured p-xylene sensitivity and its typical abundance relative to its isomers.

In this work, we use hourly averaged molar mixing ratios of benzene (C_6; measured as protonated m/z 79 by PTR-MS), toluene (C_7; protonated m/z 93), and C_8 aromatic compounds (protonated m/z 107; ethylbenzene + m-, o-, and p-xylene) measured at the KCMP tall tower during 2010 and 2011. Potential interferences for C_6-C_8 aromatics measured by quadrupole PTR-MS are thought to be minor (Warneke et al., 2001; de Gouw et al., 2003; de Gouw and Warneke, 2007). Detection limits for benzene, toluene, and C_8 aromatic compounds over the course of the study were approximately 17 pptv, 20 pptv, and 30 pptv respectively. The total measurement uncertainty is calculated hourly based on the sum of the detection limit and a relative error propagated from the main sources of instrumental uncertainty (mass flow measurement, calibration factors and fit, mixing ratio standard errors for each averaging interval, etc.). The total hourly uncertainty calculated in this way averages ≤10% for benzene and C_8 aromatics, and <20% for toluene (and in most cases is <40%). A more detailed description of the measurement methods and the field site is provided in earlier papers (Hu et al., 2011; 2013). All data presented here, along with concurrent measurements of other VOCs at the KCMP tall tower, are available for download at www.atmoschem.umn.edu/data.

5.2.2 Aircraft observations

We use airborne observations from six recent aircraft studies over the US (Table 5.1; Figure 5.1) to test the broader representativeness of our findings from the tall tower measurements. These include: CALNEX (California; May/June 2010); DISCOVER-AQ Baltimore-Washington DC (July 2011); DC3 (Central US; May/June 2012);

DISCOVER-AQ California (January/February 2013); SENEX (Southeastern US; June/July 2013); and DISCOVER-AQ Texas (September 2013). Mixing ratios of C_6-C_8 aromatic compounds (and an array of other compounds) were measured by PTR-MS during each of these campaigns. As shown in Figure 5.1, the aircraft campaigns span a range of urban, rural, and remote areas across the Western, Central, Southern, and Eastern US. They thus provide a useful counterpoint to the tall tower measurements for assessing the extent that emission biases found for the US Upper Midwest appear to manifest in other areas of the contiguous US.

5.2.3 GEOS-Chem forward model

We use the GEOS-Chem CTM (version 9.1.3) to interpret the KCMP tall tower and aircraft observations in terms of their constraints on US C_6-C_8 aromatic emissions. GEOS-Chem is an Eulerian CTM (Bey et al., 2001) driven by NASA Goddard Earth Observing System assimilated meteorological fields (GEOS-5.2.0). In this work, we use a nested-grid full-chemistry simulation over North America for 2010 and 2011. The nested domain covers 10°-70°N and 140°-40°W, with 0.5° × 0.667° horizontal resolution (latitude by longitude, approximately 56 km × 53 km at 45°N) and 47 vertical layers extending up to 0.01 hPa (14 layers are below 2 km altitude). Model transport is computed on a 10 minute time step, while emissions and chemistry are computed on a 20 minute time step. A one-year spin-up for 2009 is used to minimize any effects from initial conditions. Lateral boundary conditions (for all species, at each vertical layer) for the nested grid simulations are based on 3-hourly output from global simulations carried out at 4° × 5° resolution.

GEOS-Chem includes detailed HO_x-NO_x-VOC-ozone chemistry coupled to aerosols as originally described by Bey et al. (2001). Details regarding more recent model developments and updates can be found at www.geos-chem.org. Here we describe aspects of the simulation most salient to the work presented in this paper.

The GEOS-Chem chemical mechanism, described by Mao et al., 2010, includes the most recent JPL/IUPAC recommendations, with isoprene oxidation following the scheme of Paulot et al. (2009a; 2009b). Oxidation of benzene and toluene by OH is calculated using rate coefficients of 2.30×10^{-12} exp[−190/T] cm^3 $molecule^{-1}$ s^{-1} for benzene and 1.80×10^{-12} exp[340/T] cm^3 $molecule^{-1}$ s^{-1} for toluene (IUPAC, 2013). For C_8 aromatics, a weighted reaction rate coefficient of 1.5×10^{-11} cm^3 $molecule^{-1}$ s^{-1} is used based on the observed concentration ratios of m-xylene, o-xylene, p-xylene and ethylbenzene from an ensemble of field campaigns (Jacob et al., 2003; Millet et al., 2004; Millet et al., 2005; Millet et al., 2006; Singh et al., 2006; Murphy et al., 2007; Singh et al., 2009; Toon et al., 2010). To our knowledge, there are no reports on the deposition rates for C_6-C_8 aromatic compounds, so as a default the GEOS-Chem model doesn't treat dry deposition for these species. We implement the dry deposition for C_6-C_8 aromatic compounds through a resistance-in-series model (Wesely, 1989), with Henry's law constants of 0.18, 0.16, and 0.15 M atm^{-1} for benzene, toluene, and C_8 aromatic compounds, respectively (Sander, 1999). Later (Section 5.7), we conduct an uncertainty analysis to test the sensitivity of our results to the specific model treatment of dry deposition.

Biomass burning emissions of C_6-C_8 aromatic and other chemical species are based on the monthly GFED3 inventory (Global Fire Emission Database version 3; van der Werf et al., 2010) and measured species: species open fire emission ratios (Andreae and Merlet, 2001). Global anthropogenic emissions of CO, NO_x, and SO_2 in GEOS-Chem are based on the EDGAR monthly inventory (Emissions Database for Global Atmospheric Research; Olivier and Berdowski, 2001). For anthropogenic VOCs including C_6-C_8 aromatic compounds, we use here the RETRO (REanalysis of the TROpospheric chemical composition; Schultz et al., 2007) and the EPA NEI08 (National Emission Inventory for 2008; EPA, 2013) emission inventories.

RETRO (version 2; available at http://retro.enes.org/data_emissions.shtml) is a 0.5° × 0.5° anthropogenic inventory, containing monthly global emissions for 24 distinct

chemical species from 1960 to 2000 (Schultz et al., 2007). As with most anthropogenic inventories, RETRO estimates emissions based on both economic (e.g., activity rates) and technological (e.g., emission factors for each activity) considerations. RETRO also incorporates behavioral aspects (e.g., effects of investments in new or improved technologies) when estimating the time dependence of anthropogenic emissions, so that an emission factor is determined for each specific technology within every activity (Schultz et al., 2007). We implement the monthly RETRO emission inventory in GEOS-Chem by regridding it to the model resolution, here 0.5° × 0.667°, and (where needed) translating the RETRO species to the corresponding GEOS-Chem tracers (see Tables 5.2 and S5.1). The resulting annual global fluxes for anthropogenic VOCs emitted in GEOS-Chem are shown in Figure S5.1. We use the most recent RETRO data (year-2000) for all ensuing years, with the understanding that US VOC emissions have changed significantly since that time (e.g., Fortin et al., 2005; Harley et al., 2006; Warneke et al., 2012; McDonald et al., 2013). RETRO emissions of C_6-C_8 aromatic VOC together account for ~23% of the total estimated global anthropogenic VOCs flux in the GEOS-Chem on a carbon basis (16 TgC versus 71 TgC; Table S5.1). Annual emissions over the contiguous US in the RETRO are 420, 1448, and 2009 GgC/y for benzene, toluene, and C_8 aromatic compounds, respectively (Table 5.2). US emissions account for approximately 25% of the total global source for these compounds in the RETRO for the year 2000 (Table 5.2).

The EPA NEI08 is a regional emission inventory covering the United States. For this work, the NEI08 data has been processed using the 2008 EPA SMOKE platform (http://cmascenter.org/smoke/) based on the CB05 chemical mechanism (Yarwood et al., 2005) on 12 km × 12 km spatial resolution and hourly temporal resolution, and regridded to the native GEOS-Chem resolution (here 0.5° × 0.667°) for years 2006 and 2010. Emissions for years other than 2006 or 2010 are scaled uniformly according to the EPA's published trend data (http://www.epa.gov/ttn/chief/trends/index.html). The resulting a priori year-2010 annual emissions over the contiguous US are 191 GgC benzene, 1010

GgC toluene, and 909 GgC C_8 aromatic compounds, or 45%, 70%, and 45% of the corresponding RETRO estimates for year-2000.

In this paper, we use RETRO to estimate VOC emissions outside of the US when constructing the boundary conditions for our nested simulations. We then carry out separate analyses with US emissions computed using both RETRO and NEI08 inventories, as a way to test the sensitivity of our findings to the a priori emission assumptions. The RETRO and NEI08 inventories differ in a number of important respects (aside from geographic extent), including spatial and temporal resolution, speciation assumptions (Table 5.2), and the relative importance attributed to various source sectors. For example, on-road versus non-road source partitioning in the RETRO and the NEI08 is substantially different for benzene (50% on-road in the RETRO versus 29% in the NEI08), but only slightly different for toluene and C_8 aromatics (See Figure 5.7). In addition, RETRO extends only to year-2000, whereas the implementation of NEI08 used here predicts emissions for our specific years of analysis (2010 and 2011). Thus any post-2000 emission changes in the US due to vehicle fleet changeover and other factors (Fortin et al., 2005; Harley et al., 2006; Warneke et al., 2012; McDonald et al., 2013) will in principle be accounted for in the NEI08, but not in the RETRO simulations.

5.3 Measured and simulated aromatic mixing ratios at the KCMP tall tower

Figure 5.2 shows hourly average mixing ratios of benzene, toluene, and C_8 aromatics measured at the KCMP tall tower during 2011. Annual mean measured mixing ratios were 91 pptv for benzene, 57 pptv for toluene, and 90 pptv for C_8 aromatics (see Table 5.3). We see in the data a pronounced seasonal cycle, with high values in winter and lower values in summer (Figure 5.2 and Table 5.3), mainly reflecting the combined influence of seasonal changes in atmospheric OH and mixing depths. Figure 5.2 also shows simulated concentrations from GEOS-Chem based on the NEI08 emission inventory (corresponding plots for the RETRO inventory are shown in Figure S5.2).

While the GEOS-Chem simulation is able to capture the general annual patterns seen in the observations, some clear seasonally-dependent biases emerge. Our base-case simulation using the NEI08 emission inventory overpredicts the observed toluene mixing ratios by a factor of 2-3 throughout the year (Figure 5.3). On the other hand, the model underpredicts the abundance of benzene and C_8 aromatics during the warm season (April-September) by 25%. During the cold season (October-March), the model has a consistent low bias for benzene (~40 pptv) while over- predicting C_8 aromatics by >60% (Figure 5.3).

The GEOS-Chem simulation based on the year-2000 RETRO emission inventory is shown in Figure S5.2 and Figure S5.3. Here, the KCMP tall tower observations reveal a substantial high bias in the model for all aromatic species throughout the year. The annual model:measurement slopes (reduced major axis) in this case are 1.6, 3.9, and 2.8 for benzene, toluene, and C_8 aromatics, respectively, reflecting a RETRO overestimate of aromatic hydrocarbon emissions for the region sampled by the KCMP tall tower.

5.4 Optimizing aromatic VOC emissions based on the tall tower measurements

Using a Bayesian inverse approach, we use the above comparisons to derive optimized C_6-C_8 aromatic emission estimates that are most consistent with observational constraints (here the KCMP tall tower measurements) and with existing bottom-up information (the a priori emission inventories described in Sect 2.3). The procedure involves minimizing the cost function $J(\mathbf{x})$ (Rodgers, 2000):

$$J(\mathbf{x}) = (\mathbf{x} - \mathbf{x}_a)^T \mathbf{S}_a^{-1} (\mathbf{x} - \mathbf{x}_a) + (\mathbf{Kx} - \mathbf{y})^T \mathbf{S}_\Sigma^{-1} (\mathbf{Kx} - \mathbf{y}) \quad (5.1)$$

Here $\boldsymbol{x}$ is the vector of sources being optimized, while $\boldsymbol{x}_a$ represents their initial guess (a priori) values. $\mathbf{K}\boldsymbol{x}$ is the vector of predicted C_6-C_8 aromatic VOC mixing ratios and $\boldsymbol{y}$ is

the corresponding vector of observations at the KCMP tall tower. $\mathbf{S}_a$ and $\mathbf{S}_\Sigma$ are the a priori and observational error covariance matrices, respectively. The minimum value of $J(\boldsymbol{x})$ thus defines the set of aromatic emissions that minimizes the error-weighted mismatch between the derived sources and their a priori values (first term on the right hand side of equation 5.1), plus the error-weighted mismatch between the tall tower data and the model predictions (the second term). **K** is the Jacobian matrix describing the forward model relationship between emissions and concentrations. In order to construct the Jacobian matrix **K**, we perturb each model source individually by 10%, rerun the model, and calculate the resulting changes to the aromatic mixing ratios at the KCMP tall tower.

Errors in the a priori emissions are set initially at 100%, based on the US inventory biases inferred in other recent studies (Parrish, 2006; Warneke et al., 2007; Pétron et al., 2012). Errors for different source sectors are assumed uncorrelated so that $\mathbf{S}_a$ is diagonal. The observational error includes contributions from the measurements and from the model. Measurement uncertainties are estimated at 17 pptv + 10%, 20 pptv + 20%, and 30 pptv + 10% for benzene, toluene, and C_8 aromatics, respectively (Section 5.2.1). The model error is estimated at 20% following Hu et al. (2013) and Kim et al. (2013). These relative uncertainties are applied to the measured and simulated concentrations accordingly, and the results added in quadrature to construct $\mathbf{S}_\Sigma$. We also derive an alternate estimate of $\mathbf{S}_a$ and $\mathbf{S}_\Sigma$ based on a maximum likelihood estimation (MLE) approach, which infers the most probable elements of $\mathbf{S}_a$ and $\mathbf{S}_\Sigma$ based on the observed and (a priori) simulated C_6-C_8 aromatic mixing ratios (Michalak et al., 2005). Later, we test the dependence of our optimization results on the above assumptions and methods for constructing the error covariance matrices.

Our analyses first assessed which source combinations could be resolved based on the KCMP tall tower observations (on an annual basis). When using the NEI08 inventory, we find that on-road emissions, non-road emissions, and the model boundary condition (i.e.,

the influence of long-range transport from outside the model domain) can each be independently distinguished: the corresponding averaging kernel elements exceed > 0.95 in each instance. Conversely, when using the RETRO inventory as the a priori estimate of US emissions, the on-road and non-road sectors cannot be distinguished as they are highly correlated in this inventory (R > 0.98). We thus combine them as a single state vector element to be optimized in this case. The fact that the tall tower data allows us to resolve on-road versus non-road sources when using NEI08 but not RETRO reflects the differing spatial distribution of these sectors in the two inventories.

In addition to the annual analysis, we perform optimizations using only warm season (April – September) and only cold season (October – March) data to test for any seasonally dependent bias in the inventories. We find that toluene and the C_8 aromatics exhibit weak sensitivity to the model boundary condition during the warm season (averaging kernel values are < 0.3), due to their short atmospheric lifetimes. Accordingly, we do not attempt to optimize the seasonal boundary condition for these compounds during the warm season (Table S5.2). In the following, we employ as our base-case analysis the seasonal inversions with NEI08 as the a priori emission inventory (Opt1 in Table S5.2). Along with the separate annual inversions and those based on the RETRO inventory, we conduct an ensemble of sensitivity inversions (described in Section 5.7) with varying model configurations and assumptions in order to test the robustness of our results.

5.5 Optimization results

Our inversion results reveal a major overestimate of 2010-2011 toluene emissions in both NEI08 (3× too high) and RETRO (4.5×) inventories. In the case of NEI08, part of this discrepancy can be attributed to speciation differences between CB05 (used to construct the emission fields) and GEOS-Chem, as CB05 toluene tracer also includes ethylbenene. However, we find that this only increases the toluene flux by ~43% nationally, and so cannot explain the observed disparity. Rather, the inferred toluene bias is primarily due to

an overprediction of non-road emissions: a posteriori scale factors based on NEI08 are 0.17 [0.04-0.20] during the cold season and 0.14 [0.06-0.22] during the warm season (numbers in brackets give the range from sensitivity tests described in Section 5.7; see Table 5.4). On the other hand, our derived on-road emission estimates for toluene are more similar to the NEI08 values, with a posteriori scale factors of 1.02 [0.92-1.11] during the warm season and 0.57 [0.55-0.64] during the cold season. Our findings thus reverse the relative importance of on-road and non-road toluene emissions: non-road emissions account for 73% (NEI08) to 78% (RETRO) of the annual domestic toluene flux in the prior inventories, compared to only 35% based on the scale factors derived from the tall tower data.

Our total derived emission sources for benzene and C_8 aromatics agree well with the NEI08; aggregated scale factor are 1.23 (benzene) and 1.22 (C_8 aromatics) during the warm season, and 0.97 (benzene) and 0.66 (C_8 aromatics) during the cold season (Table 5.4). However, the optimization does reveal some significant season- and source-specific biases. We find that on-road emissions for benzene and C_8 aromatics are overestimated in the NEI08 by as much as a factor of 2 during the warm season (Table 5.4), with a posteriori scale factors of 1.93 [1.87-2.06] for benzene, and 2.23 [2.09-2.36] for C_8 aromatics. However, this bias is not present during the cold season, when the optimized fluxes are within 25% of the prior NEI08 values (Table 5.4). There thus appears to be a seasonal bias in the NEI08 on-road emissions of benzene and C_8 aromatics, at least for the US Upper Midwest region sampled by the KCMP tall tower.

The non-road sector accounts for most of the US benzene and C_8 aromatic source in the NEI08, and this is also the case with our optimized emissions. Our derived non-road emissions for benzene agree with the NEI08 estimates: a posteriori scale factors are 1.07 [0.84-1.44] and 0.97 [0.86-1.77] during the cold and warm season, respectively. The corresponding scale factors for C_8 aromatics 0.40 [0.11-0.57] during the cold season and

0.90 [0.48-1.10] during the warm season, suggesting an inventory underestimate for non-road C_8 aromatics emissions during winter.

Employing RETRO as the a priori inventory within the US results in scale factors ranging 0.35 to 0.50 for benzene and C_8 aromatics (Table S5.3), reflecting a 2-3 fold source overestimate for these compounds. As we see later, the a posteriori fluxes that we derive are consistent regardless of whether NEI08 or RETRO is used as a priori.

Aromatic VOC emissions outside the US are computed based on RETRO for our base-case simulation, as well as for all the sensitivity analyses described in Section 5.7. In all cases, there optimizations reveal a large model underestimate of the C_6-C_8 aromatic abundance upwind of the US, with a posteriori scale factors of 2.03- 4.02 for benzene, 1.65-2.14 for toluene, and 3.40-4.92 for C_8 aromatics. This may reflect an emission bias over East Asia; Liu et al. (2012) concluded on the basis of space-borne glyoxal measurements that Chinese aromatic emissions are 6 times greater than the bottom-up estimate of Zhang et al. (2009).

Figure 5.3 compares the mixing ratios of benzene, toluene, and C_8 aromatics observed at the KCMP tall tower during 2011 with those from our base-case a priori and best-estimate a posteriori simulations (using the NEI08 inventory). For all species, we see improved model:observation agreement with a posteriori simulation, as indicated by higher correlation coefficients (R; 0.85 versus 0.78, 0.63 versus 0.58, and 0.51 versus 0.48, for benzene, toluene, and C_8 aromatics) and slopes closer to one (1.03 versus 0.75, 1.02 versus 2.88, and 1.13 versus 1.47, respectively) compared to the a priori simulation. In general, we see a major revision for toluene, and more modest adjustments for C_8 aromatics and for benzene. The seasonal model:observation regression slopes are also greatly improved in the a posteriori simulations. We derive similar a posteriori model-observation comparisons when using RETRO as the a priori inventory (Figure S5.3).

A feature of the regressions in Figure 5.3 and Figure S5.3 is that the model:observation correlation coefficients increase with the lifetime of species at hand (e.g., $R = 0.51$ for C_8 aromatics versus 0.85 for benzene for our best-estimate a posteriori run based on NEI08). This mainly reflects model difficulty in capturing find-scale processes (e.g., spatially heterogeneous emissions, as well as chemistry and mixing effects) that become increasingly important for shorted-lived species. The fact that the optimized simulation substantially can improve the model:observation slopes in all cases, but only moderately increase the correlation coefficients, suggests *i*) that the overall biases in the model emissions are mostly corrected in the a posteriori simulations, and *ii*) that significantly improving the model:observation correlation would require improved representations of other model processes.

Figure 5.4 compares the observed benzene:toluene relationship with that in the a priori and a posteriori simulations. Such aromatic hydrocarbon relations have been widely used as indices of atmospheric processes like photochemical loss and transport/dilution (e.g., (McKeen and Liu, 1993; McKeen et al., 1996)), since both species are usually co-emitted directly from anthropogenic sources. As shown in Figure 5.4, our best-estimate optimized simulation (Opt1) clearly reproduce the observed benzene:toluene relationship, while two a priori simulations fail to do so. Such improvement is largely driven by a better benzene:toluene emission ratio in the best-estimate simulation than in a priori (e.g., the best-estimated total US emission ratio for benzene:toluene is 0.66, versus 0.19 in the NEI08, and 0.30 in the RETRO).

5.6 Source contributions to atmospheric aromatics in the US Upper Midwest

Figure 5.6 shows the seasonal contribution from long-range transport (i.e., the nested model boundary condition), domestic on-road sources, and non-road sources for benzene and toluene at the KCMP tall tower according to our best-estimate optimization. The

derived source apportionment for C_8 aromatics is very similar to that of toluene and is not plotted.

We find that long-range transport is a major contributor to atmospheric benzene during winter in the Upper Midwest, accounting for up to 60% of the total abundance at that time of year. This arises as a direct consequence of the large upwards adjustment to the model boundary condition that is indicated by the tall tower data, and which is common feature of all sensitivity tests. The influence of long-range transport on wintertime mixing ratios of toluene (up to 20%) and C_8 aromatics (up to 15%) is more modest as a result of their shorter atmospheric lifetimes.

In terms of domestic aromatic sources, our best-estimate optimization (Opt1) shows that on-road mobile emissions are generally of equal or more importance than non-road emissions for all C_6-C_8 aromatic compounds during the warm season (Table 5.4). However, our optimized simulation has a large uncertainty in sector information especially for the toluene non-road emissions (Section 5.5).

5.7 Uncertainty analysis

The best-estimate optimization described above is performed on a seasonal basis (warm season/cold season), with NEI08 as the prior US emission inventory, and with the forward and inverse model configured as described in Section 5.2.3 and 5.4. In this section, we repeat the optimization while varying a number of key forward model parameters, error estimates, and observation selection criteria in order to obtain a comprehensive uncertainty estimate for our results (Table S5.2). This includes:

- Use of differing a priori inventories (NEI08 and RETRO) for US aromatic VOC emissions;

- Including and excluding bromine chemistry, which modifies the model distribution of OH and O_3 as described by Parrella et al. (2012).
- Varying the reactive uptake coefficients for HO_2 on aqueous aerosols with (γ = 0.2 or 0.4), which modifies the global HO_x fields in the model (Mao et al., 2013);
- Including and excluding dry depositions for aromatic VOCs, and also including and excluding reactive uptakes for these compounds (Karl et al., 2010);
- Use of two alternative boundary layer mixing schemes (local and nonlocal; (Holtslag and Boville, 1993; Lin and McElroy, 2010);
- Decreasing NO_x emissions over North America by 40%;
- Alternate assumptions for changing the error covariance matrices: *i*) doubling and halving Sa, *ii*) doubling and halving SΣ, and *iii*) constructing $\mathbf{S}_a$ and $\mathbf{S}_\Sigma$ using Maximum Likelihood Estimation (Michalak et al., 2005);
- Varying the time frame and temporal resolution of the optimization: *i*) annual inversion for 2010, *ii*) annual inversion for 2011, *iii*) annual inversion for 2010+2011, and *iv*) seasonal inversion (warm season/cold season) for 2011.

Table S5.2 shows results from the resulting 24 sensitivity inversions. These sensitivity runs may not span every single possible cause of error in the analysis, but they do assess the main sources of uncertainty and their relative magnitudes. We find doubling or halving the a priori error covariance matrix ($\mathbf{S}_a$) does not change the emission estimates by >1%, so this test is not included in Table S5.2.

In a relative sense, we find that the total and on-road emissions for each species (benzene, toluene, C_8 aromatics) are better constrained than is the contribution from non-road sources. For each case the inferred on-road emissions vary by only ~30% across all the sensitivity invensions, where the inferred non-road emissions differ by up to 70% (Table S5.2). Across all the sensitivity runs, the derived total emissions fall within ±50% of our best-estimate optimization (Opt1) for benzene, toluene, and C_8 emissions.

The suite of test inversions summarized in Table S5.2 indicates that our derived emissions are most sensitive to the assumptions used to construct $\mathbf{S}_\Sigma$ (e.g., Opt6-9) and to model treatment of reactive uptakes (e.g., Opt16-17). Here, the inferred non-road and total emissions diverge as much as ~70% and ~50%, respectively, from the best-estimate, with the on-road source varying by up to ~30%. By comparison, use of alternate prior inventories (NEI08 versus RETRO), alternate PBL mixing schemes, and perturbations to model chemistry (40% decrease in US NO_x emissions; changing the reactive uptake efficiency for HO_2; including bromine chemistry) all had a much smaller influence in the results, with discrepancies of less than 25% compared to the best-estimate.

An inherent bias in our a priori NEI08 emission arises from speciation differences between that inventory and GEOS-Chem (Table 5.2). The NEI08 inventory used in our best-estimate analysis is based on CB05 speciation (Yarwood et al., 2005), which lumps other monoalkyl aromatics with toluene, and other polyalkyl aromatics with C_8 aromatics. By contrast, the PTR-MS measurements resolve VOCs based on their mass, so that all C_8 aromatics (xylenes + ethylbenzene) are measured together while benzene and toluene are detected as individual compounds. The chemical mechanism employed in GEOS-Chem for this work corresponds to this latter speciation. We performed an analysis to quantify the expected bias in the NEI08 a priori toluene and C_8 aromatic emissions due to this discrepancy. We find that, nationally, emissions of the lumped CB05 TOLU tracer (toluene + ethlybenzene) are ~43% higher than those of toluene itself, while emissions of the lumped CB05 XYLE tracer (xylenes + other polyalkyl aromatics) are 25% higher than those of C_8 aromatics alone. These speciation differences will also vary spatially and between sectors. However, even the largest sector-specific a priori speciation biases (e.g., a priori non-road TOLU emissions in the NEI08 are ~2.2 times those of toluene itself) are substantially smaller than the corresponding top-down correction factors derived here (e.g., an inferred 4.5-16× reduction of toluene non-road emissions). As shown above, our a posteriori flux estimates are not sensitive to the choice of prior inventory or to its assigned error covariance; this speciation discrepancy can

therefore be expected to bias the NEI08 a priori emission estimates for toluene and C_8 aromatics, but should not notably affect the a posteriori results.

5.8 Aircraft comparisons and implications for aromatic VOC emissions in the United States

An implicit assumption in the above optimizations is that the spatial distribution of each individual emission sector is described accurately in the prior inventories. As we saw earlier, however, there is some spatial disparity between RETRO and NEI08, indicating a degree of uncertainty in this regard. In this section, we test the extent to which aromatic emission corrections inferred from the KCMP tall tower measurements apply more broadly across the contiguous US. To this end, we employ recent aircraft measurements covering six key regions across the US: California (CALNEX, DISCOVER-AQ California), East Coast (DISCOVER-AQ Baltimore-Washington DC), Central US (DC3), Southeast (SENEX), and Texas (DISCOVER-AQ Texas); see Table 5.1 and Figure 5.1.

Figure 5.5 compares the average vertical profiles of benzene and toluene for each of these campaigns (in black) with our base-case a priori (NEI08; red) and best-estimate a posteriori (green, Opt1) simulations. Corresponding plots for simulations using RETRO as the a priori US inventory are shown in Figure S5.4. The comparisons for C_8 aromatics are plotted in Figure S5.5. Model simulations are for the year 2011, whereas the aircraft campaigns span 2010-2013. However, we expect year-to-year emission changes over this time period to be within the overall uncertainty in our analysis (Section 5.7). All simulations are sampled along the flight tracks at the time-of-day and day-of-year of the observations, and airborne data have been filtered to remove the influence of individual biomass burning plumes (acetonitrile > 200 pptv).

For benzene, we see in Figure 5.5 a general increase in the simulated vertical profiles with the best estimate a posteriori simulation, and improved model:measurement

agreement across all the aircraft campaigns. In some cases (notably DISCOVER-AQ California and Texas), the model is still too low compared to observations within boundary-layer, though the bias is reduced. The two main factors contributing to this shift are: *i*) the nearly doubling (scale factor = 1.93) of the on-road benzene emissions during the warm season when five out of the six campaigns were carried out; and *ii*) the large inferred increase (2-3×) in the model boundary condition, reflecting long-range transport of benzene into North America. The latter is important only in winter, when the benzene lifetime increases to several months.

In the case of toluene, our inferred ~85% reduction for non-road emissions (a posteriori scale factors of 0.17 and 0.14 during the cold and warm season, respectively) strongly improves the model:measurement agreement over most areas of the US (Central, East, and Southeastern), but with the two notable exceptions of California and Houston, TX (CALNEX, DISCOVER-AQ California, DISCOVER-AQ Texas; Figure 5.5). In these locations, a priori toluene emissions based on NEI08 appear to be more reliable than our a posteriori result, highlight very large local non-road emissions, possibly related to petroleum refineries/petrochemical facilities over these two regions.

We see worse comparisons with RETRO simulations for benzene, with the agreement becoming worse in every case but one (CALNEX; Figure S5.4). On the other hand, for toluene the a posteriori simulation based on RETRO agrees very well with the aircraft data everywhere, with the sole exception of Houston TX. Such different agreements reflect the spatial disparity between RETRO and NEI08. Nevertheless, as seen earlier for the tall tower data, in all cases, the observed benzene:toluene relationships are much better captured by the best-estimate a posteriori simulation than by the a priori (right panels in Figure 5.5 and Figure S5.4).

Based on the comparisons above, we conclude that the benzene biases inferred from the KCMP tall tower measurements are generally present across the EPA's NEI08 inventory

(but not the RETRO) within the contiguous US; likewise, the inferred emission biases for toluene apply to most areas of the contiguous US, with clear exceptions in California and Texas for the NEI08 and RETRO. For C_8 aromatic emission (Figure S5.5), the emission biases can also be applied to most areas of the contiguous US for both NEI08 and RETRO inventories.

Applying the emission scale factors from our best-estimate optimization (Opt1 in Table S5.2), we estimate total anthropogenic emission fluxes in the contiguous US for 2011 of 209 GgC for benzene (with an uncertainty range from the 24 sensitivity runs of 180-297 GgC; Figure 5.7), 310 GgC for toluene (195-372 GgC), and 822 GgC for C_8 aromatics (uncertainty range 403-1028 GgC). Annually, the best-estimate top-down values for benzene and C_8 aromatics agree well with our a priori emission based on the EPA's NEI08 inventory, within the uncertainties of the analysis (Figure 5.7). However, toluene emissions are substantially overestimated by our a priori emissions based on our model implementation of NEI08 inventory (961 GgC in the a priori NEI08 versus 340 GgC in our best-estimate a posteriori) by a factor of almost three for most areas in the US except in California and Texas. Figure 5.7 also shows that the fractions of on-road mobile emissions in our best-estimate are greater than in the EPA NEI08 inventory, suggesting on-road sources for BTEX compounds should be more important than in the current understanding, possibly reflecting the NEI08 is currently overestimating emission reduction effect over times related to on-road transportation sources.

We find that toluene emission is substantially overestimated all year-round in our model implementation of the EPA's NEI08 in the upper Midwest region and most areas in the central and eastern US. Such overestimation is mostly driven by non-road sources and is partly due to speciation differences in CB05 (Figure 5.8). Our best-estimate optimization implies benzene and C_8 aromatics on-road emissions are underestimated by the EPA NEI08 inventory, especially during warm season (Table 5.4). These possibly reflect that tailpipe and fuel evaporative emissions are not well represented in inventories. The

doubled on-road sources for benzene and C_8 aromatic emissions during the warm season also change the seasonal distribution of emission for these compounds, with slightly higher total emissions during the warm season than in the cold season in our best-estimate optimization (Figure 5.8 and Table 5.4). However, such inference on seasonal and sectional emissions should be used with cautions, because the sensitivity runs show the uncertainties for estimating non-road sources and seasonal emissions are large (e.g., ±70%, ±67%, and ±68% for non-road benzene, toluene, and C_8 aromatics, respectively), while on-road sources and the total emission tend to be constrained by the optimization (±51% or better; Table S5.2 and Figure 5.7).

We find that US C_6-C_8 aromatic emissions in the RETRO inventory are overestimated by as factors of 2.0, 4.5, and 2.4 for benzene, toluene, and C_8 aromatics, respectively. Part of this overestimate likely reflect the substantial anthropogenic VOC emission reductions that occurred in the US between 2000 (the most recent RETRO year used here) and 2010-2011 (Fortin et al., 2005; Harley et al., 2006; Warneke et al., 2012; McDonald et al., 2013). Regardless of whether the NEI or RETRO inventory are used as a priori over the US, we derive statically identical a posterior flux estimates (Figure 5.7 and Figure 5.8). In the future, sustained measurements are needed in other key regions in the US to *i*) explore the reasons for the spatial and temporal sector emission biases as seen in this study, and, to *ii*) monitor future changes and the evolving importance of long-range transport for these compounds and other air pollutants.

Table 5.1. Datasets used in this work

Campaign	Timeframe	Location	Instrument	PI (Reference)
KCMP tall tower	2010-2011	MN, US	PTR-MS	Millet (this paper; www.atmoschem.umn.edu/data)
DC3 (DC300)	May/June 2012	Central US	PTR-MS	Wisthaler (http://www2.acd.ucar.edu/dc3)
DISCOVER-AQ California (DISCCA)	January/ February 2013	San Joaquin Valley, CA, US	PTR-MS	Wisthaler (http://discover-aq.larc.nasa.gov/)
DISCOVER-AQ Baltimore-Washington DC (DISCDC)	June/July 2011	Baltimore MD / - Washington, D.C, US	PTR-MS	Wisthaler (http://discover-aq.larc.nasa.gov/)
CALNEX (CALNX)	May/June 2010	CA, US	PTR-MS	de Gouw (http://www.esrl.noaa.gov/csd/projects/calnex/)
SENEX (SENEX)	June/July 2013	Southeastern US	PTR-MS	de Gouw (http://www.esrl.noaa.gov/csd/projects/senex/)
DISCOVER-AQ Texas (DISCTX)	September 2013	Houston, TX, US	PTR-MS	Wisthaler (http://discover-aq.larc.nasa.gov/)

Table 5.2. Speciation differences for C_6-C_8 aromatic compounds in PTR-MS measurements, the EPA NEI08, and RETRO inventories

Species	PTR-MS	NEI08 CB05		RETRO		
			US emissions (2010, GgC)		US emissions (2000, GgC)	Global emissions (2000, GgC)
Benzene	Benzene	Benzene	191	Benzene	420	3212
Toluene	Toluene	Toluene and other monoalkyl aromatics such as ethlybenzene	1010	Toluene	1448	5601
C_8 aromatics	ethylbenzene + m-, o-, and p-xylene	Xylenes and other polyalkyl aromatics	909	Xylenes and other aromatics mostly ethlybenzene	2009	7220

Table 5.3. Seasonal mixing ratios (ppbv) of benzene, toluene, and C_8 aromatics measured at the KCMP tall tower.

	Spring[1]		Summer[2]		Autumn[3]		Winter[4]	
	Mean (standard deviation)	Median (10^{th}-90^{th} percentiles)	Mean (standard deviation)	Median (10^{th}-90^{th} percentiles)	Mean (standard deviation)	Median (10^{th}-90^{th} percentiles)	Mean (standard deviation)	Median (10^{th}-90^{th} percentiles)
benzene	89 (46)	83 (35 – 145)	48 (23)	43 (24 – 78)	80 (42)	76 (29 – 131)	160 (44)	152 (115 – 214)
toluene	35 (42)	23 (6 – 76)	38 (36)	29 (6 – 85)	58 (52)	45 (15 – 109)	96 (65)	79 (42 – 165)
C_8-aromatics	54 (52)	39 (13 – 108)	77 (56)	61 (26 – 158)	99 (81)	79 (34 – 181)	125 (101)	95 (42 – 239)

[1] Spring: March–May; [2] Summer: June–August; [3] Autumn: September–November; [4] Winter: December–February.

Table 5.4. Emission correction factors from the best-estimate optimizations relative to the EPA's NEI08 inventory. Uncertainty ranges from sensitivity tests are shown in parenthesis.

	Benzene			Toluene			C_8 aromatics		
NEI08 (Opt1)	Non-road	On-road	Boundary condition	Non-road	On-road	Boundary condition	Non-road	On-road	Boundary condition
Cold	1.07 (0.84-1.44)	0.75 (0.73-0.93)	2.69 (2.21-3.53)	0.17 (0.04-0.2)	0.57 (0.55-0.64)	1.85 (1.65-1.89)	0.40 (0.11-0.57)	1.23 (1.11-1.32)	3.86 (3.40-4.03)
	0.97*			0.28*			0.66*		
Warm	0.97 (0.86-1.77)	1.93 (1.87-2.06)	2.80 (2.17-4.02)	0.14 (0.06-0.22)	1.02 (0.92-1.11)	--	0.90 (0.48-1.10)	2.23 (2.09-2.36)	--
	1.23*			0.36*			1.23*		

* The mean aggregated scale factors for the total US emission source in each season.

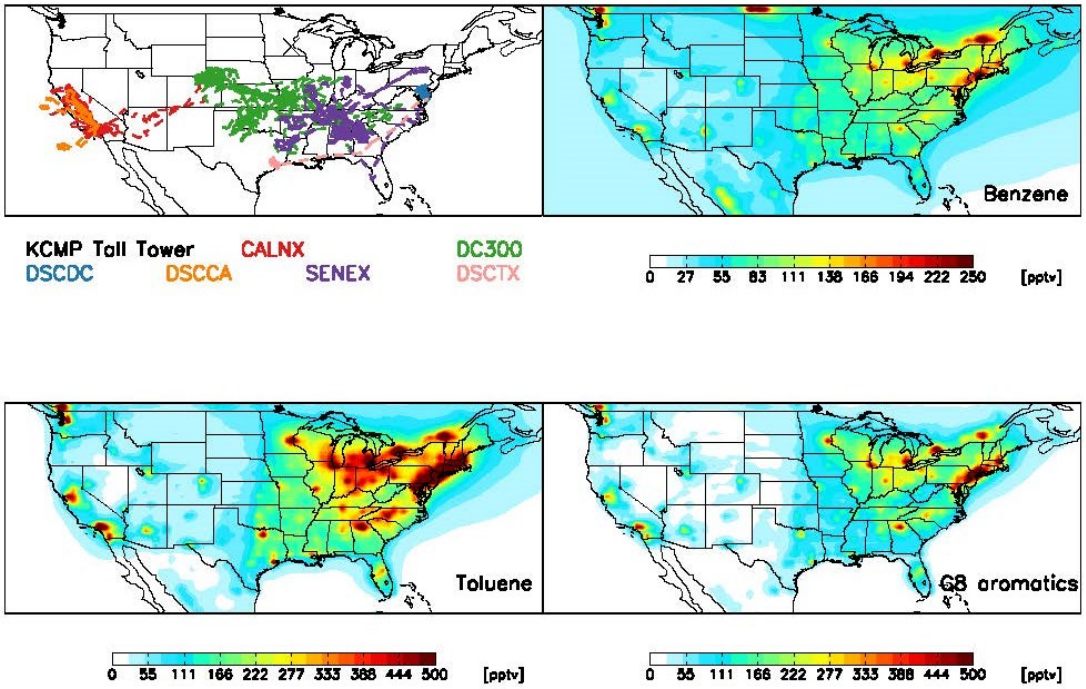

Figure 5.1. Simlated surface mixing ratios (P >900 hPa, annual mean) of C_6-C_8 aromatic compounds in the contingous US for the year 2011 based on NEI08 emission inveontry. Also shown are the location of KCMP tall tower used in the inverse analysis, along with flight tracks for six aircraft campaign measurements used to examine the broad application of the emission biases found for the US Upper Midwest. CALNX: CALNEX; DC300: DC3; DSCDC: DISCOVER-AQ California; DISCDC: DISCOVER-AQ Baltimore-Washington DC; SENEX: SENEX; DISCTX: DISCOVER-AQ Texas.

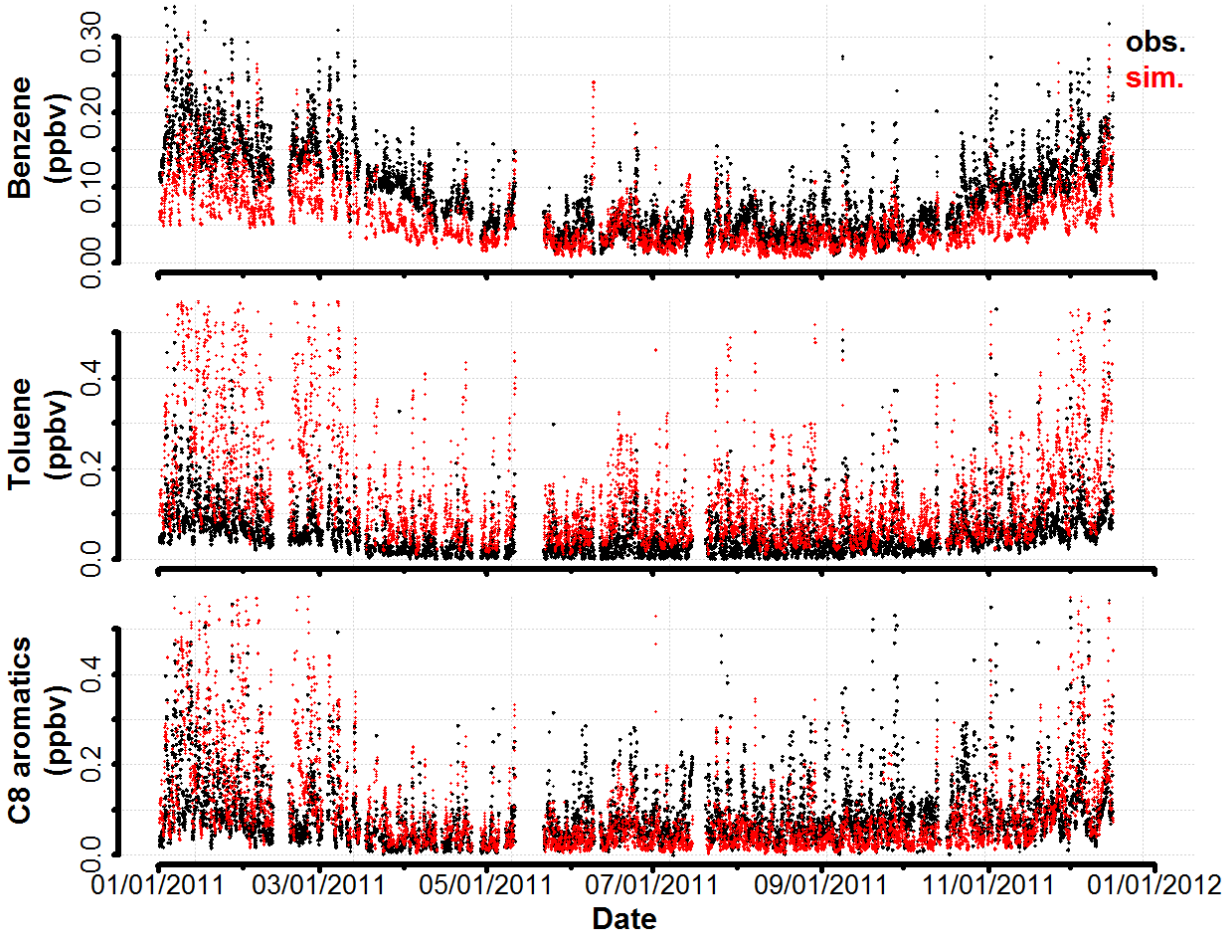

Figure 5.2. Annual cycle in benzene, toluene, and C_8 aromatics observed at the KCMP tall tower for the year 2011(black). The base-case a priori aromatic compounds simulated by GEOS-Chem based on the EPA's NEI08 inventory are shown in red. All data points are 1 h means.

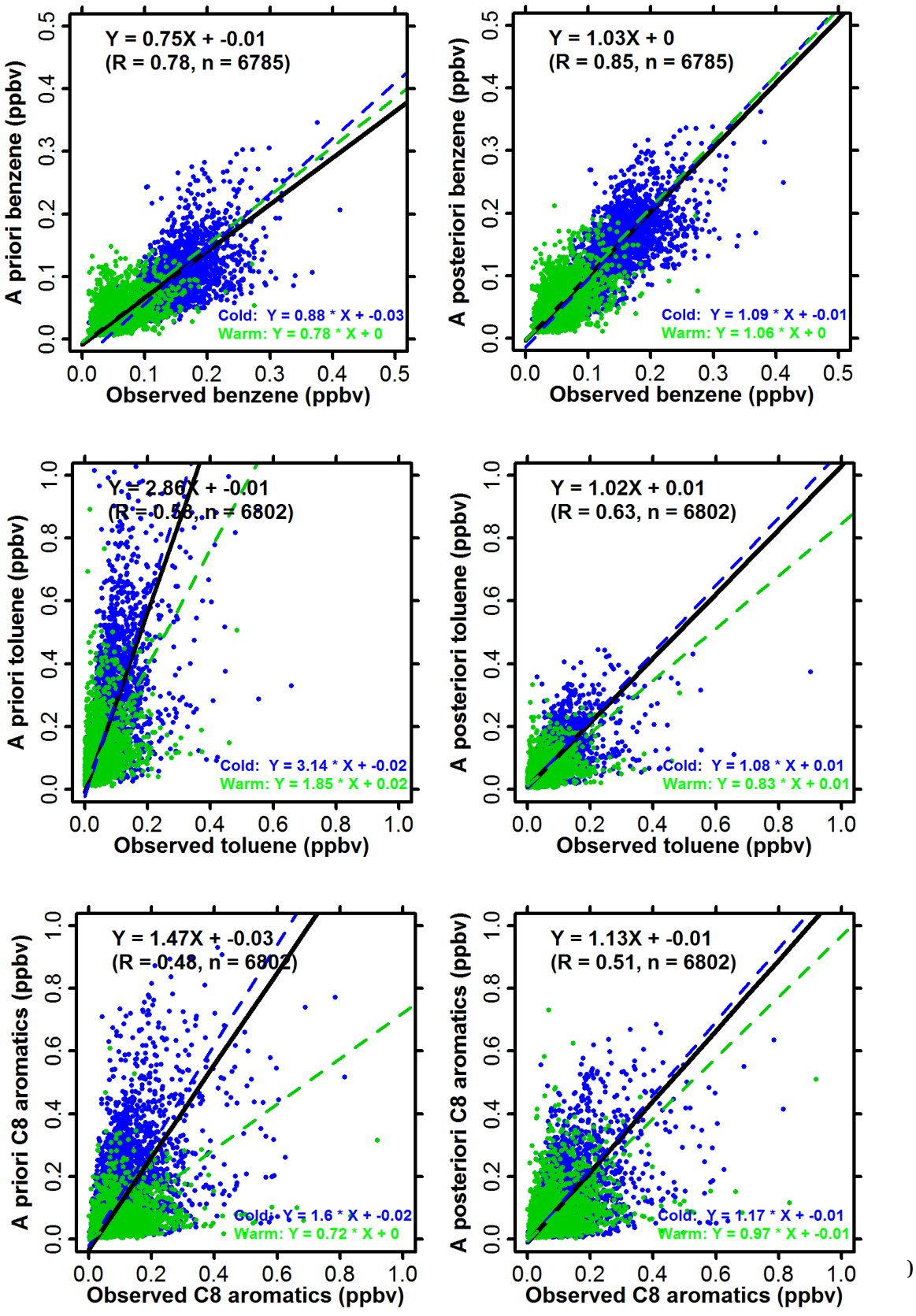
Y = 0.75X + -0.01
(R = 0.78, n = 6785)
Cold: Y = 0.88 * X + -0.03
Warm: Y = 0.78 * X + 0
A priori benzene (ppbv)
Observed benzene (ppbv)
Y = 1.03X + 0
(R = 0.85, n = 6785)
Cold: Y = 1.09 * X + -0.01
Warm: Y = 1.06 * X + 0
A posteriori benzene (ppbv)
Observed benzene (ppbv)
Y = 2.86X + -0.01
(R = 0.53, n = 6802)
Cold: Y = 3.14 * X + -0.02
Warm: Y = 1.85 * X + 0.02
A priori toluene (ppbv)
Observed toluene (ppbv)
Y = 1.02X + 0.01
(R = 0.63, n = 6802)
Cold: Y = 1.08 * X + 0.01
Warm: Y = 0.83 * X + 0.01
A posteriori toluene (ppbv)
Observed toluene (ppbv)
Y = 1.47X + -0.03
(R = 0.48, n = 6802)
Cold: Y = 1.6 * X + -0.02
Warm: Y = 0.72 * X + 0
A priori C8 aromatics (ppbv)
Observed C8 aromatics (ppbv)
Y = 1.13X + -0.01
(R = 0.51, n = 6802)
Cold: Y = 1.17 * X + -0.01
Warm: Y = 0.97 * X + -0.01
A posteriori C8 aromatics (ppbv)
Observed C8 aromatics (ppbv)

)

Figure 5.3. Atmospheric aromatic mixing ratios from GEOS-Chem simulations (left: a priori using the EPA's NEI08; right: a posteriori best-estimate) compared to observations at the KCMP tall tower in 2011, colored by warm and cold seasons. Data points are 1 h mean values.

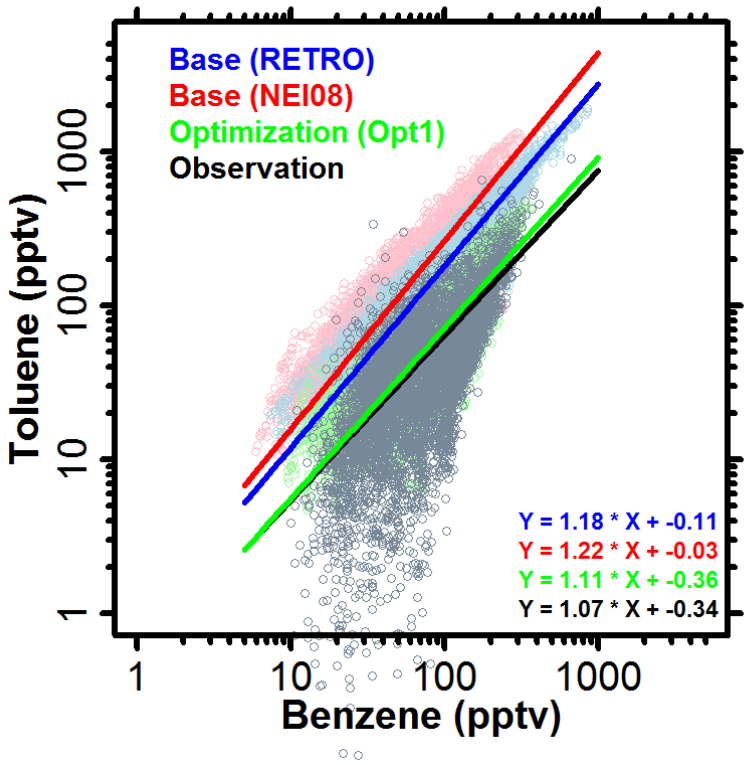

Figure 5.4. The log-log plot for benzene versus toluene in the KCMP tall tower observation (black), a priori (blue and red), and a posteriori best-estimate (green). Solid lines are best fits (major axis regression), with regression parameters given in the inset. The regression slope and intercept in the measurements are highly dependent on the selection of toluene data near the PTR-MS detection limit (~ 15-25 pptv; e.g., when removing toluene data below 15 pptv: Y=1.13*X-0.46; 25pptv: Y=1.03*X – 0.24). The best fit in the observations shown in the figure are taken with toluene mixing ratios > 20 pptv.

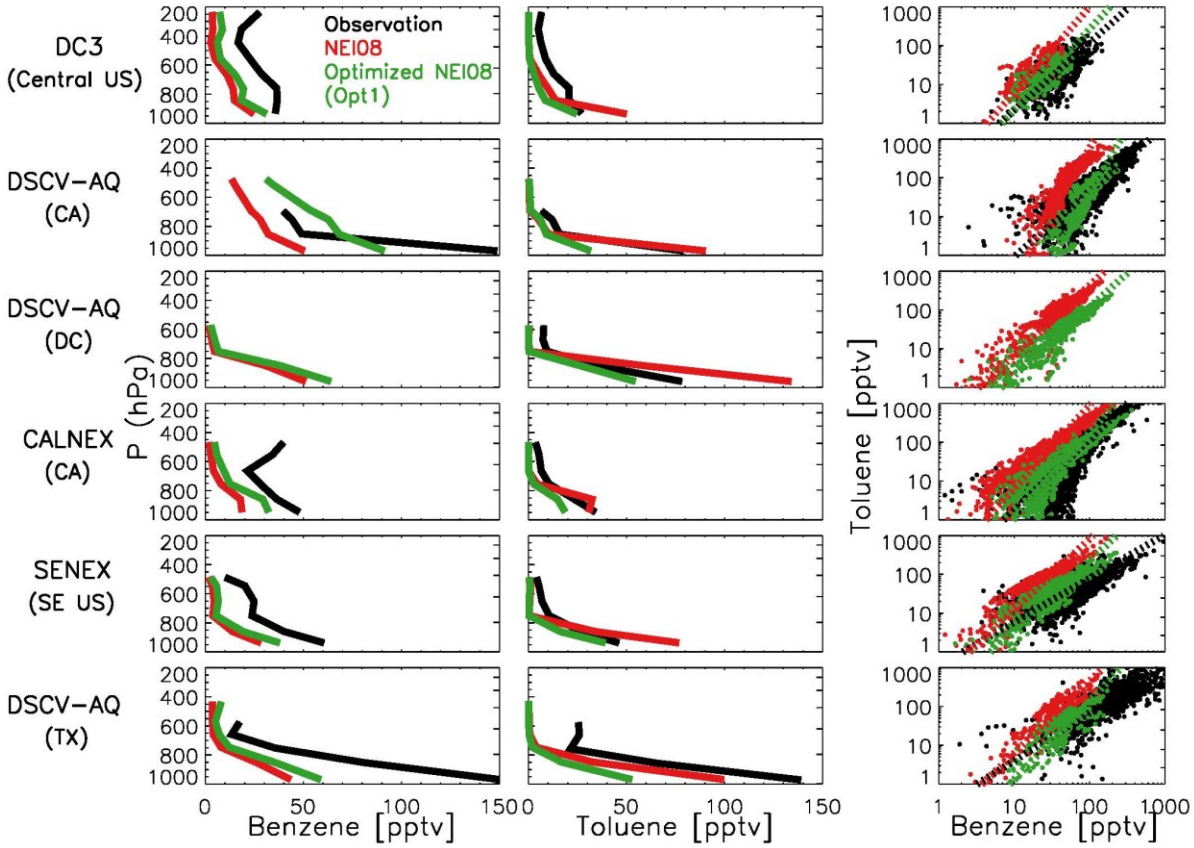

Figure 5.5. Vertical profiles (median for each vertical level; left and middle panel) in a priori base-case (red) and a posteriori best-estimate (green) simulations based on the EPA's NEI08 compared with that in six recent aircraft campaigns (black). The right panel shown the log-log plot for benzene versus toluene (data in the boundary layer, P > 800 hPa), with dashed lines as best fits from major axis regression. DSCV-AQ (CA): DISCOVER-AQ California; DISCV-AQ (DC): DISCOVER-AQ Baltimore-Washington DC; DSCV-AQ (TX): DISCOVER-AQ Texas.

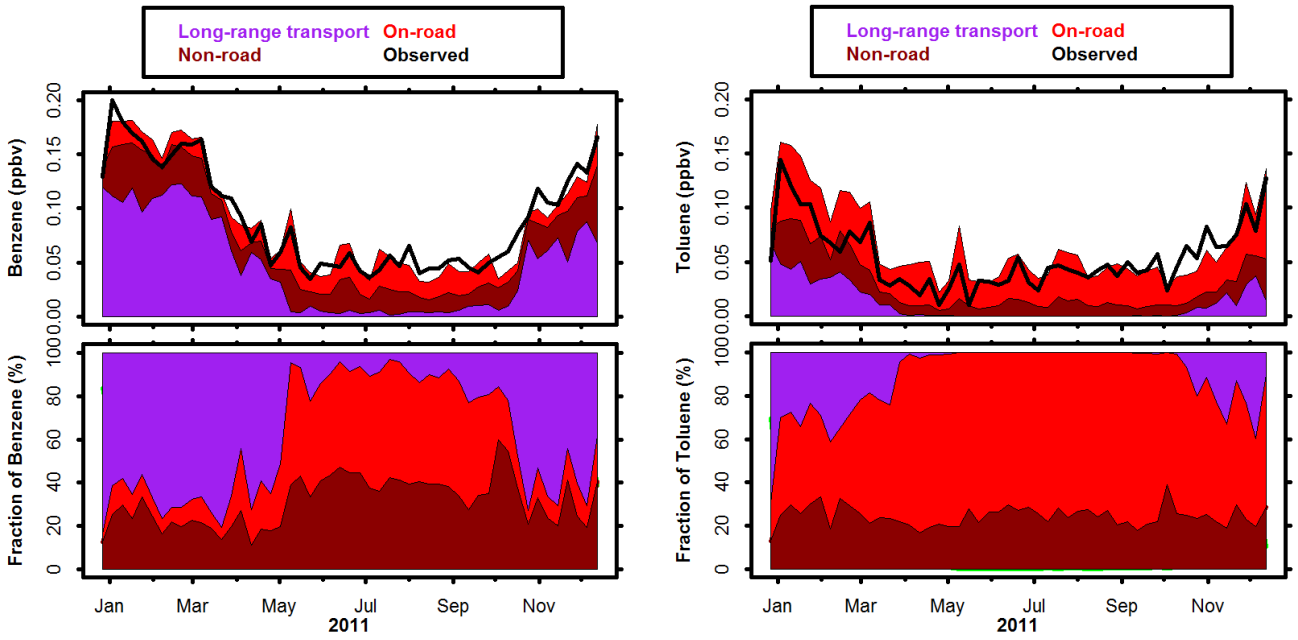

Figure 5.6. Top panels (left: benzene; right: toluene): Stack plot of the seasonal mixing ratios (weekly mean) from various sources in the best-estimate GEOS-Chem simulation at the KCMP tall tower. Also shown are the observed mixing ratios at the tall tower (black line). Bottom panels: Fractional contribution of these sources to the total modeled benzene (left) and toluene (right) abundance in the optimized simulation. Source apportionments for C_8 aromatics are similar to these of toluene.

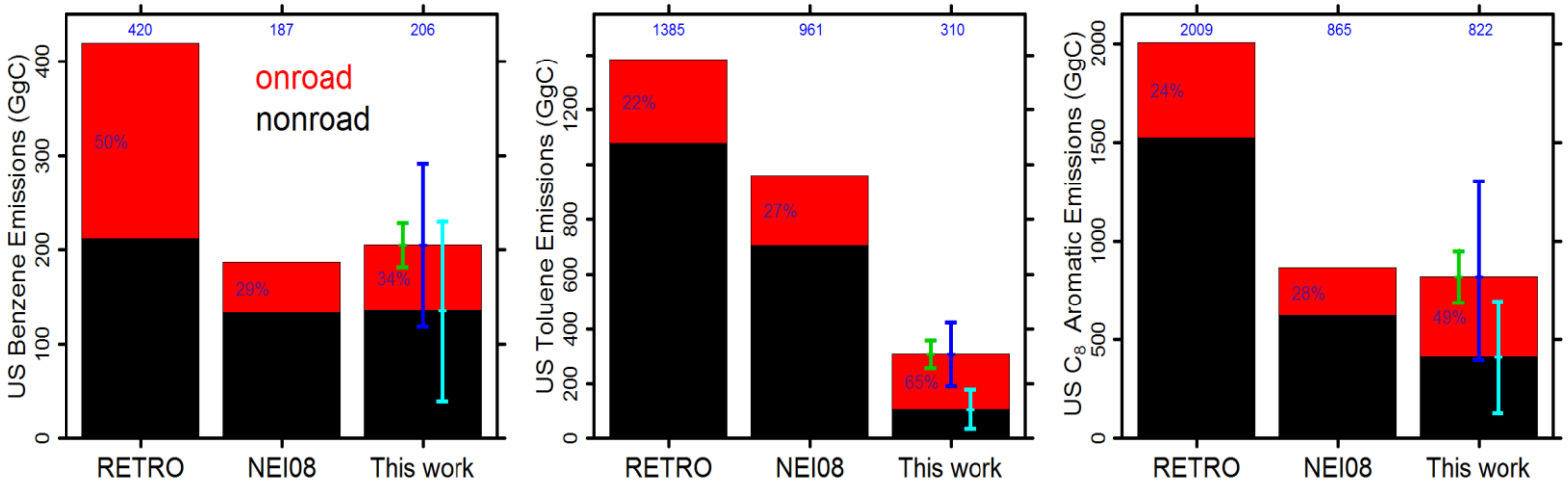

Figure 5.7. Annual aromatic emissions in the contiguous US in the RETRO (based on 2000) and NEI08 (based on 2011) a priori emission inventories, compared to the best-estimate a posteriori emissions. Also shown the fraction of on-road emissions (percentage numbers in the red area of each bar) and the total emissions (blue numbers above each bar). The uncertainty ranges from 24 sensitivity runs (Table S5.2) are shown for the a posteriori total emissions (blue error bars), on-road emissions (green), and non-road emissions (cyan).

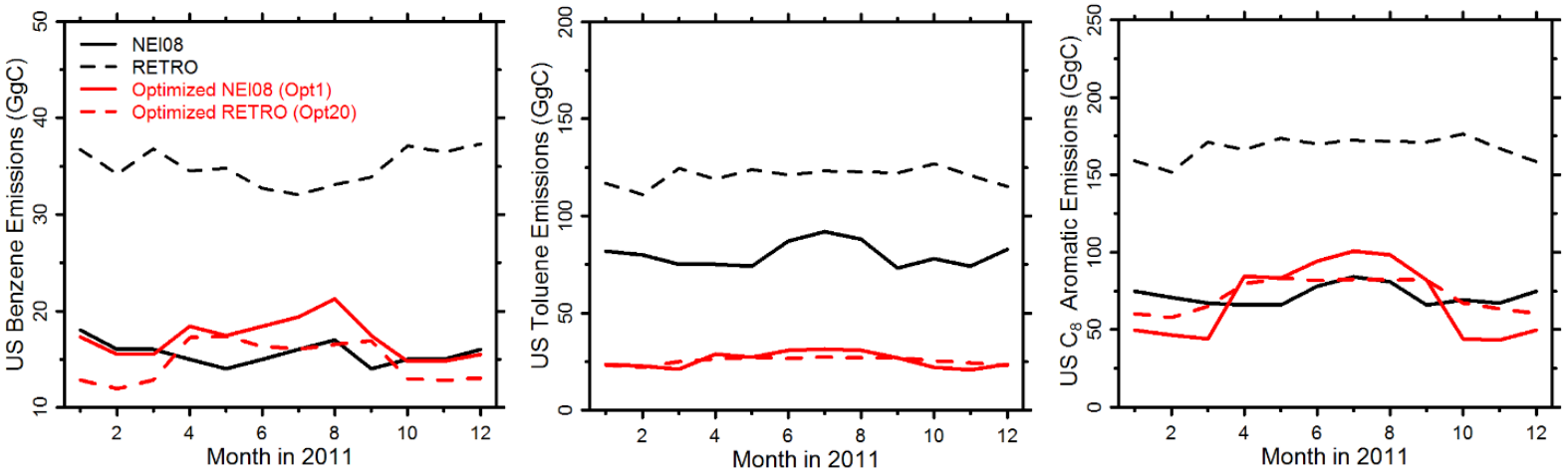

Figure 5.8. Monthly total emissions for benzene (left panel), toluene (middle), and C_8 aromatics (right) in the a priori NEI08 (black solid line) and RETRO (black dashed line) inventories, compared to the a posteriori estimates based on NEI08 (red solid line; Opt1 in Table S5.2) and RETRO (red dashed line; Opt20 in Table S5.2).

Supplemental Information for Chapter 5

Table S5.1. Mapping RETRO species to GEOS-Chem tracers

GEOS-Chem tracer	Applicable RETRO species	Global emissions (TgC/y)	Comments
ALK4	Butanes Pentanes Hexanes and Higher Alkanes	32.56	ALK4 is alkanes >= 4 carbon atoms
ACET	Ketones	2.63	Assume acetone accounts for 75% of the total ketones
MEK	Ketones	0.88	Assume methyl ethyl ketone accounts for 25% of the total ketones
ALD2	Other Alkanals	0.93	Assume all alkanals are acetaldehyde since no RCHO emissions are provided
PRPE	Propene	2.35	PRPE is lumped >= C3 alkenes
C3H8	Propane	2.88	
CH2O	Methanal	0.46	
C2H6	Ethane	4.09	
C2H4	Ethene	5.55	
BENZ	Benzene	3.21	
TOLU	Toluene	5.60	
XYLE	Xylene and other aromatics	7.22	Assume "other aromatics" is solely ethylbenzene (personal communication, RETRO group, 2013). XYLE is C_8 aromatic compounds including o-, m-, p-xylenes and ethylbenzene.
C2H2	Ethyne	2.28	
HCOOH	Acids	0.49	Assume HCOOH accounts for 25% of the total acids based on Chebbi et al. (1996)
Total		71.14	

Table S5.2. A posteriori emission estimates for the contiguous US in the best-estimate inversion and 24 sensitivity analyses.

		Benzene				Toluene				Xylenes			
Opt number	Note	On-road	Non-road	US total	$J_{final}/J_{initial}$[1]	On-road	Non-road	US total	$J_{final}/J_{initial}$[1]	On-road	Non-road	US total	$J_{final}/J_{initial}$[1]
	A priori; NEI08; 2011; GgC	54	133	187		256	705	961		241	624	865	
1a	NEI08; 2011; Seasonal[2]: cold; DryDep[3]; GgC	22	72		0.29	76	58		0.2	161	117		0.87
1b	NEI08; 2011; Seasonal[2]: warm; DryDep[3]; GgC	48	67		0.62	125	51		0.34	246	298		0.91
1	Opt 1; GgC	70	139	209		201	109	310		407	415	822	
Sensitivity runs: deviation from the best-estimate Opt1													
2	NEI08; 2011; DryDep[3]; Annual[4]	-16%	18%	6%	0.41	-9%	23%	2%	0.27	-21%	7%	-7%	0.99
3	NEI08; 2011; Annual[4]	-11%	13%	5%	0.49	-9%	23%	2%	0.25	-22%	5%	-8%	0.99
4	NEI08; 2010; Annual[4]	-10%	-3%	-5%	0.65	-1%	8%	2%	0.28	-11%	4%	-3%	0.99
5	NEI08; 2010-2011; Annual[4]	-11%	5%	0%	0.57	-5%	13%	1%	0.27	-16%	5%	-5%	0.99
6	NEI08; 2011; Seasonal[2]; MLE[5]	-3%	-17%	-12%	0.52 (cold);0.78 (warm)	-7%	-67%	-28%	0.03 (cold);0.10 (warm)	-8%	-54%	-31%	0.41 (cold); 0.96 (warm)

7	NEI08; 2011; Annual[4]; MLE[5]	-33%	-4%	-14%	0.65	-25%	-61%	-37%	0.04	-32%	-68%	-51%	0.58
8	NEI08; 2011; Seasonal[2]; $\mathbf{S}_{mod}$ *2[6]	4%	10%	8%	0.72 (cold);0.70 (warm)	-1%	26%	8%	0.14 (cold);0.21 (warm)	4%	27%	16%	0.98 (cold); 0.86 (warm)
9	NEI08; 2011; Annual[4]; $\mathbf{S}_{mod}$ *2[6]	0%	24%	16%	0.58	-6%	36%	9%	0.17	-13%	35%	12%	0.99
10	NEI08; 2011; Seasonal[2]; γ_{HO2} *2[7]	3%	-4%	-2%	0.38 (cold); 0.69 (warm)	-2%	-3%	-2%	0.18 (cold); 0.31 (warm)	-2%	-5%	-3%	0.84 (cold); 0.92 (warm)
11	NEI08; 2011; Annual[4]; γ_{HO2} *2[7]	-13%	10%	2%	0.52	-11%	17%	-1%	0.24	-22%	1%	-11%	0.98
12	NEI08; 2011; Seasonal[2]; E_{NOx} *0.6[8]	3%	-6%	-3%	0.36 (cold); 0.67 (warm)	0%	-13%	-5%	0.18 (cold); 0.31 (warm)	1%	-8%	-3%	0.85 (cold); 0.92 (warm)
13	NEI08; 2011; Annual[4]; E_{NOx} *0.6[8]	-13%	10%	2%	0.5	-8%	10%	-2%	0.24	-20%	1%	-10%	0.98
14	NEI08; 2011; Seasonal[2]; with Br chemsitry[9]	3%	-1%	0%	0.36 (cold); 0.65 (warm)	0%	0%	0%	0.19 (cold); 0.34 (warm)	-1%	0%	0%	0.86 (cold); 0.91 (warm)
15	NEI08; 2011; Annual[4]; with Br chemsitry[9]	-13%	13%	4%	0.49	-9%	23%	2%	0.25	-22%	5%	-8%	0.99
16	NEI08; 2011;	6%	57%	39%	0.3 (cold);	8%	36%	18%	0.28	4%	17%	11%	0.92

	Seasonal[2]; DryDep with relative uptake[10]				0.47 (warm)				(cold); 0.47 (warm)				(cold); 0.88 (warm)
17	NEI08; 2011; Annual[4]; DryDep with relative uptake[10]	-11%	70%	42%	0.37	-2%	61%	20%	0.36	-16%	16%	0%	0.99
18	NEI08; 2011; Seasonal[2]; PBL local[11]	10%	7%	8%	0.39 (cold); 0.62 (warm)	8%	0%	5%	0.23 (cold); 0.41 (warm)	-1%	4%	1%	0.87 (cold); 0.91 (warm)
19	NEI08; 2011; Annual[4]; PBL local[11]	-6%	21%	12%	0.5	-3%	23%	6%	0.3	-23%	7%	-8%	0.99
20	RETRO; 2011; Seasonal[2]; DryDep[3]			-14%	0.34 (cold); 0.35 (warm)			-2%	0.13 (cold); 0.08 (warm)			5%	0.43 (cold); 0.48 (warm)
21	RETRO; 2011; Annual[4]; DryDep[3]			-13%	0.35			-2%	0.11			3%	0.45
22	RETRO; 2011; Seasonal[2];			-12%	0.36 (cold); 0.34 (warm)			-2%	0.12 (cold); 0.08 (warm)			15%	0.47 (cold); 0.48 (warm)
23	RETRO; 2011; Annual[4]			-10%				-2%	0.13			15%	0.45
24	RETRO; 2010; Annual[4]			-8%				3%	0.13			25%	0.54
	Min[12]	-33%	-17%	-14%		-25%	-67%	-37%		-32%	-68%	-51%	

Max[12]	10%	70%	42%		8%	61%	20%		4%	35%	25%

[1] Cost function reduced from their a priori; [2] Optimizations using only warm season (April – September) or only cold season (October – March) data; see Section 4 and Table 3 for source combinations for different seasons; [3] With dry deposition as described in Section 2.3; [4] Optimizations using a full year of data; [5] Estimation of $\mathbf{S}_a$ and $\mathbf{S}_\Sigma$ based on a maximum likelihood estimation approach; [6] Doubling the model error which is a major part of the observational error covariance matrix $\mathbf{S}_\Sigma$; [7] doubling the reactive uptake coefficient for HO_2 on aqueous aerosols from 0.2 to 0.4; [8] Decreasing NO_x emissions over North America by 40%; [9] Including bromine chemistry; [10] Including reactive uptakes of aromatics during dry depositions; [11] Using a local boundary layer mixing scheme; [12] Minimum or maximum of deviation from Opt1 based on Opt2 to Opt24.

Table S5.3. Emission correction factors for the best-estimate optimizations relative to the bottom-up RETRO inventory.

	Benzene		Toluene		C_8 aromatics	
RETRO (Opt20)	U.S. emission	Boundary condition	U.S. emission	Boundary condition	U.S. emission	Boundary condition
Cold	0.35	2.74	0.2	2.14	0.38	4.92
Warm	0.50	2.20	0.22	1	0.48	1

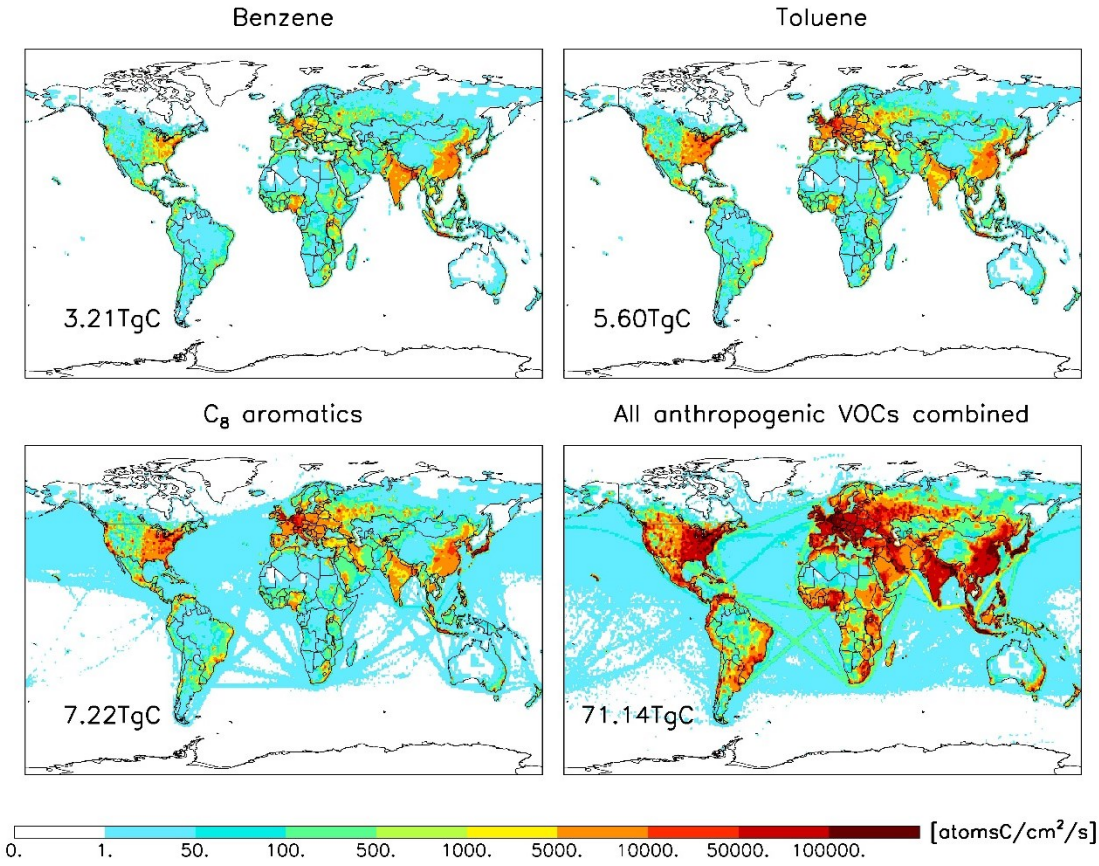

Figure S5.1. Annual emissions of C_6-C_8 aromatics and all anthropogenic VOCs combined in GEOS-Chem based on the RETRO inventory for the year 2000. Numbers inset show the aggregated annual flux for the corresponding GEOS-Chem tracer (see Table S1).

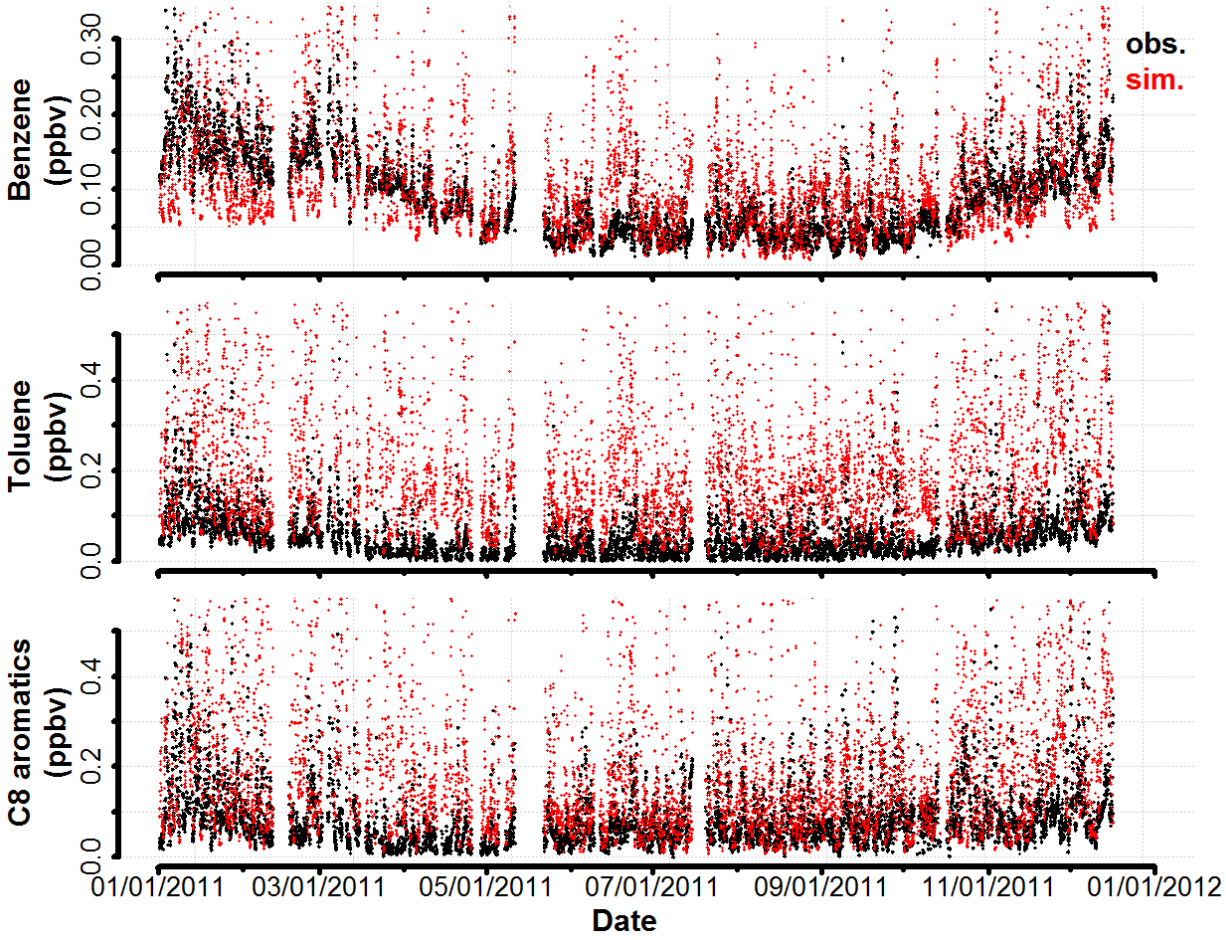

Figure S5.2. Annual cycle in benzene, toluene, and C_8 aromatics observed at the KCMP tall tower for the year 2011(black). Also shown (in red) are predicted values from the GEOS-Chem a priori simulation based on the RETRO inventory. All data points are 1 h means.

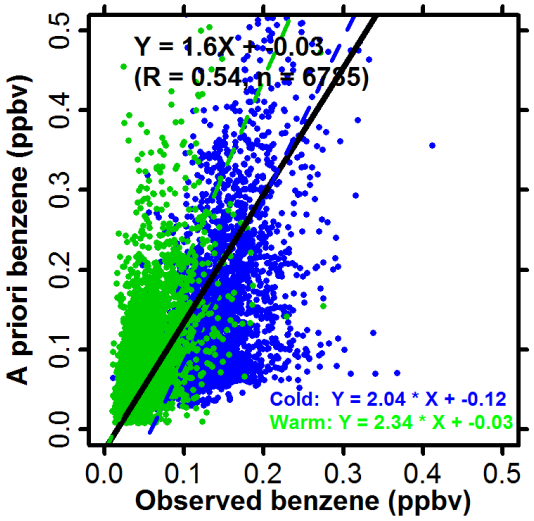
Y = 1.6X + -0.03
(R = 0.54, n = 6785)
Cold: Y = 2.04 * X + -0.12
Warm: Y = 2.34 * X + -0.03
A priori benzene (ppbv)
Observed benzene (ppbv)
0.0
0.1
0.2
0.3
0.4
0.5

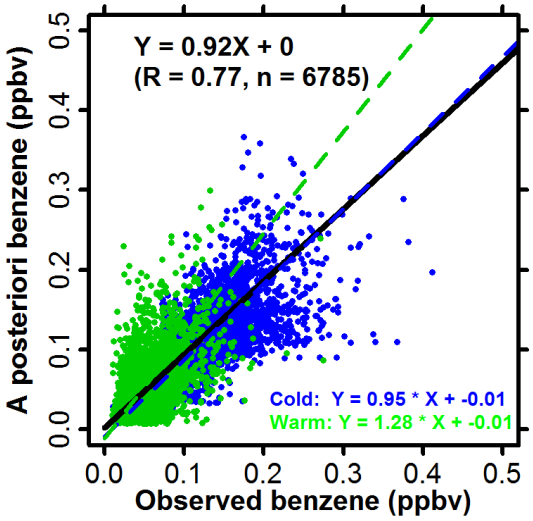
Y = 0.92X + 0
(R = 0.77, n = 6785)
Cold: Y = 0.95 * X + -0.01
Warm: Y = 1.28 * X + -0.01
A posteriori benzene (ppbv)
Observed benzene (ppbv)
0.0
0.1
0.2
0.3
0.4
0.5

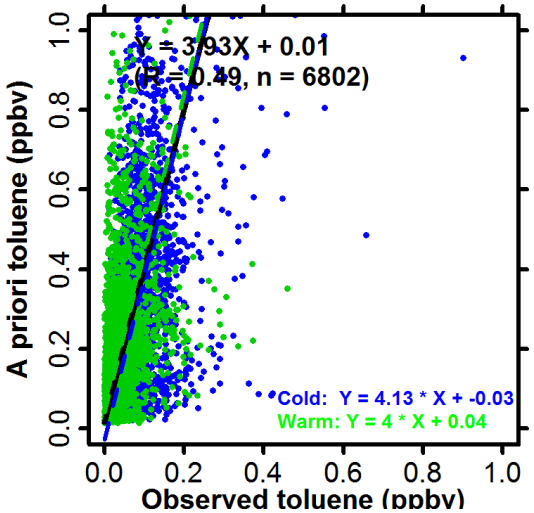
Y = 3.93X + 0.01
(R = 0.49, n = 6802)
Cold: Y = 4.13 * X + -0.03
Warm: Y = 4 * X + 0.04
A priori toluene (ppbv)
Observed toluene (ppbv)
0.0
0.2
0.4
0.6
0.8
1.0

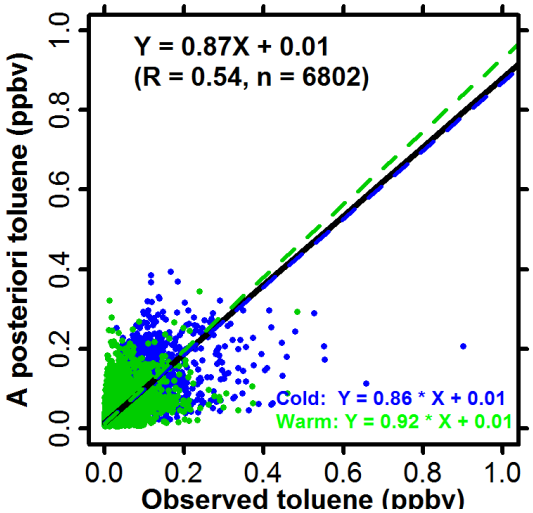
Y = 0.87X + 0.01
(R = 0.54, n = 6802)
Cold: Y = 0.86 * X + 0.01
Warm: Y = 0.92 * X + 0.01
A posteriori toluene (ppbv)
Observed toluene (ppbv)
0.0
0.2
0.4
0.6
0.8
1.0

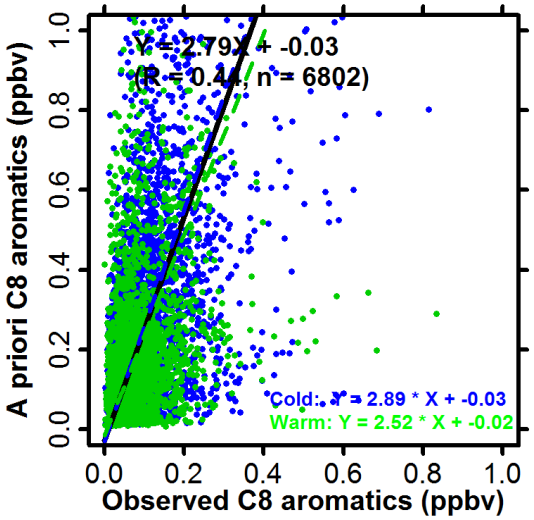
Y = 2.79X + -0.03
(R = 0.44, n = 6802)
Cold: Y = 2.89 * X + -0.03
Warm: Y = 2.52 * X + -0.02
A priori C8 aromatics (ppbv)
Observed C8 aromatics (ppbv)
0.0
0.2
0.4
0.6
0.8
1.0

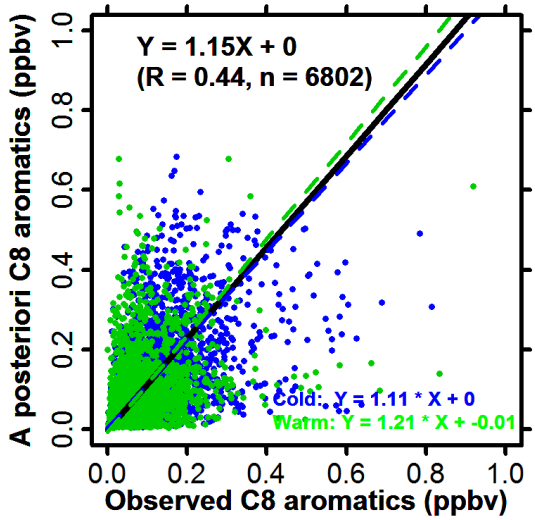
Y = 1.15X + 0
(R = 0.44, n = 6802)
Cold: Y = 1.11 * X + 0
Warm: Y = 1.21 * X + -0.01
A posteriori C8 aromatics (ppbv)
Observed C8 aromatics (ppbv)
0.0
0.2
0.4
0.6
0.8
1.0

Figure S5.3: Atmospheric aromatic mixing ratios at the KCMP tall tower. Predicted values from the GEOS-Chem a priori (left column) and a posteriori (right) RETRO-based simulations compared to observations from 2011, and colored by seasons. Data points are 1 h mean values.

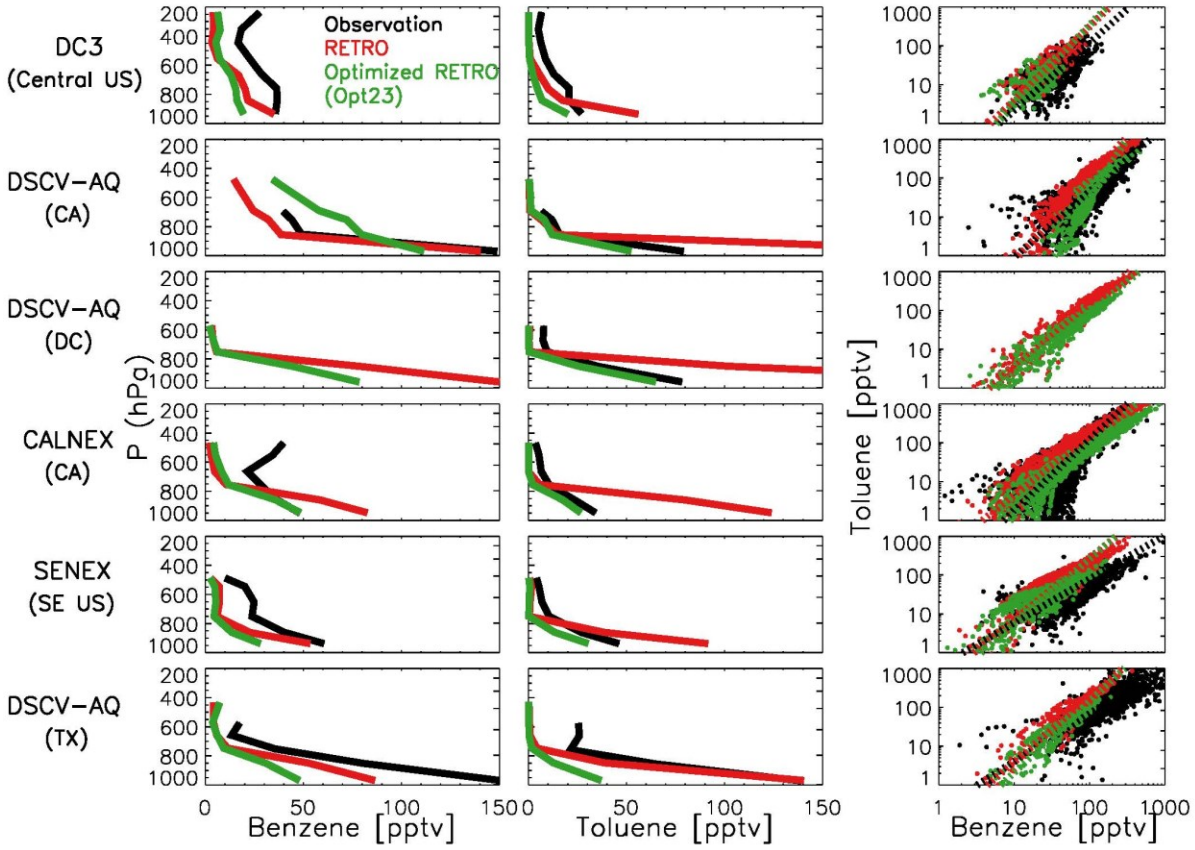

Figure S5.4. Airborne measurements of benzene and toluene over the United States. Left columns: median observed (black) and simulated (red: a priori; green: a posteriori) vertical profiles for six recent aircraft campaigns. Right column: relationship between benzene and toluene (boundary-layer data only; $P > 800$ hPa) on a log-log scale, with dashed lines showing the best fit from a major axis regression. Model simulations shown here are based on the RETRO inventory. DSCV-AQ (CA): DISCOVER-AQ California; DISCV-AQ (DC): DISCOVER-AQ Baltimore-Washington DC; DSCV-AQ (TX): DISCOVER-AQ Texas.

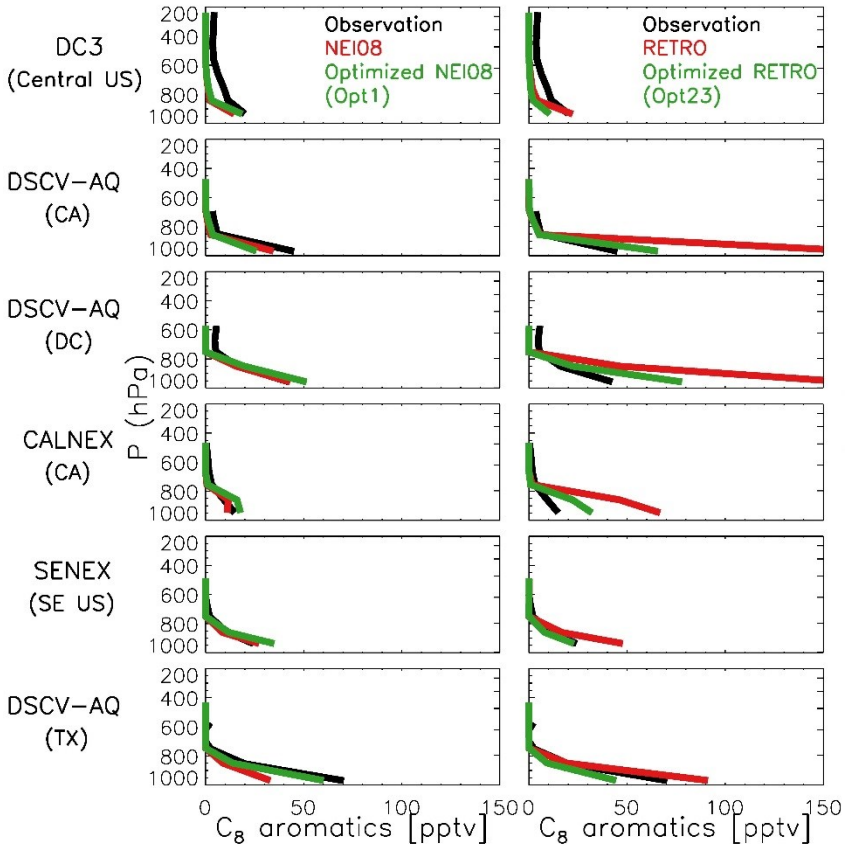

Figure S5.5. Airborne measurements of C_8 aromatics over the United States. Plotted are the median observed (black) and simulated (red: a priori; green: a posteriori) vertical profiles for six recent aircraft campaigns. The left column shows simulations based on the EPA's NEI08 inventory, while the right column shows simulations based on the RETRO inventory. DSCV-AQ (CA): DISCOVER-AQ California; DISCV-AQ (DC): DISCOVER-AQ Baltimore-Washington DC; DSCV-AQ (TX): DISCOVER-AQ Texas.

6 Conclusions and future directions

This chapter summarizes the main conclusions of this dissertation, and suggests directions for future study.

6.1 Sources and seasonality of atmospheric methanol based on tall tower measurements in the US Upper Midwest

Methanol is the most abundant VOC observed at the KCMP tall tower. The seasonal cycle of observed methanol concentrations is generally similar to that simulated by a state-of-science chemical transport model (GEOS-Chem CTM), except the seasonal peak occurs ~1 month earlier in the observations, apparently reflecting a model underestimate of emission rates for younger versus older leaves. Based on a source tracer approach, we estimate that anthropogenic emissions account for ~40% of the ambient methanol abundance during winter and 10% during summer. The seasonal importance of methanol as a source of HCHO and CO is highest (accounting for up to 20% of their production rates) in spring through early summer, when biogenic methanol emissions are high but isoprene emissions are still relatively low. The biased seasonality in the model suggests that the photochemical role for methanol early in the growing season is presently underestimated.

6.2 North American acetone sources determined from tall tower measurements and inverse modeling

Acetone is the second most abundant VOC observed at the KCMP tall tower. An inverse analysis of the tall tower observations reveals that biogenic acetone emissions from broadleaf trees, shrubs, and herbaceous plants are presently underestimated (~37%), but emissions from needleleaf trees plus secondary production from biogenic precursors are overestimated by a similar amount (~40%). Our inverse analysis shows that North American primary + secondary anthropogenic acetone sources in the model (based on the US EPA's NEI 2005 inventory) are accurate to within approximately 20%. An optimized GEOS-Chem simulation incorporating the above findings captures 70% of the variance in the observed hourly measurements. The resulting North American acetone source of 11

Tg a^{-1}, including both primary emissions and secondary production, and with roughly equal contributions from anthropogenic and biogenic sources, is nearly as large as the total continental VOC source (all compounds combined) from fossil fuel combustion.

6.3 Isoprene emissions and impacts over an ecological transition region in the US Upper Midwest

Based on an intercomparison of independent measurement techniques and a source-tracer analysis, we find that anthropogenic isoprene contributes to 30% of the observed PTR-MS signal at m/z 69 signal on average during summertime at the KCMP tall tower. Interferences for MVK+MACR at m/z 71 are small (7%). The KCMP tall tower is impacted by local as well as regional isoprene sources, as diagnosed by daytime enhancements of isoprene under southwest winds and by MVK+MACR enhancements under other wind directions. Model-measurement comparisons using the GEOS-Chem CTM imply that isoprene emissions in the immediate vicinity of the KCMP tall tower are accurately captured by MEGANv2.1 biogenic inventory, but that larger-scale regional emissions are underestimated, reflecting the heterogeneous land cover and uncertain isoprene fluxes in this transitional landscape. We find that isoprene emissions play a key role in seasonal shifts between NO_x and VOC limited chemical regimes, and that role is still currently underestimated for the area surrounding the Twin Cities of Minneapolis and St. Paul due to the model underprediction of regional isoprene fluxes.

6.4 Emissions of C_6-C_8 aromatic compounds in the United States: Constraints from tall tower and aircraft measurements

A Bayesian inverse analysis based on two full years of measurements at the KCMP tall tower suggests that: *i*) the RETRO global emission inventory significantly overestimates US aromatic emissions by factors of 2.0, 4.5, and 2.4 for benzene, toluene, and C_8 aromatics during 2010-2011; *ii*), the US EPA's NEI08 inventory likewise overestimates the toluene flux by a factor of 3, partly reflecting a bias in the estimated non-road emissions; and *iii*) total annual emissions of benzene and C_8 aromatics in the EPA's NEI08 are accurate to within the constraints provided by the KCMP tall tower

observations, but the on-road emissions of these compounds are underestimated by a factor of 2 during the warm season (April – October). We find also that C_6-C_8 aromatic sources upwind of North America are more than double the prior estimate, likely reflecting a substantial underestimate of aromatic sources in East Asia (by at least a factor of 2). We find that up to 60% of the observed benzene mixing ratios (up to 20% for toluene and 15% for C_8 aromatics) during winter in the U.S. Upper Midwest can be attributed to sources outside North America. Independent aircraft measurements suggest that the emission biases found for C_6-C_8 aromatic VOCs based on our tall tower measurements in the Upper Midwest also apply to other parts of the contiguous U.S., with exceptions in California and Texas. Our resulting best estimates of year-2011 emissions in the contiguous US are 206 GgC for benzene, 310 GgC for toluene, and 822 GgC for C_8 aromatic compounds.

6.5 Implications of this dissertation

This dissertation developed the first-ever long term in-situ tall tower measurements of VOC concentrations. The analyses of this unique dataset advanced scientific understanding of the sources of key atmospheric VOCs and their impacts on other air pollutants. This dissertation demonstrated that the bottom-up errors in aggregated biogenic and anthropogenic emission estimates are better than a factor of two for most of the compounds examined here. However, a number of major seasonal and sectoral biases are evident and merit further attention. In addition, development of high resolution, accurate land cover and meteorological data for use in CTMs is a key need for future improvement. Lastly, given the dramatic ongoing changes in domestic and international emission sources, and projected future climate variations, sustained measurements are still needed in other key regions in the US to monitor these changes and the evolving importance of long-range transport of air pollutants.

6.6 Directions for future research

6.6.1 The role of the ocean in climate and atmospheric composition

Chapter 3 of this dissertation on North American acetone sources has highlighted the importance of the oceans in controlling the global budgets of important atmospheric trace gases. 70% of the Earth's surface is ocean, however, we know little about its role in atmospheric chemistry. Future work toward understanding ocean-atmosphere exchange will need to address the following questions: what biological and physical-chemical mechanisms control the emission and uptake of VOCs and other reactive species by the ocean surface? What are the contributions of these emissions to marine aerosols? How do oceanic emissions affect air quality in coastal cities? How do they affect the global tropospheric background for various longer-lived species? How will atmosphere-ocean exchange be impacted by climate change? This area of work will require field measurements to study air-sea trace gas exchange over key ocean regions, inverse modeling to estimate emission rates from satellite data, and developing coupled ocean modules for atmospheric chemical transport models that will allow us to interpret observations in terms of underlying emission processes and VOC chemistry.

6.6.2 Emission-energy-climate interactions

Many emissions associated with rapidly changing aspects of the energy sector are poorly constrained. These changes include land cover alteration associated with biofuel crop production, and the rapid US expansion of oil and gas production via coastal drilling and hydraulic fracturing. Biofuel-driven land cover change could replace some present agricultural crops/grassland with other plants that are stronger isoprene-emitters (Ashworth et al., 2013), or that are potential emitters of other reactive gases (Graus et al., 2013). Oil and gas production is an important source of atmospheric methane (Pétron et al., 2012) and of hazardous air pollutants (Warneke et al., 2014), but can also play a role in reducing regional CO_2, NO_x, and SO_2 emissions by providing opportunities to switch to a less polluting energy source (from coal to natural gas) (de Gouw et al., 2014). Future work is urgently needed to establish detailed emission inventories for these energy-related activities, and to extensively evaluate those inventories. This would require

multiple research platforms such as ground-based and airborne field measurements, observations from space, and 3-D atmospheric modeling to evaluate the impact of these emissions on local air quality and global climate, and to predict their future changes and effects. Since Minnesota is downwind of some major oil/gas production areas (e.g., South Dakota, North Dakota), future observations from the KCMP tall tower could help to resolve some of these key energy-related research questions. In addition, multi-species observations from space (e.g., methanol, formic acid, NO_2, methane) can also provide unique perspectives for resolving oil/gas-related emissions from other sources.

6.6.3 Transported air pollutants and their role in US air quality

This dissertation has demonstrated the importance of long-range transport for atmospheric benzene in North America (Chapter 5). Future research is needed to address how extensive such impacts are for different parts of the US, and for other air pollutants (e.g., ozone), as well as the role of long-range transport of air pollution in affecting human health in the US. More long-term measurements of VOCs, aerosols, NO_x, CO and O_3 are needed across the US to quantify the contribution to each from international sources. In addition, realistic emission inventories for developing countries are crucial for accurate model simulations of international pollutant transportation. Future efforts should focus on investigating emissions from India, China, and African countries, leveraging the use of satellite observations since field measurements are typically sparse in developing countries.

6.6.4 How will atmospheric photochemistry change over the US as a result of decreasing domestic emissions combined with increasing international emissions from developing countries?

Evidence shows that anthropogenic emissions within the US are declining (Warneke et al., 2012; McDonald et al., 2013; de Gouw et al., 2014), while transported pollutants from other countries are likely to increase. On the other hand, biogenic VOC emissions are likely to stay the same or decline due to the net effect of increasing temperature and rising ambient CO_2 concentrations (Guenther et al., 2012). Overall, this could mean that:

some airsheds in the US will shift from their current high-NO_x environment to a low-NO_x environment, while other areas could see a higher air pollutant load due to increasing long-range transport. Either scenario could significantly impact the NO_x-VOC-chemical conditions, which in turn would require divergent adaptation strategies for ozone control in different regions. This complicated issue can be addressed by incorporating realistic emission scenarios in high-resolution global chemical transport model simulations.

6.6.5 Formation of secondary organic aerosol (SOA) through interactions between anthropogenic and biogenic compounds

Anthropogenic emissions have been proposed to play an important role in the formation of biogenic SOA (Weber et al., 2007) through various mechanisms, including: *i*) biogenic VOC oxidation in high sulfate and high NO_x environments (Goldstein et al., 2009), and *ii*) anthropogenic organic aerosol providing a pre-existing condensed medium for partitioning of semivolatile products of biogenic origin (Carlton et al., 2010). To better understand such processes, we need: 1) laboratory studies of the interactions between anthropogenic and biogenic emissions in a variety of combinations and conditions; 2) extensive gas and aerosol measurements in field locations that experience a confluence of biogenic and anthropogenic sources, such as the KCMP tall tower site discussed in this dissertation; 3) concurrent satellite observations of formaldehyde, glyoxal, NO_2, SO_2, and aerosol optical depth to link VOC emissions and chemistry to SOA formation.

References

2008 National Emissions Inventory: Review, Analysis and Highlights: http://www.epa.gov/ttnchie1/net/2008report.pdf, access: January 2014.

2010 Census: Table 20. Large Metropolitan Statistical Areas--Population: http://www.census.gov/compendia/statab/2012/tables/12s0020.xls, access: May, 2014.

Aiello, M., and McLaren, R.: Measurement of airborne carbonyls using an automated sampling and analysis system, Environ. Sci. Technol., 43, 8901-8907, doi:10.1021/es901892f, 2009.

Alvarado, A., Tuazon, E.C., M. Aschmann, S., Arey, J., and Atkinson, R.: Products and mechanisms of the gas-phase reactions of OH radicals and O_3 with 2-methyl-3-buten-2-ol, Atmos. Environ., 33, 2893-2905, 1999.

Andreae, M.O., and Merlet, P.: Emission of trace gases and aerosols from biomass burning, Global Biogeochem. Cy., 15, 955-966, doi: 10.1029/2000GB001382 2001.

Arneth, A., Monson, R.K., Schurgers, G., Niinemets, Ü., and Palmer, P.I.: Why are estimates of global terrestrial isoprene emissions so similar (and why is this not so for monoterpenes)?, Atmos. Chem. Phys., 8, 4605-4620, doi: 10.5194/acp-8-4605-2008, 2008.

Arnold, F., Bürger, V., Droste-Fanke, B., Grimm, F., Krieger, A., Schneider, J., and Stilp, T.: Acetone in the upper troposphere and lower stratosphere: Impact on trace gases and aerosols, Geophys. Res. Lett., 24, 3017-3020, 1997.

Arnold, S.R., Chipperfield, M.P., and Blitz, M.A.: A three-dimensional model study of the effect of new temperature-dependent quantum yields for acetone photolysis, J. Geophys. Res., 110, D22305, doi:10.1029/2005JD005998, 2005.

Ashworth, K., Wild, O., and Hewitt, C.N.: Impacts of biofuel cultivation on mortality and crop yields, Nature Clim. Change, 3, 492-496, doi: 10.1038/nclimate1788, 2013.

Atkinson, R., Baulch, D., Cox, R., Crowley, J., Hampson, R., Hynes, R., Jenkin, M., Rossi, M., and Troe, J.: Evaluated kinetic and photochemical data for atmospheric chemistry: Volume II. Gas phase reactions of organic species, Atmos. Chem. Phys., 6, 3625-4055, doi:10.5194/acp-6-3625-2006, 2006.

Baan, R., Grosse, Y., Straif, K., Secretan, B., El Ghissassi, F., Bouvard, V., Benbrahim-Tallaa, L., Guha, N., Freeman, C., Galichet, L., and Cogliano, V.: A review of human carcinogens—Part F: Chemical agents and related occupations, Lancet Oncol., 10, 1143-1144, doi:10.1016/S1470-2045(09)70358-4, 2009.

Baker, B., Guenther, A., Greenberg, J., and Fall, R.: Canopy level fluxes of 2-methyl-3-buten-2-ol, acetone, and methanol by a portable relaxed eddy accumulation system, Environ. Sci. Technol., 35, 1701-1708, doi:10.1021/es001007j, 2001.

Barkley, M.P., Palmer, P.I., Ganzeveld, L., Arneth, A., Hagberg, D., Karl, T., Guenther, A., Paulot, F., Wennberg, P.O., Mao, J., Kurosu, T.P., Chance, K., Müller, J.F., De Smedt, I., Van Roozendael, M., Chen, D., Wang, Y., and Yantosca, R.M.: Can a

"state of the art" chemistry transport model simulate Amazonian tropospheric chemistry?, J. Geophys. Res., 116, D16302, doi: 10.1029/2011jd015893, 2011.

Bey, I., Jacob, D.J., Yantosca, R.M., Logan, J.A., Field, B.D., Fiore, A.M., Li, Q., Liu, H.Y., Mickley, L.J., and Schultz, M.G.: Global modeling of tropospheric chemistry with assimilated meteorology: Model description and evaluation, J. Geophys. Res., 106, 23073-23095, doi:10.1029/2001JD000807, 2001.

Blitz, M.A., Heard, D.E., Pilling, M.J., Arnold, S.R., and Chipperfield, M.P.: Pressure and temperature-dependent quantum yields for the photodissociation of acetone between 279 and 327.5 nm, Geophys. Res. Lett., 31, L06111, doi:10.1029/2003GL018793, 2004.

Boersma, K.F., Jacob, D.J., Trainic, M., Rudich, Y., DeSmedt, I., Dirksen, R., and Eskes, H.J.: Validation of urban NO2 concentrations and their diurnal and seasonal variations observed from the SCIAMACHY and OMI sensors using in situ surface measurements in Israeli cities, Atmos. Chem. Phys., 9, 3867-3879, doi: 10.5194/acp-9-3867-2009, 2009.

Borbon, A.s., Fontaine, H., Veillerot, M., Locoge, N., Galloo, J.C., and Guillermo, R.: An investigation into the traffic-related fraction of isoprene at an urban location, Atmos. Environ., 35, 3749-3760, doi: 10.1016/S1352-2310(01)00170-4, 2001.

Brown, S.S., Dubé, W.P., Bahreini, R., Middlebrook, A.M., Brock, C.A., Warneke, C., de Gouw, J.A., Washenfelder, R.A., Atlas, E., Peischl, J., Ryerson, T.B., Holloway, J.S., Schwarz, J.P., Spackman, R., Trainer, M., Parrish, D.D., Fehshenfeld, F.C., and Ravishankara, A.R.: Biogenic VOC oxidation and organic aerosol formation in an urban nocturnal boundary layer: aircraft vertical profiles in Houston, TX, Atmos. Chem. Phys., 13, 11317-11337, doi: 10.5194/acp-13-11317-2013, 2013.

Carlton, A.G., Pinder, R.W., Bhave, P.V., and Pouliot, G.A.: To what extent can biogenic SOA be controlled?, Environ. Sci. Technol., 44, 3376-3380, doi: 10.1021/es903506b, 2010.

Carslaw, D.C., and Ropkins, K.: *openair* - An R package for air quality data analysis, Environ. Modell. Softw., 27-28, 52-61, doi: 10.1016/j.envsoft.2011.09.008, 2012.

Chatfield, R.B., Gardner, E.P., and Calvert, J.G.: Sources and sinks of acetone in the troposphere: Behavior of reactive hydrocarbons and a stable product, J. Geophys. Res., 92, 4208-4216, 1987.

Chen, D., Wang, Y., McElroy, M.B., He, K., Yantosca, R.M., and Le Sager, P.: Regional CO pollution and export in China simulated by the high-resolution nested-grid GEOS-Chem model, Atmos. Chem. Phys., 9, 3825-3839, doi:10.5194/acp-9-3825-2009, 2009.

Chen, Y.-H., and Prinn, R.G.: Estimation of atmospheric methane emissions between 1996 and 2001 using a three-dimensional global chemical transport model, J. Geophys. Res., 111, D10307, doi: 10.1029/2005jd006058, 2006.

Choi, W., Faloona, I.C., Bouvier-Brown, N.C., McKay, M., Goldstein, A.H., Mao, J., Brune, W.H., LaFranchi, B.W., Cohen, R.C., Wolfe, G.M., Thornton, J.A., Sonnenfroh, D.M., and Millet, D.B.: Observations of elevated formaldehyde over a forest canopy suggest missing sources from rapid oxidation of arboreal hydrocarbons, Atmos. Chem. Phys., 10, 8761-8781, doi: 10.5194/acp-10-8761-2010, 2010.

Christian, T.J., Kleiss, B., Yokelson, R.J., Holzinger, R., Crutzen, P.J., Hao, W.M., Shirai, T., and Blake, D.R.: Comprehensive laboratory measurements of biomass-burning emissions: 2. First intercomparison of open-path FTIR, PTR-MS, and GC-MS/FID/ECD, J. Geophys. Res., 109, D02311, doi: 10.1029/2003jd003874, 2004.

Colorado Department of Public Health and Environment (CDPHE) (2008), Denver metropolitan area and North Front Range 8-hour ozone state implementation plan - Emissions inventory: http://www.colorado.gov/airquality/documents/deno308/Emission_Inventory_TSD_DraftFinal.pdf, access:

Corcoran, J.M.: Assessing the spatial variability of net ecosystem carbon dioxide production in the Upper Midwest, M.S. thesis, University of Minnesota-Twin Cities, US, 123 pp, 2009.

Crounse, J.D., Paulot, F., Kjaergaard, H.G., and Wennberg, P.O.: Peroxy radical isomerization in the oxidation of isoprene, Phys. Chem. Chem. Phys., 13, 13607-13613, doi: 10.1039/c1cp21330j, 2011.

de Gouw, J.A., Howard, C.J., Custer, T.G., and Fall, R.: Emissions of volatile organic compounds from cut grass and clover are enhanced during the drying process, Geophys. Res. Lett., 26, 811-814, 1999.

de Gouw, J.A., Goldan, P.D., Warneke, C., Kuster, W.C., Roberts, J.M., Marchewka, M., Bertman, S.B., Pszenny, A.A.P., and Keene, W.C.: Validation of proton transfer reaction-mass spectrometry (PTR-MS) measurements of gas-phase organic compounds in the atmosphere during the New England Air Quality Study (NEAQS) in 2002, J. Geophys. Res., 108, 4682, doi: 10.1029/2003JD003863, 2003.

de Gouw, J.A., Warneke, C., Karl, T., Eerdekens, G., van der Veen, C., and Fall, R.: Sensitivity and specificity of atmospheric trace gas detection by proton-transfer-reaction mass spectrometry, Int. J. Mass Spectrom., 223, 365-382, doi: 10.1016/S1387-3806(02)00926-0, 2003.

de Gouw, J.A., Middlebrook, A.M., Warneke, C., Goldan, P.D., Kuster, W.C., Roberts, J.M., Fehsenfeld, F.C., Worsnop, D.R., Canagaratna, M.R., Pszenny, A.A.P., Keene, W.C., Marchewka, M., Bertman, S.B., and Bates, T.S.: Budget of organic carbon in a polluted atmosphere: Results from the New England Air Quality Study in 2002, J. Geophys. Res., 110, D16305, doi: 10.1029/2004JD005623, 2005.

de Gouw, J.A., and Warneke, C.: Measurements of volatile organic compounds in the earth's atmosphere using proton-transfer-reaction mass spectrometry, Mass Spectrom. Rev., 26, 223-257, doi: 10.1002/mas.20119, 2007.

de Gouw, J.A., Parrish, D.D., Frost, G.J., and Trainer, M.: Reduced emissions of CO2, NOx, and SO2 from U.S. power plants owing to switch from coal to natural gas with combined cycle technology, Earth's Future, 2, 75-82, doi: 10.1002/2013ef000196, 2014.

de Reus, M., Fischer, H., Arnold, F., de Gouw, J., Holzinger, R., Warneke, C., and Williams, J.: On the relationship between acetone and carbon monoxide in different air masses, Atmos. Chem. Phys., 3, 1709-1723, doi:10.5194/acp-3-1709-2003, 2003.

Development of baseline 2006 emissions from oil and gas activity in the Denver-Julesburg Basin, WRAP Phase III report: http://www.wrapair.org/forums/ogwg/documents/2008-04_06_Baseline_Emissions_DJ_Basin_Technical_Memo_(04-30).pdf, access:

Dufour, G., Szopa, S., Barkley, M. P., Boone, C. D., Perrin, A., Palmer, P. I., and Bernath, P. F.: Global upper-tropospheric formaldehyde: Seasonal cycles observed by the ACE-FTS satellite instrument, Atmos. Chem. Phys., 9, 3893-3910, doi:10.5194/acp-9-3893-2009, 2009.

Duncan, B.N., Logan, J.A., Bey, I., Megretskaia, I.A., Yantosca, R.M., Novelli, P.C., Jones, N.B., and Rinsland, C.P.: Global budget of CO, 1988-1997: Source estimates and validation with a global model, J. Geophys. Res., 112 (D22), D22301, doi: 10.1029/2007JD008459, 2007.

Duncan, B.N., Yoshida, Y., Olson, J.R., Sillman, S., Martin, R.V., Lamsal, L., Hu, Y., Pickering, K.E., Retscher, C., Allen, D.J., and Crawford, J.H.: Application of OMI observations to a space-based indicator of NO_x and VOC controls on surface ozone formation, Atmos. Environ., 44, 2213-2223, doi: 10.1016/j.atmosenv.2010.03.010, 2010.

Dunlea, E.J., Herndon, S.C., Nelson, D.D., Volkamer, R.M., San Martini, F., Sheehy, P.M., Zahniser, M.S., Shorter, J.H., Wormhoudt, J.C., Lamb, B.K., Allwine, E.J., Gaffney, J.S., Marley, N.A., Grutter, M., Marquez, C., Blanco, S., Cardenas, B., Retama, A., Ramos Villegas, C.R., Kolb, C.E., Molina, L.T., and Molina, M.J.: Evaluation of nitrogen dioxide chemiluminescence monitors in a polluted urban environment, Atmos. Chem. Phys., 7, 2691-2704, doi: 10.5194/acp-7-2691-2007, 2007.

Elias, T., Szopa, S., Zahn, A., Schuck, T., Brenninkmeijer, C., Sprung, D., and Slemr, F.: Acetone variability in the upper troposphere: analysis of CARIBIC observations and LMDz-INCA chemistry-climate model simulations, Atmos. Chem. Phys, 11, 8053-8074, doi:10.5194/acp-11-8053-2011, 2011.

Environmental Protection Agency National Emission Inventory for 2005: http://www.epa.gov/ttnchie1/net/2005inventory.html, access: 1 December, 2011.

EPA AirData: Access to monitored air quality data from EPA's Air Quality System (AQS) Data Mart: https://ofmext.epa.gov/AQDMRS/aqdmrs.html, access: August, 2013.

EPA: Environmental Protection Agency National Emission Inventory for 1999: http://www.epa.gov/ttnchie1/net/1999inventory.html, last access: 1 March 2011, 1999.

Fall, R., and Benson, A.A.: Leaf methanol - the simplest natural product from plants, Trends Plant Sci., 1, 296-301, doi: 10.1016/S1360-1385(96)88175-0, 1996.

Fall, R.: Abundant oxygenates in the atmosphere: A biochemical perspective, Chem. Rev., 103, 4941-4951, doi: 10.1021/cr0206521, 2003.

Fiore, A.M., Horowitz, L.W., Purves, D.W., Levy, H., Evans, M.J., Wang, Y., Li, Q., and Yantosca, R.M.: Evaluating the contribution of changes in isoprene emissions to surface ozone trends over the eastern United States, J. Geophys. Res., 110, D12303, doi: 10.1029/2004jd005485, 2005.

Fischer, E.V., Jacob, D.J., Millet, D.B., Yantosca, R.M., and Mao, J.: The role of the ocean in the global atmospheric budget of acetone, Geophys. Res. Lett., 39, L01807, doi:10.1029/2011GL050086, 2012.

Folberth, G., Hauglustaine, D., Lathiere, J., and Brocheton, F.: Interactive chemistry in the Laboratoire de Météorologie Dynamique general circulation model: model description and impact analysis of biogenic hydrocarbons on tropospheric chemistry, Atmos. Chem. Phys., 6, 2273-2319, doi:10.5194/acp-6-2273-2006, 2006.

Folkers, A., Huve, K., Ammann, C., Dindorf, T., Kesselmeier, J., Kleist, E., Kuhn, U., Uerlings, R., and Wildt, J.: Methanol emissions from deciduous tree species: Dependence on temperature and light intensity, Plant Biol., 10, 65-75, doi: 10.1111/j.1438-8677.2007.00012.x, 2008.

Folkins, I., and Chatfield, R.: Impact of acetone on ozone production and OH in the upper troposphere at high NO_x, J. Geophys. Res., 105, 11,585-11,600, 2000.

Fortin, T.J., Howard, B.J., Parrish, D.D., Goldan, P.D., Kuster, W.C., Atlas, E.L., and Harley, R.A.: Temporal changes in U.S. benzene emissions inferred from atmospheric measurements, Environ. Sci. Technol., 39, 1403-1408, doi: 10.1021/es049316n, 2005.

Fu, T.-M., Jacob, D.J., Palmer, P.I., Chance, K., Wang, Y.X., Barletta, B., Blake, D.R., Stanton, J.C., and Pilling, M.J.: Space-based formaldehyde measurements as constraints on volatile organic compound emissions in east and south Asia and implications for ozone, J. Geophys. Res., 112, D06312, doi: 10.1029/2006jd007853, 2007.

Galbally, I.E., and Kirstine, W.: The production of methanol by flowering plants and the global cycle of methanol, J. Atmos. Chem., 43, 195-229, doi: 10.1023/A:1020684815474, 2002.

Gierczak, T., Burkholder, J.B., Bauerle, S., and Ravishankara, A.R.: Photochemistry of acetone under tropospheric conditions, Chem. Phys., 231, 229-244, 1998.

Goldan, P.D., Trainer, M., Kuster, W.C., Parrish, D.D., Carpenter, J., Roberts, J.M., Yee, J.E., and Fehsenfeld, F.C.: Measurements of hydrocarbons, oxygenated hydrocarbons, carbon monoxide, and nitrogen oxides in an urban basin in Colorado: Implications for emission inventories, J. Geophys. Res., 100, 22771-22783, 1995.

Goldstein, A.H., Goulden, M.L., Munger, J.W., Wofsy, S.C., and Geron, C.D.: Seasonal course of isoprene emissions from a midlatitude deciduous forest, J. Geophys. Res., 103, 31045-31056, doi: 10.1029/98JD02708, 1998.

Goldstein, A.H., and Schade, G.W.: Quantifying biogenic and anthropogenic contributions to acetone mixing ratios in a rural environment, Atmos. Environ., 34, 4997-5006, 2000.

Goldstein, A.H., and Galbally, I.E.: Known and unexplored organic constituents in the Earth's atmosphere, Environ. Sci. Technol., 41, 1514-1521, doi: 10.1021/es072476p, 2007.

Goldstein, A.H., Koven, C.D., Heald, C.L., and Fung, I.Y.: Biogenic carbon and anthropogenic pollutants combine to form a cooling haze over the southeastern

United States, Proc. Natl. Acad. Sci. U.S.A., 106, 8835-8840, doi: 10.1073/pnas.0904128106, 2009.
Graus, M., Eller, A.S.D., Fall, R., Yuan, B., Qian, Y., Westra, P., de Gouw, J., and Warneke, C.: Biosphere-atmosphere exchange of volatile organic compounds over C4 biofuel crops, Atmos. Environ., 66, 161-168, doi: 10.1016/j.atmosenv.2011.12.042, 2013.
Griffis, T.J., Baker, J.M., Sargent, S.D., Eriksson, M., Corcoran, J., Chen, M., and Billmark, K.: Influence of C_4 vegetation on $^{13}CO_2$ discrimination and isoforcing in the Upper Midwest, United States, Global Biogeochem. Cy., 24, GB4006, doi: 10.1029/2009GB003768, 2010.
Griffis, T.J., Lee, X., Baker, J.M., Russelle, M.P., Zhang, X., Venterea, R., and Millet, D.B.: Reconciling the differences between top-down and bottom-up estimates of nitrous oxide emissions for the U.S. Corn Belt, Global Biogeochem. Cy., 27, 746-754, doi: 10.1002/gbc.20066, 2013.
Guenther, A., Hewitt, C.N., Erickson, D., Fall, R., Geron, C., Graedel, T., Harley, P., Klinger, L., Lerdau, M., McKay, W.A., Pierce, T., Scholes, B., Steinbrecher, R., Tallamraju, R., Taylor, J., and Zimmerman, P.: A global-model of natural volatile organic-compound emissions, J. Geophys. Res., 100, 8873-8892, 1995.
Guenther, A., Karl, T., Harley, P., Wiedinmyer, C., Palmer, P.I., and Geron, C.: Estimates of global terrestrial isoprene emissions using MEGAN (Model of Emissions of Gases and Aerosols from Nature), Atmos. Chem. Phys., 6, 3181-3210, doi: 10.5194/acp-6-3181-2006, 2006.
Guenther, A.B., Jiang, X., Heald, C.L., Sakulyanontvittaya, T., Duhl, T., Emmons, L.K., and Wang, X.: The Model of Emissions of Gases and Aerosols from Nature version 2.1 (MEGAN2.1): an extended and updated framework for modeling biogenic emissions, Geosci. Model Dev. Discuss., 5, 1503-1560, doi:10.5194/gmdd-5-1503-2012, 2012.
Guo, H., Ling, Z.H., Cheung, K., Wang, D.W., Simpson, I.J., and Blake, D.R., Acetone in the atmosphere of Hong Kong: Abundance, sources and photochemical precursors, Atmos. Environ., 65, 80-88, doi:10.1016/j.atmosenv.2012.10.027, 2013.
Harley, P.C., Monson, R.K., and Lerdau, M.T.: Ecological and evolutionary aspects of isoprene emission from plants, Oecologia, 118, 109-123, doi: 10.1007/s004420050709, 1999.
Harley, P., Greenberg, J., Niinemets, U., and Guenther, A.: Environmental controls over methanol emission from leaves, Biogeosciences, 4, 1083-1099, doi: 10.5194/bg-4-1083-2007, 2007.
Harley, R.A., Hooper, D.S., Kean, A.J., Kirchstetter, T.W., Hesson, J.M., Balberan, N.T., Stevenson, E.D., and Kendall, G.R.: Effects of reformulated gasoline and motor vehicle fleet turnover on emissions and ambient concentrations of benzene, Environ. Sci. Technol., 40, 5084-5088, doi: 10.1021/es0604820, 2006.
Heald, C.L., Jacob, D.J., Jones, D.B.A., Palmer, P.I., Logan, J.A., Streets, D.G., Sachse, G.W., Gille, J.C., Hoffman, R.N., and Nehrkorn, T.: Comparative inverse analysis of satellite (MOPITT) and aircraft (TRACE-P) observations to estimate Asian

sources of carbon monoxide, J. Geophys. Res., 109, D23306, doi:10.1029/2004JD005185, 2004.
Heikes, B.G., Chang, W.N., Pilson, M.E.Q., Swift, E., Singh, H.B., Guenther, A., Jacob, D.J., Field, B.D., Fall, R., Riemer, D., and Brand, L.: Atmospheric methanol budget and ocean implication, Global Biogeochem. Cy., 16, 1133, doi: 10.1029/2002GB001895, 2002.
Helmig, D., Bocquet, F., Pollmann, J. and Revermann, T.: Analytical techniques for sesquiterpene emission rate studies in vegetation enclosure experiments, Atmos. Environ., 38, 557-572, doi:10.1016/j.atmosenv.2003.10.012, 2004
Henze, D.K., Seinfeld, J.H., Ng, N.L., Kroll, J.H., Fu, T.M., Jacob, D.J., and Heald, C.L.: Global modeling of secondary organic aerosol formation from aromatic hydrocarbons: high- vs. low-yield pathways, Atmos. Chem. Phys., 8, 2405-2420, doi: 10.5194/acp-8-2405-2008, 2008.
Holtslag, A., and Boville, B.: Local versus nonlocal boundary-layer diffusion in a global climate model, J. Clim., 6, 1825-1842, 1993.
Holzinger, R., Warneke, C., Hansel, A., Jordan, A., Lindinger, W., Scharffe, D.H., Schade, G., and Crutzen, P.J.: Biomass burning as a source of formaldehyde, acetaldehyde, methanol, acetone, acetonitrile, and hydrogen cyanide, Geophys. Res. Lett., 26, 1161-1164, doi: 10.1029/1999GL900156, 1999.
Hu, L., Millet, D.B., Mohr, M.J., Wells, K.C., Griffis, T.J., and Helmig, D.: Sources and seasonality of atmospheric methanol based on tall tower measurements in the US Upper Midwest, Atmos. Chem. Phys., 11, 11145-11156, doi:10.5194/acp-11-11145-2011, 2011.
Hu, L., Millet, D.B., Kim, S.Y., Wells, K.C., Griffis, T.J., Fischer, E.V., Helmig, D., Hueber, J., and Curtis, A.J.: North American acetone sources determined from tall tower measurements and inverse modeling, Atmos. Chem. Phys., 13, 3379-3392, doi: 10.5194/acp-13-3379-2013, 2013.
Hudman, R.C., Jacob, D.J., Turquety, S., Leibensperger, E.M., Murray, L.T., Wu, S., Gilliland, A.B., Avery, M., Bertram, T.H., Brune, W., Cohen, R.C., Dibb, J.E., Flocke, F.M., Fried, A., Holloway, J., Neuman, J.A., Orville, R., Perring, A., Ren, X., Sachse, G.W., Singh, H.B., Swanson, A., and Wooldridge, P.J.: Surface and lightning sources of nitrogen oxides over the United States: Magnitudes, chemical evolution, and outflow, J. Geophys. Res., 112, D12S05, doi: 10.1029/2006JD007912, 2007.
Hudman, R.C., Murray, L.T., Jacob, D.J., Millet, D.B., Turquety, S., Wu, S., Blake, D.R., Goldstein, A.H., Holloway, J., and Sachse, G.W.: Biogenic versus anthropogenic sources of CO in the United States, Geophys. Res. Lett., 35, L04801, doi: 10.1029/2007GL032393, 2008.
Jaars, K., Beukes, J.P., van Zyl, P.G., Venter, A.D., Josipovic, M., Pienaar, J.J., Vakkari, V., Aaltonen, H., Laakso, H., Kulmala, M., Tiitta, P., Guenther, A., Hellén, H., Laakso, L., and Hakola, H.: Ambient aromatic hydrocarbon measurements at Welgegund, South Africa, Atmos. Chem. Phys. Discuss., 14, 4189-4227, doi: 10.5194/acpd-14-4189-2014, 2014.

Jacob, D.J., Horowitz, L.W., Munger, J.W., Heikes, B.G., Dickerson, R.R., Artz, R.S., and Keene, W.C.: Seasonal transition from NO_x- to hydrocarbon-limited conditions for ozone production over the eastern United States in September, J. Geophys. Res., 100, 9315-9324, doi: 10.1029/94jd03125, 1995.

Jacob, D.J., Field, B.D., Jin, E.M., Bey, I., Li, Q.B., Logan, J.A., Yantosca, R.M., and Singh, H.B.: Atmospheric budget of acetone, J. Geophys. Res., 107, 4100, doi:10.1029/2001JD000694, 2002.

Jacob, D.J., Crawford, J.H., Kleb, M.M., Connors, V.S., Bendura, R.J., Raper, J.L., Sachse, G.W., Gille, J.C., Emmons, L., and Heald, C.L.: Transport and chemical evolution over the Pacific (TRACE-P) aircraft mission: Design, execution, and first results, J. Geophys. Res., 108, 9000, doi: 10.1029/2002jd003276, 2003.

Jacob, D. J., Field, B. D., Li, Q. B., Blake, D. R., de Gouw, J., Warneke, C., Hansel, A., Wisthaler, A., Singh, H. B., and Guenther, A.: Global budget of methanol: Constraints from atmospheric observations, J. Geophys. Res., 110, D08303, doi:10.1029/2004JD005172, 2005.

Jaeglé, L., Jacob, D.J., Wennberg, P.O., Spivakovsky, C.M., Hanisco, T.F., Lanzendorf, E.J., Hintsa, E.J., Fahey, D.W., Keim, E.R., Proffitt, M.H., Atlas, E.L., Flocke, F., Schauffler, S., McElroy, C.T., Midwinter, C., Pfister, L., and Wilson, J.C.: Observed OH and HO_2 in the upper troposphere suggest a major source from convective injection of peroxides, Geophys. Res. Lett., 24, 3181-3184, 1997.

Jaeglé, L., Jacob, D.J., Brune, W.H., and Wennberg, P.O.: Chemistry of HO_x radicals in the upper troposphere, Atmos. Environ., 35, 469-489, doi:10.1016/S1352-2310(00)00376-9, 2001.

Janson, R., De Serves, C., and Romero, R.: Emission of isoprene and carbonyl compounds from a boreal forest and wetland in Sweden, Agric. Forest Meteorol., 98, 671-681, 1999.

Jardine, K.J., Sommer, E.D., Saleska, S.R., Huxman, T.E., Harley, P.C., and Abrell, L.: Gas phase measurements of pyruvic acid and its volatile metabolites, Environ. Sci. Technol., 44, 2454-2460, doi:10.1021/es903544p, 2010.

Johnson, D., Jenkin, M.E., Wirtz, K., and Martin-Reviejo, M.: Simulating the formation of secondary organic aerosol from the photooxidation of aromatic hydrocarbons, Environ. Chem., 2, 35-48, doi: 10.1071/EN04079, 2005.

Jordan, C., Fitz, E., Hagan, T., Sive, B., Frinak, E., Haase, K., Cottrell, L., Buckley, S., and Talbot, R.: Long-term study of VOCs measured with PTR-MS at a rural site in New Hampshire with urban influences, Atmos. Chem. Phys., 9, 4677-4697, doi: 10.5194/acp-9-4677-2009, 2009.

Kaiser, E.W., Siegl, W.O., Cotton, D.F., and Anderson, R.W.: Effect of fuel structure on emissions from a spark-ignited engine. 2. Naphthene and aromatic fuels, Environ. Sci. Technol., 26, 1581-1586, 1992.

Karl, T.G., Spirig, C., Rinne, J., Stroud, C., Prevost, P., Greenberg, J., Fall, R., and Guenther, A.: Virtual disjunct eddy covariance measurements of organic compound fluxes from a subalpine forest using proton transfer reaction mass spectrometry, Atmos. Chem. Phys., 2, 279-291, doi:10.5194/acp-2-279-2002, 2002.

Karl, T., Guenther, A., Spirig, C., Hansel, A., and Fall, R.: Seasonal variation of biogenic VOC emissions above a mixed hardwood forest in northern Michigan, Geophys. Res. Lett., 30, 2186, doi:10.1029/2003gl018432, 2003.

Karl, T., Potosnak, M., Guenther, A., Clark, D., Walker, J., Herrick, J.D., and Geron, C.: Exchange processes of volatile organic compounds above a tropical rain forest: Implications for modeling tropospheric chemistry above dense vegetation, J. Geophys. Res, 109, D18306, doi:10.1029/2004JD004738, 2004.

Karl, T., Guenther, A., Yokelson, R.J., Greenberg, J., Potosnak, M., Blake, D.R., and Artaxo, P.: The tropical forest and fire emissions experiment: Emission, chemistry, and transport of biogenic volatile organic compounds in the lower atmosphere over Amazonia, J. Geophys. Res., 112, D18302, doi: 10.1029/2007JD008539, 2007.

Karl, T., Apel, E., Hodzic, A., Riemer, D.D., Blake, D.R., and Wiedinmyer, C.: Emissions of volatile organic compounds inferred from airborne flux measurements over a megacity, Atmos. Chem. Phys., 9, 271-285, doi: 10.5194/acp-9-271-2009, 2009.

Karl, T., Harley, P., Emmons, L., Thornton, B., Guenther, A., Basu, C., Turnipseed, A., and Jardine, K.: Efficient atmospheric cleansing of oxidized organic trace gases by vegetation, Science, 330, 816-819, doi: 10.1126/science.1192534, 2010.

Karl, T., Hansel, A., Cappellin, L., Kaser, L., Herdlinger-Blatt, I., and Jud, W.: Selective measurements of isoprene and 2-methyl-3-buten-2-ol based on NO^+ ionization mass spectrometry, Atmos. Chem. Phys., 12, 11877-11884, doi: 10.5194/acp-12-11877-2012, 2012.

Kim, S.Y., Millet, D.B., Hu, L., Mohr, M.J., Griffis, T.J., Wen, D., Lin, J.C., Miller, S.M., and Longo, M.: Constraints on carbon monoxide emissions based on tall tower measurements in the U.S. Upper Midwest, Environ. Sci. Technol., 47, 8316-8324, doi: 10.1021/es4009486, 2013.

Kleinman, L.I.: Low and high NOx tropospheric photochemistry, J. Geophys. Res., 99, 16831-16838, doi: 10.1029/94jd01028, 1994.

Lamb, B., Guenther, A., Gay, D., and Westberg, H.: A national inventory of biogenic hydrocarbon emissions, Atmos. Environ., 21, 1695-1705, doi: 10.1016/0004-6981(87)90108-9, 1987.

Lamsal, L.N., Martin, R.V., van Donkelaar, A., Steinbacher, M., Celarier, E.A., Bucsela, E., Dunlea, E.J., and Pinto, J.P.: Ground-level nitrogen dioxide concentrations inferred from the satellite-borne Ozone Monitoring Instrument, J. Geophys. Res., 113, D16308, doi: 10.1029/2007jd009235, 2008.

Lappalainen, H.K., Sevanto, S., Back, J., Ruuskanen, T.M., Kolari, P., Taipale, R., Rinne, J., Kulmala, M., and Hari, P.: Day-time concentrations of biogenic volatile organic compounds in a boreal forest canopy and their relation to environmental and biological factors, Atmos. Chem. Phys., 9, 5447-5459, doi: 10.5194/acp-9-5447-2009, 2009.

Lathière, J., Hauglustaine, D., Friend, A., Noblet-Ducoudre, D., Viovy, N., and Folberth, G.: Impact of climate variability and land use changes on global biogenic volatile organic compound emissions, Atmos. Chem. Phys., 6, 2129-2146, doi:10.5194/acp-6-2129-2006, 2006.

Legreid, G., Loov, J. B., Staehelin, J., Hueglin, C., Hill, M., Buchmann, B., Prevot, A. S. H., and Reimann, S.: Oxygenated volatile organic compounds (OVOCs) at an urban background site in Zurich (Europe): Seasonal variation and source allocation, Atmos. Environ., 41, 8409–8423, doi:10.1016/j.atmosenv.2007.07.026, 2007.

Levi, M.A.: Comment on "Hydrocarbon emissions characterization in the Colorado Front Range: A pilot study" by Gabrielle Pétron et al, J. Geophys. Res., 117, D21203, doi: 10.1029/2012jd017686, 2012.

Levi, M.A.: Reply to "Reply to 'Comment on "Hydrocarbon emissions characterization in the Colorado Front Range – A Pilot Study"' by Michael A. Levi" by Gabrielle Pétron et al, J. Geophys. Res., 118, 3044-3046, doi: 10.1002/jgrd.50299, 2013.

Lewis, A., Hopkins, J., Carpenter, L., Stanton, J., Read, K., and Pilling, M.: Sources and sinks of acetone, methanol, and acetaldehyde in North Atlantic marine air, Atmos. Chem. Phys., 5, 1963-1974, doi:10.5194/acp-5-1963-2005, 2005.

Lin, J.T., and McElroy, M.B.: Impacts of boundary layer mixing on pollutant vertical profiles in the lower troposphere: Implications to satellite remote sensing, Atmos. Environ., 44, 1726-1739, doi:10.1016/j.atmosenv.2010.02.009, 2010.

Lin, J.T., and McElroy, M.B.: Impacts of boundary layer mixing on pollutant vertical profiles in the lower troposphere: Implications to satellite remote sensing, Atmos. Environ., 44, 1726-1739, doi:10.1016/j.atmosenv.2010.02.009, 2010.

Lindinger, W., Hansel, A., and Jordan, A.: On-line monitoring of volatile organic compounds at pptv levels by means of proton-transfer-reaction mass spectrometry (PTR-MS) - Medical applications, food control and environmental research, Int. J. Mass Spectrom., 173, 191-241, doi: 10.1016/S0168-1176(97)00281-4, 1998.

Liu, Y.J., Herdlinger-Blatt, I., McKinney, K.A., and Martin, S.T.: Production of methyl vinyl ketone and methacrolein via the hydroperoxyl pathway of isoprene oxidation, Atmos. Chem. Phys., 13, 5715-5730, doi: 10.5194/acp-13-5715-2013, 2013.

Liu, Z., Wang, Y., Gu, D., Zhao, C., Huey, L.G., Stickel, R., Liao, J., Shao, M., Zhu, T., Zeng, L., Liu, S.-C., Chang, C.-C., Amoroso, A., and Costabile, F.: Evidence of reactive aromatics as a major source of peroxy acetyl nitrate over China, Environ. Sci. Technol., 44, 7017-7022, doi: 10.1021/es1007966, 2010.

Liu, Z., Wang, Y., Vrekoussis, M., Richter, A., Wittrock, F., Burrows, J.P., Shao, M., Chang, C.-C., Liu, S.-C., Wang, H., and Chen, C.: Exploring the missing source of glyoxal (CHOCHO) over China, Geophys. Res. Lett., 39, L10812, doi: 10.1029/2012gl051645, 2012.

MacDonald, R.C., and Fall, R.: Acetone emission from conifer buds, Phytochemistry, 34, 991-994, 1993b.

MacDonald, R.C., and Fall, R.: Detection of substantial emissions of methanol from plants to the atmosphere, Atmos. Environ. A. Gen., 27, 1709-1713, doi:10.1016/0960-1686(93)90233-O, 1993a.

Madronich, S., and Calvert, J.G.: Permutation reactions of organic peroxy radicals in the troposphere, J. Geophys. Res., 95, 5697-5715, 1990.

Mao, J., Jacob, D.J., Evans, M.J., Olson, J.R., Ren, X., Brune, W.H., Clair, J.M.S., Crounse, J.D., Spencer, K.M., Beaver, M.R., Wennberg, P.O., Cubison, M.J., Jimenez, J.L.,

Fried, A., Weibring, P., Walega, J.G., Hall, S.R., Weinheimer, A.J., Cohen, R.C., Chen, G., Crawford, J.H., McNaughton, C., Clarke, A.D., Jaeglé, L., Fisher, J.A., Yantosca, R.M., Le Sager, P., and Carouge, C.: Chemistry of hydrogen oxide radicals (HO_x) in the Arctic troposphere in spring, Atmos. Chem. Phys., 10, 5823-5838, doi:10.5194/acp-10-5823-2010, 2010.

Mao, J., Fan, S., Jacob, D.J., and Travis, K.R.: Radical loss in the atmosphere from Cu-Fe redox coupling in aerosols, Atmos. Chem. Phys., 13, 509-519, doi: 10.5194/acp-13-509-2013, 2013.

Marais, E.A., Jacob, D.J., Kurosu, T.P., Chance, K., Murphy, J.G., Reeves, C., Mills, G., Casadio, S., Millet, D.B., Barkley, M.P., Paulot, F., and Mao, J.: Isoprene emissions in Africa inferred from OMI observations of formaldehyde columns, Atmos. Chem. Phys., 12, 6219-6235, doi: 10.5194/acp-12-6219-2012, 2012.

Marandino, C., De Bruyn, W., Miller, S., Prather, M., and Saltzman, E.: Oceanic uptake and the global atmospheric acetone budget, Geophys. Res. Lett, 32, L15806, doi:10.1029/2005GL023285, 2005.

Martin, R.V., Jacob, D.J., Yantosca, R.M., Chin, M., and Ginoux, P.: Global and regional decreases in tropospheric oxidants from photochemical effects of aerosols, J. Geophys. Res., 108, 4097, doi:10.1029/2002JD002622, 2003.

Martín-Reviejo, M., and Wirtz, K.: Is benzene a precursor for secondary organic aerosol?, Environ. Sci. Technol., 39, 1045-1054, doi: 10.1021/es049802a, 2005.

McDonald, B.C., Gentner, D.R., Goldstein, A.H., and Harley, R.A.: Long-term trends in motor vehicle emissions in U.S. urban areas, Environ. Sci. Technol., 47, 10022-10031, doi: 10.1021/es401034z, 2013.

McKeen, S., Gierczak, T., Burkholder, J., Wennberg, P., Hanisco, T., Keim, E., Gao, R.S., Liu, S., Ravishankara, A., and Fahey, D.: The photochemistry of acetone in the upper troposphere: A source of odd-hydrogen radicals, Geophys. Res. Lett., 24, 3177-3180, 1997.

McKeen, S.A., and Liu, S.C.: Hydrocarbon ratios and photochemical history of air masses, Geophys. Res. Lett., 20, 2363-2366, 1993.

McKeen, S.A., Liu, S.C., Hsie, E.Y., Lin, X., Bradshaw, J.D., Smyth, S., Gregory, G.L., and Blake, D.R.: Hydrocarbon ratios during PEM-WEST A: A model perspective, J. Geophys. Res., 101, 2087-2109, 1996.

McLaren, R., Singleton, D.L., Lai, J.Y.K., Khouw, B., Singer, E., Wu, Z., and Niki, H.: Analysis of motor vehicle sources and their contribution to ambient hydrocarbon distributions at urban sites in Toronto during the Southern Ontario oxidants study, Atmos. Environ., 30, 2219-2232, doi: 10.1016/1352-2310(95)00178-6, 1996.

Michalak, A.M., Hirsch, A., Bruhwiler, L., Gurney, K.R., Peters, W., and Tans, P.P.: Maximum likelihood estimation of covariance parameters for Bayesian atmospheric trace gas surface flux inversions, J. Geophys. Res., 110, D24107, 2005.

Millet, D.B., Goldstein, A.H., Allan, J.D., Bates, T.S., Boudries, H., Bower, K.N., Coe, H., Ma, Y.L., McKay, M., Quinn, P.K., Sullivan, A., Weber, R.J., and Worsnop, D.R.: Volatile organic compound measurements at Trinidad Head, California, during

ITCT 2K2: Analysis of sources, atmospheric composition, and aerosol residence times, J. Geophys. Res., 109, D23S16, doi: 10.1029/2003JD004026, 2004.
Millet, D.B., Donahue, N.M., Pandis, S.N., Polidori, A., Stanier, C.O., Turpin, B.J., and Goldstein, A.H.: Atmospheric volatile organic compound measurements during the Pittsburgh Air Quality Study: Results, interpretation, and quantification of primary and secondary contributions, J. Geophys. Res., 110, D07S07, doi: 10.1029/2004JD004601, 2005.
Millet, D.B., Jacob, D.J., Turquety, S., Hudman, R.C., Wu, S.L., Fried, A., Walega, J., Heikes, B.G., Blake, D.R., Singh, H.B., Anderson, B.E., and Clarke, A.D.: Formaldehyde distribution over North America: Implications for satellite retrievals of formaldehyde columns and isoprene emission, J. Geophys. Res., 111, D24S02, doi: 10.1029/2005JD006853, 2006.
Millet, D.B., Goldstein, A.H., Holzinger, R., Williams, B.J., Allan, J.D., Jimenez, J.L., Worsnop, D.R., Roberts, J.M., White, A.B., Hudman, R.C., Bertschi, I.T., and Stohl, A.: Chemical characteristics of North American surface layer outflow: Insights from Chebogue Point, Nova Scotia, J. Geophys. Res, 111, D23S53, doi: 10.1029/2006jd007287, 2006.
Millet, D.B., Jacob, D.J., Boersma, K.F., Fu, T.-M., Kurosu, T.P., Chance, K., Heald, C.L., and Guenther, A.: Spatial distribution of isoprene emissions from North America derived from formaldehyde column measurements by the OMI satellite sensor, J. Geophys. Res., 113, D02307, doi: 10.1029/2007JD008950, 2008.
Millet, D.B., Jacob, D.J., Custer, T.G., de Gouw, J.A., Goldstein, A.H., Karl, T., Singh, H.B., Sive, B.C., Talbot, R.W., Warneke, C., and Williams, J.: New constraints on terrestrial and oceanic sources of atmospheric methanol, Atmos. Chem. Phys., 8, 6887-6905, doi: 10.5194/acp-8-6887-2008, 2008.
Millet, D.B., Guenther, A., Siegel, D.A., Nelson, N.B., Singh, H.B., de Gouw, J.A., Warneke, C., Williams, J., Eerdekens, G., Sinha, V., Karl, T., Flocke, F., Apel, E., Riemer, D.D., Palmer, P.I., and Barkley, M.: Global atmospheric budget of acetaldehyde: 3-D model analysis and constraints from in-situ and satellite observations, Atmos. Chem. Phys., 10, 3405-3425, doi: 10.5194/acp-10-3405-2010, 2010.
Monson, R.K., Grote, R., Niinemets, Ü., and Schnitzler, J.-P.: Modeling the isoprene emission rate from leaves, New Phytol., 195, 541-559, doi: 10.1111/j.1469-8137.2012.04204.x, 2012.
Monson, R.K., Jones, R.T., Rosenstiel, T.N., and Schnitzler, J.-P.: Why only some plants emit isoprene, Plant. Cell. Environ., 36, 503-516, doi: 10.1111/pce.12015, 2013.
Montzka, S.A., Trainer, M., Goldan, P.D., Kuster, W.C., and Fehsenfeld, F.C.: Isoprene and its oxidation products, methyl vinyl ketone and methacrolein, in the rural troposphere, J. Geophys. Res., 98, 1101-1111, doi: 10.1029/92JD02382, 1993.
Müller, J.-F.: Geographical distribution and seasonal variation of surface emissions and deposition velocities of atmospheric trace gases, J. Geophys. Res., 97, 3787-3804, doi: 10.1029/91jd02757, 1992.
Müller, J.F., Stavrakou, T., Wallens, S., De Smedt, I., Van Roozendael, M., Potosnak, M.J., Rinne, J., Munger, B., Goldstein, A., and Guenther, A.B.: Global isoprene emissions estimated using MEGAN, ECMWF analyses and a detailed canopy

environment model, Atmos. Chem. Phys., 8, 1329-1341, doi: 10.5194/acp-8-1329-2008, 2008.

Murphy, J.G., Day, D.A., Cleary, P.A., Wooldridge, P.J., Millet, D.B., Goldstein, A.H., and Cohen, R.C.: The weekend effect within and downwind of Sacramento - Part 1: Observations of ozone, nitrogen oxides, and VOC reactivity, Atmos. Chem. Phys., 7, 5327-5339, doi: 10.5194/acp-7-5327-2007, 2007.

Myneni, R.B., Yang, W., Nemani, R.R., Huete, A.R., Dickinson, R.E., Knyazikhin, Y., Didan, K., Fu, R., Negrón Juárez, R.I., Saatchi, S.S., Hashimoto, H., Ichii, K., Shabanov, N.V., Tan, B., Ratana, P., Privette, J.L., Morisette, J.T., Vermote, E.F., Roy, D.P., Wolfe, R.E., Friedl, M.A., Running, S.W., Votava, P., El-Saleous, N., Devadiga, S., Su, Y., and Salomonson, V.V.: Large seasonal swings in leaf area of Amazon rainforests, Proc. Natl. Acad. Sci. U.S.A., 104, 4820-4823, doi: 10.1073/pnas.0611338104, 2007.

National Research Council: Rethinking the Ozone Problem in Urban and Regional Air Pollution, The National Academies Press, 1991.

Ng, N.L., Kroll, J.H., Chan, A.W.H., Chhabra, P.S., Flagan, R.C., and Seinfeld, J.H.: Secondary organic aerosol formation from m-xylene, toluene, and benzene, Atmos. Chem. Phys., 7, 3909-3922, doi: 10.5194/acp-7-3909-2007, 2007.

NOAA-MRCC: National Oceanic and Atmospheric Administration Midwestern Regional Climate Center, http://mrcc.isws.illinois.edu/index.jsp, last access: 1 March 2011.

Oleson, K.W., Lawrence, D.M., Bonan, G.B., Flanner, M.G., Kluzek, E., Lawrence, P.J., Levis, S., Swenson, S.C., Thornton, P.E., Dai, A., Decker, M., Dickinson, R., Feddema, J., Heald, C.L., Hoffman, F., Lamarque, J., Mahowald, N., Niu, G., Qian, T., Randerson, J., Running, S., Sakaguchi, K., Slater, A., Stockli, R., Wang, A., Yang, Z., Zeng, X., and Zeng, X.: Technical Description of version 4.0 of the Community Land Model (CLM). NCAR Technical Note NCAR/TN-478+STR, doi: 10.5065/D6FB50WZ, 2010.

Olivier, J.G.J., and Berdowski, J.J.M. (2001), Global emission sources and sinks, in *The Climate System*, edited by J. Berdowski, R. Guicherit, and B.J. Heij, pp. 33-78, A.A. Balkema Publishers/Swets & Zeitlinger Publishers, Lisse, The Netherlands.

Palmer, P.I., Jacob, D.J., Fiore, A.M., Martin, R.V., Chance, K., and Kurosu, T.P.: Mapping isoprene emissions over North America using formaldehyde column observations from space, J. Geophys. Res., 108, 4180, doi: 10.1029/2002jd002153, 2003.

Palmer, P.I., Jacob, D.J., Jones, D.B.A., Heald, C.L., Yantosca, R.M., Logan, J.A., Sachse, G.W., and Streets, D.G.: Inverting for emissions of carbon monoxide from Asia using aircraft observations over the western Pacific, J. Geophys. Res., 108, 8828, doi:10.1029/2003JD003397, 2003.

Palmer, P.I., Abbot, D.S., Fu, T.-M., Jacob, D.J., Chance, K., Kurosu, T.P., Guenther, A., Wiedinmyer, C., Stanton, J.C., Pilling, M.J., Pressley, S.N., Lamb, B., and Sumner, A.L.: Quantifying the seasonal and interannual variability of North American isoprene emissions using satellite observations of the formaldehyde column, J. Geophys. Res., 111, D12315, doi: 10.1029/2005JD006689, 2006.

Park, C., Schade, G.W., and Boedeker, I.: Characteristics of the flux of isoprene and its oxidation products in an urban area, J. Geophys. Res., 116, D21303, doi: 10.1029/2011jd015856, 2011.
Parrella, J.P., Jacob, D.J., Liang, Q., Zhang, Y., Mickley, L.J., Miller, B., Evans, M.J., Yang, X., Pyle, J.A., Theys, N., and Van Roozendael, M.: Tropospheric bromine chemistry: implications for present and pre-industrial ozone and mercury, Atmos. Chem. Phys., 12, 6723-6740, doi: 10.5194/acp-12-6723-2012, 2012.
Parrish, D.D.: Critical evaluation of US on-road vehicle emission inventories, Atmos. Environ., 40, 2288-2300, doi: 10.1016/j.atmosenv.2005.11.033, 2006.
Paulot, F., Crounse, J.D., Kjaergaard, H.G., Kürten, A., St. Clair, J.M., Seinfeld, J.H., and Wennberg, P.O.: Unexpected Epoxide Formation in the Gas-Phase Photooxidation of Isoprene, Science, 325, 730-733, doi: 10.1126/science.1172910, 2009a.
Paulot, F., Crounse, J.D., Kjaergaard, H.G., Kroll, J.H., Seinfeld, J.H., and Wennberg, P.O.: Isoprene photooxidation: new insights into the production of acids and organic nitrates, Atmos. Chem. Phys., 9, 1479-1501, doi:10.5194/acp-9-1479-2009, 2009b.
Pétron, G., Frost, G., Miller, B.R., Hirsch, A.I., Montzka, S.A., Karion, A., Trainer, M., Sweeney, C., Andrews, A.E., Miller, L., Kofler, J., Bar-Ilan, A., Dlugokencky, E.J., Patrick, L., Moore, C.T., Ryerson, T.B., Siso, C., Kolodzey, W., Lang, P.M., Conway, T., Novelli, P., Masarie, K., Hall, B., Guenther, D., Kitzis, D., Miller, J., Welsh, D., Wolfe, D., Neff, W., and Tans, P.: Hydrocarbon emissions characterization in the Colorado Front Range: A pilot study, J. Geophys. Res., 117, D04304, doi: 10.1029/2011jd016360, 2012.
Pétron, G., Karion, A., Sweeney, C., Miller, B.R., Montzka, S.A., Frost, G., Trainer, M., Tans, P., Andrews, A., Kofler, J., Helmig, D., Guenther, D., Dlugokencky, E., Lang, P., Newberger, T., Wolter, S., Hall, B., Novelli, P., Brewer, A., Conley, S., Hardesty, M., Banta, R., White, A., Noone, D., Wolfe, D., and Schnell, R.: A new look at methane and non-methane hydrocarbon emissions from oil and natural gas operations in the Colorado Denver-Julesburg Basin, J. Geophys. Res., 2013JD021272, doi: 10.1002/2013jd021272, 2014.
Piccot, S.D., Watson, J.J., and Jones, J.W.: A global inventory of volatile organic compound emissions from anthropogenic sources, J. Geophys. Res., 97, 9897-9912, doi: 10.1029/92jd00682, 1992.
Pierotti, D., Wofsy, S.C., Jacob, D., and Rasmussen, R.A.: Isoprene and its oxidation products: Methacrolein and methyl vinyl ketone, J. Geophys. Res., 95, 1871-1881, doi: 10.1029/JD095iD02p01871, 1990.
Pollmann, J., Ortega, J. and Helmig, D.: Analysis of atmospheric sesquiterpenes: Sampling losses and mitigation of ozone interferences, Environ. Sci. & Technol., 39, 9620-9629, doi:10.1021/es050440w, 2005.
Potter, C., Klooster, S., Bubenheim, D., Singh, H.B., and Myneni, R.: Modeling terrestrial biogenic sources of oxygenated organic emissions, Earth Interact., 7, 1-15, 2003.
Read, K.A., Carpenter, L.J., Arnold, S.R., Beale, R., Nightingale, P.D., Hopkins, J.R., Lewis, A.C., Lee, J.D., Mendes, L., and Pickering, S.J.: Multiannual observations of

acetone, methanol, and acetaldehyde in remote tropical Atlantic air: Implications for atmospheric OVOC budgets and oxidative capacity, Environ. Sci. Technol., 46, 11028-11039, doi:10.1021/es302082p, 2012.

Reissell, A., Harry, C., Aschmann, S.M., Atkinson, R., and Arey, J.: Formation of acetone from the OH radical- and O_3-initiated reactions of a series of monoterpenes, J. Geophys. Res., 104, 13869-13879, 1999.

Riemer, D., Pos, W., Milne, P., Farmer, C., Zika, R., Apel, E., Olszyna, K., Kliendienst, T., Lonneman, W., Bertman, S., Shepson, P., and Starn, T.: Observations of nonmethane hydrocarbons and oxygenated volatile organic compounds at a rural site in the southeastern United States, J. Geophys. Res., 103, 28111-28128, 1998.

Rodgers, C.D.: Inverse methods for atmospheric sounding: Theory and practice, World Sci., Singapore, 2000.

Salisbury, G., Williams, J., Holzinger, R., Gros, V., Mihalopoulos, N., Vrekoussis, M., Sarda-Esteve, R., Berresheim, H., von Kuhlmann, R., Lawrence, M., and Lelieveld, J.: Ground-based PTR-MS measurements of reactive organic compounds during the MINOS campaign in Crete, July-August 2001, Atmos. Chem. Phys., 3, 925-940, doi:10.5194/acp-3-925-2003, 2003.

Sander, R.: Compilation of Henry's Law Constants for Inorganic and Organic Species of Potential Importance in Environmental Chemistry (Version 3), http://www.henrys-law.org, 1999.

Sander, S.P., Golden, D., Kurylo, M., Moortgat, G., Wine, P., Ravishankara, A., Kolb, C., Molina, M., Finlayson-Pitts, B., and Huie, R.: Chemical kinetics and photochemical data for use in atmospheric studies, JPL Publ., 06-2, 684, 2011.

Sasaki, K., Saito, T., Lämsä, M., Oksman-Caldentey, K.-M., Suzuki, M., Ohyama, K., Muranaka, T., Ohara, K., and Yazaki, K.: Plants Utilize Isoprene Emission as a Thermotolerance Mechanism, Plant. Cell. Physiol., 48, 1254-1262, doi: 10.1093/pcp/pcm104, 2007.

Schade, G.W., and Goldstein, A.H.: Fluxes of oxygenated volatile organic compounds from a ponderosa pine plantation, J. Geophys. Res., 106, 3111-3123, doi:10.1029/2000JD900592, 2001.

Schade, G.W., and Goldstein, A.H.: Seasonal measurements of acetone and methanol: Abundances and implications for atmospheric budgets, Global Biogeochem. Cy., 20, GB1011, doi:10.1029/2005gb002566, 2006.

Schnitzhofer, R., Wisthaler, A., and Hansel, A.: Real-time profiling of organic trace gases in the planetary boundary layer by PTR-MS using a tethered balloon, Atmos. Meas. Tech., 2, 773-777, doi: 10.5194/amt-2-773-2009, 2009.

Schultz, M., Backman, L., Balkanski, Y., Bjoerndalsaeter, S., Brand, R., Burrows, J., Dalsoeren, S., de Vasconcelos, M., Grodtmann, B., and Hauglustaine, D.: REanalysis of the TROpospheric chemical composition over the past 40 years (RETRO) - A long-term global modeling study of tropospheric chemistry: Final Report, Jülich/Hamburg, Germany, 2007.

Sharkey, T.D., Loreto, F., and Delwiche, C.F.: High carbon dioxide and sun/shade effects on isoprene emission from oak and aspen tree leaves, Plant. Cell. Environ., 14, 333-338, doi: 10.1111/j.1365-3040.1991.tb01509.x, 1991.

Sharkey, T.D., Singsaas, E.L., Vanderveer, P.J., and Geron, C.: Field measurements of isoprene emission from trees in response to temperature and light, Tree. Physiol., 16, 649-654, doi: 10.1093/treephys/16.7.649, 1996.

Sharkey, T.D., Wiberley, A.E., and Donohue, A.R.: Isoprene Emission from Plants: Why and How, Ann. Bot., 101, 5-18, doi: 10.1093/aob/mcm240, 2008.

Shim, C., Wang, Y., Choi, Y., Palmer, P.I., Abbot, D.S., and Chance, K.: Constraining global isoprene emissions with Global Ozone Monitoring Experiment (GOME) formaldehyde column measurements, J. Geophys. Res., 110, D24301, doi: 10.1029/2004jd005629, 2005.

Sillman, S., Logan, J.A., and Wofsy, S.C.: The sensitivity of ozone to nitrogen oxides and hydrocarbons in regional ozone episodes, J. Geophys. Res., 95, 1837-1851, doi: 10.1029/JD095iD02p01837, 1990.

Simpson, I., Akagi, S., Barletta, B., Blake, N., Choi, Y., Diskin, G., Fried, A., Fuelberg, H., Meinardi, S., and Rowland, F.: Boreal forest fire emissions in fresh Canadian smoke plumes: C_1-C_{10} volatile organic compounds (VOCs), CO_2, CO, NO_2, NO, HCN and CH_3CN, Atmos. Chem. Phys., 11, 6445-6463, doi:10.5194/acp-11-6445-2011, 2011.

Singh, H.B., and Hanst, P.L.: Peroxyacetyl nitrate (PAN) in the unpolluted atmosphere: An important reservoir for nitrogen oxides, Geophys. Res. Lett., 8, 941-944, 1981.

Singh, H.B., Salas, L.J., Cantrell, B.K., and Redmond, R.M.: Distribution of aromatic hydrocarbons in the ambient air, Atmos. Environ. (1967), 19, 1911-1919, 1985.

Singh, H., O'Hara, D., Herlth, D., Sachse, W., Blake, D., Bradshaw, J., Kanakidou, M., and Crutzen, P.: Acetone in the atmosphere: Distribution, sources, and sinks, J. Geophys. Res., 99, 1805-1819, 1994.

Singh, H.B., Kanakidou, M., Crutzen, P.J., and Jacob, D.J.: High mixing ratios and photochemical fate of oxygenated hydrocarbons in the global troposphere, Nature, 378, 50-54, doi:10.1038/378050a0, 1995.

Singh, H.B., Chen, Y., Tabazadeh, A., Fukui, Y., Bey, I., Yantosca, R., Jacob, D., Arnold, F., Wohlfrom, K., Atlas, E., Flocke, F., Blake, D., Blake, N., Heikes, B., Snow, J., Talbot, R., Gregory, G., Sachse, G., Vay, S., and Kondo, Y.: Distribution and fate of selected oxygenated organic species in the troposphere and lower stratosphere over the Atlantic, J. Geophys. Res., 105, 3795-3805, doi:10.1029/1999JD900779, 2000.

Singh, H.B., Salas, L.J., Chatfield, R.B., Czech, E., Fried, A., Walega, J., Evans, M.J., Field, B.D., Jacob, D.J., Blake, D., Heikes, B., Talbot, R., Sachse, G., Crawford, J.H., Avery, M.A., Sandholm, S., and Fuelberg, H.: Analysis of the atmospheric distribution, sources, and sinks of oxygenated volatile organic chemicals based on measurements over the Pacific during TRACE-P, J. Geophys. Res., 109, D15S07, doi:10.1029/2003jd003883, 2004.

Singh, H.B., Brune, W.H., Crawford, J.H., Jacob, D.J., and Russell, P.B.: Overview of the summer 2004 Intercontinental Chemical Transport Experiment–North America (INTEX-A), J. Geophys. Res., 111, D24S01, doi: 10.1029/2006JD007905, 2006.

Singh, H.B., Brune, W.H., Crawford, J.H., Flocke, F., and Jacob, D.J.: Chemistry and transport of pollution over the Gulf of Mexico and the Pacific: spring 2006 INTEX-B campaign overview and first results, Atmos. Chem. Phys., 9, 2301-2318, doi: 10.5194/acp-9-2301-2009, 2009.

Sinha, V., Williams, J., Meyerhöfer, M., Riebesell, U., Paulino, A.I., and Larsen, A.: Air-sea fluxes of methanol, acetone, acetaldehyde, isoprene and DMS from a Norwegian fjord following a phytoplankton bloom in a mesocosm experiment, Atmos. Chem. Phys., 7, 739-755, doi:10.5194/acp-7-739-2007, 2007.

Sjostedt, S.J., Leaitch, W.R., Levasseur, M., Scarratt, M., Michaud, S., Motard-Côté, J., Burkhart, J.H., and Abbatt, J.P.D.: Evidence for the uptake of atmospheric acetone and methanol by the Arctic Ocean during late summer DMS-Emission plumes, J. Geophys. Res., 117, D12303, doi:10.1029/2011JD017086, 2012.

Stavrakou, T., Müller, J.F., De Smedt, I., Van Roozendael, M., van der Werf, G.R., Giglio, L., and Guenther, A.: Global emissions of non-methane hydrocarbons deduced from SCIAMACHY formaldehyde columns through 2003-2006, Atmos. Chem. Phys., 9, 3663-3679, doi: 10.5194/acp-9-3663-2009, 2009.

Stavrakou, T., Guenther, A., Razavi, A., Clarisse, L., Clerbaux, C., Coheur, P.-F., Hurtmans, D., Karagulian, F., Mazière, M.D., Vigouroux, C., Amelynck, C., Schoon, N., Laffineur, Q., Heinesch, B., Aubinet, M., and Müller, J.-F.: First space-based derivation of the global atmospheric methanol emission fluxes, Atmos. Chem. Phys., 11, 4873-4898, doi: 10.5194/acp-11-4873-2011, 2011.

Steinbacher, M., Zellweger, C., Schwarzenbach, B., Bugmann, S., Buchmann, B., Ordóñez, C., Prevot, A.S.H., and Hueglin, C.: Nitrogen oxide measurements at rural sites in Switzerland: Bias of conventional measurement techniques, J. Geophys. Res., 112, D11307, doi: 10.1029/2006jd007971, 2007.

Stroud, C.A., Roberts, J.M., Goldan, P.D., Kuster, W.C., Murphy, P.C., Williams, E.J., Hereid, D., Parrish, D., Sueper, D., Trainer, M., Fehsenfeld, F.C., Apel, E.C., Riemer, D., Wert, B., Henry, B., Fried, A., Martinez-Harder, M., Harder, H., Brune, W.H., Li, G., Xie, H., and Young, V.L.: Isoprene and its oxidation products, methacrolein and methylvinyl ketone, at an urban forested site during the 1999 Southern Oxidants Study, J. Geophys. Res., 106, 8035-8046, doi: 10.1029/2000jd900628, 2001.

Taddei, S., Toscano, P., Gioli, B., Matese, A., Miglietta, F., Vaccari, F.P., Zaldei, A., Custer, T., and Williams, J.: Carbon dioxide and acetone air-sea fluxes over the southern Atlantic, Environ. Sci. Technol., 43, 5218-5222, doi:10.1021/es8032617, 2009.

Task group on atmospheric chemical kinetic data evaluation by International Union of Pure and Applied Chemistry (IUPAC): http://iupac.pole-ether.fr, access: July 2013.

The Clean Air Act Amendments of 1990 List of Hazardous Air Pollutants: http://www.epa.gov/ttnatw01/orig189.html, access: January 2014.

Tie, X., Guenther, A., and Holland, E.: Biogenic methanol and its impacts on tropospheric oxidants, Geophys. Res. Lett., 30, 1881, doi: 10.1029/2003GL017167, 2003.

Toon, O.B., Starr, D.O., Jensen, E.J., Newman, P.A., Platnick, S., Schoeberl, M.R., Wennberg, P.O., Wofsy, S.C., Kurylo, M.J., Maring, H., Jucks, K.W., Craig, M.S., Vasques, M.F., Pfister, L., Rosenlof, K.H., Selkirk, H.B., Colarco, P.R., Kawa, S.R., Mace, G.G., Minnis, P., and Pickering, K.E.: Planning, implementation, and first results of the Tropical Composition, Cloud and Climate Coupling Experiment (TC4), J. Geophys. Res, 115, D00J04, doi: 10.1029/2009jd013073, 2010.

Tyndall, G.S., Cox, R.A., Granier, C., Lesclaux, R., Moortgat, G.K., Pilling, M.J., Ravishankara, A.R., and Wallington, T.J.: Atmospheric chemistry of small organic peroxy radicals, J. Geophys. Res., 106, 12157-12182, 2001.

USDA Cropland Data Layer (CDL), Prepared by the National Agricultural Statistics Service, United States Department of Agriculture, Washington D.C.: http://www.nass.usda.gov/research/Cropland/SARS1a.htm, access: March 2014.

van der Werf, G.R., Randerson, J.T., Giglio, L., Collatz, G.J., Kasibhatla, P.S., and Arellano, A.F.: Interannual variability in global biomass burning emissions from 1997 to 2004, Atmos. Chem. Phys., 6, 3423-3441, doi: 10.5194/acp-6-3423-2006, 2006.

van der Werf, G.R., Randerson, J.T., Giglio, L., Collatz, G.J., Mu, M., Kasibhatla, P.S., Morton, D.C., DeFries, R.S., Jin, Y., and van Leeuwen, T.T.: Global fire emissions and the contribution of deforestation, savanna, forest, agricultural, and peat fires (1997-2009), Atmos. Chem. Phys., 10, 11707-11735, doi:10.5194/acp-10-11707-2010, 2010.

van Donkelaar, A., Martin, R.V., Pasch, A.N., Szykman, J.J., Zhang, L., Wang, Y.X., and Chen, D.: Improving the accuracy of daily satellite-derived ground-level fine ferosol concentration estimates for North America, Environ. Sci. Technol., 46, 11971-11978, doi:10.1021/es3025319, 2012.

Veres, P., Gilman, J.B., Roberts, J.M., Kuster, W.C., Warneke, C., Burling, I.R., and de Gouw, J.: Development and validation of a portable gas phase standard generation and calibration system for volatile organic compounds, Atmos. Meas. Tech., 3, 683-691, doi:10.5194/amt-3-683-2010, 2010.

Wang, J.-L., Chew, C., Chang, C.-Y., Liao, W.-C., Lung, S.-C.C., Chen, W.-N., Lee, P.-J., Lin, P.-H., and Chang, C.-C.: Biogenic isoprene in subtropical urban settings and implications for air quality, Atmos. Environ., 79, 369-379, doi: 10.1016/j.atmosenv.2013.06.055, 2013.

Wang, Y.X., McElroy, M.B., Jacob, D.J., and Yantosca, R.M.: A nested grid formulation for chemical transport over Asia: Applications to CO, J. Geophys. Res., 109, D22307, doi:10.1029/2004JD005237, 2004.

Warneke, C., Karl, T., Judmaier, H., Hansel, A., Jordan, A., Lindinger, W., and Crutzen, P.J.: Acetone, methanol, and other partially oxidized volatile organic emissions from dead plant matter by abiological processes: Significance for atmospheric HOx chemistry, Global Biogeochem. Cy., 13, 9-17, doi: 10.1029/98GB02428, 1999.

Warneke, C., Holzinger, R., Hansel, A., Jordan, A., Lindinger, W., Poschl, U., Williams, J., Hoor, P., Fischer, H., Crutzen, P.J., Scheeren, H.A., and Lelieveld, J.: Isoprene and

its oxidation products methyl vinyl ketone, methacrolein, and isoprene related peroxides measured online over the tropical rain forest of Surinam in March 1998, J. Atmos. Chem., 38, 167-185, 2001.

Warneke, C., van der Veen, C., Luxembourg, S., de Gouw, J.A., and Kok, A.: Measurements of benzene and toluene in ambient air using proton-transfer-reaction mass spectrometry: calibration, humidity dependence, and field intercomparison, Int. J. Mass Spectrom., 207, 167-182, 2001.

Warneke, C., McKeen, S.A., de Gouw, J.A., Goldan, P.D., Kuster, W.C., Holloway, J.S., Williams, E.J., Lerner, B.M., Parrish, D.D., Trainer, M., Fehsenfeld, F.C., Kato, S., Atlas, E.L., Baker, A., and Blake, D.R.: Determination of urban volatile organic compound emission ratios and comparison with an emissions database, J. Geophys. Res., 112, D10s47, doi: 10.1029/2006jd007930, 2007.

Warneke, C., de Gouw, J.A., Del Negro, L., Brioude, J., McKeen, S., Stark, H., Kuster, W.C., Goldan, P.D., Trainer, M., Fehsenfeld, F.C., Wiedinmyer, C., Guenther, A.B., Hansel, A., Wisthaler, A., Atlas, E., Holloway, J.S., Ryerson, T.B., Peischl, J., Huey, L.G., and Hanks, A.T.C.: Biogenic emission measurement and inventories determination of biogenic emissions in the eastern United States and Texas and comparison with biogenic emission inventories, J. Geophys. Res., 115, D00F18, doi: 10.1029/2009jd012445, 2010.

Warneke, C., de Gouw, J.A., Holloway, J.S., Peischl, J., Ryerson, T.B., Atlas, E., Blake, D., Trainer, M., and Parrish, D.D.: Multiyear trends in volatile organic compounds in Los Angeles, California: Five decades of decreasing emissions, J. Geophys. Res., 117, D00V17, doi: 10.1029/2012JD017899, 2012.

Warneke, C., Karl, T., Judmaier, H., Hansel, A., Jordan, A., Lindinger, W., and Crutzen, P.J.: Acetone, methanol, and other partially oxidized volatile organic emissions from dead plant matter by abiological processes: Significance for atmospheric HO_x chemistry, Global Biogeochem. Cy., 13, 9-17, doi:10.1029/98GB02428, 1999.Wells, K.C., Millet, D.B., Hu, L., Cady-Pereira, K.E., Xiao, Y., Shephard, M.W., Clerbaux, C.L., Clarisse, L., Coheur, P.F., Apel, E.C., de Gouw, J., Warneke, C., Singh, H.B., Goldstein, A.H., and Sive, B.C.: Tropospheric methanol observations from space: retrieval evaluation and constraints on the seasonality of biogenic emissions, Atmos. Chem. Phys., 12, 3941-3982, doi:10.5194/acp-12-5897-2012, 2012.

Warneke, C., Geiger, F., Edwards, P.M., Dube, W., Pétron, G., Kofler, J., Zahn, A., Brown, S.S., Graus, M., Gilman, J., Lerner, B., Peischl, J., Ryerson, T.B., de Gouw, J.A., and Roberts, J.M.: Volatile organic compound emissions from the oil and natural gas industry in the Uinta Basin, Utah: point sources compared to ambient air composition, Atmos. Chem. Phys. Discuss., 14, 11895-11927, doi: 10.5194/acpd-14-11895-2014, 2014.

Weber, R.J., Sullivan, A.P., Peltier, R.E., Russell, A., Yan, B., Zheng, M., de Gouw, J., Warneke, C., Brock, C., Holloway, J.S., Atlas, E.L., and Edgerton, E.: A study of secondary organic aerosol formation in the anthropogenic-influenced southeastern United States, J. Geophys. Res., 112, D13302, doi: 10.1029/2007jd008408, 2007.

Wells, K.C., Millet, D.B., Hu, L., Cady-Pereira, K.E., Xiao, Y., Shephard, M.W., Clerbaux, C.L., Clarisse, L., Coheur, P.F., Apel, E.C., de Gouw, J., Warneke, C., Singh, H.B., Goldstein, A.H., and Sive, B.C.: Tropospheric methanol observations from space: retrieval evaluation and constraints on the seasonality of biogenic emissions, Atmos. Chem. Phys., 12, 3941-3982, doi:10.5194/acp-12-5897-2012, 2012.

Wells, K.C., Millet, D.B., Cady-Pereira, K.E., Shephard, M.W., Henze, D.K., Bousserez, N., Apel, E.C., de Gouw, J., Warneke, C., and Singh, H.B.: Quantifying global terrestrial methanol emissions using observations from the TES satellite sensor, Atmos. Chem. Phys., 14, 2555-2570, doi: 10.5194/acp-14-2555-2014, 2014.

Wennberg, P., Hanisco, T., Jaeglé, L., Jacob, D., Hintsa, E., Lanzendorf, E., Anderson, J., Gao, R.S., Keim, E., and Donnelly, S.: Hydrogen radicals, nitrogen radicals, and the production of O_3 in the upper troposphere, Science, 279, 49-53, 1998.

Wesely, M.L.: Parameterization of surface resistances to gaseous dry deposition in regional-scale numerical models, Atmos. Environ., 23, 1293-1304, 1989.

Williams, J., Holzinger, R., Gros, V., Xu, X., Atlas, E., and Wallace, D.W.R.: Measurements of organic species in air and seawater from the tropical Atlantic, Geophys. Res. Lett., 31, L23S06, doi:10.1029/2004gl020012, 2004.

Xue, L.K., Wang, T., Gao, J., Ding, A.J., Zhou, X.H., Blake, D.R., Wang, X.F., Saunders, S.M., Fan, S.J., Zuo, H.C., Zhang, Q.Z., and Wang, W.X.: Ozone production in four major cities of China: sensitivity to ozone precursors and heterogeneous processes, Atmos. Chem. Phys. Discuss., 13, 27243-27285, 2013.

Yarwood, G., Rao, S., Yocke, M., and Whitten, G.: Updates to the Carbon Bond chemical mechanism: CB05, Final report to the US EPA, RT-0400675, 8, 2005.

Zhang, L., D.J. Jacob, N.V. Smith-Downey, D.A. Wood, D. Blewitt, C.C. Carouge, A. van Donkelaar, D.B.A. Jones, L.T. Murray, and Y. Wang, Improved estimate of the policy-relevant background ozone in the United States using the GEOS-Chem global model with 1/2°×2/3° horizontal resolution over North America, Atmos. Environ., 45, 6769-6776, doi:10.1016/j.atmosenv.2011.07.054, 2011.

Zhang, Q., Streets, D.G., Carmichael, G.R., He, K.B., Huo, H., Kannari, A., Klimont, Z., Park, I.S., Reddy, S., Fu, J.S., Chen, D., Duan, L., Lei, Y., Wang, L.T., and Yao, Z.L.: Asian emissions in 2006 for the NASA INTEX-B mission, Atmos. Chem. Phys., 9, 5131-5153, doi: 10.5194/acp-9-5131-2009, 2009.

Zhang, X., Lee, X., Griffis, T., Baker, J., Erickson, M., Hu, N., and Xiao, W.: The influence of plants on atmospheric methane in an agriculture-dominated landscape, Int J Biometeorol, 1-15, doi: 10.1007/s00484-013-0662-y, 2013.

Appendix

Appendix 1. Schematic of the PTR-MS inlet/calibration system. MFC 1- MFC 4: mass flow controllers 1-4; V1-V6: 3-way valves 1-6. Blue arrows show the flow directions with typical flow rates indicated.

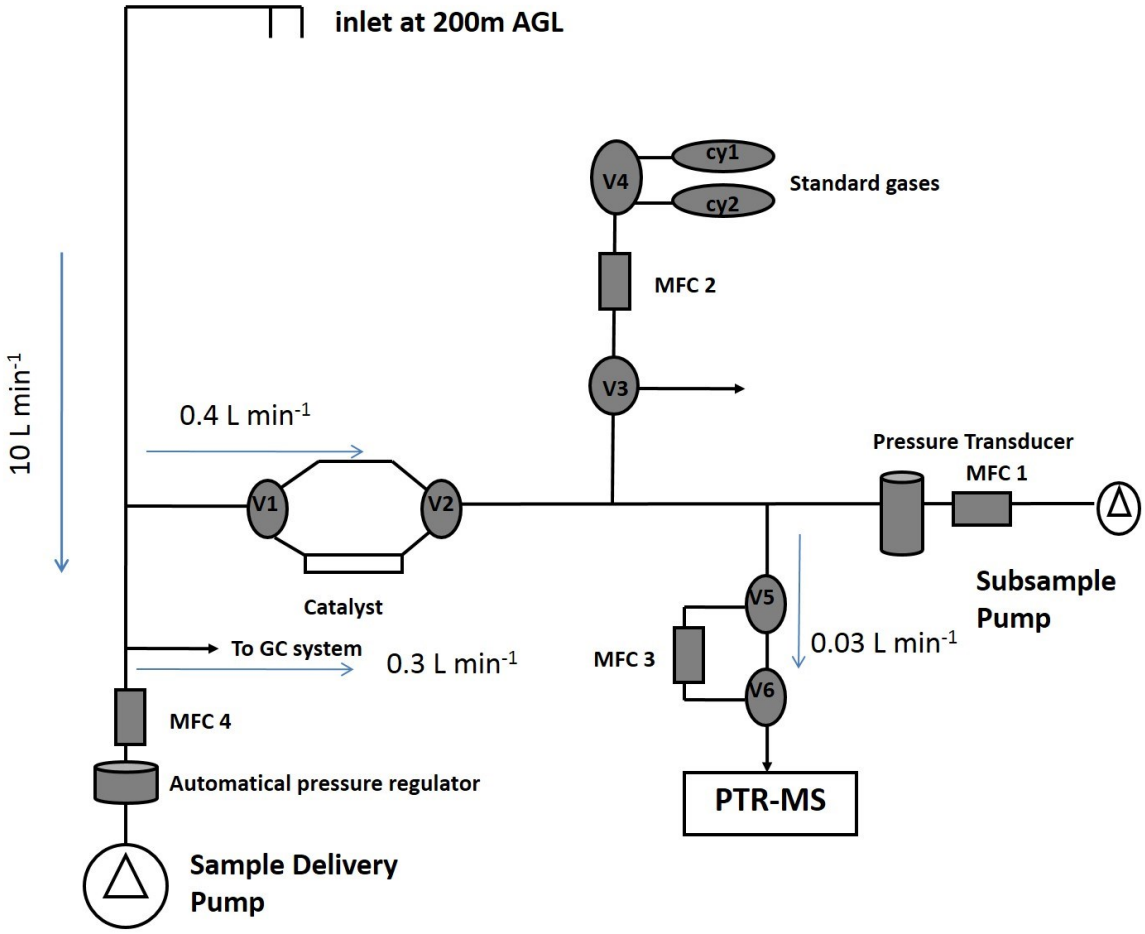

Appendix 2. VOC standard specifications

Unit: ppbv
Cylinder #: CC286005
Preparation Date: 12/3/2008 2000 psi
Reanalysis Date: 1/6/2012 1599 psi

Compound	Original	Reanalysis	% Difference
Methacrolein	177.7	112.0	-37.0
p-Xylene	43.9	44.1	0.5
1,2,4-Trimethylbenzene	23.7	24.0	1.3
a-Pinene	139.0	137.9	-0.8
2-Pentanone	149.4	146.4	-2.0
Methanol	202.8	28.9	-85.7
Methyl Ethyl Ketone	151.9	149.2	-1.8
2-Hexanone	138.1	131.4	-4.9

Cylinder #: CC285872
Preparation Date: 12/4/2008 2000 psi
Reanalysis Date: 1/6/2012 1546 psi

Compound	Original	Reanalysis	% Difference
Acetaldehyde	155.5	24.7	-84.1
Isoprene	49.9	53.3	6.8
Acetone	152.6	152.9	0.2
Acetonitrile	35.8	31.2	-12.8
Methyl Vinyl Ketone	149.8	13.7	-90.9
Benzene	27.9	28.7	2.9
Toluene	26.3	27.4	4.2
3-Carene	158.1	149.8	-5.2
Nopinone	146	123.2	-15.6

Appendix 3. Typical PTR-MS and sampling system settings.

Parameter	Value	Comments
PC (mbar)	355	Pressure controller to determine the pressure in the reaction chamber
FC (sccm)	6.5	Flow controller for the water flow
U SO (V)	75	Voltage of source out to optimize the O_2 and H_3O^+ ratio
U S (V)	110	Voltage of source to optimize the O_2 and H_3O^+ ratio
U Drift (V)	600	Voltage of drift tube
U QL (V)	50	Voltage of the extraction lens out of the reaction chamber
U NC (V)	6	Nosecone voltage is an important lens current
Source (mA)	6.5-8	Water source current
T drift (°C)	60	Temperature in the drift tube
T inlet (°C)	60	Inlet temperature
Rea (mbar)	2.10-2.25	Pressure in the reaction chamber
T catalyst (°C)	450	Temperature for catalyst converter
Subsampling pressure (torr)	530-570	Pressure transducer in Appendix 1
Subsampling flow (sccm)	250-500	MFC 1 in Appendix 1

Appendix 4. Figures of merit for compounds investigated here

Compound	Protonated m/z	Sensitivity (ncps/ppbv)[a]	Detection Limit (pptv)[b]	Humidity factor X_R [c]
methanol	33	11	203	0.38
acetone	59	18	28	0.58
isoprene	69	7	38	0.5
MVK+MACR	71	3	-	0.5
benzene	79	10	17	-0.2
toluene	93	13	35	0.1
C_8 aromatics	107	8	46	0.1
C_9 aromatics	121	7	45	0.1

[a] Sensitivities are from measurements during July 20, 2011-August 08, 2011; [b] Detection limits are defined as 3 times the error in the volume mixing ratios, following Equation (2.17) of de Gouw and Warneke (2007); [c] X_R values to correct the measurements for the influence of humidity, are from Table 1 of de Gouw et al. (2003).

de Gouw, J.A., Goldan, P.D., Warneke, C., Kuster, W.C., Roberts, J.M., Marchewka, M., Bertman, S.B., Pszenny, A.A.P., and Keene, W.C.: Validation of proton transfer reaction-mass spectrometry (PTR-MS) measurements of gas-phase organic compounds in the atmosphere during the New England Air Quality Study (NEAQS) in 2002, J. Geophys. Res., 108, 4682, doi: 10.1029/2003jd003863, 2003.
de Gouw, J.A., and Warneke, C.: Measurements of volatile organic compounds in the earth's atmosphere using proton-transfer-reaction mass spectrometry, Mass Spectrom. Rev., 26, 223-257, doi: 10.1002/mas.20119, 2007.